PROCEEDINGS

of the

NORTH DAKOTA ACADEMY OF SCIENCE

ABSTRACTS

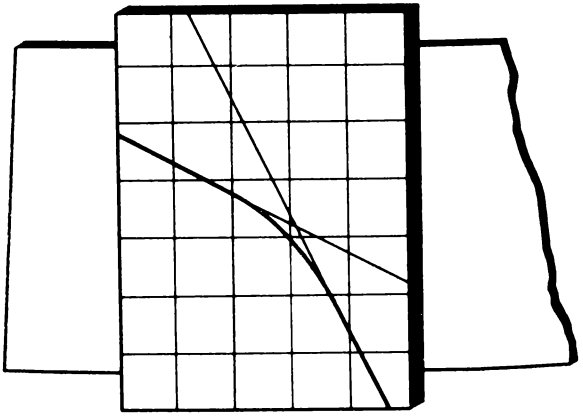

69th Annual Meeting

APRIL 29-30

Minot State College, Minot, North Dakota

Volume 31 • Part I • April, 1977

THE PROCEEDINGS OF THE NORTH DAKOTA ACADEMY OF SCIENCE is published jointly through the Academy by the University of North Dakota North Dakota State University, Minot State Collge, Dickinson State College, and Valley City State College. The Proceedings appears in two parts: Part I, Abstracts, and Part II, Papers. Part I contains only abstracts of papers presented at the annual meeting of the Academy, usually in late April. Part II contains complete papers submittd in manuscript form at the time of the annual meeting and are usually published within a year. Printing is by the University of North Dakota Press. Strictly editorial matters should be directed to the editor, Dorothea McCullough, Associate Professor of Communications, North Dakota State University, 1114 College St., Fargo, North Dakota 58102. Instructions for submission of abstracts and complete papers are obtained by writing to the secretary of the Academy (see below).

SUBSCRIPTIONS: Members of the Academy receive both parts of the Proceedings. Annual dues are $5.00 for regular members and $3.00 for student members. Correspondence concerning subscription, as well as instructions to authors and other related matters, should be directed to: North Dakota Academy of Science. Office of the Secretary, Box 8123, University Station Grand Forks, North Dakota 58202.

PROCEEDINGS
of the
NORTH DAKOTA
ACADEMY OF SCIENCE

ABSTRACTS

Volume 31, Part I April 1977

NORTH DAKOTA ACADEMY OF SCIENCE

(Official State Academy; founded December, 1908)

1976-77

OFFICERS AND OTHER MEMBERS OF EXECUTIVE COMMITTEE

EDITORIAL ADVISORY COMMITTEE

EDITOR

69th Annual Meeting

APRIL 29-30, 1977

Minot State College, Minot, North Dakota

EDITOR'S NOTE

The abstracts are arranged alphabetically by author or first author if more than one author is involved. An author index to all authors is on page 36 and 37.

PERIODIC DROUGHT IN NORTH DAKOTA. D. B. Baker. Dept. of Geography, University of N. Dak., Grand Forks, N. Dak. 58202

Precipitation records for six weather stations in North Dakota were subjected to harmonic (Fourier) analysis for the period from 1900 to 1975. Long term cyclic trens in precipitation, ranging from approximately two to fifty years, were identified. On the basis of these trends, years of drought danger for the areas of the weather stations can be identified. The spatial mapping of predicted intensities of the danger years allows the extent of the affected areas to be estimated. The mapping of long term trends identify the areas of permanent drought difficulty within the state to be delineated.

TRANSIENT SATURATED-UNSATURATED GROUNDWATER FLOW: A NUMERICAL SIMULATION. J. J. Brown and M. H. Somerville. Engineering Experiment Station, School of Engineering and Mines, University of North Dakota, Grand Forks, ND 58202

A first attempt to develop a versatile mathematical model of a transient saturated-unsaturated groundwater flow is presented. The model can be used to assess the hydrologic consequences of surface mining.

The numerical algorithm used to simulate the solution to the analytical model is the finite element method using Galerkin's weighted residual method with linear triangular finite elements. The transient time step is approximated using a forward finite difference technique.

Excellent results were obtained in the steady state when compared against known solutions. The transient response to a flow regime was shown to be incorrect. Instabilities resulting from the choice of approximating functions or from the grid size used are prevalent in the transient mode.

An analysis of the hydrologic response of the groundwater flow system to surface mining is conducted as a series of steady state analyses on changing cross sections. Thus the model can be used to predict the large scale effects of surface mining.

The results of this study indicate that further study is justified and that an experimental verification of the model is warranted. Supported in part by Natural Gas Pipeline Co. of America.

THE REDUCTION OF PRIMARY PRODUCTIVITY IN BREWER LAKE (RESERVOIR) BY PERIODIC HYPOLIMNETIC DISCHARGE. G. W. COMITA, Zoology Dept. N. D. St. Univ. Fargo, N. D. 58102 and N. D. Game and Fish Dept., Bismarck, N. D. 58501.

Brewer Lake, N. D. was monitored weekly during the ice-free period of three years: 1974, the first year after being filled, when no bottom drainage was done and a strong fish-kill occurred; 1975, with intermittent bottom drainage a slight fish-kill was noted and in 1976, with continuous bottom drainage no fish-kill occurred. iPO_4 (kg m^{-2} yr^{-1}) was reduced each year: 0.88, 0.34, 0.33 and a simultaneous reduction in primary productivity was recorded (kg C m^{-2} yr^{-1}), gross: 1.82, 2.52, 1.34; net: 1.05, 0.90, 0.60. Solar and sky radiation (kcal m^{-2} yr^{-1}) was 566,794 in 1974, 555,910 in 1975 and 825,640 in 1976. Photosynthetic efficiencies (% of SSR) also reduced, gross: 1974, 2.88, 1975, 4.06, 1976, 1.45; net: 1974, 1.66, 1975, 1.46, 1976, 0.65.

Some parameters increased (kg $m^{-2}yr^{-1}$), dissolved oxygen: 43.7, 48.0, 46.9; ammonia: 0.53, 0.48, 1.20; urea: 0.42, 1.56, 3.73; nitrate: 3.03, 3.42, 4.79; chlorophylls: -a, 0.13, 0.14, 0.23; -b, 0.05, 0.07, 0.11 and -c, 0.09, 0.06, 0.10.

ALGAE, NUTRIENTS, AND THE DEVILS LAKE ECOSYSTEM. Cecilia M. Conway and L. E. Shubert. Dept. of Biology, Univ. N. Dak., Grand Forks, N. Dak. 58202.

Devils Lake, the largest natural lake in North Dakota, is very saline and hypereutrophic. High ambient concentrations of nitrogen (N) and phosphorus (P) in the bays of Devils Lake contribute to massive blue-green algal blooms during the growing season. Nutrient analysis of Big Coulee, Main Bay-Devils Lake, and East Bay-Devils Lake has provided evidence of an accumulation factor. Total dissolved salts increased from 855 ppm, to 2343 ppm, to 6247 ppm respectively. Increases in sodium were primarily responsible, but increases in N and P were also significant. Nutrient fluxes in the Devils Lake ecosystem were correlated with algal bioassays.

Supported by Grant #A-053-NDAK from the USDI,OWRT AND WRRI and Grant # 3170-78 from UND/NSF Faculty Research.

TREE AND SHRUB STRATUM COMPOSITION ON THE KILLDEER MOUNTAINS. *E. James Crompton, Keith T. Killingbeck* and *Richard H. Bares*. Dept. of Biol., Univ. N. Dak., Grand Forks, N.D. 58202

A vegetation study conducted on the Killdeer Mountains located in Dunn County, North Dakota, examined species composition and vegetation attributes of the forest communities in relation to selected topographic features. Six forest community types were identified. Aspen (*Populus tremuloides*), bur oak (*Quercus macrocarpa*) and paper birch (*Betula papyrifera*) had the highest Importance Values of the 11 species found in the tree stratum. Juneberry (*Amelanchier alnifolia*) and beaked hazel (*Corylus cornuta*) dominated the 17 species in the shrub stratum. Mean tree stratum density, basal area and age were 1667 stems/ha, 19.1 m^2/ha and 43 years. Mean shrub stratum density and crown cover were 3273 stems/ha and 1630 m^2/ha. Aspect appeared to be the most important topographic parameter influencing community structure and distribution. Tree stratum density on north-facing slopes (2182 stems/ha) was 72% higher than on south-facing slopes (1267 stems/ha). In the tree stratum, bur oak dominated south- and east-facing slopes at all slope positions but aspen and birch dominated all positions on west- and north-facing slopes. All major tree stratum species were also prevalent in the shrub stratum indicating the continued regeneration of the forest overstory. *Support: N.D. Regional Environmental Assessment Program grant to Dr. M.K. Wali.*

AQUATIC MOLLUSKS IN SOUTHWESTERN NORTH DAKOTA. A. M. Cvancara, Dept. of Geol., Univ. of N. Dak., Grand Forks, N. Dak. 58202 and J. B. Van Alstine, Div. of Sci. and Math., Univ. Minn. at Morris, Morris, Minn. 56267

Aquatic mollusks were searched for at 85 stations in southwestern North Dakota south and west of the Missouri River during the summers of 1967 (19 stations), 1968 (47), 1969 (14), and 1976 (29). Twenty-four of the 1976 stations had been examined in previous collecting years. Sixty-seven of the stations were on streams and 18 on lakes and ponds. Twenty-six of the stations yielded no live mollusks, which were conspicuously absent at the Missouri, Little Missouri, and Yellowstone River stations. Twenty-six species were found alive: 6 mussels (unionacean bivalves), 5 pill clams (sphaeriid bivalves), and 15 snails (2 prosobranch and 13 pulmonate gastropods). This compares with 12 mussels, 9 pill clams, and 22 snails known elsewhere in the state. The most frequently found mussel, pill clam, and snail species were *Anodonta grandis* Say, *Pisidium (Cyclocalyx) compressum* Prime, and *Physa integra* Haldeman. The mussel *Proptera laevissima* (Lea) is known from North Dakota only from the lower reaches of the tributaries of the Missouri River. Of the 24 stations recollected in 1976, 19 showed an increase in the number of species (1-3) or no change, and five showed a decrease (1-2). Notable shifts in the species composition occurred at only four stations, as reflected by a Dice similarity coefficient of 0.33 or less. Size and permanency of water body (all mollusks), bottom stability (all mollusks), total sulfate content of the water (all mollusks), and fish host (mussels) may be primary ecologic factors affecting mollusk occurrence in southwestern North Dakota. Supported by N. Dak. Water Resources Research Institute and Regional Environmental Assessment Program (REAP).

DROUGHT AND FAMINES. W. A. Dando. Dept. of Geog., Univ. of N. Dak., Grand Forks, N. Dak. 58202

Droughts or intersive water defiencies for proper plant growth and development is synonymous with famine in the literature. Assessment of drought on agricultural production is a complex three-fold problem of perception involving the identification of water deficiency, recognition of its effects, and appraisal of its impact. A Symap analysis of the 1891, 1921, 1933, and the 1946 droughts in the USSR revealed reduction in yields. Famines in the following winter or spring were not located in the area of drought. Drought caused a reduction in yields or a crop failure; man causes famines. Case studies in the USSR and an analysis of 8000 famines in the world since 4000 B.C. refutes the hypothesis that droughts produce famines.

LOCAL STEROID CONCENTRATING MECHANISM IN THE REPRODUCTIVE VASCULATURE OF THE EWE. J.S. Davis, G.J. Yutrzenka, S.W. Walsh, and S. J. Brumleve. Department of Physiology and Pharmacology, Sch. of Med., Univ. N. Dak., Grand Forks, ND 58201

It has been shown in species with extensive areas of surface contact that hormones may be transferred from vein to artery. A counter-current exchange mechanism for progesterone has been demonstrated between uteroovarian venous and ovarian arterial blood in the ewe. The route of transfer was verified by experiments in which 1,2-^{3}H-progesterone (55.7 Ci/mmol) was infused into the uterine vein (1.32 uCi/min) and measuring the amount of radioactive progesterone in the ovarian artery and simultaneously in a mesenteric artery of similar size. The amount of radioactivity was significantly higher in ovarian arterial blood than in mesenteric arterial blood. (This research was supported in part by School of Medicine General Research Support Grant No. 5 SO 1RR 05407.)

NICKEL ATOM REACTIONS AND REPOLYMERIZATION IN ALKANES. REACTIVITY AND SURFACE SPECIES ON RESULTANT NICKEL PARTICLES. Steve Davis, and K. J. Klabunde, Department of Chemistry, University of North Dakota, Grand Forks, North Dakota 58202

Highly dispersed nickel particles have been prepared by co-condensation of nickel atoms and alkanes at -196°C. After warmup to room temperature and removal of excess solvent, pyrrophoric powders were obtained which have been found to be very active hydrogenation catalysts for benzene. Characterization of these nickel-alkane products has been initiated. The nickel crystallite sizes are very small (<100Å) and gross sintering occurs above 250°C. A great affinity toward oxygen has been observed with the release of CO_2 from the nickel surface at elevated temperatures after the sample had been exposed to small quantities of air. Pyrolysis products yielded none of the original alkane. Only CO_2, CH_4, and H_2 were released upon pyrolysis of the nickel-pentane samples. Extensive cracking of the original alkane was presumed. Hydrogenation of nickel-pentane samples were carried out to initiate a displacement of any carbon residue. Products obtained were consecutively C_2H_6 through C_5H_{12} indicating a high degree of dissociation of the initial alkane. The presence of either carbides or hydrocarbon fragments may be revealed through deuterium exchange studies.

THE HISTOLOGY OF THE SPLEEN OF THE BUSH BABY: GALAGO SENAGALENSIS. J. E. Dravland, Dept. of Anatomy, Sch. of Med., Univ. of N.D., Grand Forks, N.D. 58202.

The histology of the spleen has been and remains a matter of controversy despite the fact that conclusions concerning one species cannot necessarily be applied to spleens in general due to significant species variations (Snook, Amer. J. Anat., 87:31, 1950). The purpose of this paper is to present the histology of the spleen of Galago and compare it to other mammalian spleens. After perfusion with formalin, the spleens of normal healthy adolescent and adult animals were dehydrated with ethanol, cleared in chloroform and embedded in TissuePrep. The blocks were cut at sections from 4 to 20μ and stained with one of a variety of techniques: hematoxylin and eosin, Masson trichrome, Hart's elastin, periodic acid-Schiff, Gomori's Prussian blue reaction and Marshall's metalophil impregnation. The general histological layout of the Galago spleen is similar to other mammals. In the red pulp, sinuses are present, although they are poorly elaborated and the circulation is apparently "open". The striking features of this spleen are the ellipsoid sheaths of Schweigger-Seidel and the marginal zone of the white pulp. Their prominance and abundant arterial supply hint at their activity in this spleen, and show that, in Galago, the spleen is an active component of the reticuloendothelial and immune systems

INFLUENCE OF ENVIRONMENTAL FACTORS ON NITRATE REDUCTION IN SELECTED CROP AND GRASS SPECIES. J. A. Dusky and D. S. Galitz. Dept. of Botany, N.D.S.U., Fargo, N. D. 58102

Nitrate reductase activity, water potential, transpiration rate, nitrate and protein content, and environmental conditions were determined for barley (Hordeum vulgare L.), wheat (Triticum aestivum L.), sunflower (Helianthus annuus L.), slender wheatgrass (Agropyron trachycaulum (Link) Malte), and Russian wild rye (Elymus junceus Fisch.)during a growing season in a greenhouse environment. It has been suggested that the level of leaf nitrate reductase is affected by the water status of the plant and the environmental conditions. Therefore, throughout the growing season physiologic and environmental factors were monitored for possible interactions. It was found that the water status of the test plants influenced measurable nitrate reductase activity. Furthermore, it was demonstrated that environmental conditions imposed on the plants also influenced nitrate reductase activities as well as the water potentials and transpiration rates. The possibility of using nitrate reductase activity as a diagnostic tool in field work analysis will be discussed.

INHIBITORS OF PROTEIN SYNTHESIS AND CHLOROPLAST DEVELOPMENT. M. E. Duysen and T. P. Freeman. Dept. of Botany, N. Dak. State Univ., Fargo, N. Dak. 58102.

Chlorophyll development is impaired by certain antibiotics during leaf greening. One of these compounds, cycloheximide, is known to inhibit the synthesis of proteins on 80 S ribosomes in the cytoplasm. Studies were undertaken to determine the dependence of the development of wheat leaf chloroplasts on cytoplasmic protein production. Cycloheximide at 5, 7, and 10 µg/ml was applied to dark-grown, primary leaf sections of 7 day-old wheat seedlings in Petri plates on filter paper, 7 hr prior to light exposure. Chloroplast morphology, total chlorophyll and carotenoids, the characteristics of the chlorophyll-protein complexes were determined after 20 hr of light. Cycloheximide prevented wheat leaf chlorophyll production and chloroplast development, especially when applied at 10 µg/ml. Plastids treated with cycloheximide in the dark prevented the breakdown of the prolamellar body even after extended periods in the light. Plastids allowed to green 4 and 10 hr in the light prior to cycloheximide treatment were morphologically impaired to develop beyond the developmental stage at the time of application. Low concentration of cycloheximide did not totally restrict greening of wheat leaves but reduced plastid pigment production and impaired the formation of protein associated with the light harvesting chlorophyll.

PROBLEMS IN LIQUEFACTION OF NORTH DAKOTA LIGNITE. Bruce W. Farnum and Joseph E. Schiller. ERDA, Grand Forks Energy Research Center, Grand Forks, North Dakota 58202

The CO-Steam Process for conversion of lignite coal into substitute fuel oil is presently under development. A slurry of coal and coal derived solvent is treated with carbon monoxide, hydrogen, and water at 450 to 500°C and up to 5000 psi pressure. Factors which lead to high viscosity of CO-Steam product were investigated. Molecular weight of the non-distillable portion (250°C, 1 Torr) was found to correlate with viscosity of 25% solutions in anthracene oil. Correlations of solution viscosity were also obtained with weak acid content, oxygen content, and preasphaltene content. No correlation was observed between solution viscosity and asphaltene content, nitrogen content, or weak base content. Solvent separation of CO-Steam products into tetrahydrofuran (THF) insoluble, THF soluble and toluene insoluble (preasphaltenes), toluene soluble and hexane insoluble (asphaltenes), and hexane soluble fractions was carried out. The composition of the four fractions was investigated by gel permeation high pressure liquid chromatography, infrared spectrophotometry, acidity, basicity, mass spectrometry, and nuclear magnetic resonance spectrometry. Rapid analytical methods for evaluation of CO-Steam products from a stirred autoclave and a continuous flow process development unit are under development.

PROTON RELEASE STUDIES IN THE MYOSIN HYDROLYSIS OF ATP. Sylvia A. Farnum and James A. Stewart. Department of Chemistry, University of North Dakota, Grand Forks, North Dakota 58202

Myosin was prepared from rabbit skeletal muscle by two different methods. Both preparations had comparable activity. The myosin catalyzed hydrolysis of adenosinetriphosphate (ATP) was studied in the absence of calcium ion at pH 9.1 by automatic titration. Theoretical calculations were made to correct for the pKa shifts, which occur upon hydrolysis. Essentially, there is no proton release below pH 6.5 The slow rate of reaction at pH 9.1 enabled us to observe the transient phase kinetics as well as the steady state kinetics. An acid-base equilibrium scheme was developed and the corresponding theoretical equation was derived. This equation was used to analyze pH-rate profiles and found to duplicate results from the literature.

CHEMISTRY OF GASIFIER WASTE WATER FROM A LURGI-PROCESS COAL GASIFICATION PLANT. J. R. Fleeker and M. C. Bromel. Depts. of Biochemistry and Bacteriology, N. Dak. State Univ., Fargo, N. Dak. 58102.

Organic and inorganic compounds were determined in gasifier waste water obtained from a Lurgi-process coal gasification plant. Alkyl carboxylic acids, phenols, and pyridine derivatives were determined by gas chromatography. Cyanide, thiocyanate, sulfide, sulfite, ammonia and phosphate were also determined. Waste water processed in the plant for recovery of commercially valuable chemicals was also analyzed. Ammonia, and the phenol and pyridine fractions were efficiently removed from the water. The organic substances found in the wastes are known to be biodegradable but at dissimilar rates. The amount of inorganic orthophosphate found was low (0.2 mg P/liter), and may be limiting as a nutrient in the biotreatment of the waste water. Supported in part by the Natural Gas Pipeline Company, Chicago.

PARASITEMIA OF YELLOW PERCH IN NORTH DAKOTA. M. D. Forstie and H. L. Holloway Jr. Biol. Dept., Univ. N. Dak., Grand Forks, N. Dak. 58202

Twenty Perca flavescens, obtained from Jamestown Reservoir and Arrowwood Lake, were examined for evidence of parasitemia. Yellow perch were collected 6 June through 10 July 1976. Blood smears were prepared using standard techniques and stained with Giemsa solution for approximately 24 hours. Five percent of the fish examined were infected with a trypanosome previously unrecognized in North Dakota. The Trypanosoma sp. is morphometrically compared to trypanosomes previously reported from freshwater fish in North America, Yellow perch in Russia, and Pike and Pickerel in Russia and North America. The trypanosome is smaller than those previously described from the North American fauna. It cannot be assigned to any of the three recognized species. Supported in part by U.S. Department of Interior, Bureau of Reclamation, grant number 4571.

PLASMALEMMAL MICROAPPENDAGES: A STUDY IN FINE STRUCTURE. D.J. Friedenbach, R. E. Merchant, P.A. Stagno. Dept. of Anat., Sch. of Med., Univ. N. Dak., Grand Forks, N. Dak. 58202.

Surface contours of endodermal cells of early chick embryos and leukocytes of canine leptomeningeal sheaths were examined by scanning and transmission electron microscopy. Normally, these cells possess plasmalemmal microappendages (microvilli, blebs, and ruffles) in variable degrees. Microvilli are cell surface extensions of variable length and uniform diameter (0.1μm). In contrast, blebs display bulbous configurations of inconsistent diameter and size. Ridge-like ruffles are primarily found near the cell margins. When endodermal cells are exposed to variations in extracellular pH or cytochalasin B, the appearance and distribution of the microappendages are altered. Similar results are obtained when subarachnoid leukocytes are challenged by the foreign protein, bacillus Calmette - Guerin (BCG). Microappendages thus appear to reflect changes within the extracellular environment and degrees of leukocyte activation in response to antigen.

Supported by USPHS Grant NS 12106 from the Institute of Neurological and Communicative Disorders and Stroke.

ULTRASTRUCTURAL FEATURES OF EARLY EMBRYOGENESIS OF THE SCREWWORM FLY, *COCHLIOMYIA HOMINIVORAX* (COQUEREL) (DIPTERA: CALLIPHORIDAE). G. Gassner and S. G. Sears. Metabolism and Radiation Research Laboratory, ARS, USDA, Fargo, N. Dak. 58102

A transmission electron microscopy study of the preblastoderm screwworm fly embryo was initiated to determine what features could be used in a comparative study of dominant lethality among various insect types of economic importance. Eggs were fixed in 4% glutaraldehyde buffered with 0.05M phosphate (pH 7.3), post-fixed in 1% osmium tetroxide, embedded in plastic, and examined by light and electron microscopy. Within 45 minutes 4-5 cleavage divisions occurred. The dividing nucleus elongates in a cytoplasm that is not membrane bound. Each tapered extremity of the nucleoplasm was capped by a low contrast cytoplasmic inclusion of about 3-4 μm in diameter. At least 3 classes of bipartite yolk spheres were present and appeared as membrane-bound core bodies. They were identified as 1) solid cores of dark contrast surrounded by a matrix of low contrast; 2) hollow cores of dark contrast containing a matrix of low contrast; and 3) multivesiculated cores containing several matrices of low contrast. Other yolk features consisted of tightly and loosely packed rosettes of glycogen, low contrast regions containing fibrillar material, and multiple membrane-bound bodies. Supported in part by United States ERDA Contract P7603214. Thanks to G. G. Holt for eggs.

TECHNIQUES FOR ALGAL PHOTOMICROGRAPHY. Micheal S. Graham and L. E. Shubert. Department of Biology, Univ. N. Dak., Grand Forks, N. Dak. 58202

There are many inherent problems associated with photomicrography, such as selection of proper film, centering of the light, proper light sources, and quality of microscopic material, to name a few. These problems can be eliminated with the proper techniques. We have developed a photomicrographic method for studying living and fixed algae. A Zeiss standard microscope equipped with phase optics and combined with a Nikon camera and automatic exposure control unit was used for this study. Intensive analysis of color reproduction was conducted to determine the best photographic film for this system. Excellent results were obtained using an electronic flash unit and Eastman Kodak Ektachrome daylight type E-4 film. Examples of our results will be illustrated. Supported by Grant # SER 76-14931 from the National Science Foundation, RULE.

PROBABLE CAUSES OF SURFACE INSTABILITY IN CONTOURED STRIP-MINE SPOILS–WESTERN NORTH DAKOTA. G. H. Groenewold, N. Dak. Geol. Survey, University Station, Grand Forks, N. Dak. 58202 and L. M. Winczewski, Dept. of Geol., Univ. N. Dak., Grand Forks, N. Dak. 58202

Preliminary reconnaissance of existing graded strip-mine spoils in western North Dakota indicates that various engineering problems exist within these materials. These include differential subsidence of the surface of the spoil, slope instability, and piping failures. Major variations in texture, composition, and packing, within the spoil, appear to be the primary factors which control spoil stability. These are, in turn, directly related to the original nature of the stripped materials, the methods of stripping, transportation, and emplacement, and the time of year during which these operations occur. Localized movement of groundwater through recontoured spoils is very common in some settings. Permeability of the graded spoils and therefore the rates and directions of groundwater movement are, in part, determined by the method of emplacement and the physical characteristics of the sediments. In addition, the time of year during which emplacement occurs can have a very strong influence on the permeability characteristics of the spoils. Recontouring during the winter months often results in the concentration and burial of large frozen blocks of spoil within the regraded materials. Initially the zones of blocky materials are characterized by a high percentage of void space and corresponding high permeability. Areas of spoil underlain by blocky zones are often highly susceptible to settling. Fractures, resulting from settling, allow surface water to migrate down through the spoils. If sufficient water is available, piping and associated collapse features will result.

PROBABILITY AMPLITUDES FOR TWO-PHOTON ABSORPTION: RARE EARTH AND ACTINIDE ION SYSTEMS. J. B. Gruber, E. D. Larson, D. N. Olsen and T. R. Stoner. Dept. of Physics, Col. of Sci. and Math., N. Dak. State Univ., Fargo, N. Dak. 58102.

Probability amplitudes have been derived for two-photon spectroscopy using time-dependent perturbation theory. Two cases are considered in detail: (1) absorption of a laser photon and an incoherent light-source photon, and (2) absorption of two laser photons. Expressions for two-photon absorption coefficients are compared with results obtained by Kleinman in 1962. Contrary to Kleinman's approach, our expressions give probability amplitudes that do not contain or require intermediate states. We find our amplitudes depend upon the polarization and intensity of the incoming laser beams. As an example, we quantify our expressions by performing a ratio calculation between two-photon and single-photon absorption by rare earth or actinide ion ($n'f^n$) systems.

DISTRIBUTION OF HYDROPSYCHIDAE (TRICHOPTERA) IN SANDHILL STREAMS OF NORTH DAKOTA. S. C. Harris and R. B. Carlson, Department of Entomology, North Dakota State University, Fargo, North Dakota 58102.

Larvae of Hydropsyche slossonae Banks, Hydropsyche betteni Ross, Hydropsyche simulans Ross, and Cheumatopsyche pasella Ross (Hydropsychidae: Trichoptera) occur in sandhill streams in southeastern North Dakota. In areas where the current was swift, H. slossonae was common. H. betteni was restricted to a riffle area immediately downstream from a stream impoundment. H. simulans and C. pasella were collected in the still water of the undercut stream banks. As the Hydropsychidae are net-spinners, the presence of H. simulans and C. pasella in an area of non-moving water is unusual.

IMPROVED DIFFERENTIAL SPECTROPHOTOMETRIC PROCEDURE FOR THE DETERMINATION OF THEOPHYLLINE IN BLOOD.

E.S. Holzberg, A.Poklis and N.G.S. Rao. State Toxicology Lab., Fargo, N.Dak., 58102

A differential ultraviolet spectrophotometric procedure for the determination of therapeutic concentrations of theophylline in blood or plasma is described. Blood is extracted with chloroform which is then extracted with 0.45N NaOH. A distilled water blank is also carried through the procedure. Phenobarbital in the extract is destroyed by heating the hydroxide extract in a water bath. The extract is then split into two portions which are adjusted to pH13 and pH1. The differential U.V. spectrum of the sample and blank is recorded between 300-260NM by running the pH13 extract as sample and the pH1 extract as reference. Recoveries of 66 blood samples spiked with 5-20 ug/ml of theophylline ranged from 99-102%.The standard error for the method was within 5%.Washing the initial chloroform extract with pH7.4 phosphate buffer effectively removes therapeutic concentration of sulfa drugs. Phenobarbital,ephedrine and papaverine,drugs often administered with theophylline for the treatment of asthma, do not interfere with the method.

BASELINE WATER QUALITY STUDY FOR A PROPOSED COAL GASIFICATION PLANT SITE.

Yung-Tse Hung, G. O. Fossum, and E. S. Mason. Dept. of Civil Engr., Univ. of North Dakota, Grand Forks, N. D. 58202

A water quality study was conducted from April to October 1975 in Dunn County, North Dakota to provide baseline water quality information for a proposed coal gasification plant site. Sampling stations consisted of nine surface water and five ground water sampling stations. Water analysis included pH, specific conductance, alkalinity, turbidity, dissolved oxygen, chemical oxygen demand, biochemical oxygen demand, total suspend -ed solids, total dissolved solids, total hardness, Ca, Mg, Na, K, SO_4, Cl, SiO_2, NO_3, PO_4, and coliforms.

Correlation analysis revealed that streamflow was negative -ly correlated to TDS and specific conductance, and specific conductance was positively correlated to TDS, Na, and total hard -ness. High concentration of TSS, low concentration of TDS, and high DO concentration were observed in river waters during spring runoff period. Lowest DO concentration occurred in July 's sampling run. During the study ground waters sampled from farm wells was found to contain high concentration of TDS concen -tration. Water parameters exceeding North Dakota state surface water quality standards included turbidity, TDS and fecal coliforms. Supported by Eng. Experiment Station, Univ. of N. D.

USE OF FLY ASH AND VOLCANIC ASH IN WASTE TREATMENT FOR PHOSPHORUS REMOVAL. Yung-Tse Hung, R. E. Gullicks, G. O. Fossum. Dept. of Civil Engr., Univ. of North Dakota, Grand Forks, N. D. 58202 and C. P. Hwang, Dept. of Civil Engr., Univ. of Saskatchewan, Saskatoon, Saskatchewan, Canada.

In this study volcanic and fly ash were investigated for their effectiveness as adsorbent for the removal of phosphorus and organic pollutants from wastewaters. Based on 24-hour batch shaking tests, percent total organic carbon removal was found to vary from 53.55% to 81.88% using fly ash as adsorbent. For an influent P concentration of 10 mg/l , P removal efficiency varied from 0 to 82% using volcanic ash as adsorbent in the shaking type batch tests. Contact time longer than half an hour did not improve P removal efficiency. Increasing volcanic ash particle size resulted in decreasing efficiency of P removal. Continuous flow type tests indicated P removal efficiency ranged from 0 to 13.2%, and 0 to 43.2% for the filtration column for minus No.8 to plus No.16 material, and minus No.30 to plus No.50 material respectively.

This study was funded in part by OWRRI Grant No. A-046-NDAK and by the Engr. Experiment Station, Univ. of North Dakota.

PHARMACOKINETIC INTERACTIONS OF DELTA-9-TETRAHYDROCANNABINOL (THC) WITH METHAQUALONE (MQ) IN RATS. S. Husain, G.T. Pryor and M.C. Braude, Dept. Physiol. & Pharmacol., Sch. of Med., Univ. of N. Dak., Grand Forks, ND 58202, Stanford Res. Inst., Menlo Park, CA 94025 and NIDA, Rockville, MD 20852.

Due to the high polydrug abuse potential of THC and MQ, studies were undertaken to investigate the reciprocal pharmacokinetic interactions of these two compounds. Male Fischer rats were given ^{14}C-THC (40 μCi, 10 mg/kg, po) and MQ (10 mg/kg, ip) after pretreatment for six days with vehicle, THC, or MQ. In other similarly pretreated groups, reciprocal experiments were conducted by following radioactivity from ^{14}C-MQ (15 μCi/kg, 10 mg/kg, ip). Plasma and brain total radioactivity was determined at 1, 2, 4, 8 and 24 hr for ^{14}C-THC or at 0.5, 1, 2.5, 6.5 and 22.5 hr for ^{14}C-MQ. Acute MQ increased plasma total radioactivity from ^{14}C-THC in rats treated acutely or subacutely with THC which was significant at 8 hr in subacutely treated rats. Brain total radioactivity from ^{14}C-THC was significantly lower at 2 and 8 hr in rats treated subacutely with MQ. In reciprocal experiments, acute THC significantly increased plasma total radioactivity from ^{14}C-MQ at 2.5 hr and then decreased it at 6.5 hr in both acutely and subacutely MQ treated rats. Similar interactive trends were reflected in brain total radioactivity (Supported by contract HSM-42-72-182).

INTESTINAL ABSORPTION RELATED TO AGE. Francis A. Jacobs and Carol Overvold. Dept. of Biochem., School of Med., Univ. of N. Dak., Grand Forks, ND 58202

An attempt has been made to relate some aspects of the age of the rat to the intestinal absorption of leucine. Long-Evans, black hooded, male rats, over an age range of 1-20 months, anesthetized with sodium pentobarbital (50 mg/kg I.P.), were used in these studies. The lumen of a jejunal segment, about 10 cm long, was perfused *in situ* with a mixture containing 4 mM L-leucine-^{14}C and 2 mM inulin-^{3}H. The perfusion mixture was recirculated through the intestinal lumen and a scintillation detector cell which measured automatically any change in ^{14}C-activity of the perfusate, thus monitoring the rate of leucine-^{14}C absorption from the intestinal lumen. The inulin-^{3}H was measured in the presence of the leucine-^{14}C by liquid scintillation counting; this was done to assess the water balance of the perfusion system. The animals absorbed leucine at about the same rate when findings were related to intestinal segment length alone, but when the parameters of animal size and age were taken into account there was indeed a definite relationship between the intestinal absorption of the amino acid leucine and the size and age in the intact rat. (Supported in part by U.S.P.H. Institutional Grant No. 5 S01 RR 05407 for General Research Support and by the United Good Neighbor Fund).

THE WEST-CENTRAL NORTH DAKOTA REGIONAL ENVIRONMENTAL IMPACT STATEMENT: AN APPLICATION OF REGIONAL ANALYSIS TO ENVIRONMENTAL STUDIES Gary E. Johnson. Dept. of Geography, Univ. of N.Dak., Grand Forks N.Dak. 58202.

The West-Central North Dakota Regional Environmental Impact Statement (EIS) is an assessment of proposed lignite coal and energy related developments scheduled for seven North Dakota counties. In a departure from traditional site-specific EIS's prepared under requirements of the National Environmental Policy Act (NEPA) of 1969, this study is regional in concept. The EIS is conducted as a state-federal partnership between the North Dakota Natural Resources Council and the Bureau of Land Management. Three levels of potential development are being examined. Level 1 projects include active proposals for two gasification plants, two electrical generating plants and the expansion of one existing lignite coal mine. Level 2 tentative proposals include the development of five lignite coal mines and one electrical generating plant. Level 3 assesses potential energy development by tracts which have been recommended for the leasing of lignite coal but are not currently associated with any specific proposal. Nine work groups are responsible for analyzing various components of the EIS. The results of this on-going study will be utilized by state and federal decision-makers in permit granting and coal leasing recommendations affecting energy development in the region.

CATALYST AND PRESSURE VARIATION STUDIES IN THE HYDROGENATION OF SOLVENT REFINED LIGNITE (SRL). David S. Jones, Kenneth J. Klabunde, Virgil I. Stenberg, Niel F. Woolsey, and Richard J. Baltisberger. Dept. of Chemistry, University of North Dakota, Grand Forks, North Dakota 58202.

We have been conducting experiments at the University under ERDA Grant E(49-18)-2211, studying the hydrogenation of SRL to form distillable liquid products. In a one liter autoclave charged with 37.5 g presulfided catalyst and 75 g SRL, we have tried 3 different initial hydrogen pressures with various commercial catalysts. The reactions were carried out for two hours at 450°C. Recovery of materials ranged from 71% to 93% including gases, liquids, and solids. Distillation fractions were obtained along with gases and unconverted SRL. We have found that 1000 psi initial hydrogen pressure gives quite low yields of light liquids and large vacuum bottoms. A pressure of 1750 psi gives much better yields and much lower vacuum bottoms. Increasing the initial pressure to 2500 psi again improves the yield, but not so drastically. The CoO-MoO_3 catalysts give the greatest conversion to liquids with NiO-MoO_3 catalysts nearly as good, but with slightly less conversion. A nickle tungsten catalyst shows the poorest conversion to light distillates. Temperature effects are also being investigated and will be discussed along with the pressure effects.

SOURIS RIVER STUDY: JULY 1973 TO JUNE 1975. D. G. Jorde. Dept. of Biology, Univ. N. Dak., Grand Forks, N. Dak. 58201

Water samples collected at fifteen sites along the Souris River (U.S.) were analyzed to determine general water quality and to identify possible sources of pollution. Eleven tests indicated that certain aspects of water quality chemistry decreased downstream from the United States entry point to the Lake Darling impoundment of the Upper Souris National Wildlife Refuge. Dilution of salts and uptake of nutrients by aquatic plants in Lake Darling generally improved the quality of released water. Downstream from Minot, water quality chemistry decreased to the Lower Souris National Wildlife Refuge. The large area and shallow characteristics of the refuge impoundments combined to improve certain water quality chemistry of water reentering Canada during summer and fall months. During winter water quality deteriorates as anaerobic conditions become pronounced. Agricultural pollution was found to be seasonal while municipal pollution was sporadic throughout the study period.

PRELIMINARY EVIDENCE OF AN AUTHIGENIC ORIGIN OF KAOLINITE IN THE GOLDEN VALLEY FORMATION (PALEOCENE-EOCENE), NORTH DAKOTA. F.R. Karner, P.F. Bjorlie and O.D. Christensen. Dept. of Geology, Univ. N. Dak., Grand Forks, ND 58202.

Mineralogic, stratigraphic and paleoclimatologic evidence indicate that the kaolinite-rich zone of the lower member (Bear Den) of the Golden Valley may have an authigenic origin and is part of a paleosol. X-ray diffraction data show that kaolinite increases in crystallinity toward the top of the kaolinite-rich zone as expected in a soil. Scanning electron microscopy confirms the presence of kaolinite crystals but has not yet provided evidence regarding their origin. The suggested paleosol sequence consists of an upper carbonaceous silty or clayey zone with organic content decreasing downward and underlain by a massive, kaolinite-rich zone containing numerous ferruginous concretions. The lowermost unit of the Bear Den Member consists of unweathered sandstones, siltstones and interbedded clays. The known paleoclimatology at the time of formation would have allowed kaolinite formation in the lowlands of the late Paleocene-early Eocene Great Plains. The kaolinite formation may be correlated with late Cretaceous-early Cenozoic tectonic stability and the development of an extensive erosion surface as presently recognized in the south-central Rocky Mountains.

MINERALOGY OF THE SENTINEL BUTTE AND TONGUE RIVER FORMATIONS (PALEOCENE), NORTH DAKOTA. F.R. Karner, D.W. Brekke, and R.M. Wilkes. Dept. of Geology, Univ. N. Dak., Grand Forks, ND 58202

Mineralogic composition has been determined by x-ray diffraction for 61 bulk samples of the Sentinel Butte Formation at Lost Bridge, 28 km north of Killdeer; and 26 clay-fraction samples of argillaceous units of the contact zone of the Sentinel Butte and Tongue River Formations at three sites near the Little Missouri River in Billings County. In the Sentinel Butte, lignites with several percent gypsum and quartz, lignites and lignitic shales with 20-50% clay minerals and 10-40% quartz are typically underlain by clays or mudstones with 15-25% quartz,5-10% feldspar,5-15% dolomite and 40-70% clay minerals. They are overlain by calcareous siltstones with 15-30% quartz, 5-10% feldspar, 1-5% calcite, 0-15% dolomite and 40-60% clay minerals. Siltstone may be overlain by calcareous sandstone with 10-20% quartz,5-10% feldspar,5-30% calcite, 1-10% dolomite and 10-40% clay minerals. The major clay minerals in both the Tongue River and Sentinel Butte belong to the montmorillonite, mica-illite,and Fe-chlorite groups. Minor amounts of kaolinite are present. The montmorillonite group makes up 60-95% of the total clay minerals in both formations. The abundances of mica and chlorite are approximately equal and range from 5-40%, varying inversely with montmorillonite. Supported in part by NSF Undergraduate Research Participation Grant EPP 75-04708.

ZIRCONIUM DISTRIBUTION IN LATE-STAGE GRANITIC ROCKS. F. R. Karner and K. Malick. Dept. of Geology, Univ. N. Dak., Grand Forks, ND 58202

Preliminary evidence suggests that Zr is depleted in late-stage granitic rocks of larger plutons by two different processes. In the mildly alkalic, Devonian Tunk Lake pluton, Maine, marginal, hypersolvus, aegirine-augite hornblende granites contain 500-1200 ppm Zr while late-stage subsolvus core granites contain 100-300 ppm. Gravity settling of zircon aided by convection is suggested to explain the Zr distribution. In the calcalkaline, Cretaceous-Paleocene Boulder Batholith, Montana normal quartz monzonite contains 100-200 ppm Zr and late-stage alaskites (aplites) contain less than 100 and usually less than 50 ppm. Separation of a Zr-poor vapor phase from quartz monzonitic liquid is suggested to explain the depletion in the alaskites.

VEGETATION AND SOILS IN A NORTH DAKOTA GALLERY FOREST. *Keith T. Killingbeck* and *Richard H. Bares*. Dept. of Biol., Univ. N. Dak., Grand Forks, N.D. 58202

Aspects of plant community structure and distribution were studied in relation to edaphic and topographic factors in a gallery forest surrounding Homme Reservoir located in northeastern North Dakota. Five forest community types found along the reservoir shores were green ash (*Fraxinus pennsylvanica* var. *subintegerrima*), aspen-elm (*Populus tremuloides, Ulmus americana*), boxelder-basswood (*Acer negundo, Tilia americana*), elm-boxelder and boxelder-birch (*Betula papyrifera*). Soil texture, soil electrical conductivity, slope angle and slope aspect were found to be associated with community distribution. Soils in the A horizon were clay loams and sandy clay loams with pH ranging from 6.9-7.4 and electrical conductivity ranging from 75-310 µmhos/cm. Tree stratum density ranged from 1089 trees/ha in the green ash community to 125 trees/ha in the boxelder-basswood community and was found to have a direct relationship with soil electrical conductivity. Of all trees tallied, 93.4% were smaller than 36 cm DBH and twice as many young green ash stems (2-6 cm DBH) than other tree stems were found. It appears that green ash will dominate this gallery forest in the future with American elm and boxelder being stable associates. *Supported by U.S. Corps Engineers: contract DACW 37-74-C-0066 to the Inst. Ecol. Studies, UND.*

HERB AND SHRUB STRATUM BIOMASS AND PRODUCTIVITY IN FIVE SOUTHWESTERN NORTH DAKOTA FOREST COMMUNITIES. *Keith T. Killingbeck, Richard H. Bares* and *E. James Crompton*. Dept. of Biol., Univ. N. Dak., Grand Forks, N.D. 58202

Biomass and productivity relations were studied in the herb and shrub strata of ash-elm (*Fraxinus pennsylvanica* var. *subintegerrima, Ulmus americana*), aspen-birch (*Populus tremuloides, Betula papyrifera*), cottonwood (*Populus deltoides*), juniper (*Juniperus scopulorum*) and pine (*Pinus ponderosa*) communities in Dunn, McKenzie, Slope and Stark Counties, North Dakota. Leaves+current twigs production (LCT) and total aboveground biomass (AGB) were estimated for the herb strata using a harvest technique and leaf production (LVS) and AGB were estimated for the shrub strata using a regression analysis based on basal stem diameter. Herb stratum LCT and AGB ranged from 26.8 $g/m^2/yr$ and 58.0 g/m^2 in the aspen-birch type to 144.8 $g/m^2/yr$ and 198.4 g/m^2 in the ash-elm type. Shrub stratum LVS and AGB ranged from 6.0 $g/m^2/yr$ and 40.0 g/m^2 in the ash-elm type to 48.1 $g/m^2/yr$ in the aspen-birch type and 547.6 g/m^2 in the pine type. Total herb+shrub stratum AGB was highest in the pine community (607.2 g/m^2) and lowest in the ash-elm community (238.4 g/m^2). Biomass:production ratios were higher in the shrub than in the herb strata. Herb and shrub stratum productivity were inversely proportional. *Support: N.D. Regional Environmental Assessment Program grant to Dr. M.K. Wali.*

ELECTROCHEMICAL STUDY OF THE FORMATION AND DECOMPOSITION OF HALOGENATED ACETOPHENONE ANION RADICALS. Curtis E. Koeppe and Duane E. Bartak, Chemistry Department, University of North Dakota, Grand Forks, ND 58202.

The decomposition pathways of halogenated acetophenone anion radicals were studied in dimethylformamide solvent. The electrochemical techniques of cyclic voltammetry, exhaustive coulometry and single-step chronoamperometry were used to ascertain the reaction pathways. The intermediacy of the acetylphenyl radical was verified by trapping the radical with an anion(cyanide) of the supporting electrolyte forming a new stable anion radical. The rate constant for the decomposition of the m-chloroacetophenone anion radical was evaluated by fitting the chronoamperometric data for m-chloroacetophenone to a computer model for an ECE mechanism(electron transfer, chemical reaction, electron transfer). Exhaustive coulometric experiments indicated that the first reduction wave of ring-substituted chloroacetophenone was an one-electron process to form the unstable anion radical. Product analysis by electrochemical and gas chromatographic methods indicated acetophenone as the major product. The above results will be compared to substituted benzonitrile and nitrobenzene anion radical decomposition.

TRACE ELEMENT EXCHANGE CHARACTERISTICS OF LEONARDITE.
A.L. Kollman and *M. Saeed*. Project Reclamation, Univ. N. Dak., Grand Forks, N.D. 58202.

Leonardite, a low rank, naturally oxidized coal material is being tested as a soil conditioner for use in revegetation of surface mine spoils. Organic matter has been widely reported to have the ability to chelate/complex metal ions. This experiment was done to determine whether organic matter (in the form of leonardite) has greater affinities for some trace elements than others and whether there is differential extractability of each element by several extraction solutions. The leonardite samples were saturated with Fe+++, Al+++, Zn++, Cu++ or Mn++ using 0.1N chloride salts, adjusted to pH 2.0. The samples were then dried and extracted with water, 0.1 N HCl, 1.0 N ammonium acetate, 0.02 M EDTA and 0.005 M DTPA all at a 1:5, sample:solution ratio, with shaking for 2 hours. Ferric ion (Fe+++) had the greatest sorption (56 meq/100 gm) followed by Cu++, Al+++ and Zn++. Manganous ion had the lowest sorption (35 meq/100 gm). Desorption was lowest with water, followed by 0.1 N HCl and 1.0 N ammonium acetate. The two chelating agents (EDTA and DTPA) caused the greatest desorption, indicating that the majority of the ions are held in a chelation complex by the leonardite.
Supported by Grant No. GO264001 from the USDI, Bureau of Mines.

MORPHINE CHEMISTRY. P. J. Kothari, S. P. Singh, V. I. Stenberg, Department of Chemistry, University of North Dakota, Grand Forks, North Dakota 58202

To understand the spectroscopic basis of the photochemistry of morphine in the singlet and triplet states, morphine and its model compounds were examined by means of their fluorescence and phosphorescence spectra. The spectra of phenol, anisole, 2-methoxy-, 3-methoxy-, 4-methoxyphenol and morphine were recorded at 77°K. No red shift was observed for the fluorescence bands for all but morphine, which had a 17 nm red shift when the solvent polarity was increased. In triplet spectra bands, phenol and anisole respectively showed 42 and 35 nm red shift in acetonitrile. The maxima of 2-methoxyphenol phosphorescence band showed 36 nm red shift compared to 4-methoxyphenol. This may be due to intramolecular hydrogen bonding in 2-methoxyphenol. In general, morphine showed 50 nm more red shift in comparison to 2-methoxyphenol, presumably due to the charge transfer between phenolic group and tertiary nitrogen atom. The irradiation of dihydromorphine with 300 nm light gave one major and three minor products. Supported in part by NIH (Grant GM 21590) and Career Development Award (1-K4-GM-9888).

NORTH DAKOTA FLEAS. VII. SIX NEW RECORDS FROM THE STATE'S PERIPHERY. Omer R. Larson. Dept. of Biology, Univ. of N. Dakota, Grand Forks, ND 58202

Continuing a decade of studies on the Siphonaptera of North Dakota, six additional records are herewith reported. Alphabetically these include: Amphipsylla siberica pollionis from red-backed voles in Bottineau County, Cediopsylla simplex from eastern cottontails in Cass County, Ceratophyllus riparius from bank swallow nests in Walsh County, Nearctopsylla genalis hygini from short-tailed shrews and Orchopeas howardii howardii from fox squirrels in Grand Forks County, and O. sexdentatus from desert cottontails in Billings County. Except for C. riparius which is transcontinental, and N. g. hygini which occurs from the Prairie Provinces southward to Iowa and Nebraska, the other species appear to have distributions in the northern Great Plains which end in the state (i.e., southern extent of A. s. pollionis in non-mountainous areas, western limits for C. simplex and O. h. howardii, and the northeastern margin of the O. sexdentatus species complex). Climate and host ranges influence such distribution patterns. With these six additions, the known flea fauna of North Dakota now numbers 42 species.

MOBILITY OF WATER IN CLAY MINERALS. Leo Laughlin, J.W. Harrell, Jr., and F.L. Howell. Dept. of Physics, Univ. of N. Dak., Grand Forks, N.D. 58201.

The mobility of sorbed water has been studied in several clays by use of pulse N.M.R. and radiotracer techniques. Proton spin-lattice and spin-spin relaxation times have been measured as a function of the amount of sorbed water and as a function of temperature. The measurements show that the mobility increases with increasing water content and varies with the type of clay and the type of cation used to saturate the clay surfaces. Correlation times for the motion of the water molecules have been deduced from the temperature dependence studies. The feasibility of using an N.M.R. technique employing a pulsed magnetic field gradient in order to measure diffusion coefficients for the sorbed water has been explored. Results obtained with this technique are compared with results obtained by using tritiated water as a tracer. (Supported in part by OWRRI Grant No. A-051-NDAK)

A COMPUTER MODEL FOR PERFORMANCE ANALYSIS OF A SOLAR HEATED RESIDENTIAL HOME IN NORTH DAKOTA. Gregory R. Loken, Mason H. Somerville, and Donald V. Mathsen. Engineering Experiment Station, University of North Dakota, Grand Forks, ND 58202.

A computer model to simulate the yearly performance of a solar assisted heat pump domestic residence heating system in Larimore, North Dakota is presented. The house modeled is a two-story structure and has 1050 square feet of collector, two water tanks and two 35000 BTUH heat pumps. Differential equations describing the collectors, house, and storage were numerically solved using a Hammings predictor corrector routine with a Runge-Kutta startup available from IBM. Other routines were used but were not successful. Local weather records providing hourly temperature and insolation conditions were used to provide the boundary conditions. The model provides yearly operating costs for the solar heated residence as a function of equipment and environmental parameters which will assist in selection of the most desirable operating mode and will allow optimization of future designs. Supported by a consortium of industries and individuals and the Engineering Experiment Station.

A FLAT-PLATE SOLAR COLLECTOR USING NON-BLACK ABSORBER ELEMENTS. D. V. Mathsen, M. H. Somerville, and G. R. Loken. Engineering Experiment Station, School of Engineering and Mines, University of North Dakota, Grand Forks, ND 58202.

A low-cost, low-maintenance collector requiring no specialized fabrication processes was desired for incorporation into a solar house built near Larimore, ND. The long-wave emissivity, ε, and the visible-range absorptivity, α, of commercial galvanized sheet are selective in nature (ε=.23, α=.66). The effective absorptivity of galvanized steel was further increased by the creation of parallelogram cavities. A prototype collector was constructed and efficiencies determined for a narrow range of the parameter, $(T_{coll}-T_{amb})/I$, where $T_{coll}-T_{amb}$ is the temperature differential across the face of the collector and I is the incoming solar energy. The experimental data, together with the results of a computer simulation program indicate a collector design competitive with commercially available designs using expensive coatings or paints with questionable life expectancies.

EXTRAVASCULAR PLASMA PROTEIN IN THE VICINITY OF IMPLANTATION SITES IN THE PREGNANT RAT UTERUS. Donald L. Matthies, Ken E. Nicolls, Christopher A. Bates. Dept. of Anat., Sch. of Med., Univ. of N. Dak., Grand Forks, N. Dak. 58201.

The vasculature near implantation sites in the rat uterus becomes permeable to dyes, e.g., Niagara Blue, and the detection of this phenomenon has been used by researchers in studying early implantation. This dye leakage could be a sign of a mechanism important to successful pregnancy. Electron microscopic studies of endothelial capillaries reveals that those near the site develop fenestrations which transport ferritin into the surrounding intercellular spaces. Molecular sieve elution of serum from dye-injected rats demonstrates that part of the dye is bound to plasma protein and part circulates in free form. Reduction of the dosage to the level where only the bound form circulates permitted the usual marking of the sites suggesting that the protein-dye complex is transported across the endothelium. Incubation of purified plasma proteins with dye and elution on Sephadex has shown that albumin is the binding protein. Electrophoresis confirmed this observation. The rat does not acquire a placental exchange membrane until halfway through pregnancy. Extravascular plasma protein and the accompanying edema could be a device by which the blastocyst derives nutrients before establishment of the membrane.

FUNGUS POSITIVE TISSUE CONTROLS IN EVALUATING PULMONARY PLAQUES IN SOUTHERN SKUA. D. A. Nix, Div. Math and Sc., Mary College, Bismarck, N.D. 58501 and H. L. Holloway, Jr., Bio. Dept., U. North Dakota, Grand Forks, N.D. 58202.

Pulmonary mycosis in wild birds is an acute or chronic infection caused by Aspergillus fumigatus. Detection of fungal plaques is usually diagnostic, but the observation should be strengthened with histologic procedures employing fungus positive tissue controls. Controls insure reliability in histologic techniques and facilitate direct comparison of pulmonary tissue from a known infected control with an unknown experimental. Experimental pulmonary tissue from a Southern skua and positive tissue from a Canada goose were simultaneously prepared, sectioned and treated with hematoxylin/eosin, Gridley and Grocott stains. Hematoxylin/eosin stained respiratory tissue and hyphae pink in positive tissue. Gridley's stained pulmonary tissue yellow and counterstained hyphae pink, while Grocott's stained the lung tissue light green and counterstained the hyphae black. Fungal hyphae were much clearer in preparations treated with Gridley and Grocott stains than hematoxylin/eosin. The positive tissue controls facilitated the effective evaluation of experimental pulmonary tissue. Supported in part by Grant #495, U.S.A.R.P., N.S.F. and Northern Plains Consortium for Education.

THE EFFECT OF He-O_2 HYPERBARIA UPON ASPIRIN-INDUCED GASTRO-INTESTINAL BLEEDING. H.A. Pakola, B. DeBoer, C.A. Zogg, and T.K. Auyong. Dept. of Physiology and Pharmacology, Sch. of Med., Univ. of N. Dak., Grand Forks, ND 58201

Ingestion of aspirin has been shown to cause gastro-intestinal irritation, ulceration, and bleeding. This effect was studied in rats exposed to hyperbaric conditions. Growing rats were fed a synthetic rat diet modified by the addition of 1% aspirin; control rats were fed the unmodified diet. Food and water were given ad libitum. The rats were maintained at 1 ATA ambient air, 1 ATA He-O_2, or 11 ATA He-O_2 environmental conditions. Data was obtained at the end of 1, 2, or 3 weeks environmental exposure. Blood salicylate levels were measured by the Trinder method; gastro-intestinal bleeding was measured by a modification of the Benzidine test. All animals fed the unmodified diet exhibited negligible blood salicylate levels and negligible gastro-intestinal bleeding. Animals fed the 1% aspirin diet exhibited near-toxic salicylate levels and marked gastro-intestinal bleeding; the degree of bleeding, however, was significantly less in the He-O_2 gaseous environments. Hyperbaria and duration of exposure did not seem to alter the intensity of the bleeding. (This investigation was supported by Contract N00014-76-C-0219 between the Office of Naval Research, Department of the Navy, and the University of North Dakota.)

SYNTHESIS AND PURIFICATION OF 2,2',^{36}4,^{36}4,5,5'-HEXACHLOROBIPHENYL FOR USE IN A METABOLIC STUDY. Margaret A. Pearson. North Dakota State Toxicology Department, NDSU, Fargo, ND 58102. Yvonne A. Greichus, James J. Worman and Barbara A. Ammann. Department of Chemistry, SDSU, Brookings, SD 57006.

Polychlorinated biphenyls have been detected in many forms of wild life and may be affecting certain life functions. In order to accomplish metabolic studies, one radioactively labelled isomer was synthesized and purified. The title compound was syntesized using a modified procedure of the one reported by Safe and Hutzinger, 1972. This method yielded a crude product of 20% yield and <1% ^{36}Cl incorporation. The hexachlorobiphenyl was purified by preparative thermal conductivity gas chromatography. The purified material gave n.m.r. and mass spectra identical to those reported by Safe(1972) and Vas(1971). A corn oil mixture of the hexachlorobiphenyl was injected into two guinea pigs. Analysis of the urine and body tissues revealed the presence of three metabolites. One metabolite was identified as radioactively labelled pentachlorophenol. This project was supported in part by Hatch Grant 7215-697.

A SCANNING ELECTRON MICROSCOPIC STUDY OF THE CHOROID PLEXUS IN THE RABBIT. Bruce Persky and Frank N. Low. Dept. of Anat., Sch. of Med., Univ. N. Dak., Grand Forks, N. Dak. 58202.

Young rabbits were anesthetized and perfused with buffered aldehydes. The choroid plexuses were removed from the lateral ventricles and postfixed in buffered OsO_4. Samples were then routinely prepared for scanning electron microscopy (SEM).

This study depicts the surface morphology of the choroid plexus of the lateral ventricle. Numerous pleomorphic epiplexus (Kolmer cell) macrophages were noted, often occupying the sulcus found between adjacent choroid plexus ependymal cells. The ventricular surface of each ependymal cell resembled a low, rounded mound covered with numerous microvilli. The microvilli varied in length and were more heavily distributed on the top of the cell than at the periphery. The sulcus positioning apparently allowed the epiplexus macrophage to attain a closer physical proximity to the underlying epithelial cells.

The cytoplasmic processes of some epiplexus macrophages were long, thin, and delicate while others were thick and proboscis-like. Occasionally pits and crater-like depressions were observed on both the cell body and cytoplasmic processes. Generally, the cytoplasmic processes flattened out and blended with the ependymal cells. (Supported by USPHS grant NS 09363 from the Institute of Neurological and Communicative Disorders and Stroke.)

"BLOOD ALCOHOL CONCENTRATIONS IN IMPAIRED DRIVERS IN NORTH DAKOTA, 1972-1976"

N.G.S. Rao and A.Poklis State Toxicology Lab.,Fargo N.Dak.,58102

The frequency distribution of blood alcohol concentrations from drivers apprehended in North Dakota during the past five years for the violation of "Driving While Under the Influence of Intoxicating Liquor" is presented. The blood alcohol concentrations (BAC) were determined by gas chromatographic analysis of blood samples or by analyzing a sample of alveolar air using the "Breathalyzer". All blood samples were analyzed by the State Toxicology Laboratory and the breath samples by law enforcement officers trained in the operation of the "Breathalyzer". During the five year period, more than 18,000 blood alcohol determinations were conducted in North Dakota. The statutory restriction for operating a motor vehicle in North Dakota is a BAC in excess of 0.10%. The average BAC of the apprehended drivers was substantially higher than the legal limit, ranging from 0.18% to 0.22%. Less than one percent of the samples analyzed had a BAC below 0.05% and more than thirty five percent were in excess of 0.20%.

REAP LAND COVER ANALYSIS OF NORTH DAKOTA. John R. Reid and A. William Johnson. ND Regional Environmental Assessment Program, Bismarck, ND, 58505.

New maps, produced for REAP, reveal the dominant land cover for each of the 53 counties and for the entire state. The county maps are at a scale of 2 miles to the inch; the state map is about 8 miles to the inch. The 10 categories of cover are: built-up, cropland, fallow, exposed subsoil or saline seep, rangeland, mixed rangeland and pasture, forests, water, wetland, and barren. The categorization was accomplished by computer processing of LANDSAT imagery, most of which was collected in 1975 and 1976, based on ground truthing. The resulting maps contain data down to the 1.12-acre level. More detailed data, based on as many as 30 categories, have been recorded on computer tapes. Land cover data will be utilized in conjunction with other areal data in a computer-based composite geodata analysis system. The maps and the stored data can be used for such things as planning transmission line routes, development of recreation areas; agricultural development, and predicting the impacts of changes in wetland drainage, farming practices, non-point source pollution studies, and economic development. Further evaluation of the categorization is expected.

NEMATODES OF THE GENUS PHILOMETRA IN NORTH DAKOTA FISH, J. D. Reinisch, D. S. Elsen, H. L. Holloway, Jr., and J. B. Owen. Dept. of Biol., U. North Dak., Grand Forks, N.D. 58202

In studies of fish parasites several large roundworms were found just beneath the skin, below the eye and in front of the preopercle of three White suckers, Catastomus commersonii Lacépède. Three large female worms, examined in lactophenol, were identified as members of the genus, Philometra. The genus was reported in the State by Hoffman (1953) from White suckers collected in Turtle River. Examination of the worms revealed the presence of cuticular bosses; a characteristic, according to Huggins (1972) of Philometra nodulosa Thomas, 1929. The original description was based on one female worm from a White sucker. The worms recovered are larger and exhibit differences from the orginal description. Significant discrepancies include dimensions of the esophageal bulb and egg. Thomas (1929) erred in describing the egg of P. nodulosa. The C. commersonii, 14 of 72 observed to be infected, were captured in Cherry Creek in May, 1976. White suckers were collected with Black bullheads, Fathead minnows and Carp. In addition, 196 White suckers have been examined from elsewhere in the State and found to be negative. Supported in part by U.S. Dept. of Interior, Bur. Reclamtion, grant numbers 4571 and 4581.

TOXIC EFFECTS OF CADMIUM AND ZINC ON SELECTED GRASS SPECIES. S. J. Rothenberger and D. S. Galitz. Dept. of Botany, N.D.S.U., Fargo, N. D. 58102

To assess possible impact of coal-fired power plant emissions selected grasses were treated with varying concentrations of zinc and cadmium. The plant species included were: Triticum aestivum L., Hordeum vulgare L., Agropyron smithii Rydb., Stipa viridula Trin., Bouteloua gracilis (H.K.B.) Lag. ex Steud., and Panicum virgatum L. Each species was treated with solutions of the chloride salts of zinc and cadmium at concentrations of 0, 1, 10, 100, and 1000 ppm. Methods of application used were: (1) solution culture, (2) vermiculite with the solution applied directly, and (3) vermiculite with the solution applied as an aerosol. Percent germination and several growth parameters were measured. Growth was slightly stimulated by 1 to 10 ppm zinc chloride, while concentrations greater than 10 ppm reduced growth drastically. Stipa viridula Trin. and Panicum virgatum L. were slightly stimulated at the seedling stage by 1 ppm cadmium. However, cadmium concentrations of 10 ppm and greater significantly inhibited both root and shoot growth in all species. The possibility of zinc and cadmium toxicity in North Dakota vegetation will be discussed.

EFFECTS OF GLUCAGON, L-EPINEPHRINE, AND CYCLIC AMP (cAMP) ON GLUCONEOGENESIS IN PERFUSED RABBIT LIVERS. G.A. Rufo, Jr. and P.D. Ray. Dept. of Biochemistry, Univ. of North Dakota School of Medicine, Grand Forks, North Dakota 58202.

Gluconeogenesis and its regulation has been studied in isolated perfused rabbit livers. The basic rate of glucose formation from 10 mM L-lactate and 40 mM dihydroxyacetone by livers isolated from 48 hr. fasted rabbits is enhanced approximately 1.7 fold by 10^{-6}M glucagon, 10^{-8}M L-epinephrine, and 10^{-4} M cAMP. The basic rate of glucose formation from 40 mM D-fructose is stimulated only 1.3 fold by these effectors. The rates of gluconeogenesis are calculated from the net increase in perfusate glucose and are corrected for glucose formed by glycogenolysis. Data imply not only the presence of a regulatory site between triose-phosphate and glucose but the absence of such a site between lactate and triose-phosphate. The concentrations of intermediary metabolites in livers were determined by assaying hepatic samples taken just prior to and thirty minutes after the addition of effector. Effectors elevated the levels of glucose-6-phosphate and fructose-6-phosphate approximately 1.8 fold over control values in livers given either L-lactate or dihydroxyacetone as substrate. These studies indicate the existence of a major regulatory site between triose-phosphate and glucose in the pathway of gluconeogenesis in rabbit liver. (Supported by NIH AM 12705)

POTASSIUM RELEASE CHARACTERISTICS OF SPOIL MATERIALS
M. Saeed. Project Reclamation, Univ. N. Dak., Grand Forks, N.D. 58202.

Potassium release characteristics of four coal mine spoil materials and one unmined soil were studied in growth chamber (25 C day and 15 C night temperatures, 12 hours of flourescent light daily with 50% relative humidity) by exhaustive cropping with barley. Five successive generations were grown. The exchangeable potassium was determined by leaching with neutral ammonium-acetate and total potassium was determined in concentrated H_2SO_4 and boiling in 1N HNO_3 extracts. The potassium extracted by cropping is related to exchangeable and total potassium.

The spoil materials contained a large reservoir of exchangeable (280 to 606 lb./acre) and total (1075 to 1573 lb./acre) potassium, with the exception of spoil from Center, N.D. Based on Woodruff's energy exchange formula and using the data from this experiment, it is felt that the Center spoil may be potentially dificient in potassium.

Supported by Grant No. G0264001 from the USDI, Bureau of Mines.

EFFECTS OF LEONARDITE ON THE GERMINATION OF SOME PRAIRIE GRASS AND LEGUME SPECIES. *N.M. Safaya* and *M.K. Wali*. Project Reclamation, Univ. N. Dak., Grand Forks, N. Dak. 58202.

Seed germination failures contribute greatly toward reduced productivity and sparse vegetation on surface mined areas. However, since different plants may exhibit differential germination tolerance to suboptimal soil conditions, 9 grass and 4 legume species were tested, under laboratory conditions for their germination potential on Glenharold minespoil. The seeds were germinated on moist filter paper, spoil, and spoil+10 and 20% additions of leonardite from two different sources. Most of the species whose germination was poor on spoil material alone responded favorably to leonardite treatment. Green needlegrass, side-oats grama, thickspike wheatgrass, crested wheatgrass, birdsfoot trefoil and emerald crown vetch were less tolerant, whereas alkali sacaton, durar hard fescue, slender wheatgrass, yellow sweet clover and alfalfa were more tolerant of the minespoil conditions. A differential response of species to different types of leonardite was also evident. Green needlegrass gave excellent response to 'Enderlin' leonardite, and crested wheatgrass to 'South Beulah' leonardite. A distinct dimorphism, affecting germination, was observed in thickspike wheat grass seed.

Supported by Grant No. G0264001 from the USDI, Bureau of Mines.

BINDING OF GOLD TO BOVINE SERUM ALBUMIN

V.A.Sagar, S. Melethil and A.Poklis Dept.Pharmacol.Toxicol and Pharmaceut.Pharm.Prac. Coll.Pharmacy, N.Dak.State Univ.,Fargo N.Dak. 58102

The binding of gold to 2% bovine serum albumin was studied by an ultrafiltration technique using CF-25^{R} cones. Five milliliter aliquots of albumin solutions containing gold concentrations ranging from 1-10 ug/ml were equilibrated for 24 hours. The solutions were then centrifuged at 271G and 0.5ml of the filtrate were collected. The gold content of both the filtrate and the remaining albumin solutions was determined by graphite furnace-atomic absorption spectrophotometry. It was found that gold was > 99.5% bound to the albumin over the concentration range studied. Preliminary studies indicate that salicylate at a concentration of 20mg%, had no effect on the binding of gold to albumin.

SOME NUTRIENT DEFICIENCY AND TOXICITY SYMPTOMS IN SLENDER WHEATGRASS. *P.A. Schwartz* and *N.M. Safaya*, Project Reclamation, Univ. N.Dak., Grand Forks, N.Dak. 58202.

In view of the importance of revegetating the surface mined areas in the Northern Great Plains Coal Province, nutritional studies on the prairie plants have become essential. This study pertains to a hydroponic experiment on slender wheatgrass (*Agropyron trachycaulum*). Plants were raised for 27 and 54 days in continuously aerated Hoagland's nutrient solution, using 1.5 l plastic pots. Deficiency of N, P, K, Fe, Mn, Zn, Cu, B and Mo was induced by omitting each nutrient singly from the solution. Control plants received all the nutrients and those for toxicity study received each nutrient at rates 4 times higher than that in the control treatment. The entire study was conducted in a growth-chamber maintained at 25°C (day)/15°C (night) temp. 12 hr. photoperiod and 50% rel. humidity. Growth was severely affected in -N, -P and -K plants but *A. trachycaulum* appeared to be most sensitive to K deficiency. Except for typical chlorosis in Fe deficient plants, and tip burning in case of B toxicity, symptoms for other elements failed to appear.

Supported by Grant No. G0264001 from the USDI, Bureau of Mines.

ADRENAL RESPONSE IN A WILD MICROTUS POPULATION: SEASONAL ASPECTS. Robert W. Seabloom. Dept. of Biology, University of N. Dak., Grand Forks, N. Dak. 58201

A population of Microtus pennsylvanicus was sampled over a 13-month period at the Whiteshell Nuclear Research Establishment near Pinawa, Manitoba. Subsequent to behavioral testing, voles were killed and their isolated adrenals were superfused and stimulated with ACTH. Superfusates were assayed fluorometrically for corticosterone. Peaks of adrenal response occurred during spring in both adult males and females, followed by a significant decline in early summer. Subadult males exhibited a peak response in early summer. Corticosterone levels from adults were generally higher than those from juveniles in the same season. Levels from nonpregnant adult females were significantly higher than those from pregnant voles. Observed differences over the annual cycle were attributed to the behavioral and hormonal states of various components of the population.

A COMPARATIVE STUDY OF THE NUCLEI AND MEMBRANE SYSTEMS OF THE BLASTODERM EMBRYOS OF INSECTS USING SCANNING ELECTRON MICROSCOPY. S. G. Sears. Metabolism and Radiation Research Laboratory, ARS, USDA, Fargo, N. Dak. 58102

A scanning electron microscopy study was done to examine the cytological features of early blastoderm membrane systems in two species of insects, Oncopeltus fasciatus (Dallas) and Pectinophora gossypiella (Saunders). Fertilized eggs were fixed in glutaraldehyde saturated heptane, 4% glutaraldehyde, and then postfixed in 1% osmium tetroxide. Two tissue fracture methods were used: 1) a modified ethanol cryofracture (CF) and 2) room temperature ethanol fracture (RF). The CF method yielded fractures through nuclei, whole cells, and certain other embryonic structures, whereas the RF method showed cleavage around cells and yolk granules, giving a three-dimensional view of the cell surfaces. Fractured nuclei containing chromosomes were seen, as well as whole cells showing small finger-like cytoplasmic projections connecting the cells to each other and to the yolk-rich interior of the embryo. Smaller cellular structures such as ribosomes, centrioles, etc., were not identified in these preparations.

Thanks to Dr. Thomas Freeman, NDSU, for taking the SEM pictures and to Dr. George Gassner, MRRL for advice and support. Supported in part by U.S. Energy Research and Development Administration Contract P7603214.

ANALYSIS OF NITROGEN COMPOUNDS IN COAL LIQUEFACTION PRODUCTS. Lu Ann Sidney and Joseph E. Schiller. ERDA, Grand Forks Energy Research Center, Grand Forks, North Dakota 58202.

Four process solvents from solvent refined coals and one CO-Steam process product were analyzed to identify and quantify the nitrogen compounds present. Initial separation of the samples was done by column chromatography on activated alumina by elution with hexane, toluene, chloroform (two fractions), and 10% ethanol/THF. Standard mixtures of nitrogen compounds were identified by GC-MS, using a Dupont 21-491B Mass Spectrometer coupled with a Varian 2740 Gas Chromatograph with a 3% OV-17 column, and compared with the mass spectrum, peak areas, and retention times obtained from the second chloroform column chromatography fractions containing the nitrogen compounds. Temperature programming of the gas chromatograph from 150° to 275° C at 8° C/min. was essential for the resolution of the pure mixtures and the coal liquids. Major nitrogen compounds which were found include: quinolines, methylquinolines, indole, acridine, 2-phenylpyridine, benzoquinolines, and carbazole. Minor peaks in the coal liquid chromatogram, consisting of isometric dimethyl- and trimethylquinolines, could not be resolved.

SOLVENT EFFECTS ON MONOSUBSTITUTED BENZENE FLUORESCENCE AND PHOSPHORESCENCE S. P. Singh, S. S. Pamar and V. I. Stenberg, Department of Chemistry and Physiology-Pharmacology, University of North Dakota, Grand Forks, North Dakota 58202.

The fluorescence and phosphorescence spectra of several monosubstituted benzene derivatives have been recorded in polar and nonpolar solvents at 77°K. In the case of singlet-singlet transitions, the maxima are independent of the nature of the solvent and both good electron donor and acceptor groups have the effect of changing the maxima to longer wavelengths relative to that of benzene. On the other hand, benzene and all substituted benzene derivatives exhibit a significant red shift for the triplet state emission in the solvent acetonitrile as compared to that in n-hexane, chloroform and ether. Surprisingly, the benzene compounds having an electron withdrawing group retained the fine structure of the phosphorescence emission while those with an electron donating group lost the fine structure on going from nonpolar to polar solvents. These observations indicate that intermolecular charge transfer CTTS (charge transfer to solvent) exists with benzene compounds having electron donating groups and intramolecular charge transfer with compounds having electron withdrawing groups. Supported in part by NIH (grant GM 21590), NIDA (grant 7-R01-DA0 1893-01), and Career Development Award 1-K4-GM-9888.

ALGAL SUCCESSION ON SURFACED MINED AREAS OF NORTH DAKOTA. T.L. Sparks and L. E. Shubert. Dept. of Biology, Univ. N. Dak., Grand Forks, N. Dak. 58202

Soil samples were collected aseptically from May to Sept. of 1975 and 1976 at established reclamation plots. The samples were innoculated in an inorganic medium and after two months the samples were analyzed for the presence of algal species. The various amendments used to enhance the reclamation process resulted in a variety of species. The change in the algal species during the growing season was compared with the several amendments tested. Blue-green algae were the most abundant on most plots. The role of nitrogen fixation by the blue-green algae and the possible use of these organisms in enhancing soil fertility is being investigated. Field innoculations of Nostoc commune, a nitrogen fixing species that was isolated from the study area, are planned. Chlorosarcinopsis pseudominor, a green algae that undergoes a pigment shift possibly as a result of a nutrient deficiency, is being investigated as a possible indicator species for soil nutrients.

Supported by Grant # G0264001 from the USDI, Bureau of Mines

DESIGN AND ANALYSIS OF A NORTH DAKOTA ANNUAL CYCLE RESIDENTIAL SOLAR HEATING SYSTEM. M. H. Somerville, D. V. Mathsen, and G. Loken. Engineering Experiment Station, School of Engineering and Mines, University of North Dakota, Grand Forks, ND 58202

The design and analysis of a prototype residential solar heating system is discussed. The system allows an aphational flexibility not found in most solar systems. This flexibility allows performance tests to be conducted in two major modes of operation, a maximum solar energy utilization mode and an annual cycle operation mode. The system is installed in a 2300 ft^2 private residence located in Larimore, North Dakota. The system consists of: two unitary heat pumps rated at 35,000 BTUH (8820 KCal/Hr) at 42°F (5.6°C); 1050 ft^2 (107 M^2) of air cooled, parallelogram cavity, galvanized sheet metal solar collectors; a water storage capability of 4,000 to 40,000 gal. (15,142 to 151,420 l); six inch (15.24 cm) wall construction; and triple glaze windows. The design heat loss is 40,000 BTUH (10,080 KCal/Hr); 25,000 gal. (94,600 l) of water will be used as the start-up storage volume. An innovative ice maker evaporator and defrost scheme are used to replace the commercial air evaporator. The annual coefficient of performance of the system is projected to be 3.0 to 3.5 when operating under the annual cycle mode and 4.0 to 4.5 when operating under the maximum utilization mode.

THE ECONOMICS OF SOLAR SPACE HEATING AND COOLING. Carl D. Svard, M. H. Somerville, and D. V. Mathsen. Engineering Experiment Station, School of Engineering and Mines, University of North Dakota, Grand Forks, ND 58202.

An economic analysis of a solar heated and cooled private home is developed. The basis of the analysis is an experimental "solar" home located at Larimore, North Dakota. This 2300 ft^2 home utilizes a solar-assisted heat pump heating and cooling system with 1050 ft^2 of forced air solar collector and 4000-40000 gallons of water storage capability. The paper includes a comparative study of the costs inherent with this system with those of conventional systems (gas, fuel, electric, and heat pump-assisted gas) for a similar sized house. Types of costs examined include those for the heating unit, fans, water storage area, evaporators, and pumps. Costs of conventional systems include the heating and cooling units, fans, and system layout. Operational costs of the same systems are simulated with the aid of a computer model of the experimental system. An economic priority of expenditure is developed based on the analysis and comparison of the systems and operations.

A TRIAL OF ELEVEN SOURCES OF *Picea abies* IN NORTH DAKOTA AND MINNESOTA. J. L. Van Deusen. U. S. Forest Service Shelterbelt Lab., Bottineau, N. Dak. 58318 and Hans Nienstaedt. North Central Forest Experiment Station, Institute of Forest Genetics Rhinelander, Wisc. 54501

Eleven seed sources of *Picea abies* from eastern Europe and Russia were tested on the Denbigh Experimental Forest in North Dakota and Pike Bay Experimental Forest in Minnesota. Overall survival at Pike Bay was uniformly good (94.4 percent) throughout the first 10 years. At Denbigh, under average growing season precipitation, survival of all sources declined to 67 percent during the first five years. After two more years, in which the growing season precipitation was unusually low, the overall plantation survival at Denbigh averaged less than 6 percent.

Norway spruce may still be a useful conifer in North Dakota shelterbelts, but its success will depend largely on careful matching of seed sources with planting sites. Container-grown stock, tested under controlled greenhouse conditions and screened for adaptability, could form the beginning of a reservoir of adapted plant material.

A NEW ADAPTATION FOR THE CARE OF BIOLOGICAL MATERIALS IN SCANNING ELECTRON MICROSCOPY. J. J. VanRybroek and D. J. Friedenbach. Dept. of Anat., Sch. of Med., Univ. of N. Dak., Grand Forks, N. Dak. 58201

The technique of biological scanning electron microscopy conventionally requires specimens to be elaborately fixed, dehydrated, critical point dried, and coated with heavy metals. These procedures imply chemical and physical manipulation of surface structures, and potential modification of surface anatomy. Cryofixation is examined here as an alternative prepatory technique.

An inexpensive 'cold stub', modified from Macalear (1972) was manufactured and adapted to a Cambridge Stereoscan S4 Scanning Electron Microscope. Comparisons of several tissues, conventionally prepared and cryofixed, were examined with respect to preparatory procedures, resolutions and sample usefulness. The application of visualizing intracellular and intramembranous substructures by scanning electron microscopy is also examined. The potential usefulness of a cryofixation procedure as an ancillary technique to conventional biological scanning electron microscopy is discussed.

DEVELOPMENT AND TESTING OF AN ICE-MAKER EVAPORATOR FOR A HEATING ONLY HEAT PUMP. James C. Wendschlag and M. H. Somerville. Engineering Experiment Station, School of Engineering and Mines, University of North Dakota, Grand Forks, ND 58202.

The development of a heat pump evaporator for use in an annual cycle heating and air-conditioning system is discussed. The evaporator was designed for operation in an ice-making mode throughout most of the heating season.

A commercially available flat plate ice-maker was selected following tests of several configurations. The selection was based primarily on its ice removal efficiency. The water pumping system necessary with this selection was designed to minimize pumping cost and maintenance.

The automatic defrost system built into the heat pump required alteration to facilitate the ice-maker evaporator. The modification of this system to provide for periodic ice removal is presented.

The experimental set-up and laboratory test procedure used for performance evaluation are given along with test results. A complete performance analysis of the design selection is compared with that of the conventional air evaporators.

SAMPLING FROM OVERLAPPING FRAMES M. E. Winger. Dept. of Math., Coll. of Arts & Sciences, Univ. of N.Dak., Grand Forks, ND 58202. Statistical experiments using techniques of sampling occasionally arise where two or more frames will better model the target population. If there is significant overlapping of sample units, the desired randomness will be adversely affected by duplication of selection probabilities. We indicate an unbiased estimator for the size of the overlap along with an estimate of its variance. Using this knowledge, the sample size may be adjusted to attain the desired precision. Examples of possible use are exhibited. (Some results arise from work being performed for the N.D. Supreme Court concerning jury selection.)

STRATIGRAPHY AND PALEONTOLOGY OF THE UPPER CRETACEOUS MORDEN MEMBER (VERMILION RIVER FORMATION) IN THE OUTCROP AREA, NORTHEASTERN NORTH DAKOTA. F. Wosick. Geol. Dept., UND, Grand Forks, ND 58202

The Morden Member is the oldest exposed bedrock unit, cropping out in eastern Cavalier County, northeastern North Dakota. It overlies the Greenhorn Formation and underlies the Niobrara Formation. Three principal sections were measured and sampled at 2-ft intervals. The member is a uniform, dark, noncalcareous, organic-rich shale. Concretion zones are the basis for surface to subsurface correlation. The Morden-Niobrara contact is marked by a change upward to calcareous shale and an oxidized zone. The Morden-Greenhorn contact is unexposed. The member is 200 ft. thick in northeastern North Dakota and thins northwestward to less than 25 ft. in northwestern Manitoba. It strikes northwest and dips to the southwest at about 8 ft/mile. About 50 species of foraminiferids have been recognized. Arenaceous benthonic forms are more abundant, but less diverse, than calcareous benthonic and planktonic forms. Haplophragmoides is the dominant genus. Both the Niobrara and Greenhorn Formations contain abundant planktonic foraminiferids. Macrofossils include ammonites, pelecypods, and gastropods. The presence of marine fossils and the thick sequence of uniform shale indicate that the Morden Member was deposited in a quiet water, stable or slowly changing marine environment.

DRUG METABOLISM AS A REFLECTION OF ANTICONVULSANT ACTIVITY OF METHAQUALONE (MTQ). G.J. Yutrzenka, T.K. Gupta, T.K. Akers, and S.S. Parmar. Dept. of Physiol. & Pharm., Sch. of Med., Univ. of N. Dak., Grand Forks, N. Dak. 58202

Anticonvulsant activity of 2-methyl-3-ortho-tolyl-4-quinzalone (MTQ) was determined against pentylenetetrazol (90 mg/kg, sc)-induced convulsions in mice. The anticonvulsant activity of MTQ (100 mg/kg, ip) decreased with increased length of administration. The degree of protection by MTQ was 100%, 80%, and 20% during pretreatment of mice for 1 hr, 2 hr, and 3 hr, respectively, prior to the administration of pentylenetetrazol. During a 4-hr pretreatment, MTQ was devoid of anticonvulsant activity. Certain metabolites (4-methoxyphenyl, 6-methoxyphenyl, and 4,6-dimethoxyphenyl substituted derivatives) of MTQ possessed no anticonvulsant activity. L-DOPA (200 mg/kg, ip), administered 2 hr prior to MTQ, decreased protection from 40% to 20%, 80% to 60%, and 90% to 80% with 40, 60, and 80 mg/kg of MTQ, respectively. These results indicate that metabolism of MTQ may account for the time-dependent decrease in its anticonvulsant activity. (Supported by USPHS Grants 5-T01-HL-05939 and I-R01-DA-01893 and by ONR Contract N00014-76-C-0219.)

AUTHOR INDEX

AUTHOR INDEX

PROCEEDINGS

of the

NORTH DAKOTA ACADEMY OF SCIENCE

PAPERS

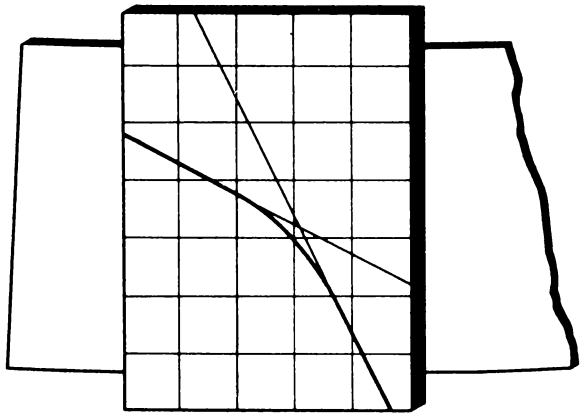

Volume 31 • Part II • April 1978

PROCEEDINGS OF THE NORTH DAKOTA ACADEMY OF SCIENCE is published jointly through the Academy by the University of North Dakota, North Dakota State University, Minot State College, Dickinson State College, and Valley City State College. The Proceedings appear in two parts: Part I, Abstracts, and Part II, Papers. Part I contains only abstracts of papers presented at the annual meeting of the Academy, usually in late April. Part II contains complete papers submitted in manuscript form at the time of the annual meeting and are usually published within a year. Printing is by the University of North Dakota Press. Strictly editorial matters should be directed to the editor, Virgil I. Stenberg, Department of Chemistry, University of North Dakota, Grand Forks, North Dakota 58202. Instructions for submission of abstracts and complete papers are obtained by writing to the Secretary of the Academy (see below).

SUBSCRIPTIONS: Members of the Academy receive both parts of the Proceedings. Annual dues are $5.00 for regular members and $3.00 for student members. Correspondence concerning subscription, as well as instructions to authors and other related matters, should be directed to North Dakota Academy of Science, Office of the Secretary, Box 8184, University Station, Grand Forks, North Dakota 58202.

PROCEEDINGS
of the
NORTH DAKOTA
ACADEMY OF SCIENCE

PAPERS

Volume 31, Part II April 1978

NORTH DAKOTA ACADEMY OF SCIENCE

(Official State Academy; founded December, 1908)

1976-77

OFFICERS AND OTHER MEMBERS OF EXECUTIVE COMMITTEE

EDITORIAL ADVISORY COMMITTEE

EDITOR

ASSOCIATE EDITORS

TABLE OF CONTENTS

INSTRUCTIONS TO AUTHORS FOR THE NORTH DAKOTA ACADEMY OF SCIENCE PROCEEDINGS

DEADLINES

Abstracts.—Both student competition and professional paper abstracts are due by the date specified by the Secretary of the Academy in the annual call for papers. Abstracts must be submitted on the prescribed form (available from the Secretary's Office) so that they can be published in time for the annual meeting of the Academy.

Papers.—Complete papers for student competition are due at the Office of the Secretary one month prior to the annual meeting, so that time is available for judging. Complete professional papers are due at the time of oral presentation.

PRESENTATION OF MANUSCRIPT

General.—The general style for papers of the Proceedings will be that used by the leading national periodicals of that discipline. It is most important that a consistent format and style be used throughout the manuscript.

Authors are to write with clarity and conciseness so that the result is professional and consistent in style. The manuscript should be in completed, final form when submitted; changes after the galley proof is set can be made only with the approval of the Editor, and costs for these changes will be assessed to the author.

All parts of the manuscript must be typed double spaced with wide margins on 8½ inch x 11 inch white paper. Each original manuscript must be accompanied by two copies (Xerox or similar copy), including illustrations.

A separate title page, numbered one, should include the authors names, their affiliation and complete addresses, including zip codes. Subsequent pages should be numbered consecutively and the principal author's name should precede each page number.

A carefully organized manuscript text may consist of the following parts introduced by major headings: INTRODUCTION, MATERIALS AND METHODS, RESULTS, DISCUSSION, ACKNOWLEDGMENTS, and REFERENCES: RESULTS and DISCUSSION may be treated together.

Headings—Major headings are centered and capitalized. Subheadings are indented, underlined for italics, and followed by a period and dash (two hyphens on the typewriter) as used in these instructions.

Figures.—Maps, drawings, graphs, structural formulas and complex tables cannot be set in type and must be drafted and reproduced as line cuts. These illustrations must be drafted in India ink so they reproduce well, and should be submitted on separate sheets ordinarily not exceeding the size of the manuscript page. Therefore, larger drawings should be reduced photographically; if so, lines, lettering and symbols must be bold enough to stand the appropriate reduction.

Photographs must be unblurred and clearly show what is intended.

Each figure (drawing or photograph) must be proportioned to fit precisely on the printed page of the *Proceedings*. A full page figure should be 4⅛ x 6¾ inches to allow *adequate space* for a caption at the base of a full page figure. To reduce publishing costs, consider carefully if a full page figure is necessary, or whether a carefully cropped photograph or smaller line cut would convey the visual impression as well.

Each figure must be identified on the back with the figure number, author's name, and with the phrase "Top of figure" at the top of the page.

Figure captions are to be typed on a separate page and included with the manuscript. An example of a figure caption is as follows:

FIGURE 1. Frequency occurrence of vegetation for each sampling station.

Tables.—Complex tables (those with vertical lines, characters on fraction of successive lines or unusually extensive characters or words) should be drafted as mentioned under Figures. Tables are to be double spaced on separate sheets, numbered (Arabic numbers) consecutively and given a short title. An example of a table caption is as follows:

TABLE 1. Effect of pH on reactivity of chymotropsin.

The same material should not be repeated in tables and figures.

References and Citations—References are to be listed at the end of the manuscript and citations given within the manuscript in a manner consistent with those used by leading national periodicals of that discipline.

Footnotes.—Footnotes are costly and are to be avoided. Footnote material can usually be incorporated in the text or included under the major heading Acknowledgments.

Acknowledgments.—Grants and other aid are to be acknowledged under the major heading Acknowledgments.

Order of the manuscript.

Full papers.—Manuscripts consist of the following parts arranged in the indicated order (each page, beginning with the title page, is to be given in a consecutive page number):

1. Title page (separate sheet)
2. Abstract
3. Manuscript text
4. Tables (separate sheets)
5. Figures captions (separate sheet)
6. Figures

Other.—Words underlined in the text are placed in italics when set in type. Authors are to use the metric system for all measurement; equivalent values of the English system may be placed in parentheses.

CHARGES, GALLEY PROOFS, AND REPRINTS

For papers in excess of five printed pages, authors will be charged $10.00 per page for each page in excess of five. Authors are encouraged to include page charges in grant or other budget requests.

Galley proofs are to be corrected and returned, within three days, to the Editor. Reprints are to be ordered (at prices shown on the order form) at the time the galley proof is returned.

ERDA'S RESEARCH PROGRAM RELATING TO LIGNITE AND OTHER LOW-RANK COALS

Gordon H. Gronhovd
Director, Grand Forks Energy Research Center
Energy Research and Development Administration
Grand Forks, North Dakota 58201

ABSTRACT

Coal is expected to play an increasingly important role in meeting the Nation's energy requirements in the near and mid-term as supplies of natural gas and oil continue to diminish and become more expensive. The Energy Research and Development Administration (ERDA) has a coal program designed to greatly expand the use of our most abundant fossil fuel and to do so in an economically and environmentally acceptable manner. Huge deposits of lignite and subbituminous coal are located in the Northern Great Plains and these low-sulfur coals are increasingly being utilized as the shift to coal grows. ERDA is supporting a number of research, development and demonstration projects relating to the use of lignite and other low-rank coals. This paper identifies these projects and the associated funding and briefly describes the ERDA Grand Forks Energy Research Center's activities and other ERDA-funded industrial projects relating to the use of low-rank coals.

INTRODUCTION

President Carter's National Energy Plan as presented to the nation on April 20, 1977, might be called a combination of "Conservation and Coal," at least for the near term. With respect to coal, he is asking that production be increased from the present 670 million tons-per-year level to 1.1 billion tons per year by 1985. This 400 million ton-per-year increase represents a tremendous challenge to the coal industry, and it is expected that the huge deposits of lignite and subbituminous coals in the Northern Great Plains will be looked to for supplying a substantial portion of this increase.

The increased use of coal by 1985 will be largely for new powerplants and for conversion of existing plants from gas and oil to coal. The President's National Energy plan does, however, also stress the need for continuing and expanded emphasis on the conversion of coal to synthetic gaseous and liquid fuels.

In this paper I will briefly describe ERDA's programs in research, development, and demonstration which are directed, in varying degrees, toward the utilization of lignite and other low-rank Western coals. These programs consist of in-house work at the Grand Forks Energy Research Center (GFERC); contract research at universities and colleges; and contract research, development, and demonstration cooperatively with industry. In Table 1, the various projects are listed and the approximate funding levels indicated.

In the interest of brevity, not all of the projects listed will be discussed in this paper. The CO_2 Acceptor and Hy-Gas projects have been reported extensively in the literature (1,2)[1] The UND project on solvent refined lignite was covered in the 1976 North Dakota Academy of Science Proceedings and another of the ERDA-funded projects at UND, the Chemistry of Coal Liquefaction, will be covered

TABLE 1. ERDA FUNDED PROJECTS RELATING TO LIGNITE AND OTHER LOW-RANK WESTERN COALS

	Project	Organization	Location of Work	ERDA FY 77 Funding	Total
I.	**Gasification**				
1.	Slagging fixed-bed	Grand Forks Energy Research Center	Grand Forks, ND	600 K	—
2.	CO_2 Acceptor	Conoco Coal Development Co.	Rapid City, SD	2.1 MM	32 MM
3.	Hygas	Inst. Gas. Tech.	Chicago, IL	2.8 MM	44 MM
4.	Gasifier and grate kiln	Bureau of Mines and industry	Minneapolis, MN	750 K	2 MM
5.	Small industrial gasifier	Land O'Lakes	Perham, MN	—	2.7 MM
6.	Small industrial gasifier	University of Minnesota	Duluth, MN	—	2.2 MM
7.	Low-Btu Gasification demonstration plant	Erie Mining Co.	Hoyt Lakes, MN	—	23 MM
8.	Comparison of liquid effluents from dry ash gasifiers	University of North Dakota	Grand Forks, ND	98 K	98 K
II.	**Liquefaction**				
9.	CO-Steam process	Grand Forks Energy Research Center	Grand Forks, ND	500 K	—
10.	Solvent Refined lignite	University of North Dakota	Grand Forks, ND	1000 K	5 MM
11.	Chemistry of lignite liquefaction	University of North Dakota	Grand Forks, ND	198 K	551 K
12.	Flash Hydrocracking of Lignite	Brookhaven Nat'l Lab.	Upton, NY	—	460 K
III.	**Combustion and Emissions Control**				
13.	Ash fouling studies	Grand Forks Energy Research Center	Grand Forks, ND	330K	—
14.	SO_2 control by ash-alkali scrubbing	Grand Forks Energy Research Center	Grand Forks, ND	300 K	—

15.	Fluidized bed combustion	Grand Forks Energy Research Center	Grand Forks, ND	200 K	—
16.	Fly ash control by ESP	Grand Forks Energy Research Center	Grand Forks, ND	310 K	—
17.	Industrial fluidized-bed combustion	FluiDyne Co. & Owatonna Tool Co.	Owatonna, MN	—	2 MM

in a separate paper at this meeting. In the space available I have chosen to discuss our in-house activities at the Grand Forks Energy Research Center and the industry cost-shared coal research, development, and demonstration activities in this geographic area.

ERDA IN-HOUSE RESEARCH AT THE GRAND FORKS ENERGY RESEARCH CENTER

A. Slagging fixed-bed gasification.

The proposed first generation commercial gasification plants in this country, including those for North Dakota, plan to use the German Lurgi process. In this process, the gasification is carried out at a nominal pressure of 400 psig with steam and oxygen. Coal is charged to the top of a descending bed, countercurrent to gases produced in the gasification zone where the steam and oxygen are introduced. Moisture and volatiles in the coal feed are released in the upper part of the bed and are carried out with the product gases. In conventional Lurgi gasifiers, shown in Figure 1, the temperature in the gasification zone must be maintained below the melting temperature of the coal ash in order to be able to discharge the ash with a mechanical rotating grate. In order to control this temperature, excess quantities of steam are injected, most of which pass through the gasifier unreacted and must be condensed at the gasifier outlet.

At GFERC we are researching a high-pressure, fixed-bed gasification method known as slagging gasification (3). In this process the operation is somewhat similar to a blast furnace. The gasifier, as shown in Figure 2, does not have a grate but it has a refractory-lined hearth and a slag taphole. The quantities of steam used are greatly reduced, as compared to the Lurgi process, and the temperature is increased to the point where the ash melts and becomes a liquid slag.

During the period from about 1958 to 1964, the GFERC slagging gasifier was developed. The following advantages over the conventional "dry ash" Lurgi gasifiers were demonstrated:

1. two- to fourfold increase in gas making capacity for a given gasifier size,
2. steam consumption reduced by a factor of 5,
3. quantity of liquid effluent greatly reduced, and
4. coals having low ash fusion temperature were well suited for the process.

The most serious disadvantage shown for the process was the problem of reliably maintaining slag flow through the taphole. This problem is aggravated by the small size of the unit. About the same time as the GFERC work was going on, the British Gas Corporation was conducting similar tests on a larger slagging

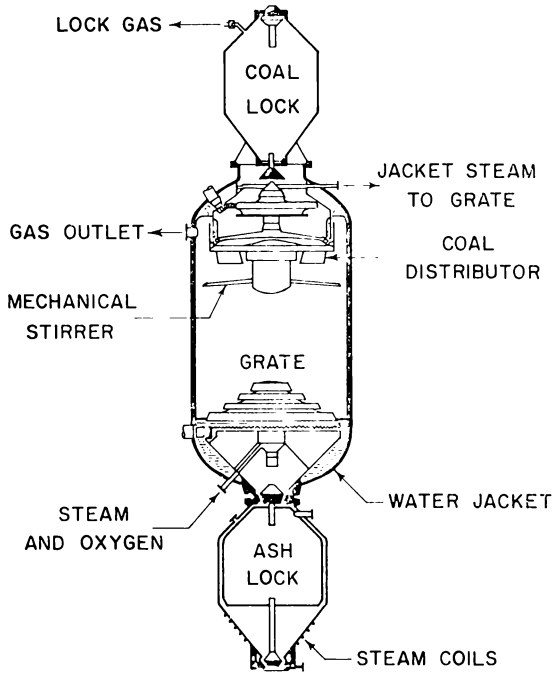

Figure 1. Conventional Lurgi Dry Ash Gasifier.

gasifier, and they obtained similar results. Table 2 shows a comparison of operating results from the GFERC slagging gasifier and a commercial dry ash Lurgi gasifier.

In 1964 the GFERC slagging gasifier program was stopped and the pilot plant was put in standby status. As a result of the accelerated interest in coal gasification, it was decided to restart the gasification project again in 1975. The major emphasis of the research program was to be on the characterization and treatment of the liquid effluent produced in the process.

Some refurbishing of the gasification pilot plant was required, including the installation of a new oxygen supply system and control instrumentation. Shakedown tests were started in the spring of 1976. During the past year the new operating crew has been trained, and the gasifier is now being operated regularly at the full pressure of 400 psig. The coal being gasified in the current series of tests is a lignite from the Indianhead Mine at Zap, North Dakota.

In the current program, samples of liquid effluents are being collected by various procedures to determine their quantity and chemical and physical characteristics. The objective of the effluent studies is to produce data which will help assess the environmental impact of fixed-bed gasifiers such as those being proposed for North Dakota. Another objective of the current program is to evaluate various candidate refractories for use in the hearth of the gasifier. This in-

TABLE 2. COMPARISON OF RESULTS FROM GFERC EXPERIMENTAL SLAGGING GASIFIER WITH COMMERCIAL DRY ASH LURGI GASIFIER

	GFERC Slagging Gasifier	Westfield Scotland Lurgi Gasifier
Cross Sectional Area, ft^2	1.5	63.6
Operating Pressure, psig	400	355
Fuel analysis, pct:		
Moisture	23	16
Ash	7	15
Product Gas Composition, pct:		
CO_2	6	25
H_2	30	40
CO	59	25
CH_4	5	10
Btu/ft^3	350	314
Gas Production, scfh/ft^2 Hearth Area	26,000	9,000
Material Requirements:		
O_2, ft^3/mscf Gas	192	155
Steam, lb/mscf Gas	10	37
MAF Fuel, lb/mscf Gas	34	28
Cold Gas Efficiency:		
Btu Coal/Btu Gas	85	81

Phase	Est. Cost, Millions of Dollars		Time After Contract Award, months Start	Finish
I	24	Conceptual design for a commercial process and for demonstration plants.	0	12
II		Detailed design of demonstration plant.	9	22
	213	Construction of demonstration plant.	22	52
III	44	Operation of demonstration plant.	52	—
	$281			

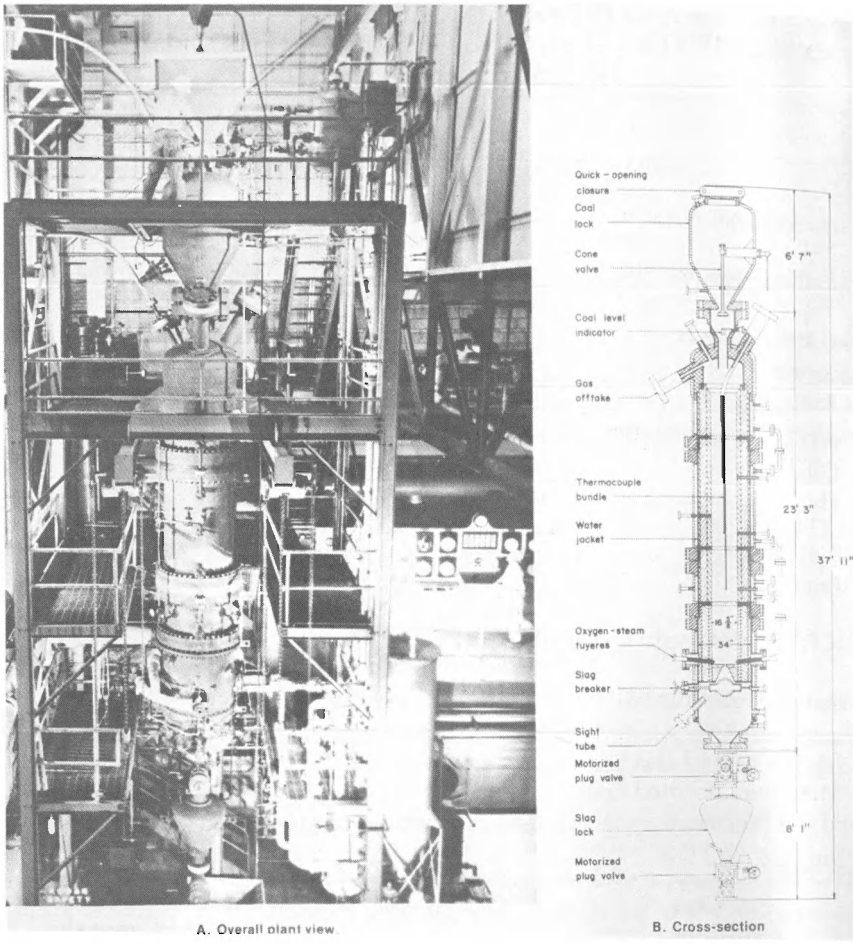

Figure 2. Slagging-ash, fixed-bed gasifier, 24-tpd capacity located at the ERDA Grand Forks Energy Research Center.

volves a laboratory screening program and actual testing in the operating gasifier.

As will be discussed in the next paragraph, slagging fixed-bed gasification has been selected for the ERDA demonstration program, and this has caused considerably increased interest in the GFERC slagging gasifier. Plans are now underway to modify and expand our program with the goal of supplying information which will aid in the design of the demonstration gasifier. Specifically, the GFERC gasification pilot plant will be modified to permit continuous operation of up to 5 days, a stirring device will be installed in the gasifier to permit the use of caking coals, and dual coal locks and a new coal handling system will be installed. These

modifications are expected to cost about 2 million dollars and are scheduled to be completed in about 18 months.

In October of 1975, ERDA issued a request for proposal (RFP) for design, construction, and operation of high Btu gasification demonstration plants. The Conoco Coal Development Company was one of the two respondents selected for contract negotiations. It is expected that a contract will be signed with Conoco in the near future. The gasification method proposed by Conoco is slagging fixed-bed similar to the GFERC process.

Conoco is joined in the proposal by the Lurgi Company and the British Gas Corporation. These groups have been conducting slagging gasification experiments in Westfield, Scotland, for the past two years under sponsorship of a group of about 15 North American companies, including Conoco.

The ERDA slagging fixed-bed gasification demonstration program is divided into the following phases:

ERDA will fund 100 percent of Phase I and 50 percent of Phases II and III. The plant is to be located in Ohio and will use a caking coal from Ohio No. 9 coalbed. The demonstration plant will use 3,757 tons per day of coal and produce 58.9 million standard cubic feet per day of gas. This is less than half the size of the 125 million SCFD dry ash Lurgi plant being planned for North Dakota. Conoco estimates the gas cost from the demonstration plant at $4.78/million Btu. Figure 3 is a flow sheet of the proposed slagging fixed-bed gasification demonstration plant.

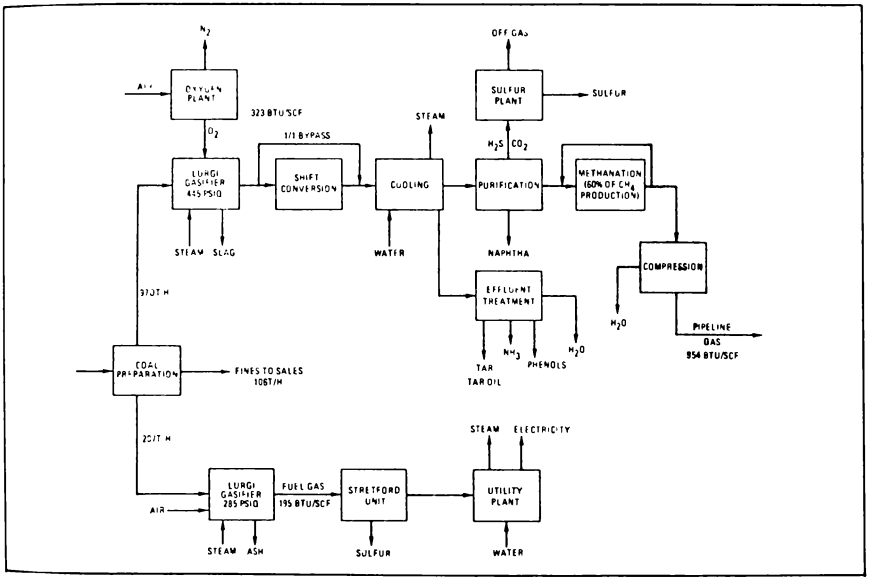

Figure 3. Process flow sheet for the proposed Conoco slagging fixed-bed gasification demonstration plant.

B. CO-Steam liquefaction process.

The CO-Steam process shown schematically in Figure 4 is a second-generation coal liquefaction technology for converting low-rank coals into environmentally acceptable liquid broiler fuel, and with additional hydrogenation, into refined products, including gasoline, distillate heating oil, and chemical feedstocks. Conversion occurs by reaction with carbon monoxide and water to provide in-situ hydrogen, nominal conditions are 4000 psi and 450° C. Factors being studied are yield, viscosity, and reduction of sulfur, nitrogen, and ash contents of the product.

Work on reaction kinetics is conducted in a modified one-liter batch autoclave which is capable of hot reactor charging and timed sampling of both gas and liquid products. Kinetic data have been obtained on the rate of disappearance of carbon monoxide and hydrogen reacting with a selected North Dakota lignite and on simultaneous changes in the molecular weight distribution and composition of the liquid product. Results point to the possibility of more rapid conversion by reaction with carbon monoxide through moderate increase in reaction temperature and improved use of hydrogen donor compounds that are produced in the process.

Analytical techniques used to characterize CO-Steam products include gas chromatography, low- and high-resolution mass spectrometry with computerized data handling, column chromatography, high pressure liquid chromatography, non-aqueous titration, UV, IR, and AA spectroscopy, and specialized separation and characterization procedures. Studies have focused on the relationship between product viscosity and other parameters, including molecular weight, asphaltene and pre-asphaltene contents, weak acid content, concentration of non-polar constituents, and oxygen content. Batch autoclave studies indicate that the high

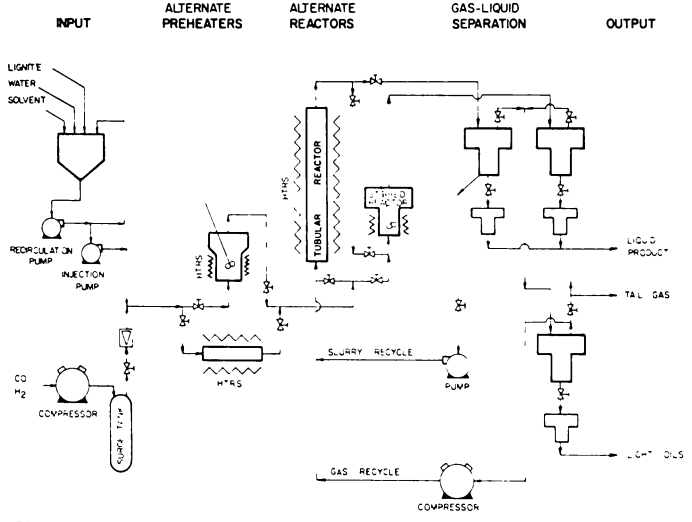

Figure 4. Schematic of continuous process unit, CO-Steam liquefaction process.

molecular weight products produced at temperatures under 400° C depolymerize to lower viscosity products slowly at 440° C but rapidly at 475° C. Major molecular species in the product oil have been quantitatively determined up to a molecular weight of 378. Analytical data provide important insights into the reaction mechanism, the role of hydrogen donor solvent, and the role of gaseous reactants.

A definite temperature dependence has been observed in the depolymerization during liquefaction. Figure 5 shows typical molecular weight distribution profiles of the CO-Steam product obtained by high pressure liquid chromatography separation on gel permeation columns. This fraction of the CO-Steam product is not distillable at 250° C and 1 mm Hg but is soluble in tetrahydrofuran, and this amounts to 20-40 pct of the MAF coal. The profiles show that at 460-470° C, the quantity of material over 600 molecular weight has been greatly decreased. Ninety pct coal-derived products made at 470° C have been found to be liquids at room temperatures.

Studies on flow pattern and turbulent mixing to improve reactor design are to be carried out in a continuous process unit sized to treat 3 to 5 lbs of coal/hr. This unit, currently undergoing shakedown, has been designed to provide flexibility for studying backmixing (residence time distribution) and turbulence through the

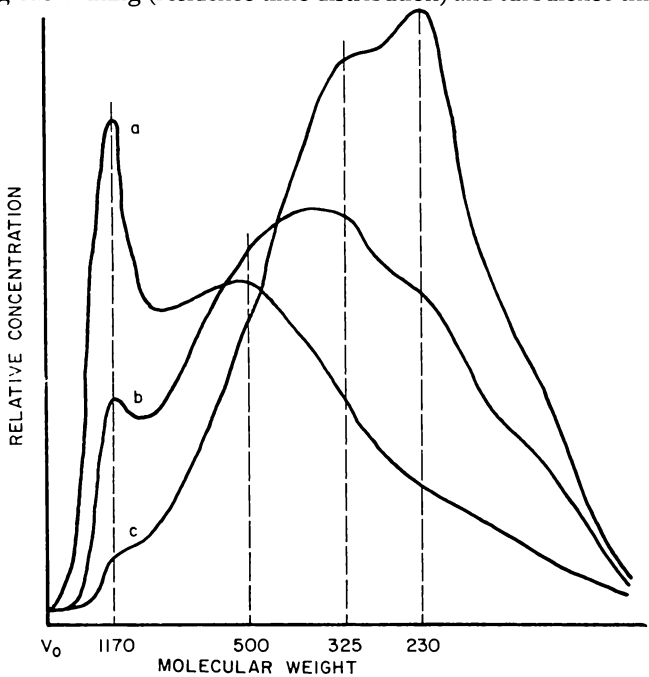

Figure 5. Typical molecular weight distribution produced at reactor temperature of a) 400° C, b) 440° C, and c) 470° C for 20 to 40% of the MAF coal charged in the CO-Steam process.

use of different reactor modules and the recycle of gas and/or slurry. After shakedown, this unit will be used to confirm favorable trends shown by the work on the time-sampled batch autoclave and to establish the effect of changes in reactor design parameters. The data on reactor design and the material balanced obtained from the continuous process unit will be used to establish specifications for a larger process development unit and to perform an economic evaluation comparing the CO-Steam process with catalytic hydrogenation technology.

C. Combustion - Ash Fouling

Nearly all of the present lignite production is used for power generation. Much progress has been made in designing powerplants for efficient use of lignite; however, some serious problems remain, the most serious of which is the deposition of ash on boiler steam tubes. Problem coals cause rapid ash deposition which can force repeated unscheduled shutdowns during difficult operating periods; the capacity of the boiler can be lowered by as much as 10 to 20 pct; the thermal efficiency can be reduced by 10 pct, and 1 pct of the steam generated can be used to operate on-line cleaning devices. The number of operating days per year can be reduced by 10 pct. The economic penalty for forced outage of a large boiler is very severe, amounting to over $100,000 per day in lost revenue for a 500 MW unit. These costs have prompted extensive research on ash fouling, starting in the 1950's and continuing until today.

Research at GFERC has included field testing in operating boilers (5), operation of a 75-lb/hr test furnace (6), and studies on the mechanism of the fouling process (7). Basic supporting studies on ash fouling at GFERC include: 1) characterization of mineral matter in Western coals, 2) examination of the microscopic structure and analysis of boiler deposits, 3) determination of the microscopic melting temperatures of fly ash particles and deposit fragments, and 4) studies on volatility of mineral constituents from coal and ash. Specialized analytical tools available to this work include X-ray fluorescence, X-ray diffraction, an electron microprobe, a scanning and analyzing electron microscope, a heated stage microscope, and a graphite furnace attached to an atomic absorption unit.

Much of the research on ash fouling at GFERC has been performed using a specially designed pulverized-coal-fired furnace. This furnace, shown in Figure 6, is designed to burn about 75 lb/hr of lignite under conditions similar to those found in commercial powerplants. Probes simulating steam tubes in large boilers are placed in locations in the ash-laden flue gas stream where the temperatures are from about 2000 to 1600° F. A standardized procedure has been developed for evaluating the relative fouling characteristics of a given coal by determination of the weight of deposit collected in a given test time. Figure 7 is a comparison of the ash deposits from a high fouling and a low fouling North Dakota lignite.

Over 100 coals have been tested in this program, and more than 400 individual tests have been run. Most of the coals tested have been lignites and subbituminous coals from the Northern Great Plains. The most consistent result obtained from the program is that the rate of ash deposition is a function of the sodium and ash contents of these coals. This effect is shown graphically in Figure

8. Unfortunately, many of the lignite deposits in North Dakota and some of the subbituminous deposits in Montana have high sodium contents. The use of these coals will require very conservative boiler design in order to achieve good boiler availability.

The GFERC test furnace has been used extensively to evaluate the ash fouling potentials of coals from new mining areas prior to design of the commercial boilers. In the last 2-3 years there has been considerable interest in developing some of the low quality lignite reserves in Texas. Test firing at GFERC has shown that some of these coals will be very difficult to use because of extremely high fouling rates.

FIGURE 6. Pulverized-coal combustor, 75-lb/hr capacity used in ash fouling studies at the ERDA Grand Forks Energy Research Center.

D. SO_2 emission control.

Most North Dakota lignites and other Western coals are low in sulfur content, as compared to Eastern bituminous coals. However, they often contain slightly too much sulfur to permit them to be burned without SO_2 control under the Federal New Source Performance Standards (NSPS) of 1.2 lb/SO_2/million Btu. The table given below shows the allowable sulfur content in various Western coals if they are to meet NSPS, assuming that all the sulfur in the coal appears as SO_2 in the stack gases.

TABLE 3. DATA ON ERDA'S SMALL INDUSTRIAL GASIFIERS AND LOW-BTU GASIFICATION DEMONSTRATION PLANT PLANNED FOR USING LOW RANK COALS

	Small Industrial Gasifiers			Demonstration Gasifiers
Contractor	Land O'Lakes and Applied Technology Co., Division of Black, Sivalls & Bryson	University of Minnesota and Foster Wheeler Corp.	Bureau of Mines and Industrial Groups	Erie Mining Co., Pickards-Mather & Co., and Arthur G. McKee
Location of Gasifier	Perham, MN	Duluth, MN	Bureau of Mines Twin Cities Research Center, Minneapolis, MN	Hoyt Lakes, MN
Application	Boiler for spray drying	Boiler for space heat and steam to campus	Induration of taconite pellets	Induration of taconite pellets
Type of Gasifier	Atmospheric, fixed bed dry ash removal	Atmospheric, fixed bed dry ash removal	Atmospheric, fixed bed dry ash removal	Atmospheric, fixed bed dry ash removal
Manufacturer	Wellman-Incandescent	Foster Wheeler STOIC	Wellman Galusha	Woodall-Duckham
Diameter	10′	10′	6′ 6″	12
Capacity	3 TPH	3 TPH	1 TPH	4 TPH x 5 Gasifiers
Type of Coal	Low-sulfur Western	Low-sulfur Western coal or briquetts	Low sulfur Western	Various types including low sulfur Montana subbituminous
Total Estimated Cost	$7.2 million	$4.8 million	$2 million	$39 million
ERDA Cost	$2.7 million	$2.2 million	$.75 million	$23 million
Percent of cost	37	46	38	100% design phase 50% construction and operation phase
Expected Operating Date	1979	1978	Dec. 1977	1980

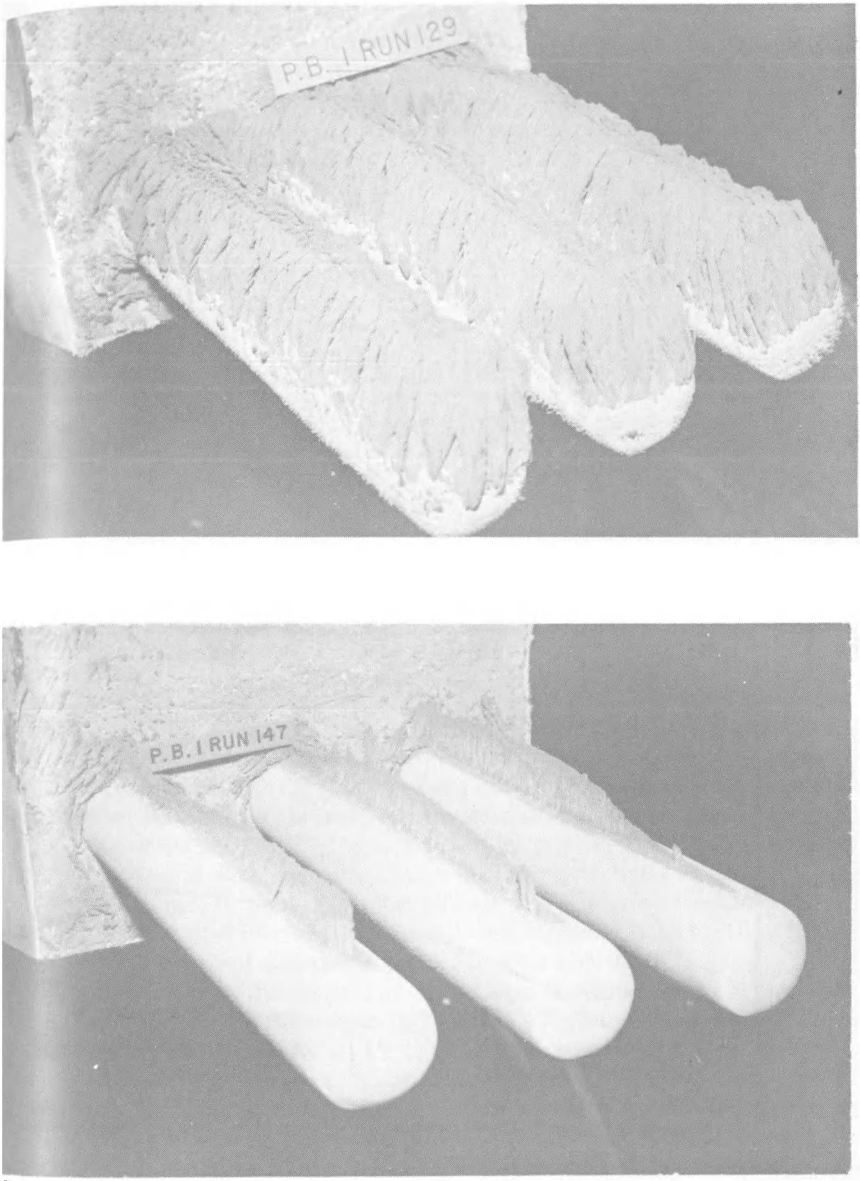

FIGURE 7. Comparison of ash deposits from a high fouling lignite (top) with those from a low fouling lignite (bot). Deposits produced in GFERC test furnace during 5 hr. test.

Most of these Western coals will require SO_2 removals in the stack of from 30 to 40 pct to meet NSPS. The most common method of SO_2 removal is by use of a stack-gas scrubber, in which lime or limestone converts the SO_2 to calcium sulfite or calcium sulfate.

North Dakota lignite and other Western low-rank coals produce ashes containing substantial alkaline oxides—CaO, MgO, Na_2O, and K_2O. For the past 5 years GFERC has been working on a process which substitutes the natural ash alkali for the lime or limestone reagent used in scrubbing systems.

This research has been conducted using a 120-scfm laboratory-scale scrubber at GFERC and a 5000-cfm pilot scrubber in a cooperative program with Minnkota Power Cooperative, Minnesota Power and Light Company, and Combustion Equipment Associates. The GFERC laboratory-scale wet scrubber is shown in Figure 9, and Figure 10 shows the 5000-scfm scrubber being tested at the Milton R. Young Generating Station at Center, North Dakota. Typical results from the 5000-cfm pilot scrubber are shown in Figure 11.

The results from this program (8) have demonstrated that ash alkali scrubbing can be used successfully and at lower cost than the lime-limestone scrubbing method. The 450 MW Unit 2 at the Milton R. Young Station will use this process. The plant is expected to be in operation by the summer of 1977.

E. Fluidized-bed combustion.

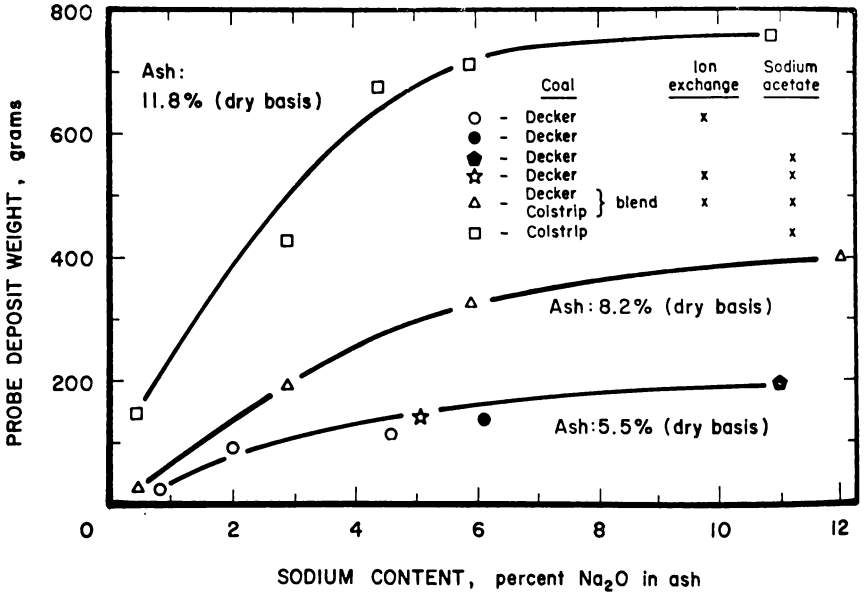

Figure 8. Probe deposit weight versus sodium content in ash at three ash levels for subbituminous coal. Data from GFERC 75-lb/hr furnace.

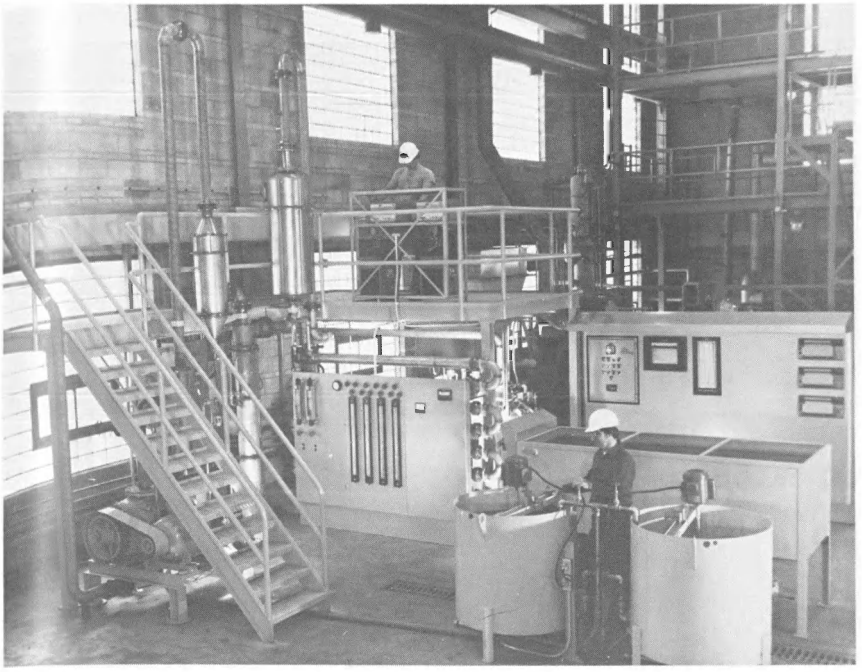

FIGURE 9. Ash-alkali pilot scrubber, 130 scfm capacity installed at the Grand Forks Energy Research Center.

There is currently a great interest in this country and abroad in developing fluidized-bed combustors (FBC) for coal. In fluidized-bed combustion, particles of coal are suspended in a stream of air passing upwards through the bed. Limestone particles can be added to the bed, and the calcium in the limestone reacts with sulfure dioxide released by the burning coal This produces calcium sulfate which can be discharged with the ash. FBC is an alternate sulfur emission control strategy and is seen by many as a more efficient and economical method than wet scrubbing. Most of the testing to date has been done with high sulfur Eastern coals using limestone or dolomite in the bed to react with the SO_2.

As stated earlier in this paper, lignite and most Western coals have high alkali contents in the ash, and these ashes will react in a fluidized-bed combustor much as the limestone or dolomite. At GFERC we have recently installed and started testing (9) a 6-inch diameter fluidized-bed combustor, shown in Figure 12. Preliminary tests with one North Dakota lignite have shown that sulfur retentions are a function of average bed temperature and range from 40 to 50 pct over the temperature range from 1200 to 1500° F. These results are very encouraging and indicate that many of the North Dakota lignites can be expected to meet NSPS when burned in a FBC. FBC has a distinct advantage over wet scrubbing when considered for sulfur control on smaller industrial furnaces.

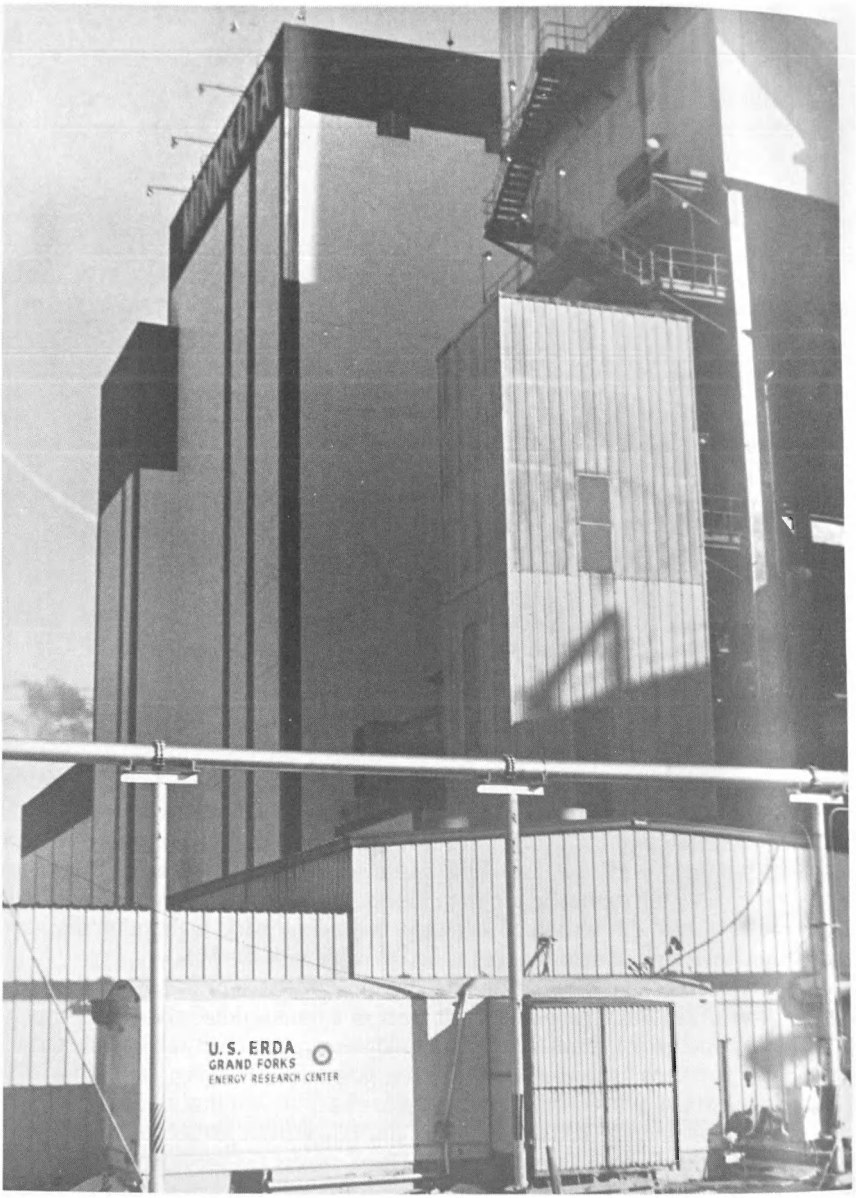

FIGURE 10. Pilot scrubber, 5000 cfm capacity, used to study ash-alkali scrubbing at the Milton R. Young station in a GFERC cooperative program.

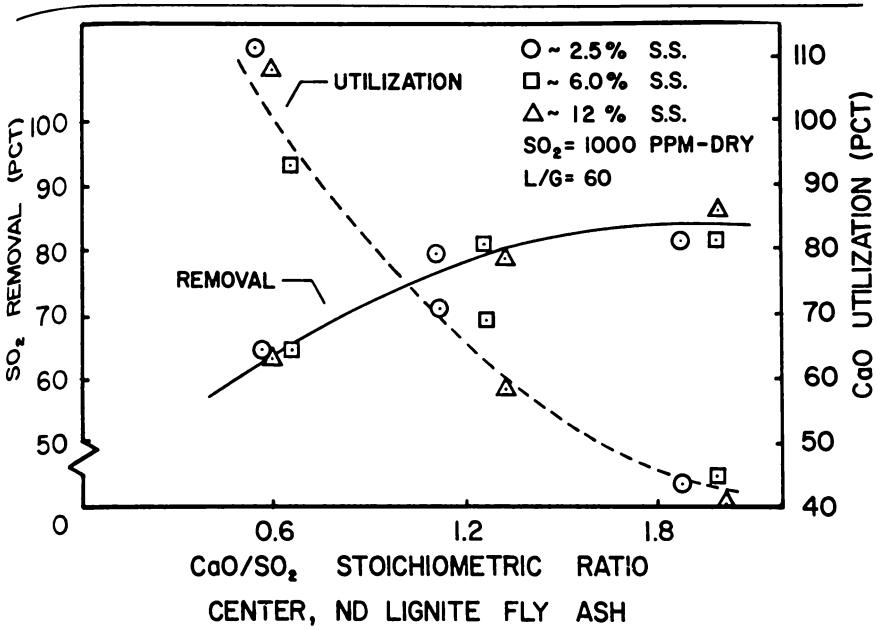

Figure 11. Sulfur dioxide removal efficiencies and calculated calcium utilization in the fly ash as a function of CaO/SO_2 ratio. Data from tests on 5000 cfm scrubber.

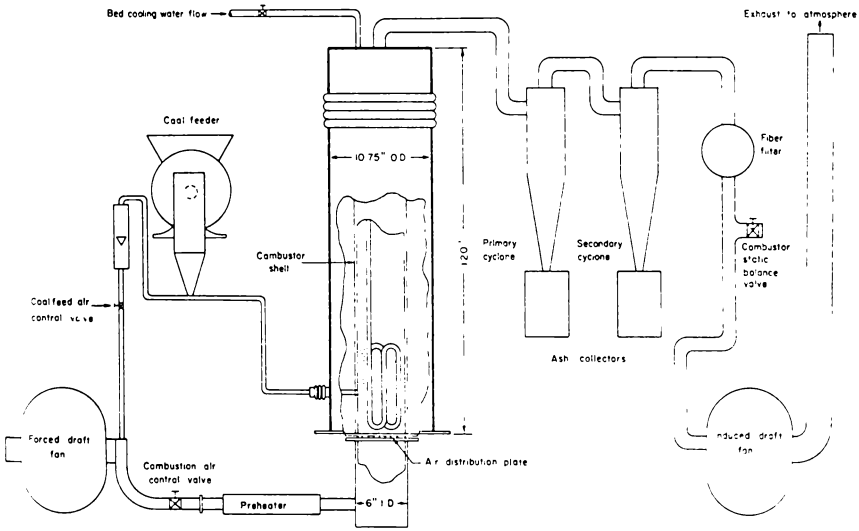

Figure 12. Schematic of fluidized-bed combustor installed at the Grand Forks Energy Research Center.

F. Fly ash control by electrostatic precipitation.

The Federal New Source Performance Standards require that fly ash emissions must not exceed 0.1 lb/million Btu heat input to the boiler. In order to meet these standards, collection efficiencies of over 99 pct are often required. The most common apparatus used to attempt to achieve these efficiencies is an electrostatic precipitator. These devices have been available for many years; however, there is

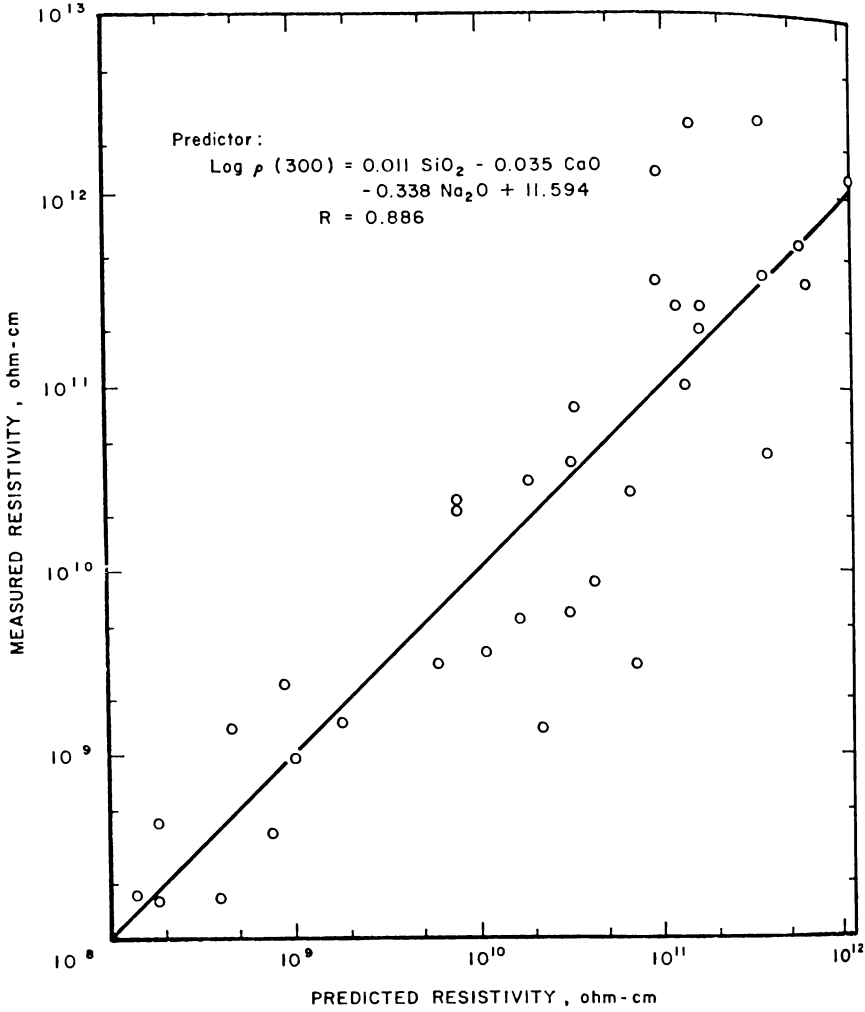

Figure 13. Measured vs. predicted resistivity at 300° F based on fly ash cnemical composition. Fly ash produced from burning lignite and other low-rank Western coals.

still considerable uncertainty in the design of units for use on low-sulfur Western coals.

GFERC has for some years conducted research to better define the factors affecting the operation of electrostatic precipitators. If is generally accepted that electrical resistivity of the fly ash is the most important single factor affecting precipitator performance. For good performance, resistivity should be in the range of 10^8 10^{11} ohm/cm. Electrical resistivity is a function of temperature and moisture content of the flue gas and of the chemistry of the fly ash. GFERC has developed a correlation relating chemical composition to resistivity based on measurements on ashes from various Western coals, as shown in Figure 13. (10).

GFERC has conducted in-house experiments using a plate-type pilot electrostatic precipitator in conjunction with the ash fouling furnace. Operation of this unit was not satisfactory until now. A new specially designed 75-lb/hr pulverized-coal-fired furnace and an associated tubular pilot electrostatic precipitator have been installed. This unit, which is shown in Figure 14, will be used to fire samples of coal from new mining areas and provide information which will permit more precise design of commercial precipitators to be used with this coal. This equipment will also be used to study dry sorbents such as Nahcolite or trona for SO_2 absorption as an alternative to wet scrubbing and to study the control of ultrafine sulfate particulates.

ERDA COST-SHARED INDUSTRIAL PROGRAMS USING LOW-RANK COALS

A. Gasifiers in industry program.

This ERDA program involves the direct use of low-Btu gas in industrial applications. Small-sized individual gasifiers are currently available and will be the first application of synthetic gas from coal in industry. Coal will be prepared for gasification and converted to a low-Btu fuel gas in a gasifier located at the industrial plant. The fuel gas will be purified to remove particulates and condensible products. The program is designed to determine the factors controlling the connection of gasifiers to the end user of the gas in industry.

As a result of a recent ERDA project opportunity notice, six proposals were selected for negotiations. Two of the proposals were for installations in Minnesota and will be tested on low-rank coals. One gasifier will be located at the Land-O'Lakes Creamery at Perham and will be used to fire a boiler for process steam. The other gasifer will be located at the Duluth Campus of the University of Minnesota and will be used to supply steam heat to the campus. It is expected that low-sulfur Western coals will be used in both of these gasifiers. Some details of these industrial gasifiers are given in Table 3.

ERDA is also participating with the Bureau of Mines and an industrial group in another program relating to industrial gasifiers. The program is designed to evaluate the use of low-BTU gas to fire a grate kiln for induration (hardening) of taconite pellets. An existing small industrial gasifier will be relocated from the iron range to the Bureau of Mines Twin City Metallurgy Research Center in Min-

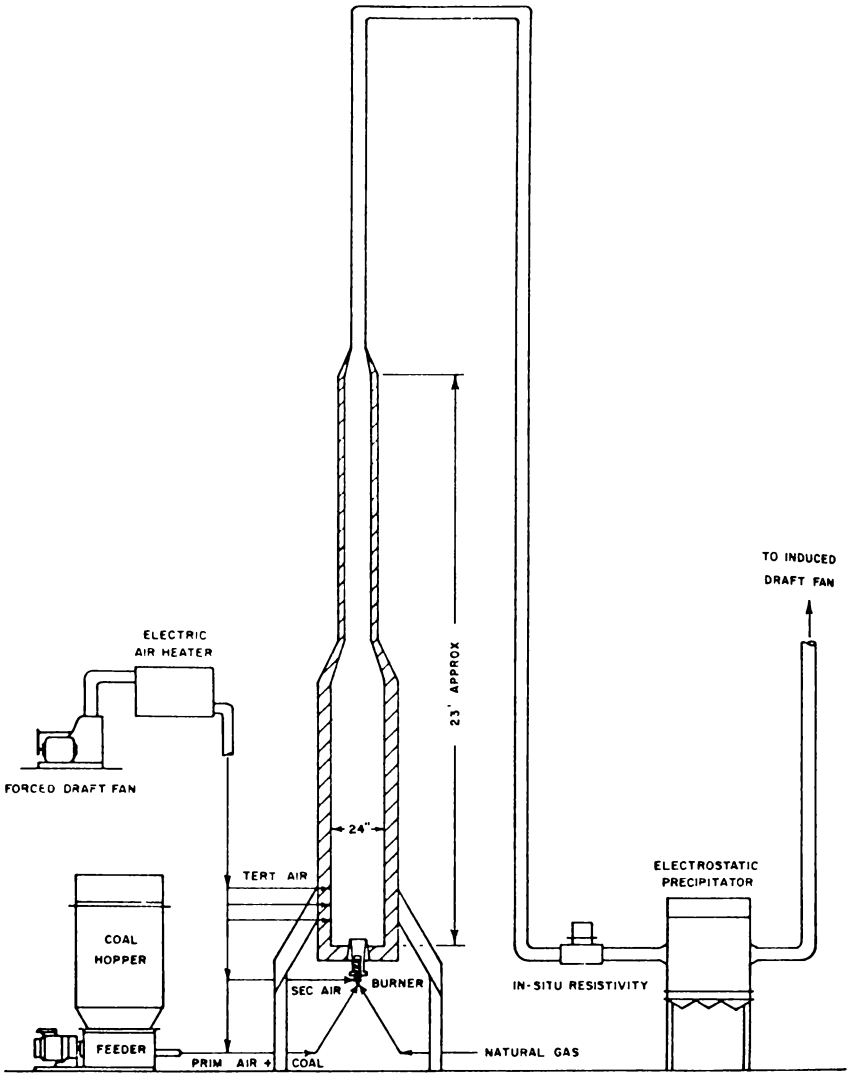

Figure 14. Schematic of test facility for electrostatic precipitation research at the Grand Forks Energy Research Center.

neapolis. This project which will also use low-rank coals, is expected to be operational by late 1977.

B. Low-Btu gasification demonstration program.

ERDA also has a program for larger-scale testing of low Btu gasifiers. As a result of a request for proposal (RFP) issued by ERDA, 15 firms submitted proposals for a low-Btu gasification demonstration plant. Two proposals were selected for negotiations, one of which was a proposal by Erie Mining Company to install a gasifier at their Hoyt Lake, Minnesota, taconite plant. The gas will be burned to supply heat for induration of taconite pellets. Woodall Duckham's atmospheric pressure fixed-bed gasifiers will be used in the demonstration facility. Some data on the gasifier program are given in Table 3. The demonstration facility will consist of five 12-ft diameter gasifiers, and they will gasify about 500 tons of coal per day. Plans are to test both a high-sulfur Illinois coal and low-sulfur Montana subbituminous coal in the program. If the operation is successful, Erie Mining Company plans to triple the size of the plant at a later date. The total cost of the demonstration program is 39 million dollars and ERDA funding is 23 million dollars.

C. Fluidized-bed combustion—industrial application.

ERDA also has a program for demonstrating the applicability of atmospheric fluidized-bed combustion to industrial applications. Four areas of industrial application are to be investigated: 1) saturated steam boilers, 2) superheated steam generator, 3) indirect fired process heater, and 4) direct fired process heater.

ERDA has negotiated a contract with the Fluidyne Company to design, construct, and test a FBC for Category (3) indirect fired process heat. The unit, to be installed at the Owatonna Coal Company, Owatonna, Minnesota, will be designed to burn 1-1/2 ton/hr of coal and supply flue gas to heat air for metal-working at 900° F. Plans are to test lignite and other low-rank coals, as well as higher sulfur coals, in this unit.

SUMMARY

ERDA's program for coal research, development, and demonstration places considerable emphasis on the use of lignite and other low-rank Western coals, as well as the high sulfur Eastern bituminous coals. In the near term there will be a great emphasis on the displacement of gas and oil by coal for power generation and industrial use. ERDA is funding projects both in-house and by contract that are designed to achieve increased use of low-rank Western coals in an environmentally acceptable manner.

Lignite and other low-rank fuels have distinct advantages for most conversion processes because of their high reactivity and non-caking properties. ERDA is funding liquefaction and gasification research relating to lignite and other low-rank coals at various scales of operation ranging from laboratory studies to demonstration plants, and it is expected that the results of these programs will have a profound influence on the fuel supply options available in the Upper Midwest in the coming years.

LITERATURE CITED

Fink, C. E., G. P. Curran, and J. D. Sudbury. CO_2 Acceptor Process Pilot Plant—1974, Rapid City, South Dakota. Technology and Use of Lignite: Proceedings of a Symposium sponsored by the Energy Research and Development Administration and the University of North Dakota, Grand Forks, ND, May 14-15, 1975 GFERC/IC-75/2, pp. 239-253.

Lee, B. S. The Hygas Process for Converting Lignite to SNG. Technology and Use of Lignite: Proceedings of a Symposium sponsored by the Energy Research and Development Administration and the University of North Dakota, Grand Forks, ND, May 14-15, 1975, GFERC/IC-75/2, pp. 230-238.

Ellman, R. C, and H. H. Schobert. Pilot Plant operation of a Fixed-Bed Slagging Gasifier, ACS, Division of Fuel Chemistry, 173rd National Meeting, March 21-25, 1977, 13 pp.

Sondreal, E. A., J. E. Schiller, C. L. Knudson, and T. H. May. Development of the CO-Steam Process for Liquefaction of Lignite and Western Subbituminous Coals. To be presented at the 1977 ERDA-und Lignite Symposium, Grand Forks, ND, May 18-19, 1977.

Sondreal, E. A., S. J. Selle, P. H. Tufte, V. H. Menze, and V. R. Laning. Correlation of Fireside Boiler Fouling with North Dakota Lignite Ash Characteristics and Power Plant Operating Conditions. Presented at the American Power Conference, Chicago, IL, April 19, 1977, 18 pp.

Tufte, P. H., G. H. Gronhovd, E. A. Sondreal, and S. J. Selle, Ash Fouling Potentials of Western Subbituminous Coals as Determined in a Pilot Plant Test Furnace. Presented at the American Power Conference, Chicago, IL, April 22, 1976, 15 pp.

Tufte, P. H. and W. Beckering. A Proposed Mechanism for Ash Fouling Burning Northern Great Plains Lignite. Journal of Engineering for Power, ASME Transactions, Vol 97, July 1975, pp. 407-412.

Ness, Harvey M., F. I. Honea, E. A. Sondreal, and P. Richmond. Pilot Plant Scrubbing of SO_2 with Fly Ash Alkali from North Dakota Lignite. To be presented at the 1977 ERDA-UND Lignite Symposium, Grand Forks, ND, May 18-19, 1977.

Selle, S. J. and L. L. Hess. Factors Affecting ESP Performance on Western Coals and Experience with North Dakota Lignite. Presented at EPA/EPRI Symposium on Particulate Control in Energy Processes, May 1976, San Francisco, CA, 20 pp.

DISTRIBUTION OF HYDROPSYCHIDAE (TRICHOPTERA) IN SANDHILL STREAMS OF SOUTHEASTERN NORTH DAKOTA

S. C. Harris and R. B. Carlson
Department of Entomology
North Dakota State University
Fargo, North Dakota 58102

ABSTRACT

Larvae of *Hydropsyche slossonae* Banks, *Hydropsyche betteni* Ross, *Hydropsyche simulans* Ross, and *Cheumatopsyche pasella* Ross (Hydropsychidae: Trichoptera) were found to occur in sandhill streams of southeastern North Dakota. In areas where the current was swift, *H. slossonae* was common. *Hydropsyche betteni* was restricted to a riffle area immediately downstream from a stream impoundment. *Hydropsyche slossonae, H. simulans*, and *C. pasella* were collected in the slow moving waters of the undercut stream banks. As the Hydropsychidae are net-spinners, the presence of *H. slossonae, H. simulans,* and *C. pasella* in an area of slow moving water is unusual.

INTRODUCTION

The larvae of the Hydropsychidae generally prefer cool, swift streams with abundant riffle areas. Members of the family spin nets, in front of retreats, to catch biota swept in by the current. This mode of feeding suggests that the distribution patterns of hydropsychid larvae should be related to stream flow rates (Chutter, 1969; Edington, 1965). This paper reports on the species distribution of the family in springbrooks, of the sandhill region of North Dakota, where the typical riffle habitat is absent.

DESCRIPTION OF STUDY AREA

Two springbrooks, Iron Springs and Ransom Springs are located in the Sheyenne delta, in Richland and Ransom Counties respectively, of southeastern North Dakota. The delta consists predominantly of fine sand and some gravel to depths of 60 feet (Baker, 1967). Iron Springs is 3.5 km long, with an average width of 2.2 m; Ransom Springs is 1.2 km long, with an average width of 1.3 m. Both springbrooks have fairly uniform substrates of fine sand with accumulations of silt and detritus at the margins. The springbrooks are spring and seepage fed over their length by the Sheyenne aquifer. Water from the aquifer is typically hard and relatively high in dissolved solids (Baker, 1967).

MATERIALS AND METHODS

Permanent sampling stations were established at eight locations along Iron Springs and at three locations along Ransom Springs. The numerals designating these sampling stations increase from the spring headwaters. A detailed description of sampling stations is contained in Harris and Carlson (1975).

Sites within the stations were sampled monthly from March to November

during 1974 and 1975 and also in January, 1975. Samples were obtained with a Neil-type, cylinder sampler from sites at the stream center and at the stream margin. The sampler enclosed 0.6 m^2 of substrate to a depth of 6 cm. Substrate materials were screened (300 mm mesh) and the remainder preserved in 70% ethyl alcohol. Specimens were removed from the substrate materials, sorted by taxa, and stored in 70% ethyl alcohol.

The springbrooks were qualitatively sampled with an aquatic net during the spring and summer of 1975 and 1976. Specimens were sorted in a white pan and transferred to 70% ethyl alcohol. Light traps of the Texas type equipped with UV bulbs, placed on the stream banks, were used to collect adults.

Water samples and measurements of physical parameters were taken at the time of sampling. Water samples were analyzed with a Hach DR-EL laboratory and the pH was determined with a Corning (Model 10) pH meter. Specific conductance was determined with a Lab-Line solu-bridge (Model MC-1). Flow was measured with a pygmy flow meter (Scientific Instruments, Wisconsin). Stream depth, width, and temperature were also recorded.

RESULTS AND DISCUSSION

Cheumatopsyche pasella and *Hydropsyche slossonae*, with the latter the most common, were the only hydropsychids collected with the Neil sampler (Table 1). In general, *H. slossonae* did not occur at the headwaters of the springbrooks (Stations I, II, RI, RII). In both springbrooks, sampling sites at the headwaters were characterized by low stream flow (12 cm/sec) and shallow water (6 cm). Flow rate and depth, along with high dissolved solids (>800 mhs/cm, specific conductance) and high iron levels (>3 mg/l), may have served to limit the occurrence of *H. slossonae* at the headwaters of Iron Springs.

TABLE 1. Hydropsychidae collected by Neil-type sampler in Iron Springs and Ransom Springs (R) from March to November 1974 and 1975, and January 1975.

Site	*H. slossonae*	*C. pasella*
I	0	0
II	1	0
III	134	2
IV	75	0
V	149	0
VI	113	0
VII	21	2
VII	32	0
RI	0	0
RII	1	0
RIII	62	0

In the downstream reaches of the springbrooks, 198 *H. slossonae* were collected at the stream margins and 288 at the stream center. At the stream margin, the mean stream flow was higher at sites where *H. slossonae* were present (Table 2). Only 9 specimens were collected at current velocities below 11 cm/sec. This might be expected since the mode of feeding of hydropsychids is current related and at low flows feeding nets are not constructed (Philipson, 1953; Scott, 1958). However, at the stream center occurrence of specimens did not seem to be related to stream flow rates (Table 2). Along with suitable current velocity, the hydropsychids require stable substrate for attachment of feeding nets. Sampling data revealed that in all cases where *H. slossonae* were collected at the stream center, the substrate contained detritus or gravel. It would seem then that at the stream margins, where material suitable for attachment of nets was abundant, stream flow governed the distribution of larvae and at the stream center, where flow rates were suitable, the substrate composition was a determining factor. Stream depth did not appear to influence distributional patterns of *H. slossonae* (Table 2).

Light traps placed on the banks along the lengths of Iron Springs and Ransom Springs yielded four species of Hydropsychidae (Table 3). Based on numbers captured, it seemed likely that *H. slossonae, H. simulans,* and *C. pasella* would occur

TABLE 2. Mean stream flow and stream depth for specific sites and times, within stations III-VIII and RIII, at which *Hydropsyche slossonae* were present (P) or absent (A) in collections. Number of observations in parenthesis.

	All sites	Sites at stream margin	Sites at stream center
Stream Flow (cm/sec)	(P) 23.0 (79) (A) 21.0 (238)	18.0 (44) 7.0 (111)	31.0 (35) 33.0 (127)
Stream Depth (cm)	(P) 14.9 (79) (A) 11.8 (247)	8.9 (44) 7.3 (110)	23.3 (35) 15.4 (137)

TABLE 3. Adult Hydropsychidae captured in light traps, positioned on the banks of Iron Srpings and Ransom Springs, during the summer of 1974 in Richland and Ransom Counties, North Dakota.

Species	Males	Females
Hydropsyche slossonae	49	40
Hydropsyche simulans	10	12
Hydropsyche piatrix	0	2
Cheumatopsyche pasella	12	42

in the springbrooks. Since *H. slossonae* was the only species commonly collected in quantitative sampling, the habitats of the other species were apparently missed.

By qualitative sampling, the habitats of *H. simulans* in sandhill springbrooks were determined to be undercut stream banks and stickjams at the stream center (Table 4). Flow rates in these undercut areas are slow, the undercutting occurring due to the collapse of the unstable sand stream banks, rather than erosion by a fast current. Both *C. pasella* and *H. slossonae* also inhabited the slow waters of the undercut stream banks. The reasons for occurrence of *H. simulans* and *C. pasella* in these slow moving waters are obscure. Perhaps as Hughes (1966) has suggested, shade may be a factor in distribution patterns. It is also possible that *H. slossonae* has a competitive advantage in the use of the limited suitable substrates that occur in the areas of higher flow, thereby limiting the other two species to marginal habitats. *Hydropsyche piatrix*, though captured in light traps (Table 3) was not collected as immatures by either sampling methods. The species probably occurs in the nearby Sheyenne River, rather than in the springbrooks.

Another species, *H. betteni* was collected in a rocky riffle immediately downstream from a stream impoundment (Table 4). The rocky riffle, which formed

TABLE 4. Hydropsychidae collected during qualitative sampling of Iron Springs and Ransom Springs during spring and summer of 1974 and 1976.

Species	Undercut streambank	Stickjam	Rocky riffle
Hydropsyche slossonae	34	51	63
Hydropsyche simulans	9	6	0
Hydropsyche betteni	0	0	16
Cheumatopsyche pasella	51	5	1

from the breakup of the impoundment dam, was the only such area in the springbrooks. Ross (1944) has reported this species to occur in a similar habitat in Illinois.

ACKNOWLEDGMENTS

The authors wish to thank Dr. Andrew Nimmo of the University of Alberta and Dr. Glenn B. Wiggins of the Royal Ontario Museum for assistance in the identification of hydropsychid adults and larvae respectively.

LITERATURE CITED

Baker, C. H. 1967. Geology and ground water resources of Richland County, North Dakota. Part I. Geology. Bull. N. Dak. Geol. Surv. 46: 1-56.

Chutter, F. M. 1969. The distribution of some stream invertebrates in relation to current speed. Int. Revue ges. Hydrobiol. 54: 413-422.

Edington, J. M. 1965. The effect of water flow on populations of net-spinning Trichoptera. Mitt. int. Verein. Theor. angew. Limnol. 13: 40-48.

Harris, S. C. and R. B. Carlson. 1975. Comparative distribution of immature *Bittacomopha clavipes* (Fabricius) and *Ptychoptera quadrifasciata* Say (Diptera: Ptychopteridae) in sandhill streams of southeastern North Dakota. Proc. N. D. Acad. Sci. 27. In Press.

Hughes, D. A. 1966. Mountain streams of the Barberton area, eastern Transvaal. Part II. The effect of vegetational shading and direct illumination on the distribution of stream fauna. Hydrobiologia 27: 437-459.

Philipson, G.N. 1953. The larva and pupa of *Hydropsyche instabilis* Curtis (Trichoptera: Hydropsychidae). Proc. Zool. Soc. Lond. 124: 547-564.

Scott, D. 1958. Ecological studies on the Trichoptera of the River Dean, Chesire. Arch. Hydrobiol. 54: 340-392.

Ross, H. H. 1944. The caddis flies or Trichoptera of Illinois. Ill. Nat. Hist. Surv. Bull. 23: 1-326.

NORTH DAKOTA FLEAS. VII. SIX NEW RECORDS FROM PERIPHERAL REGIONS OF THE STATE

Omer R. Larson
Department of Biology
University of North Dakota, Grand Forks, North Dakota 58202

INTRODUCTION

This paper continues the reports of a decade of studies on the Siphonaptera of North Dakota. Scattered collections from the past several years, an old vial of bird fleas, and a series of specimens at the University of Minnesota yielded six species not previously reported from North Dakota and are herewith reported. These six additions are considered in the context of their North American and probable North Dakota distributions. They, along with earlier check-lists and the Genoways and Jones (1972) collections, bring the state's known flea fauna to 42 species.

METHODS

All fleas were preserved in 70 percent ethanol prior to bleaching in 10 percent potassium hydroxide. Whole mounts were prepared by conventional techniques described previously (Woods and Larson, 1970). All accession numbers refer to specimens cataloged in the University of North Dakota Parasitology Collection.

RESULTS AND DISCUSSION

Family Pulicidae

Cediopsylla simplex (Baker)

No. 891-892 from *Sylvilagus floridanus similis* Nelson, Cass Co., 4 February 1973, 4 females.

Cediopsylla Jordan is a common and widespread genus of North American leporids. The 100th meridian is an approximate boundary between *C. simplex* to the east, and *C. inaequalis inaequalis* (Baker) to the west, although the species overlap in eastern Nebraska (Rapp and Gates, 1957). *Cediopsylla i. inaequalis* is known to occur in Slope and Bowman Counties of southwestern North Dakota (Voth and James, 1966), and from unpublished records of *S. audubonii baileyi* (Merriam) in Billings County. The distribution of *Cediopsylla* spp. between the Red River Valley and the North Dakota Badlands is unknown.

Family Hystrichopsyllidae

Nearctopsylla genalis hygini (Rothschild)

No. 874-876 from *Blarina brevicauda brevicauda* (Say), Grand Forks Co., 23 October 1972, 3 females.

Two valid subspecies of *N. genalis* are recognized east of the Rocky Mountains from shrews, moles, and their mustelid predators. One of these, *N. g. genalis* (Baker), extends from Michigan eastward to the Atlantic. The other subspecies, *N. g. hygini*, occurs in the northern Great Plains, from Alberta, Saskatchewan and Manitoba, southward to Iowa and Nebraska. Several specimens from the last two localities were re-identified at the British Museum of Natural History as *N. g. hygini* (Hopkins and Rothschild, 1962). Although the University of North Dakota Parasitology Collection contains *N. g. hygini* from Minnesota (2 from Itasca State Park and 7 from Dakota County), the eastward distribution of this subspecies remains unknown. Specimens from Cook County, Minnesota were not identified to subspecies (Timm, 1975), nor were others from Bayfield County, Wisconsin (Knipping, et al. 1950), or northwestern Illinois (Verts, 1961). The distribution of *N. g. hygini* in North Dakota may well reach the Missouri River. West of that, *B. b. brevicauda* is absent, and shrews in general are scarce.

Family Leptopsyllidae

Amphipsylla sibirica pollionis (Rothschild)

No. 521 from *Clethrionomys gapperi loringi* (Bailey), near Lake Metigoshe in Bottineau Co., 5 May 1961, 1 female.

Amphipsylla sibirica is a polytypic species of northern and montane areas of the Holarctic region. In North America it is represented by two subspecies, *A. s. pollionis* and *A. s. washingtona* Hubbard, the latter considered a full species according to Holland (1958). *Amphipsylla s. pollionis* ranges from Alaska and the Yukon, southward along the Rocky Mountains through Alberta. Holland (op. cit.) also reported a disjunct population from northern Labrador. The only previous locality record from the contiguous United States is from southeastern Idaho, where specimens were described as similar to *A. s. pollionis* (Allred, 1968). Its occurrence in North Dakota is the most southern, non-mountainous record in North America, a thousand miles from the nearest known populations in Alberta. In addition to our specimen, seven others from the same lot of fleas are in the University of Minnesota Entomology Collection.

Family Ceratophyllidae

Ceratophyllus styx riparius (Jordan and Rothschild)

No. 559-563 from nests of *Riparia riparia riparia* (L.), Homme Dam site in Walsh Co., 26 July 1949, 5 males, 5 females.

Ceratophyllus styx is also a polytypic, Holarctic parasite. It is represented across North America by one subspecies, *C. s. riparius.* The true host is the bank swallow, *R. riparia,* and in North Dakota the flea can be expected wherever this bird nests.

Orchopeas howardii howardii (Baker)

No. 906-907 from *Sciurus niger rufiventer* E. Geoffroy St.-Hilaire, near Thompson in Grand Forks Co., 15 September 1973, 2 males, 2 females.

This is a common and widely distributed flea on gray, red, fox and flying squirrels east of the 100th meridian. Its true host appears to be the gray squirrel. In eastern North Dakota and north-central Minnesota, tree-dwelling squirrels may typically have *Monopsyllus vison* (Baker) and *O. caedens* (Jordan) (Woods and Larson, 1970; Benton, et al., 1971). The occurrence of *O. h. howardii* in North Dakota is unknown, but the introduction of gray squirrels into Minot, Bismarck, Valley City, Jamestown and the Killdeer Mountains (Hibbard, 1956) over the past 75 years, may mean that the flea also occurs in those localities. Similar transplantation of squirrels from eastern North America has introduced *O. h. howardii* into portions of California, England and Ireland.

Orchopeas sexdentatus agilis (Rothschild)

No. 913 from *Sylvilagus audubonii baileyi* (Merriam), 2 mi. w. of Medora in Billings Co., 29 December 1973, 1 male, 1 female.

Orchopeas sexdentatus ssp. has been collected from many species of mammals, but is typically associated with woodrats (*Neotoma* spp.) throughout that host's range. Lewis (1975) listed 8 subspecies from North America, with 7 of these occurring west of the Mississippi River. The flea's variable morphology makes many subspecific identifications tenuous, especially from the montane areas of the west. However, *O. s. agilis* is one of the more distinctive subspecies. It is a common flea, known to occur from the Pacific Northwest to eastern Montana (Jellison and Senger, 1973). Examination of woodrats from the North Dakota Badlands should yield additional records of *O. s. agilis.*

ACKNOWLEDGMENTS

Appreciation is extended to Dr. Edwin Cook for permission to examine *Amphipsylla sibirica pollionis* in the University of Minnesota Entomology Collection, and for sharing those specimens. Thanks are also due Michelle Erickson for library and technical assistance in the preparation of this paper.

LITERATURE CITED

Allred, D. M. 1968. Fleas of the National Reactor Testing Station. Grt. Basin Nat. 28:73-87.

Benton, A. H., O. R. Larson, and B. A. VenHuizen. 1971. Siphonaptera from Itasca State Park region. J. Minnesota Acad. Sci. 37:91-92.

Genoways, H. H. and J. K. Jones, Jr. 1972. Mammals from southwestern North Dakota. Occas. Pap. Mus. Texas Tech Univ. 6. 36 pp.

Hibbard, E. A. 1956. Range and spread of the gray and the fox squirrels in North Dakota. J. Mammal. 37:525-531.

Holland, G. P. 1958. Distribution patterns of northern fleas (Siphonaptera). Proc. 10th Intl. Congr. Ent. (1956). 1:645-658.

Hopkins, G. H. E. and M. Rothschild. 1962. An illustrated catalogue of the Rothschil collection of fleas (Siphonaptera) in the British Museum (Natural History). Vol. III. Hystrichopsyllidae. Brit. Mus. Nat. Hist. 560 pp.

Jellison, W. L. and C. Senger. 1973. Fleas of Montana. Montana Agric. Exp. Stn. Res. Rept. 29. 75 pp.

Knipping, P. A., B. B. Morgan, and R. J. Dicke. 1950. Preliminary list of some fleas from Wisconsin. Tr. Wisconsin Acad. Sci. Arts Lett. 40:199-206.

Lewis, R. E. 1975. Notes on the geographical distribution and host preferences in the order Siphonaptera. Part 6. Ceratophyllidae. J. Med. Ent. 11:658-676.

Rapp, W. F., Jr. and D. B. Gates. 1957. A distributional checklist of the fleas of Nebraska. J. Kansas Ent. Soc. 30:50-53.

Timm, R. M. 1975. Distribution, natural history, and parasites of mammals of Cook County, Minnesota. Occas. Pap. Bell Mus. Nat. Hist. Univ. Minnesota. 14. 56 pp.

Verts, B. J. 1961. Observations on the fleas (Siphonaptera) of some small mammals in northwestern Illinois. Am. Midl. Nat. 66:471-476.

Voth, D. R. and T. R. James. 1966. Parasites of the white-tailed jackrabbit in southwestern North Dakota. Proc. North Dakota Acad. Sci. 19:15-18.

Woods, D. E. and O. R. Larson. 1970. North Dakota fleas. II. Records from man and other mammals. Proc. North Dakota Acad. Sci. 23:31-40.

A TRIAL OF ELEVEN SOURCES OF *PICEA ABIES* IN NORTH DAKOTA AND MINNESOTA

James L. Van Deusen
Rocky Mountain Forest and Range Experiment Station
North Dakota State University-Bottineau Branch Campus
Bottineau, North Dakota 58318

and

Hans Nienstaedt
North Central Forest Experiment Station
Institute of Forest Genetics
Rhinelander, Wisconsin 54501

ABSTRACT

Eleven seed sources of *Picea abies* from eastern Europe and Russia were tested on the Denbigh Experimental Forest in North Dakota and Pike Bay Experimental Forest in Minnesota. Overall survival at Pike Bay was uniformly good (94.4 percent) throughout the first 10 years. At Denbigh, under average growing season precipitation, survival of all sources declined to 67 percent during the first five years. After two more years, in which growing season precipitation was unusually low, the overall plantation survival averaged less than 6 percent.

Norway spruce may still be a useful conifer in North Dakota shelterbelts, but its success will depend largely on careful matching of seed sources with planting sites. Container-grown stock, tested under controlled greenhouse conditions and screened for adaptability, could form a reservoir of adapted plant material.

INTRODUCTION

Foresters and farmers have long recognized the need for coniferous trees that will survive and grow well in the northern Great Plains. A dilemma has developed, however, because more rapidly growing broadleaved trees are favored over the slow growing adapted conifers.

Conifers, however, have desirable traits absent in broadleaved tress. Their year-round foliage affords winter protection for humans, livestock, and wildlife. They also provide an esthetically pleasing contrast to an often bleak winter landscape. In addition, once the coniferous shelterbelt reaches the desired density, it can be maintained without frequent pruning.

The limited number of proven coniferous species we now have is not sufficient to meet the varied needs of tree planters in the northern Great Plains. Thus, it is important to continually search for adapted, rapidly growing conifers that can provide evergreen shelterbelts for this region.

Norway spruce (*Picea abies* (L.) Karst.) is one possibility for northern Great Plains shelterbelts. Norway spruce trees are occasionally found in old farmsteads, undoubtedly planted from seeds carried along by early residents.

Prior to our test, the only experimental planting of Norway spruce on the Denbigh Experimental Forest had failed. However, Hoag (1965) observed Nor-

way spruce trees in North Dakota plantations. He contends that the Norway spruce is adaptable to North Dakota. Similarly, Ross (1931) reported Norway spruce as "almost hardy" at Indian Head, Saskatchewan, Canada.

Geographic origin often determines the difference between success and failure for introduced plant material. Early plantings of Norway spruce in North Dakota were probably from German and possibly Scandinavian sources. Trees from these sources may not have been adapted to northern Plains conditions. However, other provenances from climatically similar regions might produce trees adapted to these sites. This hypothesis is strengthened by Logginov's (1964) success of Norway spruce establishment in shelterbelts in the Steppe of the Ukraine from seed of "local" sources. Similarly, Larsen (1956) also reported better results growing Norway spruce in Denmark and southern Sweden from seed of more southerly regions of central Europe than from sources in Finland.

Slabaugh and Rudolph (1957) tested 12 European sources of Norway spruce in Michigan. After the first 15 years they found average heights to range from 1.2 m (3.8 feet) for a Yugoslavian source to 2.2 m (7.3 feet) for a Polish source. They also observed significant differences in frost damage among the 15 sources.

THE STUDY

A small provenance test of Norway spruce seeds from various sources was begun in 1957 on the Denbigh Experimental Forest near Towner, North Dakota and the Pike Bay Experimental Forest near Cass Lake, Minnesota. At the time the study was established, both experimental forests were under direction of the Lakes States Forest Experiment Station. The Denbigh site was intended to test trees under conditions representative of grassland or prairie regions, while the Pike Bay site was more representative of the northern boreal forest.

Seed source locations for the 11 test sources are shown in Table 1. All seed sources except 1864 originated from 6° to 16° north of the planting site, but represented regions of relatively low rainfall and continental temperatures. Provenances 1852 and 1863 represent climates most similar to the North Dakota planting site; whereas, 1853 and 1862 most resemble the Minnesota site. The European origin of 1864 is not known.

Sources 648, 649, 652, 653, and 654 were seeded in the nursery at Rhinelander, Wisconsin in the spring of 1957, transplanted as 2-0 in 1959, and again as 2-2 in 1961. The remaining planting stock was shipped as 3-0 stock to Rhinelander from Petawawa Forest Experiment Station, Ontario, Canada and grown for 2 years in a nursery 50 miles north in Michigan.

All trees were handplanted in tilled ground at Denbigh and on cleared ground at Pike Bay. The plantation design consisted of 4-tree plots of each source, in 10 replications, planted 2.1 x 2.1 meters apart. Trees that died during the first year were replaced in the spring of 1963.

At Denbigh, competing vegetation was subdued by mechanical cultivation each year, with one application of Amazine during the 1966 growing season. At Pike Bay, Amazine was used without any cultivation.

Table 1. Location and climatic characterization of Norway spruce provenances tested on the Denbigh and Pike Bay Experimental Forests.

Seed source	Provenance	North latitude	East longitude	Mean annual temp (°C)[2/]	Precip (mm)[2]	Frost free season (days)[2]
648	Taborinski Dist., U.S.S.R.	58° 30'	64° 30'	0.2	515	105
649	Ust-Vymski Dist., Komi A.S.S.R.	62° 15'	50° 45'	1.6	500	88
652	Zhelesnodorozhny Dist., Komi A.S.S.R.	62° 45'	51° 00'	1.6	500	88
653	Shkalouski Dist., U.S.S.R.	54° 15'	30° 15'	5.8	620	146
654[1/]	Upper Travdinski Dist., U.S.S.R.	58° 00'	65° 30'	1.6	500	88
1844	Olsztyn, Poland	53° 45'	20° 30'	7.3	518	153
1852	Bashkiria, U.S.S.R.	54° 00'	57° 00'	2.5	417	130
1853	Bauske, Latvia	56° 30'	27° 45'	5.3	626	132
1862	Minsk, U.S.S.R.	55° 00'	27° 00'	5.3	626	132
1863	Kaluga, U.S.S.R.	54° 30'	36° 15'	4.7	469	135
1864	Petawawa Forest Experiment Station, Chalk River, Ontario, Canada	46° 00'	77° 30'			150[3/]
	Planting site, North Dakota	48° 45'	100° 00'[4/]	4.1	420	139
	Planting site, Minnesota	47° 30'	94° 45'[4/]	3.8	675	140

[1/] *Picea obovata*

[2/] Based on 1 to 3 weather stations in the region of origin and must be considered approximation.

[3/] Based on Station Zwickau, East Germany.

[4/] West longitude.

RESULTS AND DISCUSSION

After 10 years in the field, the confounding effects of nursery production of the stock are no longer demonstrable. Significant differences among sources are indicated for survival and height variables in most instances where performance seemed good enough to warrant analysis, and where subsequent performance seemed to justify it. From a practical standpoint, however, there is little or no information to be gained by such analyses. Inspection of the means reveal where the practically important differences lie.

Survival.—On the Denbigh Experimental Forest, survival of all sources after six field seasons was unacceptably low, and by the seventh year the plantation average was less than six percent. Two sources had died out completely by 1968 (Table 2). At Pike Bay, in contrast, survival after 10 field seasons was remarkably good for all sources, with a plantation average of almost 95 percent. Because trees from all provenances were growing well at Pike Bay through 1971, their performance will not be discussed in detail in this report.

Survival at Denbigh, even though lower at each successive measurement than at Pike Bay, was averaging enough after 5 years (70 percent) to be encouraging (Table 2). Ranking of sources was about the same from one year to another within plantations, but survival at Pike Bay was consistently better than at Denbigh.

Tests of other spruce species at Denbigh have been comparable to the first five years of this trial. Mean survival after five years in the field at Denbigh for seven sources of blue spruce, *Picea pungens* was 62 percent (Dawson and Rudolf 1966), while 68 percent of 15 sources of white spruce (*Picea glauca*) survived (Nienstaedt 1977). However, none of the critical, cyclical droughts characteristic of the Great Plains occurred during 1962-1965 at Denbigh. It was not until the fifth growing season that droughty conditions appeared. Growing season precipitation, and departure from normal, at Granville, North Dakota (U.S. Weather Bureau substation 10 miles west of the experimental forest) is shown in Table 3.

In midsummer 1966, precipitation was below normal, and the 1967 summer was also unusually dry. It was not until near the end of the 1968 growing season that critically low soil moisture was beginning to be replenished. The water table at Denbigh was relatively high, but spruces were characterisitcally shallow-rooted (Preston 1950). Seedlings in only their fourth or fifth growing season probably were not tapping it.

In 1966 and 1967 precipitation was less than 280 mm (11.0 inches) during April through September, and the combined growing-season precipitation for those 2 years was 503 mm (19.8 inches). Records from nearby Granville, North Dakota show precipitation was that scarce for two consecutive years only three times between 1931 and 1974. It was impossible to determine how much moisture would have been needed during the critical years of 1966 and 1967 to prevent so many spruces from dying, but perhaps few might have survived if irrigated periodically during 1967 while the trees were still little more than seedlings.

TABLE 2. Adaptive responses of Norway spruce by year and seed source at Denbigh, North Dakota and Pike Bay, Minnesota.

		Denbigh Experimental Forest					Pike Bay Experimental Forest					
		1964	1966		1968	1964	1966		1971		1972
Seed Origin number	Latitude (°N)	Survival (%)[1]	Survival (%)	Ave. ht. (cm.)[2]	Survival (%)	Survival (%)	Winter injury[2,3]	Survival (%)	Ave. ht. (cm.)	Survival (%)	Ave. ht. (cm.)	Spring frost damage (%)[2]
652	63	58 c	35 d	33.5	2	92 a	149	92a	38.7	85 a	73.2 c	19.8
649	62	58 c	45 cd	48.5	10	98 a	137	98 a	51.2	88 a	103.9 b	17.6
648	58	85 ab	65 abc	47.5	5	100 a	142	100 a	49.7	92 a	108.2 ab	21.2
654	58	72 bc	52 bcd	54.9	8	100 a	143	100 a	54.6	95 a	120.1 ab	15.5
1844	54	95 a	85 a	60.0	0	98 a	102	95 a	55.5	90 a	106.4 b	23.8
1853	56	90 ab	70 ab	62.8	5	100 a	113	95 a	65.4	88 a	115.2 ab	19.6
1862	55	90 ab	65 abc	72.5	5	98 a	100	95 a	66.4	92 a	113.7 ab	18.8
653	54	90 ab	78 a	68.3	0	100 a	91	98 a	59.1	98 a	106.1 b	20.5
1863	54	75 bc	60 abc	62.5	12	98 a	121	98 a	56.4	98 a	124.1 ab	15.7
1852	54	88 ab	80 a	55.2	12	100 a	119	98 a	54.9	98 a	133.9 a	21.2
1864	46	85 ab	65 abc	70.7	2	95 a	90	90 a	60.4	88 a	117.7 ab	25.3

[1] Survival and height means followed by a common letter are not significantly different at the P = .05 level.
[2] No analyses made of these data.
[3] Accumulated score—the highest score indicates the least amount of damage.

TABLE 3. Growing season precipitation (mm) at the Denbigh Experimental Forest.[1]

Year	April	May	June	July	Aug.	Sept.	Total	Departure from normal
1962	11	104	75	67	56	5	318	- 6
1963	69	82	135	54	28	18	386	+ 62
1964	45	72	129	58	97		447	+122
1965	26	80	65	105	43	83	402	+ 78
1966	30	53	65	44	72	12	276	- 48
1967	106	21	33	3	22	43	228	- 96
1968	16	61	67	43	155	58	400	+ 76

[1]Precipitation actually recorded at Granville, North Dakota, 10 miles west of the Denbigh Experimental Forest.

Based on 1966 data, seed sources from milder climates with long growing seasons (the more southerly populations) survived best at Denbigh. Correlation coefficients r = .81** and r = .62* for growing season and latitude are both significant. In addition, the most vigorous seed sources tended to survive best: r = .63* for 1966 survivals.

Height Growth.—Average heights of more than half the provenances after five field seasons at Denbigh were greater than their counterparts at Pike Bay (Table 2). The provenances which grew best at Denbigh originated from latitudes ranging only 54° to 55° North, excepting provenance 1864 for which the European source is not known. Heights differed significantly among sources at Pike Bay in 1971. Only source 652 from the northernmost latitude was significantly shorter on the average than trees from other provenances, although geographic trends in height were not well defined.

White spruce or any other North American spruce species were not included in the test, but white spruce seed sources were compared to the adjacent stands of Norway spruce at Denbigh and Pike Bay. The Norway spruce heights compared favorably with white spruce only until age five. After 15 years at Pike Bay, Norway spruce averaged about half the height of the white spruce.

Winter Injury and Spring Frost Damage.—Winter injury, which results in needle browning and subsequent needle drop, was estimated periodically in both plantations. It has been a major cause of damage to Norway spruce planted in the Lake States in open field conditions.

Table 2 shows the relationships between winter injury and seed origins, and compares winter injury with other tree characteristics. Seed sources collected

from areas with more severe, short growing seasons, generally more northerly regions, had the least amount of damage. Branches protected by deep winter snow packs do not sustain winter injury. Therefore, a negative correlation between tree height and winter injury might be expected while trees were small, but it was not significant.

Damage from late spring frost also affects Norway spruce planted in the open. In this respect, the species was similar to native white spruce. In 1972 at Pike Bay, trees from two of the most southerly populations showed the most severe (24-25%) damage to new shoot growth (Table 2). Repeated spring frost injury can materially reduce height growth and cause ultimate failure of spruce plantings. It may partially explain the poorer performance of Norway spruce in comparison with white spruce at Cass Lake, Minnesota.

CONCLUSIONS AND RECOMMENDATIONS

Even though seed sources tested at Denbigh have not done well over long time periods thus far, they survived and grew satisfactorily under average Denbigh environmental conditions. Therefore, Norway spruce should not be entirely written off as ill-suited to North Dakota. The tests provide some information to guide the future search for populations adapted to the rigorous climate in the northern Plains.

Based on survival at Denbigh and growth at both Denbigh and Cass Lake, Minnesota, it is clear that northern populations are not adapted. The search probably should not extend north of 55° to 56°N, the latitudes of collections 1853 and 1862.

It is likely that the search area should be limited to the south as well, but data are not available in this respect. Climatic data from Europe and performance in tests elsewhere suggest that the sampling be concentrated in the Polish populations, with limited sampling in contiguous Sudeten, Czechoslovakian and Romanian populations.

The testing program could include greenhouse screening, where new sources are grown in containers under limited soil moisture and other environmental stresses. Those seedlings which satisfactorily withstand the extreme conditions likely to be encountered in the field can be vegetatively propagated and field tested on a variety of sites.

One additional source of material would be well-established Norway spruces growing near North Dakota homesteads. Greenhouse trials of open-of control-pollinated progency from such trees might yield seedlings for further vegetative propagation and testing.

LITERATURE CITED

Dawson, David H. and Paul O. Rudolf. 1966. Performance of seven seed sources of blue spruce in central North Dakota. U.S. Forest Serv. Res. Note NC-5, 4 p. North Central Forest Exp. Stn., St. Paul, Minn.

Hoag, Donald G. 1965. Trees and shrubs of the northern Plains. Inst. for Regional Studies, Fargo, N. Dakota. 376 p.

Larsen, C. Syrach. 1956. Genetics in silviculture. Oliver and Boyd. Edinburgh, Scotland. 224 p.

Logginov, B. I. 1964. Principles of field-protective forestation. U.S. Dep. Agric. and Nat'l Sci. Foundation. 302 p.

Nienstaedt, Hans. 1977. Unpublished data on file. North Central Forest Exp. Stn., Institute of Forest Genetics, Rhinelander, WI.

Preston, Richard J. 1950. North American Trees. Iowa State University Press, Ames, Iowa. 371 p.

Ross, Norman M. 1931. Tree planting in the prairies of Manitoba, Saskatchewan, and Alberta. Dept. Int. Forest Service, Canada. Bulletin 1. 64 p.

Slabaugh, Paul E. and Paul O. Rudolf. 1957. The influence of seed source on Scotch pine and Norway spruce planted in Lower Michigan (fifteen year results) In: Papers of the Michigan Academy of Sciences, Arts, and Letters. XLI (1956):41-52.

VEGETATION AND SOILS OF A GALLERY FOREST BORDERING HOMME RESERVOIR, NORTH DAKOTA

Keith T. Killingbeck and *Richard H. Bares*
Department of Biology
University of North Dakota
Grand Forks, North Dakota 58202

ABSTRACT

Plant community structure and distribution were studied in relation to edaphic and topographic factors in a gallery forest surrounding Homme Reservoir located in northeastern North Dakota. Five forest community types found along the reservoir shores were green ash (*Fraxinus pennsylvanica* var. *subintegerrima*), aspen-elm (*Populus tremuloides, Ulmus americana*), boxelder-basswood (*Acer negundo, Tilia americana*), elm-boxelder and boxelder-birch (*Betula papyrifera*). Soil particle size and electrical conductivity, slope angle and slope aspect were found to be associated with community distribution. Soils in the A horizon were clay loams and sandy clay loams with pH ranging from 6.9 - 7.4 and electrical conductivity from 75 - 310 μmhos/cm. Tree stratum density ranged from 1089 trees/ha in the green ash community to 125 trees/ha in the boxelder-basswood community and had a direct relationship with soil electrical conductivity. Of all trees tallied, 93.4% were smaller than 36 cm DBH. Twice as many stems of young green ash (2-6 cm DBH) were found than of any other tree species. It appears that green ash will dominate this gallery forest in the future with American elm and boxelder being stable associates.

INTRODUCTION

Forests and woodlands occupy only a small portion of North Dakota's landscape yet are an important renewable resource which must be maintained. These communities, located predominantly along perennial and ephemeral watercourses, decrease the loss of topsoil from wind and water erosion, maintain nutrient influxes, provide diverse wildlife habitat and moderate temperatures. Of all natural forest types found in the state, the ash-elm gallery forest is the most important with respect to total acreage and volume of wood (Warner and Chase 1956).

Only in recent years have studies been initiated to gather information on ash-elm gallery forest structure and function. Research concerning forest vegetation along the Sheyenne River (Nelson 1964), the Red River (Wanek 1967) and the Forest River (Wikum and Wali 1974; Killingbeck 1976) has added to our knowledge and should enable more efficient management of these forests.

The present study was conducted along the margin of Homme Reservoir in northeastern North Dakota during the summer of 1974 to 1) describe the structure and distribution of the gallery forest communities, 2) quantify and relate selected edaphic and topographic parameters to community distribution, and 3) to obtain information for prediction of future trends in canopy composition of the forest.

METHODS AND MATERIALS

Community structure was quantified in three forest strata. Tree stratum data

were collected by the point-quarter method (Cottam et. al. 1953; Phillips 1959). Shrub stratum (plants between 1 and 3 m) information was obtained from 2x2 m quadrats placed at each of 34 randomized sampling points located along 11 transect lines. From the data collected, Importance Values (relative density + relative dominance + relative frequency) were computed for all tree and shrub species.

The herb stratum (plants less than 1 m) coverage was documented using a .5 x .5 m quadrat at each point. A single estimate of coverage was made for the entire species complement. Plant identification and taxonomic nomenclature were based on Stevens (1963).

Soil samples from the A horizon were taken along each transect. Samples were air dried and the 2-mm fraction was taken for analysis. Soil particle size was determined by the hydrometer method (Bouyoucos 1951) and soils were assigned to texture classes. A Radiometer Model 51 pH Meter and a Radiometer Model CDB2e Conductivity Meter were used to measure pH and electrical conductivity on a 1:2.5 soil:water suspension (Jackson 1958). Slope gradients were measured at each sampling point with an Abney Level.

DESCRIPTION OF AREA

Homme Reservoir is located in Section 19, T. 157 N., R 55 W. of Walsh County, North Dakota on the South Branch of the Park River, 6.4 km west of the town of Park River (Fig. 1). The area is on the eastern margin of the Williston Basin which extends into portions of South Dakota, Montana, Manitoba and Saskatchewan (Carlson 1966). The present topography and the layer of glacial drift covering the area are a result of glacial action during the Late Wisconsin time of the Pleistocene Epoch (Bluemle 1973).

The Park River itself is a tributary of the Red River of the North. The drainage basin of the South Branch of the Park River varies in elevation from 244 to 458 m above sea level and comprises an area of over 76,900 ha (Farmer, et al. 1974). The reservoir maintains an elevation of 329 m above sea level at maximum pool elevation and has a surface area of 76.4 ha (U.S. Corps of Engineers 1952). A maximum of 6.6 km of shoreline surrounds the reservoir and over 80% of this is occupied by gallery forest.

The soils surrounding the reservoir are predominantly Buse-Barnes loams which developed from glacial till, and Fairdale and LaPrairie soils which formed from alluvial deposits (U.S.D.A. 1972). Both soil types are Mollisoils (U.S.D.A. 1975). The climate is continental with a mean annual precipitation of 43.9 cm, a mean annual temperature of 4.0°C, and a growing season of 122 days (U.S. Dept. Commerce 1965).

RESULTS

A major portion of the vegetation bordering the Park River prior to 1948, when construction of the Homme Dam and Reservoir began (U.S. Corps Engineers 1955), was gallery forest. Gallery forests are those which are found along streams and rivers in regions where low precipitation and/or high

evaporation would otherwise prevent successful tree growth. From analysis of 1937 air photos provided by the Production Marketing Association, U.S.D.A., the area which is now the reservoir floor appears to have been occupied by gallery forest, pastureland and agricultural land. Although no quantitative data are available on pre-dam vegetation, boxelder, bur oak, green ash, American elm, chokecherry, wild plum, paper birch, hazel, ironwood and basswood were the most abundant woody species (U.S. Corps Engineers 1952).

In the present study, five gallery forest community types were found along the margin of the Homme Reservoir. A green ash community was located along the north shore of the reservoir (Fig. 1) on alluvial deposits. The soils were all of the Fairdale and LaPrairie types and were clay loams. The high clay content and flat topography resulted in poor drainage which in part accounted for the relatively high electrical conductivity (Table 2). Green ash dominated the tree stratum (Table 1) having a density of 1,022 trees/ha which was the highest density recorded for any tree species in the study. Total tree stratum density was 1089 trees/ha. Bur oak was the only other species in the tree stratum, but it was not found in the shrub stratum. Juneberry and green ash dominated the shrub stratum. The herb stratum coverage (61%) under the green ash canopy was the highest recorded in the study.

Directly west of the green ash community was an aspen-elm community. These two community types were the only ones to be found on the alluvial Fairdale and LaPrairie soils. A horizons were sandy clay loams with pH values slightly

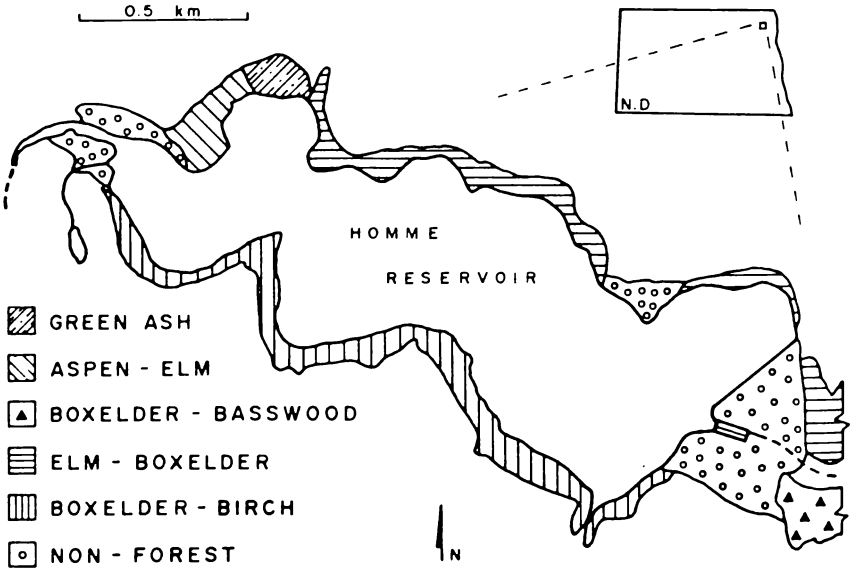

FIGURE 1. Gallery forest communities bordering the Homme Dam and Reservoir.

TABLE 1. Analysis of vegetation for the tree and shrub strata of five gallery forest communities surrounding Homme Reservoir. (I = relative density; II = relative dominance; III = relative frequency; IV = Importance Value)

	I	II	III	IV
GREEN ASH COMMUNITY				
Tree Stratum				
Green ash (*Fraxinus pennsylvanica* var. *subintegerrima*)	93.8	55.9	80.0	229.7
Bur oak (*Quercus macrocarpa*)	6.2	44.1	20.0	70.3
Shrub Stratum				
Juneberry (*Amelanchier alnifolia*)	56.4	34.7	28.8	91.9
Green ash (*Fraxinus pennsylvania* var. *subintegerrima*)	10.9	22.5	28.8	62.2
Beaked hazel (*Corylus cornuta*)	12.7	17.7	19.3	49.7
Downy arrowwood (*Viburnum affine*)	10.9	19.1	28.8	48.8
Chokecherry (*Prunus virginiana*)	7.3	5.3	19.3	32.9
Ironwood (*Ostrya virginiana*)	1.8	0.8	9.6	12.2
ASPEN - ELM COMMUNITY				
Tree Stratum				
Aspen (*Populus tremuloides*)	50.0	41.0	37.5	128.5
American elm (*Ulmus americana*)	31.3	46.6	25.0	102.9
Boxelder (*Acer negundo*)	12.5	8.9	25.0	46.4
Green ash (*Fraxinus pennsylvanica* var. *subintegerrima*)	6.3	3.4	12.5	22.2
Shrub Stratum				
Boxelder (*Acer negundo*)	30.8	32.5	33.3	96.6
American elm (*Ulmus americana*)	15.4	41.5	16.7	73.6
Tall nettle (*Urtica procera*)	30.8	14.0	16.7	61.5
Juneberry (*Amelanchier alnifolia*)	15.4	9.2	16.7	41.3
Aspen (*Populus tremuloides*)	7.7	2.8	16.7	27.2
BOXELDER - BASSWOOD COMMUNITY				
Tree Stratum				
Boxelder (*Acer negundo*)	57.1	40.9	50.0	148.0
Basswood (*Tilia americana*)	28.6	39.6	25.0	93.2
Elm (*Ulmus americana*)	14.3	19.5	25.0	58.8
ELM - BOXELDER COMMUNITY				
Tree Stratum				
American elm (*Ulmus americana*)	34.1	47.0	38.2	119.3
Boxelder (*Acer negundo*)	31.8	18.1	28.8	78.7
Bur oak (*Quercus macrocarpa*)	20.5	26.5	18.9	65.9
Green ash (*Fraxinus pennsylvanica* var. *subintegerrima*)	13.6	8.4	14.1	36.1
Shrub Stratum				
Chokecherry (*Prunus virginiana*)	82.7	75.2	36.4	194.3
Green ash (*Fraxinus pennsylvanica* var. *subintegerrima*)	6.7	8.6	18.2	33.6
American elm (*Ulmus americana*)	1.3	10.9	9.1	21.3
Boxelder (*Acer negundo*)	4.0	4.0	9.1	17.1
Buckbrush (*Symphoricarpos occidentalis*)	2.7	0.8	9.1	12.7
Hawthorne (*Crataegus rotundifolia*)	1.3	1.5	9.1	11.9
Bur oak (*Quercus macrocarpa*)	1.3	0.9	9.1	11.3

BOXELDER - BIRCH COMMUNITY

Tree Stratum				
Boxelder (*Acer negundo*)	26.9	19.7	20.1	66.7
Green ash (*Fraxinus pennsylvanica* var. *subintegerrima*)	21.2	15.2	20.1	56.5
American elm (*Ulmus americana*)	15.4	19.4	16.6	51.4
Bur oak (*Quercus macrocarpa*)	9.6	29.9	10.0	49.5
Ironwood (*Ostrya virginiana*)	13.5	4.7	16.6	34.8
Basswood (*Tilia americana*)	9.6	10.6	10.0	30.2
Paper birch (*Betula papyrifera*)	3.8	0.6	6.5	10.9
Shrub Stratum				
Juneberry (*Amelanchier alnifolia*)	3.8	31.2	20.1	70.0
Green ash (*Fraxinus pennsylvanica* var. *subintegerrima*)	11.4	28.7	15.0	55.1
Ironwood (*Ostrya virginiana*)	12.9	12.2	15.0	41.1
Boxelder (*Acer negundo*)	5.7	8.4	5.0	19.1
Buckbrush (*Symphoricarpos occidentalis*)	7.1	5.0	5.0	17.1
Blackhaw (*Viburum lentago*)	8.6	3.4	5.0	17.0
Chokecherry (*Prunus virginiana*)	4.3	2.8	9.8	16.9
Paper birch (*Betula papyrifera*)	4.3	2.5	5.0	11.8
American elm (*Ulmus americana*)	1.4	2.8	5.0	9.2
Beaked hazel (*Corylus cornuta*)	2.9	1.2	5.0	9.1
Smooth wild rose (*Rosa blanda*)	1.4	1.2	5.0	7.6
Downy arrowwood (*Viburnum affine*)	1.4	0.5	5.0	6.9

TABLE 2. Selected soil characteristics for each community type. (SCL, sandy clay loam; CL, clay loam)

Community	pH	Electrical Conductivity (μmhos/cm)	Sand	Silt	Clay	Texture Class
			%			
Green ash	7.3	310	46.0	25.0	29.0	CL
Aspen-Elm	6.9	140	60.5	11.8	27.7	SCL
Boxelder-Basswood	7.4	75	51.5	18.5	30.0	SCL
Elm-Boxelder	7.1	88	67.7	8.0	24.3	SCL
Boxelder-Birch	7.3	184	56.9	18.6	24.5	SCL

lower than those of A horizons in other community types. Aspen, the dominant in the community, had a density of 407 trees/ha. Boxelder, though less important than aspen and American elm in the tree stratum, was the most important shrub stratum species. This was the only community in which aspen appeared in the shrub stratum. Herb stratum coverage was 40%.

A small area below the dam along the Park River was occupied by a boxelder-basswood community. The Buse-Barnes soils were sandy clay loams with the lowest electrical conductivity found in the study (Table 2). Boxelder dominated

the tree stratum but had a density of only 71 trees/ha. The total tree stratum density (125 trees/ha) was the lowest of all community types. Basswood and American elm made up the rest of the tree stratum. This area appears to have been grazed in the recent past which may account for the virtually nonexistent shrub stratum and sparse herb stratum coverage (25%).

Much of the north shore of the reservoir and an area north of the Park River below the dam was covered by an elm-boxelder community. The terrain angled up and away from the shoreline with slope gradients reaching a maximum of 28 degrees (mean slope 14 degrees). The sandy clay loam texture of the Buse-Barnes loams and the sloping relief resulted in well drained soils. The tree canopy was dominated by American elm followed by boxelder and bur oak. The density of this relatively open canopy was 473 trees/ha. The small green ash component of the tree stratum was composed predominantly of young trees. The shrub stratum was dominated by chokecherry and contained hawthorns, which were not found in any other community type. The low coverage in the herb stratum (30%) was, in part, a result of dense shrub cover.

A boxelder-birch community, the most extensive around the reservoir, occupied the whole south shoreline. The terrain was varied but steep slopes of up to 43 degrees were common. All soils were well drained Buse-Barnes loams. Seven species were found in the tree stratum and 12 in the shrub stratum. Boxelder, green ash, American elm and bur oak dominated the forest canopy which had an overall density of 1085 trees/ha. The steep, north-facing slopes of this community were the only areas where paper birch occurred. The most important shrub stratum members were Juneberry, green ash and ironwood. Of the "tree" species which were observed in the shrub stratum, green ash was by far the most dominant. Herb stratum coverage (37%) was relatively low.

DISCUSSION

The five gallery forest communities surrounding the Homme Reservoir appeared to be variants of the ash-elm forest type described by Warner and Chase (1956). This major forest type makes up over one-third of North Dakota's forested area. All forest elements in the present study were deciduous with most being representatives of the eastern deciduous forest. However, several plant species, such as Juneberry and paper birch, were of boreal origin (Rudd 1951).

Both topographic and edaphic factors affected the distribution of the five community types in this study. The green ash community was restricted to soils with the highest levels of dissolved salts and the highest silt + clay fraction (Table 2). These values indicate potentially high levels of nutrient reserves in the soil since the large clay fraction provides great numbers of exchange sites for ion adsorption. This community had a higher tree density (1089 trees/ha) than any other. The nutrient status of the soils may, in part, explain this high density.

In contrast to the green ash community, the higher content of sand in the soils under the adjacent aspen-elm community provided better drainage with less accumulation of salts. Since shade intolerant aspen was the dominant species in the

tree stratum, it is possible that a previous disturbance in this localized area eliminated most of the original trees, enabling aspen to invade the area. Although some aspen regeneration was occurring, the soils were probably too sandy for optimum aspen growth (Bares 1976; Stoeckeler 1948).

The two communities covering the largest extent of reservoir margin, boxelder-birch and elm-boxelder, occupied opposite sides of the reservoir. The elm-boxelder community was found only on the south-facing shoreline on moderate slopes. The boxelder-birch type was located exclusively on north-facing slopes which were generally steeper than those on the opposite shore. Of the two, the boxelder-birch community had soils with higher silt + clay content and electrical conductivity (Table 2). These differences along with the moderating effect on temperature and evaporation by the north-facing aspect may account for dif-

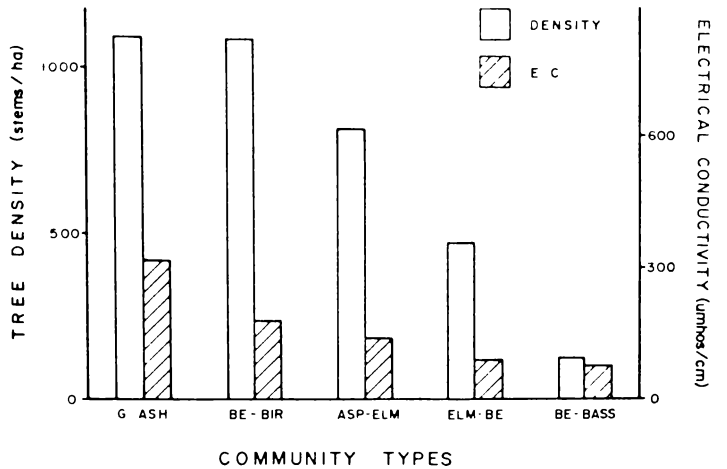

FIGURE 2. Relationship between total tree density and A horizon soil electrical conductivity for the five community types studied.

ferences in species diversity (Table 1) and total tree density, between the boxelder-birch (1085 trees/ha) and elm-boxelder (473 trees/ha) communities.

A direct relationship existed between soil electrical conductivity and tree stratum density for all communities (Fig. 2) indicating the influence of this edaphic factor on community structure as well as community distribution. Since soil conductivity is a measure of total dissolved salts, high tree density may be, in part, a result of relatively high levels of nutrients. A similar relationship was found between tree density and A horizon soil conductivity on two opposing slopes in another North Dakota gallery forest along the Forest River (Killingbeck 1976).

Much of the vegetation surrounding the Homme Reservoir can be categorized as young gallery forest in a state of transition. Over 93% of all trees tallied were

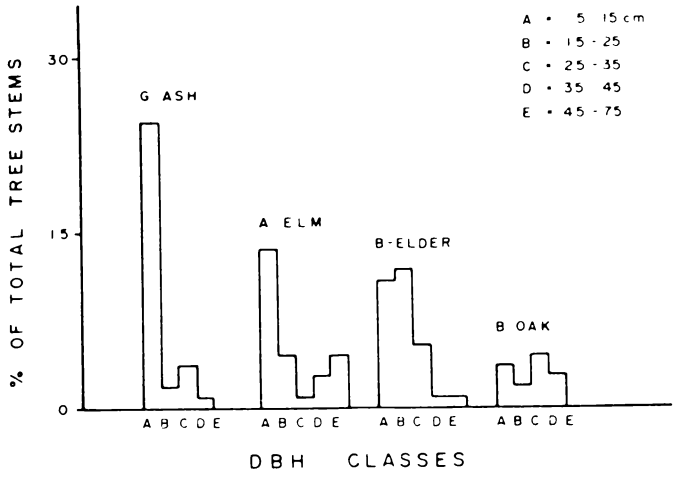

FIGURE 3. DBH class distribution given for the four major tree species as a percentage of the total tree stems of the four major tree species.

smaller than 36 cm DBH. In all but the boxelder-birch community, green ash comprised much of the young growth. Almost 20% of all tree stems were green ash. Of the four major tree species stems, 24.5% were green ash (Fig. 3). Of all ash stems, 79.4% were in the 2-6 cm DBH class indicating the predominance of young green ash growth. Of the four communities having a shrub stratum, three of these had green ash as the most dominant "tree" species.

Regeneration of American elm and boxelder appears to be sufficient to assure their future presence in the forest communities. Bur oak, however, was found only in the shrub stratum of one community and had few young stems in the tree stratum (Fig. 3). It seems very probable, therefore, that green ash will dominate the forest canopy in the future with American elm and boxelder being stable associates.

ACKNOWLEDGMENTS

Funds for this study were provided by the U.S. Corps of Army Engineers of St. Paul District under contract no. DACW 37-74-C-0066 to the Institute of Ecological Studies, University of North Dakota. Thanks are extended to Dr. Mohan K. Wali, University of North Dakota, for comments on the manuscript.

LITERATURE CITED

Bares, R. H. 1976. Nutrient relations of some Northern Minnesota forest communities. Master's Thesis, Univ. of North Dakota, Grand Forks. 93 p.

Bleumle, J. P. 1973. Geology of Nelson and Walsh Counties, North Dakota. North Dakota Geol. Surv. Bull. 57, Part 1. 70 p.

Bouyoucos, J. 1951. A recalibration of the hydrometer method for making mechanical analysis of soils. Agron. J. 43: 434-438.

Carlson, C. G. and S. B. Anderson. 1965. Sedimentary and tectonic history of North Dakota part of Williston Basin. Bull. Amer. Assoc. Petrol. Geol. 49: 1833-1846.

Cottam, G., J. T. Curtis and B. W. Hale. 1953. Some sampling characteristics of a population of randomly distributed individuals. Ecology 34: 741-745.

Farmer, C. E., L. M. Winczewski, K. T. Killingbeck, G. E. Johnson, R. D. Ludtke, R. H. Pilatzke, A. Carmichael and J. P. Jorgenson. 1974. Environmental Impact Assessment of the Homme Dam and Reservoir, North Dakota. Res. Rpt. No. 7., Inst. Ecol. Stud., Univ. of North Dakota, Grand Forks. 189 p.

Jackson, M. L. 1958. Soil Chemical Analysis. Prentice-Hall, Inc., Englewood Cliffs, New Jersey. 498 p.

Killingbeck, K. T. 1976. Aspects of nutrient cycling and productivity in an eastern North Dakota gallery forest. Ph.D. Dissertation. Univ. of North Dakota, Grand Forks. 184 p.

Nelson, P. W. 1964. The forests of the lower Sheyenne River valley, North Dakota. M.S. Thesis, North Dakota State Univ., Fargo. 148 p.

Phillips, E. A. 1959. Methods of Vegetation Study. Holt, Reinhardt & Winston, Inc., New York. 107 p.

Rudd, V. E. 1951. Geographical affinities of the flora of North Dakota. Am. Mid. Nat. 45: 722-739.

Stevens, O. A. 1963. Handbook of North Dakota Plants. North Dakota Institute for Regional Studies, Fargo, North Dakota. 324 p.

Stoeckeler, J. H. 1948. The growth of quaking aspen as affected by soil properties and fire. J. For. 46: 727-737.

U.S. Corps of Engineers. 1952. Homme Reservoir, Park River, North Dakota. Master Recreation Plan. St. Paul District. 21 p.

U.S. Corps of Engineers. 1955. Flood Control, South Branch Park River, North Dakota, Homme Dam and Reservoir, Reservoir Regulation Manual. St. Paul District. 28 p.

U.S. Department of Agriculture. 1937. Air photos. Production Marketing Association Staff.

U.S. Department of Agriculture. 1960. Soil Classification: A Comprehensive System, 7th Approximation (revised edition). Soil Survey Staff, Soil Conservation Service. 265 p.

U.S. Department of Agriculture. 1972. Soil Survey of Walsh County. Soil Conservation Service. 126 p.

U.S. Department of Commerce. 1965. Climatic Survey of the United States, 1951 through 1960, North Dakota. Weather Bureau. 265 p.

Wanek, W. J. 1967. The gallery forest vegetation of the Red River of the North. Ph.D. Dissertation. North Dakota State Univ., Fargo. 211 p.

Warner, J. R. and C. D. Chase. 1956. The Timber Resource of North Dakota. U.S.D.A. Forest Service, Lakes States For. Exp. Sta. Paper No. 36. 39 p.

Wikum, D. A. and M. K. Wali. 1974. Analysis of a North Dakota gallery forest: Vegetation in relation to topographic and soil gradients. Ecol. Monogr. 44: 441-464 + appendix.

SOME NUTRIENT DEFICIENCY AND TOXICITY SYMPTOMS IN SLENDER WHEATGRASS

Patricia A. Schwartz and N. M. Safaya
Project Reclamation
University of North Dakota
Grand Forks, North Dakota 58202

ABSTRACT

In view of the importance of revegetating the surface mined areas in the Northern Great Plains Coal Province, nutritional studies on the prairie plants have become essential. This study pertains to a hydroponic experiment on slender wheatgrass (*Agropyron trachycaulum* (Link) Malte). Plants were raised for 27 and 54 days in continuously aerated Hoagland's nutrient solution, using 1.5 liter plastic pots. Deficiency of N, P, K, Fe, Mn, Zn, Cu, B and Mo was induced by omitting each nutrient singly from the solution. Control plants received all the nutrients and those for toxicity study received Zn, Cu, B or Mo at rates 4 times higher than that in the control treatment. The study was conducted in a growth-chamber maintained at 25°C (day)/15°C (night) temp., 12 hr. photoperiod and 50% rel. humidity. Growth of *A. trachycaulum* was severely affected by -N, -P and -K treatments. However, the plants appeared to be most sensitive to K deficiency which caused extremely reduced shoot and root growth with progressive loss of dry matter. Except for typical chlorosis in Fe deficient plants, and tip burning in case of B excess, deficiency or toxicity symptoms of other micronutrients failed to appear. In the -N and -P nutrient media the shoot/root ratio was substantially reduced. A comparison of plant growth accomplished in control, Zn deficient, and Zn excess treatments revealed that this species has perhaps very low requirement for Zn. A mutual antagonistic relationship between K and Fe was observed.

INTRODUCTION

Among the diagnostic criteria used for assessing the nature and magnitude of nutrient disorders in plants, specific visual symptoms, and plant analysis techniques have been used with great success (Wallace, 1961; Chapman, 1965). However, the earlier notions which frequently implied a quantitative and even qualitative uniformity in the mineral requirements of plants are undergoing a radical change (Gerloff, 1963). It is being increasingly realized that different species and even varieties and ecotypes differ greatly in their mineral requirements (Bradshaw and Snaydon, 1959; Millikan, 1961; Vose, 1963; Brown et al., 1972). The variability in plants to absorb certain nutrients at different rates from solutions of similar concentration, has been considered important in relation to their ecological distribution (Bollard and Butler, 1966; Loneragan, 1968). It is also known that the specific symptoms of deficiency or excess of an element exhibited by a certain species may greatly differ from those exhibited by another species. Thus, in order to be able to make use of foliar diagnostic techniques in assessing the nutritional status of any plant, a prior knowledge of its specific responses to the deficiency and excess of nutrient elements is essential. Exhaustive information on such aspects is available for a large number of cultivated species. But, as stated by Billings (1957), "there are all too few mineral nutrition studies on wild plants of any kind." Even twenty years after this statement, enthusiasm for undertaking such studies on uncultivated species has been generally lacking.

Nutritional studies on uncultivated species are essential with respect to the revegetation of disturbed lands resulting from surface mining operations. In the Northern Great Plains surface mining for coal has lain bare large acreages of land, and to reclaim these areas emphasis is being given to the reintroduction of desirable native species. Slender wheatgrass (*Agropyron trachycaulum* (Link) Malte) is a native species of the Midwest prairie. It forms a significant component of the prairie vegetation. Obviously, before its reintroduction in the surface mined areas, which generally exhibit fertility problems of various kinds, an understanding of its responses to various nutrient stresses would be greatly useful. With this purpose in mind, a preliminary hydroponic experiment designed to produce symptoms of different nutrient deficiencies and toxicities was conducted using slender wheatgrass as the test plant.

MATERIAL AND METHODS

Seeds of slender wheatgrass were germinated and the resulting seedlings of uniform size allowed to grow for periods of 27 and 54 days in 1.5 liter of modified Hoagland's nutrient solution placed in plastic pots. Four polyethylene tubes (4 cm long and 1 cm in diameter) were passed through holes in the lid of each culture vessel. The ends of the tubes were closed with nylon mesh to facilitate the direct placement of seeds on the surface of nutrient solution. Eight plants were grown in each culture vessel. Different deficiency treatments were created by following Dutt and Bergman's (1966) scheme of omitting singly, N, P, K, Fe, Mn, Zn, Cu, B and Mo from the otherwise complete nutrient solution which served as the control. In other treatments, Zn, Cu, B or Mo were supplied to plants at rates four times higher than in the control. All the treatments were replicated twice. The composition of stock solutions and amount of each taken to make the dilute nutrient solution of each treatment are summarized in Tables 1 and 2. The final concentrations of different salts in the complete nutrient medium were:

1.00 mM $NH_4H_2PO_4$	5.75 mM $Ca(NO_3)_2$
1.45 mM $CaCl_2$	2.00 mM $MgSO_4$
6.00 mM KNO_3	6.00 μM H_3BO_3
1.23 μM $MnCl_2.4H_2O$	0.20 μM $ZnCl_2$
0.06 μM $CuCl_2.2H_2O$	0.03 μM $H_2MoO_4.H_2O$

Iron at the rate of 795 μg/l was provided as Fe-EDTA (iron complex of disodium ethylenediaminetetraacetic acid). All solutions were prepared with distilled-deionized water. The cultures were continuously aerated and occasional additions of distilled-deionized water were made to each culture vessel to maintain the initial volume. Solutions were completely renewed at biweekly intervals. The entire study was conducted in an environment controlled growth chamber maintained at 25° C day and 15° C night temperature, 12 hour photoperiod and 50% relative humidity.

The plants growing under different nutrient treatments were examined for the appearance of nutrient deficiency and toxicity symptoms regularly. At the end of

27 and 54 days plants were photographed, removed from their respective solutions, washed with distilled-deionized water and separated into root and shoot fractions. The plant samples were dried for 36 hours at 70°C in a force-draft oven and their dry weights were taken. Shoot material from each treatment was ground in a stainless steel mill and after drying it again wet ashed using 1 ml concentrated H_2SO_4 and 0.25 ml of 30% H_2O_2 per 50 mg sample. Total P was determined by chlorostannous molybdophosphoric blue method as described by Johnson and Ulrich (1959) using a Bausch and Lomb spectronic 21. Analysis for K, Ca, Mg, Fe and Zn was carried out on a Perkin Elmer Model 403 atomic absorption spectrophotometer.

RESULTS AND DISCUSSION

i. Visual Symptoms: Slender wheatgrass plants growing in solutions from which N, P, K or Fe respectively were omitted exhibited characteristic symptoms of each deficiency (Fig. 1). However, except for a general decrease in growth, specific symptoms of the deficiencies of other elements failed to appear. In treatments with elevated (x4) Zn, Cu, B or Mo concentrations in the culture solutions, the Zn-treated plants alone were reduced in size and those receiving high B exhibited discrete tip burning on all the leaves. The characteristic deficiency symptoms for N, P, K and Fe as recorded for this species are summarized below.

TABLE 1. Stock Solutions

Chemical	Amount (g/l)	Molarity (M)
A. $NH_4H_2PO_4$	46	0.40
B. NH_4NO_3	80	1.00
C. $Ca(NO_3)_2$	378	2.30
D. $CaCl_2$	58	0.58
E. $MgSO_4.7H_2O$	198	0.80
F. KH_2PO_4	54	0.40
G. KNO_3	242	2.40
H. K_2SO_4	174	1.00
I. H_3BO_3	1.44	2.40×10^{-2}
J. $CuCl_2.2H_2O$	0.04	0.024×10^{-2}
K. $MnCl_2.4H_2O$	0.90	0.460×10^{-2}
L. $ZnCl_2$	0.12	0.088×10^{-2}
M. $H_2MoO_4.H_2O$	0.02	0.012×10^{-2}

N. Fe EDTA (2.68 gm of disodium ethylenediaminetetraacetate were dissolved in 500 ml of distilled water and heated and while still hot 1.98 gm of $FeSO_4.7H_2O$ were added to this and stirred vigorously).

TABLE 2. Milliliters of various stock solutions taken for making 1.5 liter dilute nutrient solution of different types.*

	A	B	C	D	E	F	G	H	I	J	K	L	M	N
Complete	3.75	X	3.75	3.75	3.75	X	3.75	X	0.4	0.4	0.4	0.4	0.4	1.5
-N	X	X	X	15.75	3.75	3.75	X	3.75	0.4	0.4	0.4	0.4	0.4	1.5
-P	X	0.75	3.75	3.75	3.75	X	3.75	X	0.4	0.4	0.4	0.4	0.4	1.5
-K	3.75	4.5	3.75	3.75	3.75	X	X	X	0.4	0.4	0.4	0.4	0.4	1.5
-Fe	3.75	X	3.75	3.75	3.75	X	3.75	X	0.4	0.4	0.4	0.4	0.4	X
-Mn	3.75	X	3.75	3.75	3.75	X	3.75	X	0.4	0.4	X	0.4	0.4	1.5
-Zn	3.75	X	3.75	3.74	3.75	X	3.75	X	0.4	0.4	0.4	X	0.4	1.5
-Cu	3.75	X	3.75	3.75	3.75	X	3.75	X	0.4	X	0.4	0.4	0.4	1.5
-B	3.75	X	3.75	3.75	3.75	X	3.75	X	X	0.4	0.4	0.4	0.4	1.5
-Mo	3.75	X	3.75	3.75	3.75	X	3.75	X	0.4	0.4	0.4	0.4	X	1.5
+Zn (X4)							Same as for complete						1.6	
+Cu (X4)							Same as for complete				1.6			
+B (X4)							Same as for complete			1.6				
+Mo (X4)							Same as for complete						1.6	

*Different stock solutions are represented as A, B, C . . . N. The chemicals used to make each one of them are shown in Table 1.

FIGURE 1. Response of slender wheatgrass to some nutrient deficiencies. (From *left* to *right*: control-no deficiency, iron deficient, phosphorus deficient, nitrogen deficient and potassium deficient plants.)

Nitrogen: Progressive fading of the leaves resulting in dusky brown color followed by tip dying; restricted growth rate leading to very small tillerless plants as compared to the control.

Phosphorus: Spindly growth; purple pigmentation on older leaves; younger leaves dark green; restricted growth.

Potassium: Extremely reduced plant growth; progressive leaf scorching starting from tips and spreading towards leaf base; the scorched areas of leaves turn ash-white and papery and finally drop off.

Iron: Yellowing and chlorosis of youngest leaves, followed by chlorosis of almost all the leaves except the oldest; growth of plants slightly restricted.

ii. *Dry matter yield:* The data pertaining to shoot and root dry matter yield of 27 and 54 day old plants as affected by different nutrient deficiencies and excesses are given in Table 3. Slender wheatgrass was found to be extremely sensitive to K deficiency which started appearing as early as 10 to 12 days after germination. The progressive loss of dry matter in K-deficient plants was obviously due to extreme withering of leaves. Root growth also was the most affected with this deficiency. In -N and -P cultures plants suffered severe reductions in shoot growth but at the 27 day stage the root weights in these

TABLE 3. Dry matter yield of 27 and 54 day old slender wheat grass plants as affected by different nutrient deficiencies and excesses.

Treatments	27 days			54 days		
	Shoot	Root	Whole Plant	Shoot	Root	Whole Plant
	mg/10 plants					
Control	90	18	108	645	106	751
-N	48	37	85	34	89	123
-P	57	30	87	57	70	127
-K	37	3	40	10	2	12
-Fe	90	48	138	283	165	448
-Mn	50	5	55	496	84	570
-Zn	114	31	145	902	137	1039
-Cu	100	24	124	216	37	253
-B	113	22	135	350	64	414
-Mo	92	13	105	444	69	513
+Zn (x4)	68	9	77	205	36	241
+Cu (x4)	90	12	102	488	84	572
+B (x4)	90	15	105	484	71	555
+Mo (x4)	62	9	71	448	70	518

TABLE 4. Chemical composition of 27 day old slender wheat grass shoots as affected by different nutrient deficiencies and excesses.

Treatment	P	K	Ca	Mg	Fe	Zn
	% dry wt.				ppm dry wt.	
Control	1.14	3.41	0.40	0.16	153	91
-N	0.79	1.97	0.20	0.05	184	184
-P	0.19	2.00	0.31	0.17	63	75
-K	2.05	0.45	0.39	0.36	773	68
-Fe	1.53	5.00	0.33	0.17	60	213
-Mn	1.44	3.63	0.56	0.23	513	75
-Zn	1.18	4.12	0.39	0.17	127	37
-Cu	1.30	3.95	0.37	0.21	120	55
-B	0.96	3.01	0.38	0.15	110	51
-Mo	1.14	3.75	0.35	0.14	109	60
+Zn (X4)	1.23	4.12	0.39	0.25	79	134
+Cu (X4)	1.22	4.10	0.48	0.16	111	69
+B (X4)	1.09	3.75	0.50	0.24	102	88
+Mo (X4)	1.10	3.40	0.38	0.13	80	70

treatments were higher than in the control plants. Both at 27 and 54 day stage -N and -P plants had very low shoot/root ratio as compared to control or other treatments. Initially plant growth did not seem to be adversely affected in cultures from which Fe, Mn, Zn, Cu, B or Mo were omitted. In fact the growth of plants in some of these treatments appeared to be better than in the complete nutrient medium. However at the 54 day stage, the growth of plants under all these treatments (except that in -Zn) was lower than the control. In this group of treatments Cu deficiency seemed to have the greatest effect in decreasing dry matter yield. However, paradoxically, the dry matter yield of plants grown in -Zn cultures was highest at both the stages of growth. From this it was obvious that cultures which did not receive Zn salt contained some traces of Zn as contamination. Since the control plants gave lower dry matter yield than those growing in the Zn-deficient cultures, it is implied further that perhaps the actual requirement of slender wheatgrass for Zn is very low and that the relatively higher amounts of Zn provided by the complete nutrient medium may be detrimental. This inference was further supported when plants supplied with 4 times higher Zn rate were found to have very low dry matter yield. High levels of Cu, B or Mo in the nutrient medium also decreased dry weight of plants, but the decrease was not of the same magnitude as observed in case of Zn excess.

iii. *Chemical Composition.* The changes resulting in the P, K, Ca, Mg, Fe and Zn content of shoots of slender wheatgrass, under different nutrient deficiencies and excesses are presented in Table 4. Nitrogen deficient plants revealed lower concentration of P, K, Ca and Mg, but higher concentration of Fe and Zn. Omission of P from nutrient medium resulted in extremely low P status of plants and also decreased their Fe content. Potassium deficient plants revealed higher concentration of P but their Fe concentration was extremely high. On the contrary plants grown in -Fe medium exhibited highest K and Zn concentrations while their Fe content was only about two and a half times lower than the control plants. Manganese deficient plants accumulated large amounts of Fe and Ca in their shoots. Plants grown in -Zn cultures revealed fairly adequate Zn status, which is further proof that these cultures were contaminated. Other treatments did not seem to have any appreciable effect on the composition of plant tops which could be considered significantly different from what was found for control plants.

The high concentration of Zn in N deficient plants is perhaps due to a lack of adequate amount of proteins in the root tissues which otherwise bind Zn in the form of certain complexes, thereby reducing its translocation to the shoot (Ozanne, 1955). Likewise high level of Fe in the shoots of Mn deficient plants can be explained on the basis of Epstein and Stout's (1951) observation that Mn application reduces the absorption and translocation of Fe. The unusually high concentration of Fe in -K plants and that of K in -Fe plants reflects an antagonistic relation between these two nutrients. Although high accumulation of Fe in the nodes of corn plants as one of the first indications of K deficiency had been observed earlier (Hoffer, 1930), a mutually an-

tagonistic relationship between Fe and K has received little mention in the literature.

ACKNOWLEDGMENTS

The study was supported by Grant No. G0264001 from the USDI, Bureau of Mines. The suggestions and criticism offered by Mr. Alden Kollman, Project Manager, are gratefully acknowledged.

LITERATURE CITED

Billings, W. D. 1957. Physiological Ecology. Ann. Rev. Plant Physiol., 8: 375-392.

Bollard, E. C. and G. W. Butler. 1966. Mineral nutrition of plants. Ann. Rev. Plant Physiol., 17:77-112.

Bradshaw, A. D. and R. W. Snaydon. 1959. Population differentiation within plant species in response to soil factors. Nature, 183, 129-30.

Brown, J. C., J. E. Ambler, R. L. Chaney, and C. D. Foy. 1972. Differential responses of plant genotypes to micronutrients. P. 389-418. In J. J. Mordvedt, P. M. Giordano and W. L. Lindsay (ed). Micronutrients in Agriculture, Soil Sci. Soc. Am. Inc., Madison, Wisc.

Chapman, Homer D. [ed.]. 1965. Diagnostic Criteria for Plants and Soils. University of California, Berkeley. P. 793.

Dutt, J. O. and E. L. Bergman. 1966. Nutrient solution culture of plants. Penn. State Agri. Ext. Ser. Veg. Crops 2.

Epstein, E. and P. R. Stout. 1951. The micronutrient cations iron, maganese, zinc and copper: their uptake by plants from the absorbed state. Soil Sci. 72:47-65.

Gerloff, G. C. 1963. Comparative mineral nutrition of plants. Ann. Rev. Plant Physiol. 14:107-124.

Hoffer, G. H. 1930. Testing corn crop chemically to aid in determining the plant food needs. Purdue Univ. Agric. Exp. Station Bull. 298.

Johnson, C. M. and A. Ulrich. 1959. Analytical methods for use in plant analysis. Bull. Calif. Agric. Exp. Stn. No. 766.

Loneragan, J. F. 1968. Nutrient requirements of plants. Nature 220:1307-1308.

Millikan, C. R. 1961. Plant varieties and species in relation to the occurrence of deficiencies and excesses of certain nutrient elements. J. Aust. Inst. Agric. Sci. *26*:220-223.

Ozanne, P. G. 1955. The effect of nitrogen on zinc deficiency in subterranean clover. Aust. J. Biol. Sci. 8:47-55.

Vose, P. B. 1963. Varietal differences in plant nutrition. Herb. Abstr. *33*: 1-13.

Wallace, T. 1961. The Diagnosis of Mineral Deficiencies in Plants by Visual Symptoms, A colour Atlas and Guide. Chemical Publishing Co., New York. P. 125+ color plates.

USE OF VOLCANIC ASH IN WASTE TREATMENT FOR PHOSPHORUS REMOVAL

Yung-Tse Hung, Ronald E. Gullicks, Guilford O. Fossum
Department of Civil Engineering
University of North Dakota
Grand Forks, North Dakota 58202

and

C. P. Hwang
Department of Civil Engineering
University of Saskatchewan
Saskatoon, Saskatchewan, Canada

ABSTRACT

Volcanic ash from Linton, North Dakota was investigated for its effectiveness as adsorbent for the removal of phosphorus (P) from wastewaters. For an influent P concentration of 10 mg/l, P removal efficiency varied from 0 to 82% in the shaking type batch tests. Contact time longer than half an hour did not improve P removal efficiency. Increasing volcanic ash particle size resulted in decreasing efficiency of P removal. Continuous flow type tests indicated P removal efficiency ranged from 0 to 13.2%, and 0 to 43.2% for the filtration column for - No. 8 to + No. 16 material, and No. 30 to + No. 50 material, respectively.

INTRODUCTION

Excessive eutrophication in lakes and streams in the country has pointed to the need for controlling plant nutrients in the wastewaters. Of the major nutrients other than carbon, removal of phosphorus (P) from wastewater treatment plan effluents has been suggested as a means of effective control by several investigators (Eberhardt, Nesbitt 1968; Sawyer 1962; Sawyer 1952). In the last 20 years phosphorus quantity in sewage has increased almost four times due to the extensive use of synthetic detergents. The removal of P from wastewater effluents has been a major area of research in the field of water pollution control. Processes applicable for P removal include ion exchange, electrochemical treatment, electrodialysis, reverse osmosis, biological treatment, chemical treatment and sorption (Elliassen, Tchobanoglous 1968). The most promising and most studied methods appear to be chemical treatment, biological treatment or the combination of the two. Sorption for P removal has been the least investigated method. Culp and Ames (1970) reported that 98% P removal by activated alumina column from secondary treated effluent was obtained in a pilot plant experiment. Selective removal of mixed phosphate from water streams by activated alumina also was studied by Yee (1965). Removal efficiencies up to 90% were accomplished without adding any salts to the water for pH adjustment.

A volcanic ash deposit in south-central North Dakota was reported by Stanton (1917). Manz (1962) reported that this deposit lies in the Fox Hills Sandstone

about 35 feet (10.67 m) above the top of the Pierre Shale. He suggested that the material was carried a long distance in the air and deposited in the area. The nearest probably source, according to the present knowledge of cretaceous volcanism in the Rocky Mountains, is the Livingston region in Montana, about 500 (804 km) miles to the West of Linton, North Dakota. It was estimated that there are over 500 million tons (453 million metric tons) of volcanic ash in this deposit. Volcanic ash is primarily mined for use as an abrasive in cleaning compounds, a pozzolanic admixture in concrete, component of concrete aggregate and acoustic plaster, railroad ballast and a soil stabilizing agent in road construction. According to the U.S. Bureau of Mines Minerals Yearbook (1973), 3.77 million tons (3.42 million metric tons) of pumic, pumicite, and volcanic cinder were sold or used by producers. Little information is available on the utilization of volcanic ash in the field of waste treatment. The purpose of this study was to evaluate the effectiveness of volcanic ash from Linton, North Dakota for use as adsorbent for P removal from domestic wastewater.

MATERIALS AND METHODS

Volcanic Ash — The sample of volcanic ash from Linton, North Dakota, was a very fine grained, angular shaped rock of 3 to 6 inch (7.62 to 15.24 cm) least dimension. It had a very low resistance to abrasion and was easily crushed to smaller particle sizes. A physical analysis is presented in Table 1.

The high ratio of surface area to volume, 10,000 cm^2/cm^3 renders the ash an excellent adsorbing media. Table 2 shows chemical analysis of a typical Linton area volcanic ash. The main constituents are silicon dioxide SiO_2, aluminum oxide Al_2O_3, iron oxide Fe_2O_3, calcium oxide CaO, and magnesium oxide MgO.

PROCEDURE

The phosphate adsorption capacity of volcanic ash was evaluated by two types of tests: (1) shaking type batch tests, and (2) continuous flow type column tests. Synthetic wastewater containing monobasic potassium phosphate KH_2PO_4 was used for the study.

TABLE 1. Some Physical Characteristics of Volcanic Ash from Linton, North Dakota.

Parameter	Value
Specific gravity	2.25 - 2.50
%retained on U.S. Sieve No. 325	3 - 10%
Blaine fineness	10,000 cm^2/cm^3
Mean particle diameter	2.7 microns

TABLE 2. Chemical Analysis of Linton Area Volcanic Ash

UNITED STATES
DEPARTMENT OF THE INTERIOR
BUREAU OF MINES

X-XAY FOURESCENCE ANALYSIS

Sample No.: GF 71-218 XB-22 Date: 3/19/71
Sample Description: 70-40 Volcanic Ash - Linton

Parameter	Percent
Iron oxide, Fe_2O_3	3.4
Titanium dioxide, TiO_2	.4
Calcium oxide, CaO	2.2
Potassium oxide, K_2O	3.0
Sulfur trioxide, SO_3	.1
Phosphorus pentoxide, P_2O_5	.1
Silicon dioxide, SiO_2	66.7
Aluminum oxide, Al_2O_3	12.5
Magnesium oxide, MgO	1.1
Sodium oxide, Na_2O	2.7
Ignition loss at 800° C	6.8
Total	99.0

Shaking Type Batch Tests—The volcanic ash sample was crushed to meet the following gradations:

U.S. Sieve No.	Volcanic Ash Sizes (mm)
(a) -No. 8 to +No. 16	1.190 to 4.760
(b) -No. 16 to +No. 30	0.590 to 1.190
(c) -No. 30 to +No. 50	0.297 to 0.590
(d) -No. 50 to +No. 100	0.149 to 0.297
(e) -No. 100	0.149

Stock solutions of KH_2PO_4 were prepared to generate synthetic wastewater containing 10 mg/l phosphorus. Synthetic wastewater of 100 ml volume was added to varying amounts of volcanic ash of the specified gradations in 250 ml Erlenmeyer flasks fitted with rubber stoppers. The flasks and contents were then agitated with a Burrell Model 75 wrist action shaker for varying lengths of time. The agitated solutions were filtered through a No. 5 Whatman filter paper to remove any volcanic ash from the synthetic wastewater and the filtrates analyzed for P concentration in accordance with Standard Methods (APHA 1971), Section 223 D.

Continuous Flow Type Column Test—The volcanic ash sample was crushed to meet gradations of -No. 8 to +No. 16 (1.19 to 4.76 mm) and -No. 30 to +No. 50 (0.297 to 0.590 mm) sieves. Stock solutions of KH_2PO_4 were prepared to generate synthetic wastewater containing 10.6 mg/l and 7.4 mg/l phosphorus for evaluation of -No. 8 to +No. 16 and -No. 30 to +No. 50, respectively. Filtration columns 18 inches in length were prepared by adding the desired gradation of volcanic ash to a 100 ml buret in known quantities. Synthetic wastewater was allowed to filter through the buret columns under gravity flow. The effluents were collected at various intervals to determine filtration rates. Effluents were filtered through a No. 5 Whatman filter paper and analyzed for P concentration by procedures indicated above.

RESULTS AND DISCUSSION

Tables 3 through 4 summarize the results of the shaking type batch tests and continuous flow column test, respectively. A complete set of laboratory data is contained in the Independent Study report for the M.S. degree in Civil Engineering by Gullicks (1977).

Shaking Type Batch Tests—The maximum P adsorption capacity of volcanic ash varied from 0.0056 mg P/g volcanic ash for -No. 8 to +No. 16 sized material to 0.0176 mg P/g volcanic ash for -No. 100 sized material. The maximum value of 0.0176 mg P/g was achieved using a volcanic ash concentration of 125,000 mg/l with contact time of one hour. Effect of mixing time on P removal is shown in Figures 1 and 2 for volcanic ash size of -No. 100 (smaller than 0.149mm) and ash concentration of 500 g/l. These indicate that P removal was virtually completed at half an hour mixing period. Further contact period did not improve P removal. Figure 2 indicates that the weight of P removed per unit weight of adsorbent (mg P/g volcanic ash) was relatively constant and was independent of mixing period. Since extended contact time could cause a physical breakdown of volcanic ash particles from the agitating action of the shaker, one hour of contact time was employed for all shaking tests.

Figure 3 presents percent P removal for different volcanic ash concentrations and sizes. The P removal efficiencies increased with increasing volcanic ash concentration. No more than 20% of P was removed when volcanic ash concentration was less than 300 g/l. The capacity of volcanic ash for P adsorption decreased with increasing particle sizes. For volcanic ash passing through sieve No. 100, the maximum P removal efficiency of 80% was obtained at a volcanic ash concentration of 500 g/l. For volcanic ash with sizes larger than sieve No. 100 opening, the maximum P removal was about 60% at volcanic ash concentration of 1000 g/l. The volcanic ash with largest particle size, -No. 8 to +No. 16 exhibited the lowest P removal efficiency.

Figure 4 presents data of weight of P removed per unit weight of volcanic ash versus P remaining in the wastewater. No definite trend was observed, which implies that P adsorption by volcanic ash may not follow the Freundlich adsorption isotherm. When weight of P removed per unit weight of volcanic ash was plotted

TABLE 3. Shaking Type Batch Tests

Particle Size	Quantity Filter Matl. g	Quantity Influent ml	Contact Time (With Agitation)	Conc. P Influent mg/l	Conc. P Effluent mg/l	% P Removed	g P removed per g Volcanic Ash
-No. 8 +No. 16	100	100	1 Hr.	9.6	4.0	58.3	5.60×10^{-6}
-No. 8 +No. 16	50	100	1 Hr.	10.4	6.8	34.6	7.20×10^{-6}
-No. 8 +No. 16	25	100	1 Hr.	10.2	9.3	8.8	3.59×10^{-6}
-No. 8 +No. 16	16.7	100	1 Hr.	10.0	10.6	0.0	0
-No. 8 +No. 16	10	100	1 Hr.	10.2	10.6	0.0	0
-No. 16 +No. 30	100	100	1 Hr.	9.6	4.0	58.3	5.60×10^{-6}
-No. 16 +No. 30	50	100	1 Hr.	10.4	6.6	36.5	7.59×10^{-6}
-No. 16 +No. 30	25	100	1 Hr.	10.0	7.8	22.0	8.80×10^{-6}
-No. 16 +No. 30	12.5	100	1 Hr.	10.0	8.9	11.0	8.80×10^{-6}
-No. 16 +No. 30	10	100	1 Hr.	10.2	10.9	0.0	0
-No. 30 +No. 50	100	100	1 Hr.	9.6	3.6	62.5	6.00×10^{-6}
-No. 30 +No. 50	50	100	1 Hr.	10.0	6.0	40.0	8.00×10^{-6}
-No. 30 +No. 50	25	100	1 Hr.	10.2	8.4	17.6	7.18×10^{-6}
-No. 30 +No. 50	16.7	100	1 Hr.	10.0	8.6	14.0	8.38×10^{-6}
-No. 30 +No. 50	10	100	1 Hr.	10.2	10.6	0.0	0
-No. 50 +No. 100	100	100	1 Hr.	9.6	3.6	62.5	6.00×10^{-6}
-No. 50 +No. 100	50	100	1 Hr.	10.0	5.4	46.0	9.20×10^{-6}
-No. 50 +No. 100	25	100	1 Hr.	9.6	7.4	22.9	8.79×10^{-6}
-No. 50 +No. 100	10	100	1 Hr.	10.2	9.9	3.0	3.06×10^{-6}
-No. 100	50	100	½ Hr.	10.0	2.2	78.0	1.56×10^{-5}
-No. 100	50	100	1 Hr.	10.0	2.2	78.0	1.56×10^{-5}
-No. 100	50	100	2 Hr.	10.0	1.8	82.0	1.64×10^{-5}
-No. 100	50	100	4 Hr.	10.0	2.6	74.0	1.48×10^{-5}
-No. 100	50	100	8 Hr.	10.0	2.0	80.0	1.60×10^{-5}
-No. 100	12.5	100	1 Hr.	10.0	7.8	22.0	1.76×10^{-5}
-No. 100	5.0	100	1 Hr.	10.0	10.6	0.0	0

TABLE 4. Contnuous Flow Column Test

Minus No. 8 to Plus No. 16
Volcanic Ash

Cumulative Total Volume Effluent ml	Δ Time Min.	P Conc. Effluent mg/l	%P Removal	Ratio *Wt. Effluent* Wt. Filter Media	mg P Removed
0	0	—	—	—	—
100	6	9.2	13.2	1.57	.140
200	7	10.0	5.7	3.15	.060
300	11	10.2	3.8	4.72	.040
400	12	10.2	3.8	6.30	.040
500	14	10.2	3.8	7.87	.040
600	15	10.6	0.0	9.45	.000
700	15	10.6	0.0	11.02	.000

1. Influent P concentration 10.6 mg/l
2. Weight filter media 63.5 g

against volcanic ash concentration in Figure 5, there was no linear correlation between these two parameters.

Continuous Flow Type Column Tests—Continuous flow tests were first conducted on -No. 8 to +No. 16 volcanic ash (1.19 to 4.76mm size) with an influent P concentration of 10.6 mg/l as listed in Table 4. The filtration run lasted 80 minutes with a computed filtration rate of 1 gpm/ft² (40.74 l/min/m²) at an average contact time of 11.3 minutes.

Table 5 summarizes the results of continuous flow tests on -No. 30 to +No. 50 volcanic ash (0.297 to 0.590mm size) with an influent P concentration of 7.4 mg/l. This filtration run lasted 26 hours with a computed filtration rate of 0.14 gpm/ft² (5.70 l/min/m²) with an average contact time of 75 minutes. Both runs were conducted using the same constant head feed solution tank. The filtration rate for finer ashes (-No. 30 to +No. 50) was significantly less than that for coarser ashes (-No. 8 to +No. 16). Phosphorus removal efficiency ranged from 0 to 13.2% and 0 to 43.2% for the continuous adsorption column for -No. 8 to +No. 16 material and -No. 30 to +No. 50 material, respectively. As shown in Figure 6,

TABLE 5. Continuous Flow Column Test

Minus No. 30 to Plus No. 50
Volcanic Ash

Cumulative Total Volume Effluent ml	Δ Time Min.	P Conc. Effluent mg/l	%P Removal	Ratio Wt. Effluent / Wt. Filter Media	mg P Removed
0	0	—	—	—	—
50	63	4.2	43.2	0.84	.160
100	47	5.2	30.0	1.69	.110
150	51	5.9	20.3	2.53	.075
200	49	6.3	15.0	3.38	.056
300	105	6.6	10.8	5.06	.040
450	165	6.4	13.5	7.59	.150
550	115	6.4	13.5	9.28	.200
650	115	6.6	10.8	10.77	.080
1000	350	7.0	5.4	16.88	.140
1500	500	7.4	0	25.29	.000

1. Influent P concentration 7.4 mg/l
2. Weight filter media 59.3 g

effluent P concentration increased rapidly during the first 200 ml volume of waste treated and then gradually approached that of influent. Adsorbing media with coarser ash particles (-No. 8 to +No. 16) showed a faster breakthrough than the finer ash particles (-No. 30, +No. 50).

Figure 7 depicts weight of P adsorbed per unit weight of volcanic ash versus filtration time for both continuous column runs. Finer volcanic ashes (-No. 30 to +No. 50) had a higher P adsorption capacity per unit weight of volcanic ash than coarser ashes (-No. 8 to +No. 16) and it took a much longer time, which was about 18 hours, for finer ashes to exhaust its P adsorption capacity compared to that for coarser ashes, which was about one hour. This could be attributed to the larger surface area and slower filtration rate for the finer volcanic ashes.

Figure 8 depicts the relationship between weight of P adsorbed per unit weight of volcanic ash and effluent P concentration. It is noted that finer ashes had a much higher P adsorption capacity than the coarser ashes. For both finer and coarser volcanic ashes (-No. 30 to +No. 50 and -No. 8 to +No. 16) a larger portion of the adsorptive capacity was used up when effluent P concentration was approaching influent P concentration.

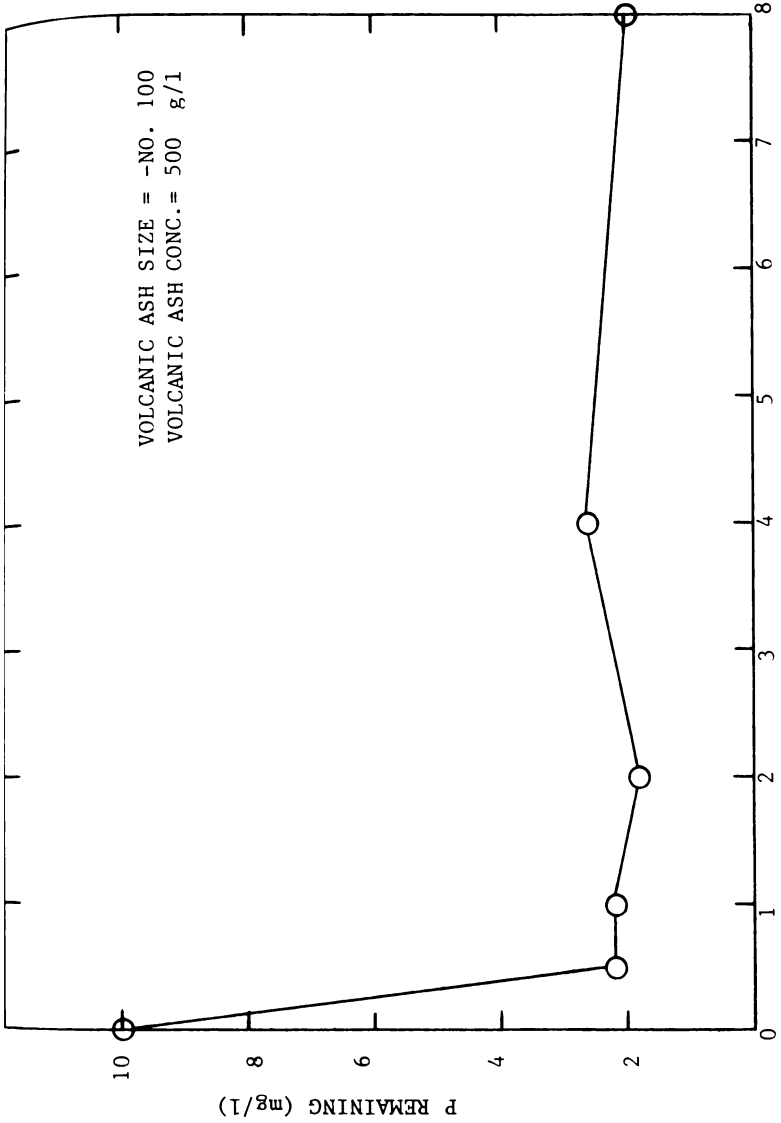

FIGURE 1. Phosphate Remaining vs. Mixing Time - Batch Test

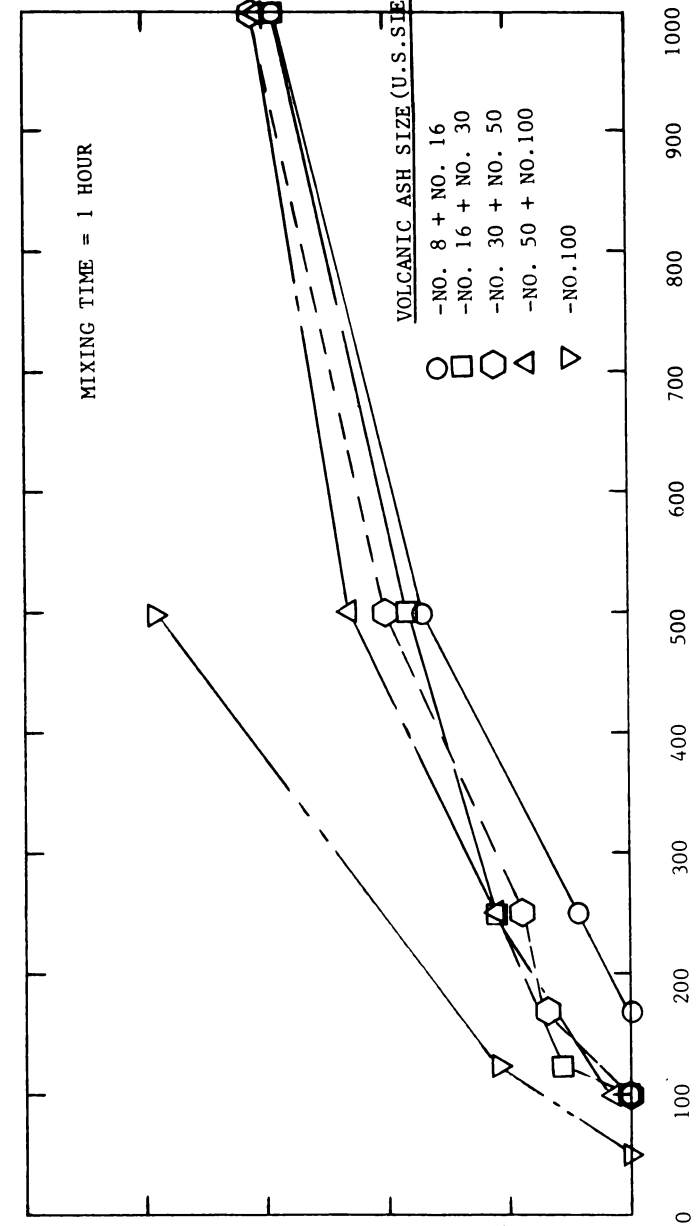

FIGURE 2. Percent P Removal vs. Mixing Time - Batch Test

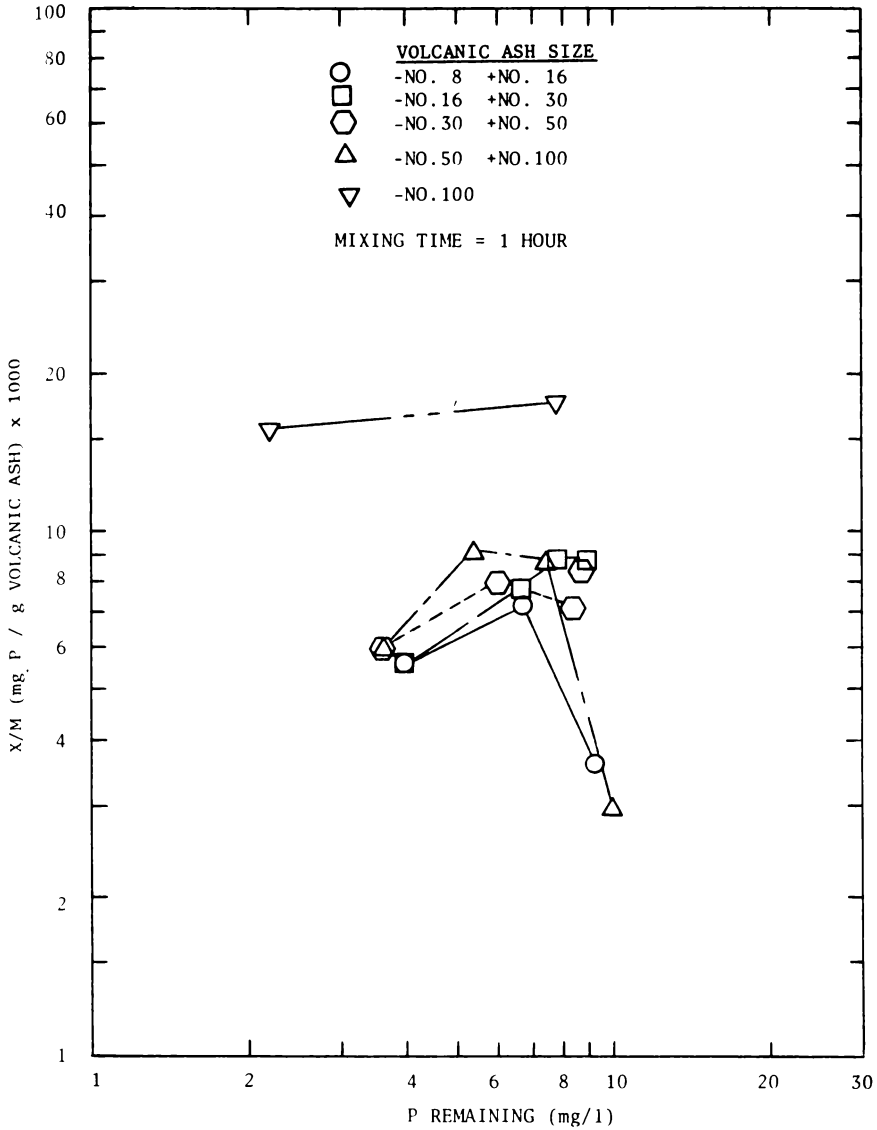

FIGURE 3. Percent P Removal vs. Volcanic Ash Concentration - Batch Test

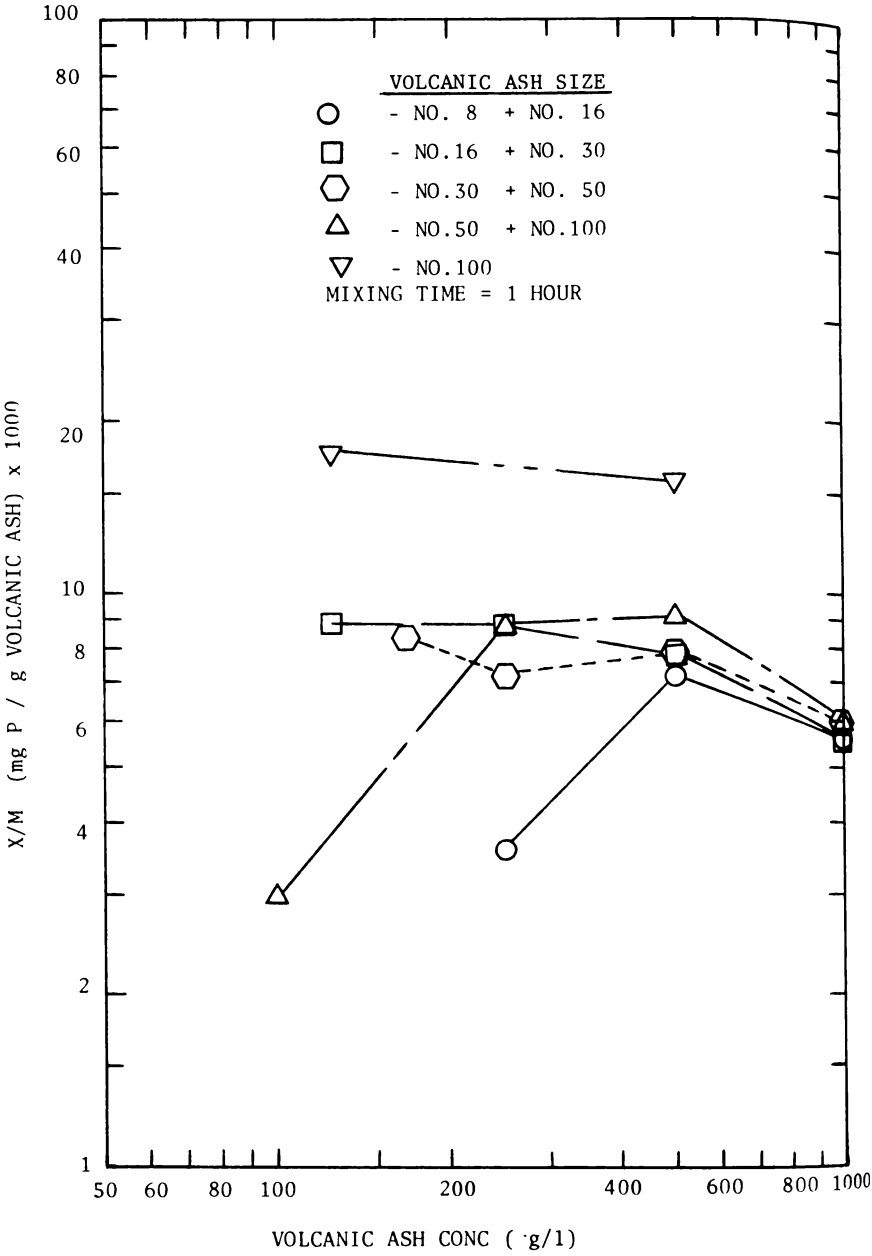

FIGURE 4. X/M vs. P Remaining - Batch Test

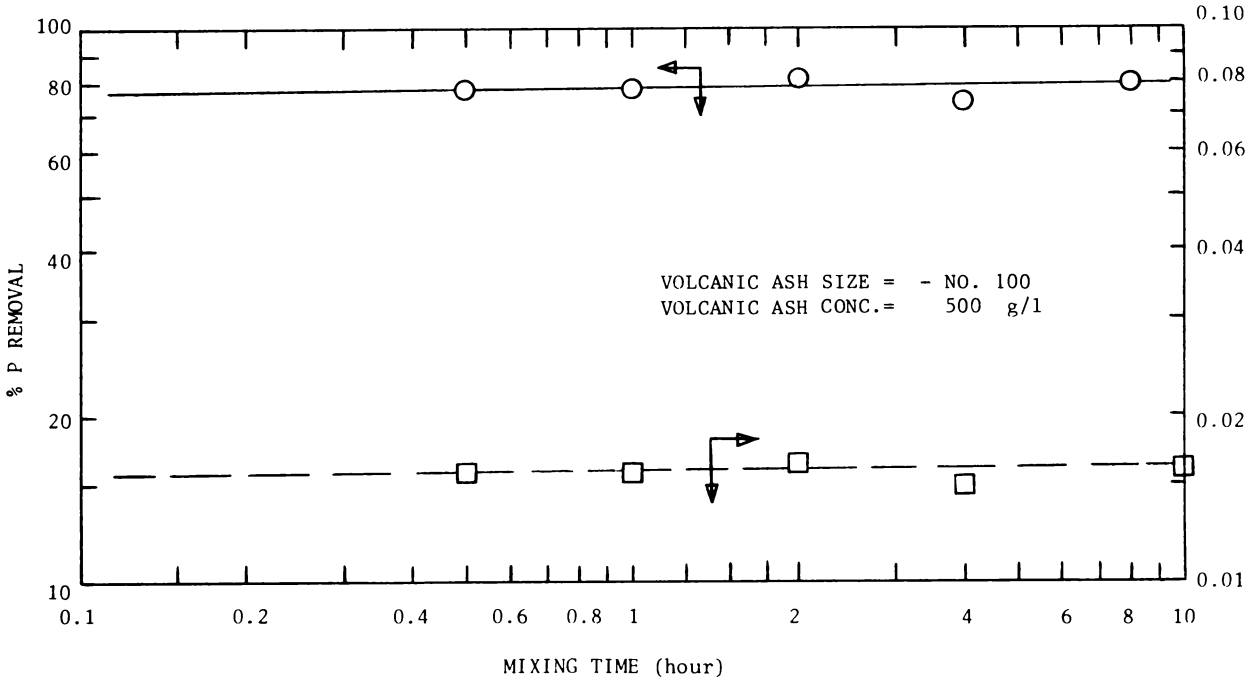

FIGURE 5. . X/M vs. Volcanic Ash Concentration - Batch Test

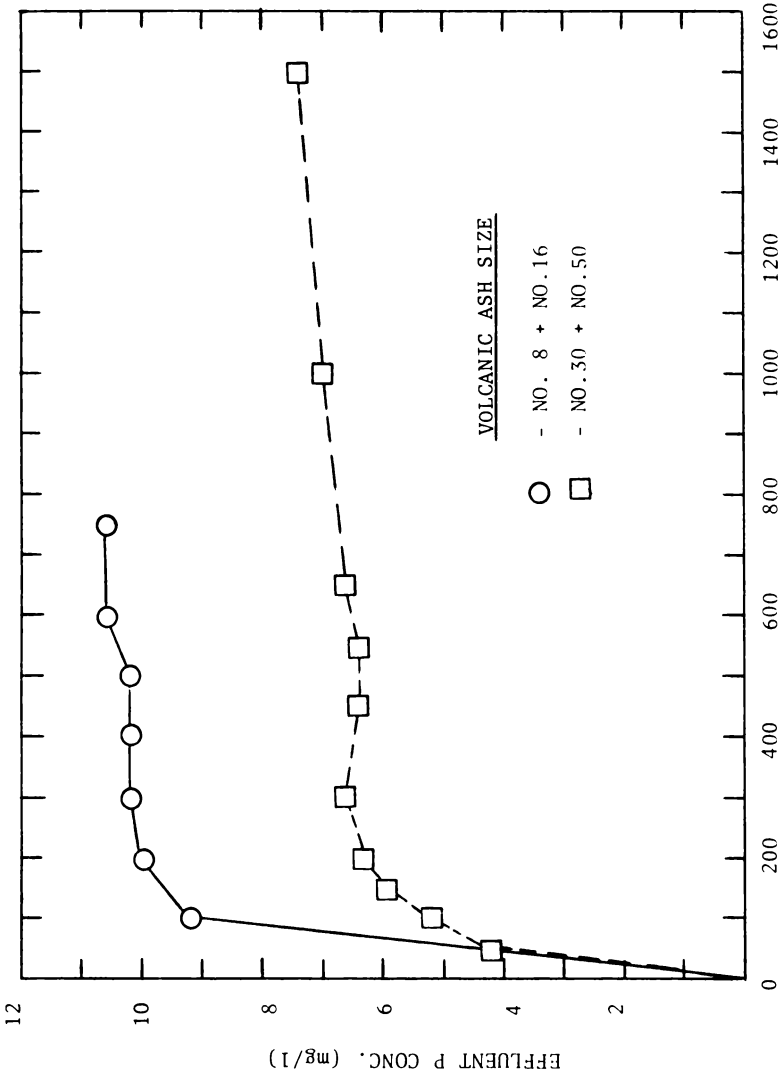

FIGURE 6. Effluent P Concentration vs. Volume of Waste Treated - Continuous Flow Column

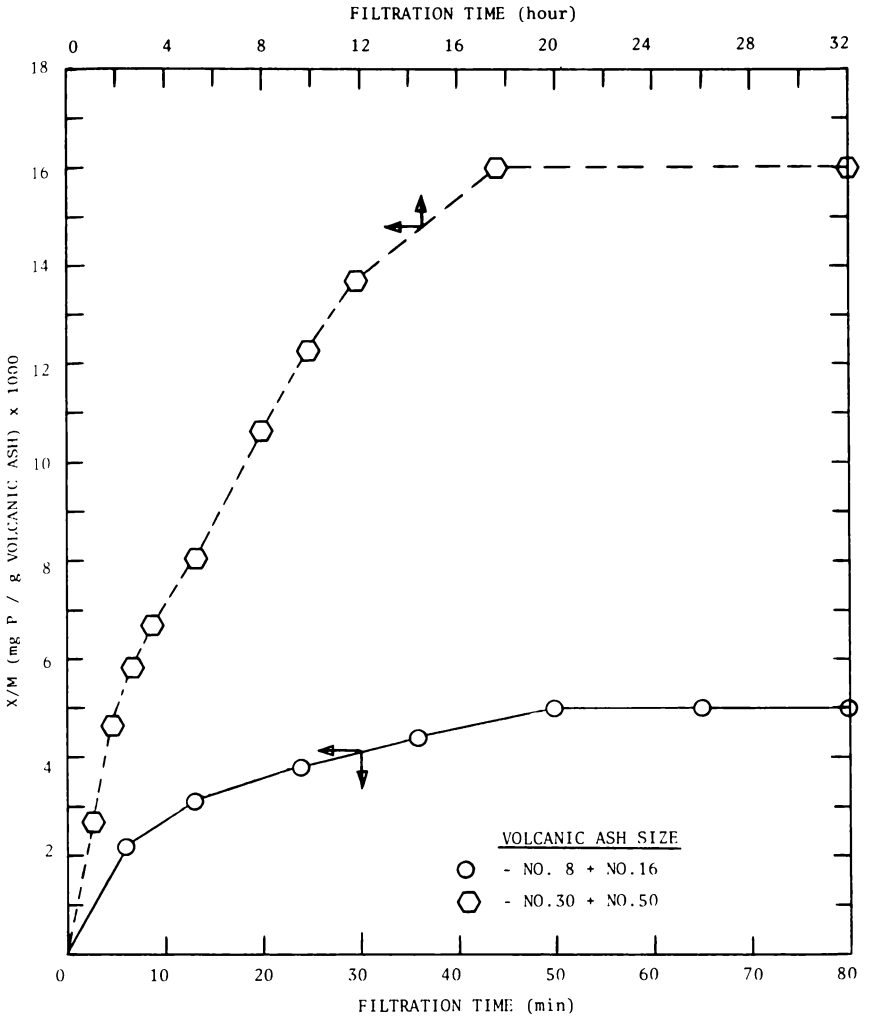

FIGURE 7. X/M vs Filtration Time.

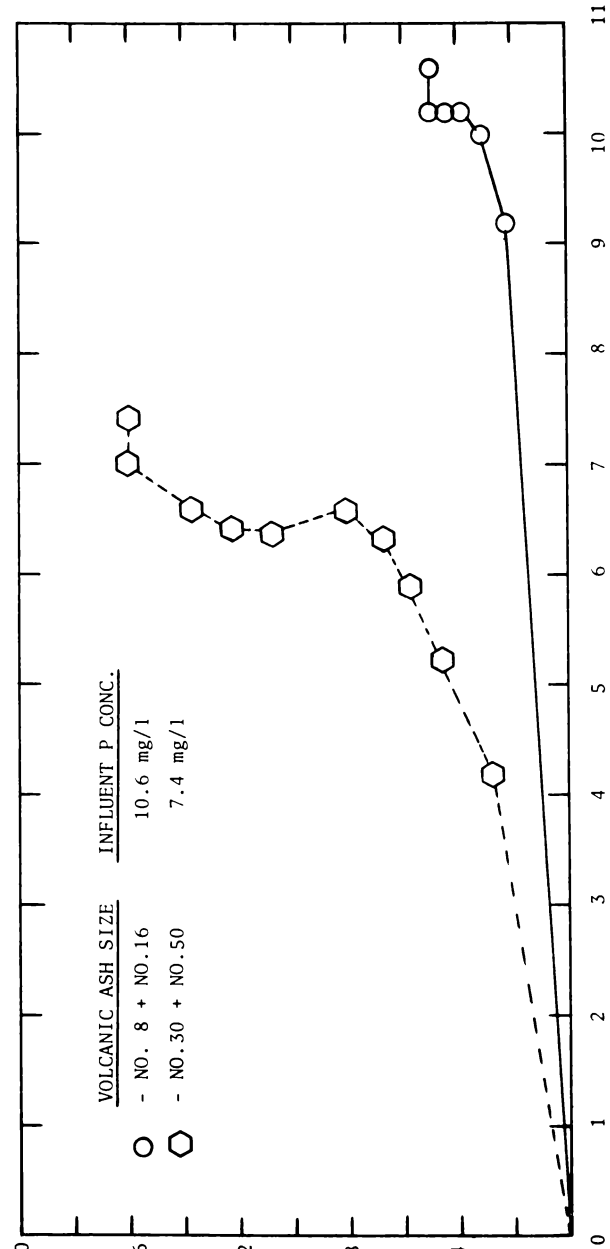

FIGURE 8. X/M vs. Effluent P Concentration - Continuous Flow Column

SUMMARY

1. Using the batch adsorption test, P removal from synthetic wastewater by volcanic ashes was virtually completed within half an hour of the mixing period.

2. In the batch adsorption test, high volcanic ash dosages were required to achieve a significant P removal efficiency. For volcanic ash with particle sizes smaller than 0.15 mm, dosage of 500 g/l was necessary to obtain 80% P reduction. For volcanic ashes with particle sizes larger than 0.14 mm, dosage of 1000 g/l was required to obtain 60% P reduction.

3. Based on the batch adsorption test conducted in this study, P adsorption by volcanic ashes did not follow Freundlich adsorption isotherm.

4. Using continuous adsorption column tests, P removal efficiency varied from 0.13.2% and 0 to 43.2% for the adsorption column of -No. 8 to +No. 16 material, and -No. 30 to +No. 50 material, respectively.

5. For continuous column study, adsorbing media of coarser ash particles (-No. 8 to +No. 16) showed a faster breakthrough than the finer ash particles. Finer volcanic ashes (-No. 30 to +No. 50) had a higher P adsorption capacity than the coarser ashes.

6. The batch adsorption unit was capable of a much higher P removal than the continuous adsorption column as defined by the limit of this study.

7. Based on this study the volcanic ash is recommended for use as adsorbent for P removal from wastewaters. The ash should be ground to a size of less than 0.14 mm and a complete-mix system should be employed for effective P removal.

LITERATURE CITED

American Public Health Association, 1971. Standard methods for the examination of water and wastewater, 13th edition.

Culp, G. L., and L. L. Ames, 1971. Phosphorus removal from wastewater by activated silica columns. Chemical Engr. Progr. Symposium Ser. No. 107, Vol. 67, Water-1970, pp. 304-309, AICHE.

Eberhardt, W. A., and J. B. Nesbitt. 1968 Chemical precipitationn of phosphorus within a high rate activated sludge process. Engineering Research Report, Pennsylvania State University, Department of Civil Engineering.

Eliassen, R., and G. Tchobanoglous, 1968. Removal of nitrogen and phosphorus. Proc. of 23rd industrial waste conf., Purdue University, p. 35-48.

Gullicks, R. E., 1977. Removal of soluble orthophosphate by adsorption on volcanic ash. M.S. Independent study. University of North Dakota.

Manz, O. E., 1962. Investigation of pozzolanic properties of the cretaceous volcanic ash deposit near Linton, North Dakota: North Dakota Geological Survey Report of Investigation, No. 38. P. 4 and 10.

Nesbitt, J. B., 1966. Removal of phosphorus from municipal sewage plant effluents. Engineering Research Bulletin, B-93. Pennsylvania State University.

Sawyer, C. N., 1952. Some new aspects of phosphates in relation to lake fertilization. Sewage and Industrial Wastes, Vol. 24, No. 6, pp. 768-776.

Sawyer, C. N., 1962. Cause, effects, and control of aquatic growths. Jour. of Water Pollution Control Federation, Vol. 34, No. 3 pp. 279-287.

Stanton, T. W., 1917. A cretaceous volcanic ash bed on the Great Plains of North Dakota. Washington Academy of Science, Jour. Vol. 7, No. 3, pp. 80-81.

U.S. Dept. of the Interior, Bureau of Mines 1973. Minerals Yearbook, Vol. 1, metals, minerals and fuels.

Yee, W. C. 1965. The selective of mixed phosphates from water streams by activated silica. Oak Ridge National Laboratory, TM-1135, Nov. 1965.

DEVELOPMENT AND TESTING OF AN ICE-MAKER EVAPORATOR FOR A HEATING ONLY HEAT PUMP

James C. Wendschlag
and
Mason H. Somerville
The Engineering Experiment Station
University of North Dakota
Grand Forks, North Dakota 58202

ABSTRACT

The development of a heat pump evaporator for use in an annual cycle heating and air conditioning system is discussed. The evaporator was designed for operation in an ice making mode throughout most of the heating season.

A commercially available flat plate ice maker was selected following tests of several configurations. The selection was based primarily on its ice removal efficiency. The water pumping system necessary with this selection was designed to minimize pumping cost and maintenance. The automatic defrost system built into the heat pump required alteration to facilitate ice harvesting.

The apparatus and experimental procedure used for performance evaluation are given along with test results. A complete performance analysis of the design selection is compared with that of the conventional air evaporators indicating that an annual cycle system is presently feasible as an alternative heating and air-conditioning system.

INTRODUCTION

New solar energy systems, along with conventional systems, are providing several alternatives for heating and cooling residential and commercial buildings. The conventional heating systems utilize combustion, electrical resistance elements, or heat pumps; while cooling requirements can be supplied by a central air-conditioning system or a reversible heat pump. The basic requirements of a solar heating system include a means of collecting solar energy, a means of storing the collected energy, and a method of transferring stored energy to the conditioned space.

A heat pump is a device that operates in a cycle, that requires work, and that accomplishes the objective of transferring heat from a low temperature body (energy storage) to a high temperature body (the conditioned space). A vapor compression heat pump schematic is shown in Figure 1 below. The working fluid is generally freon. Heat is transferred to the evaporator where the low pressure, low temperature saturated liquid freon is evaporated. The gaseous freon is then compressed. Heat is then removed in the condenser, condensing the high pressure and temperature freon. The freon is then expanded in an isenthalpic process (capillary tube) to a low temperature, low pressure saturated liquid completing the cycle.

The annual cycle energy system (ACES) (Fischer, 1976), a solar energy system, is an alternative heating and air-conditioning system with significant

potential for reducing energy consumption for space heating (Figure 2). Basically, an ACES system utilizes an ice-maker heat pump (Fischer, 1976) to remove energy from a water storage tank during the winter while heating the house. This is done while freezing the storage tank's contents. The ice formed during the winter is stored to provide the summer air-conditioning. Melting the ice during the summer, with naturally occurring solar energy, returns the energy to the water that was extracted the previous winter. The key to an ACES system is a suitable evaporator system which expedites ice removal. Since ice has a low thermal conductivity, a thick layer on the evaporator severely decreases the performance of the heat pump. The performance can be maintained by periodically removing the ice from the evaporator surface.

The coefficient of performance (COP) of the heat pump may be expressed as:

$$COP = \frac{\text{Heat Rejected to Dwelling}}{\text{Electrical Input Heating} + \text{Electrical Input Defrosting}}$$

Minimizing the defrost energy maximizes the COP. This is best accomplished by minimizing the time required to remove the ice. This paper discusses several evaporator designs and schemes to remove (harvest) the ice.

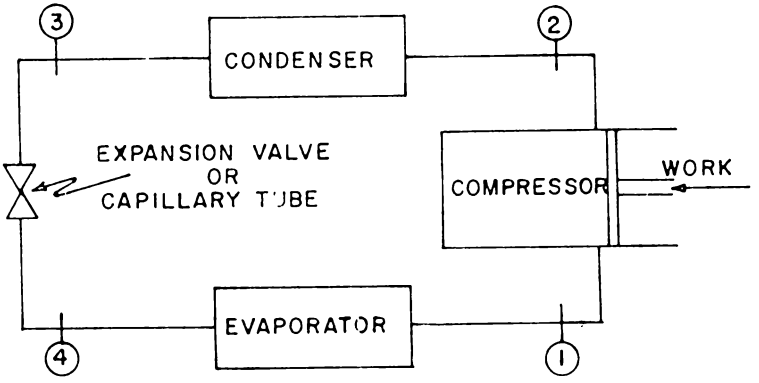

FIGURE 1. A simple heat pump cycle: (1) gaseous freon at low temperature and low pressure, (2) gaseous freon at high temperature and high pressure, (3) liquid freon at high temperature and high pressure, (4) liquid freon at low temperature and low pressure.

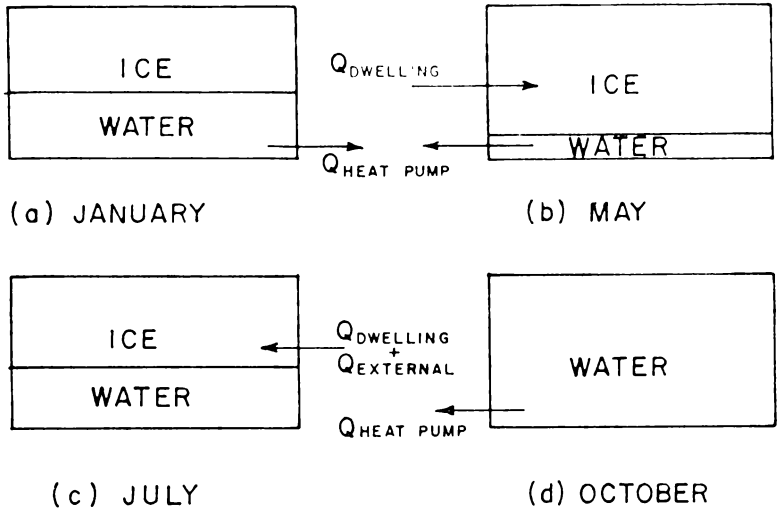

FIGURE 2. Principle of the ACES system: (A) heat pump supplies heat to dwelling while forming ice, (B) heating season ending and air-conditioning season beginning, (C) air-conditioning load used to melt the ice, storing summer heat. Direct solar assist or outside air may be required to melt some of the ice, (D) beginning of the heating season with all ice melted.

CONCEPT DEVELOPMENT

Several ice-maker evaporator designs were fabricated and tested in the laboratory. Determination of the energy requirements for ice removal was the primary objective of these tests. Additionally, heat pump performance was determined as a function of ice thickness during these tests.

Several designs were built and tested. All were successful in removing heat from the storage water; however, ice harvesting was unsuccessful in all but one. The designs unsuccessful in harvesting the ice are shown in Figure 3. The successful design tested utilized commercially available flat plate evaporators suspended over the tank (Fischer, 1976). The experimental setup is shown in Figure 4.

The thermal conductivity of the type 304 stainless steel plates ($k = 5.8$ W/mK) is low enough to prevent ice formation outside of the evaporator tube area. Manual operation of the heat pump reveals that the ratio of defrost time to operation time for successful ice removal was approximately constant at 0.0167 for operating times between ten and ninety minutes. Since the heat pump runs at constant power, ice harvesting requires approximately 1.7% of the energy provided to the pumps. This has a minor impact on the overall COP. Furthermore, virtually all of the energy expended during harvesting is added to the storage water and is therefore recoverable.

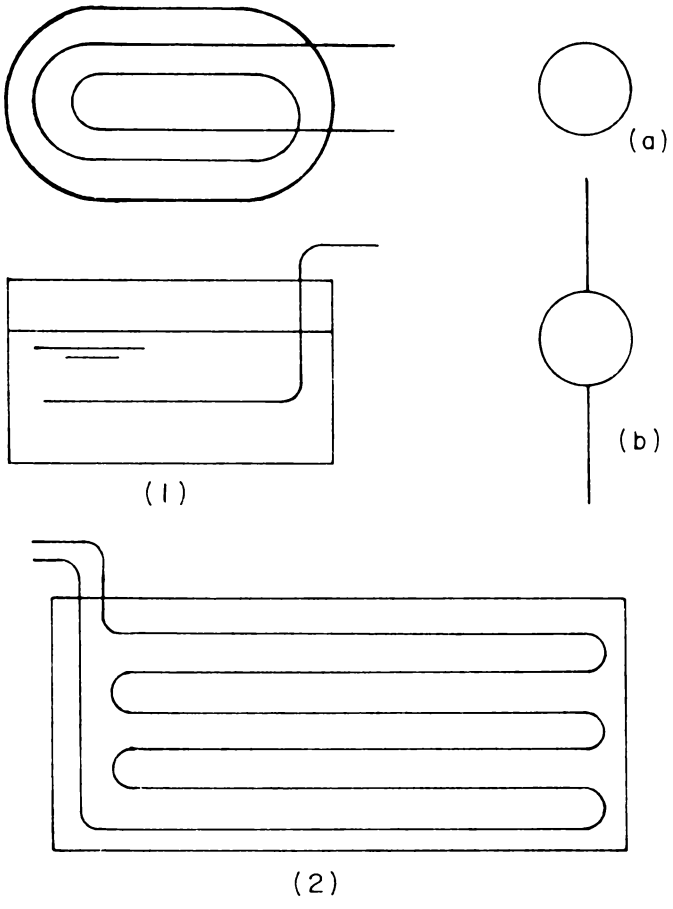

FIGURE 3. Preliminary evaporator designs: (1) coiled copper tube, a) plain tube, b) finned tube, (2) copper tubing sealed between two copper plates.

DEVELOPMENT OF THE ICE MAKER EVAPORATOR

Two ice-maker evaporator plates connected in parallel proved to provide sufficient area (3.2m^2) to operate the donated heat pumps for more than an hour with continuous ice formation and still supply 90% of the no-ice (0°C) heat rate, 7,000 W (24,000 Btu/hr). Two additional aspects of this setup required further development. These are: the evaporator plate water distribution system and the design and selection of the controls to automatically harvest the ice.

Since the selected design required a flow of water over the plates, a pumping

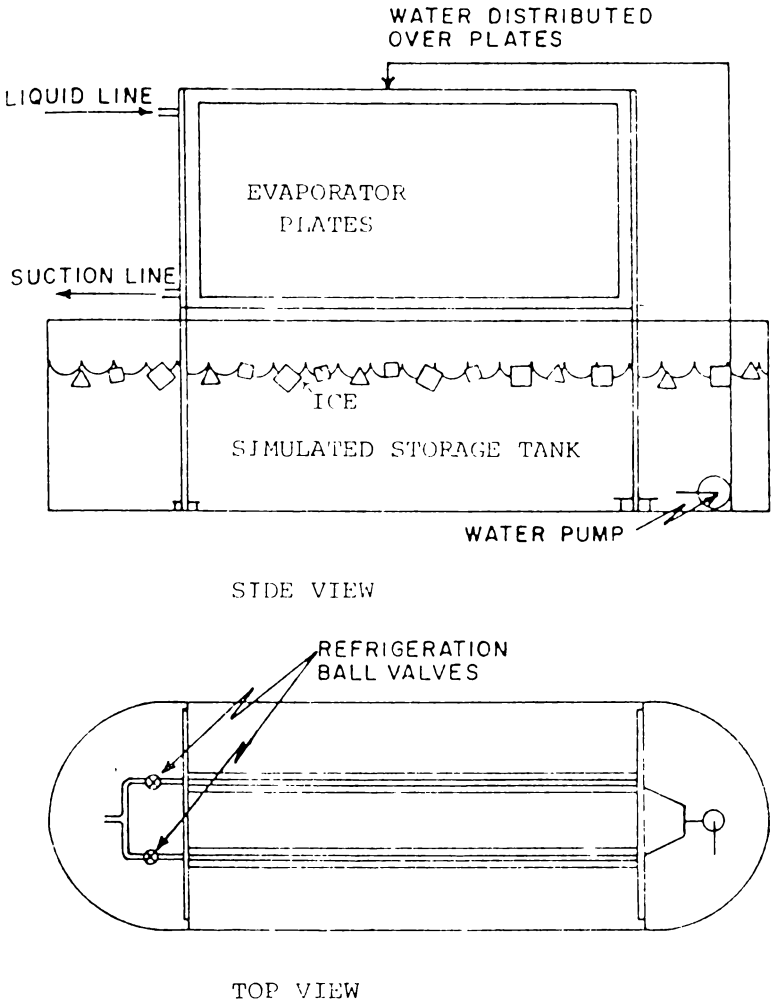

FIGURE 4. Parallel ice-maker evaporators suspended over test tank.

and water distribution system had to be developed. Several alternatives were designed and tested in the laboratory. Emphasis was placed on minimizing the pump power and probable maintenance requirements.

Copper tubes [1.27 cm (0.50 inch)] were placed along the top of each side of the evaporator. Holes [0.25 mm (0.10 inch)], drilled at 1.26 cm (0.50 inch) intervals along the tube, distributed 95 lpm (25 gpm) of water uniformly over both sides of both evaporator plates. Initial tests (uniform hole size) revealed that the

hole size had to decrease from the center of the tube to the ends in order to achieve a uniform flow distribution (Figure 5).

Ice harvesting is effected by forcing superheated freon to bypass the condenser and expansion device and go directly to the evaporator where it melts the ice immediately adjacent to the plates causing the sheets of ice to fall into the storage tank.

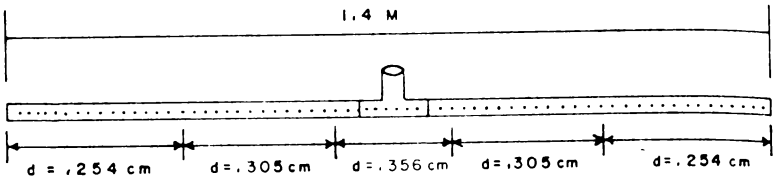

FIGURE 5. Hole size specifications for water distribution tubes.

Temperature switches, pressure switches, and timers were investigated to control the initiation and termination of ice harvesting. The sensing elements of the switches were placed on the suction line of the heat pump. A short period of time (90 seconds) was required for the heat pump to regain operating equilibrium immediately following termination of defrost. During this period the suction temperature and pressure dropped to levels lower than the harvest initiation set points required for the switches. This caused a continuous on-off cycling of the defrost system once initiated. Use of suction line conditions consequently proved inadequate to control the harvesting of the ice.

Harvesting of the ice is never required until the water temperature reaches 0°C (32°F). This allows one to use the water temperature to initiate a controlled time cycled defrost. A timer was selected which allows on-off adjustments from 18 seconds to 1,800 seconds (30 minutes). The timer was set to provide 30 seconds for harvesting the ice following every 30 minutes of operation. Adjustments allowing greater harvest time or defrost frequency can be easily made if required. A combination timer-temperature switch was selected as the best solution (Figure 6).

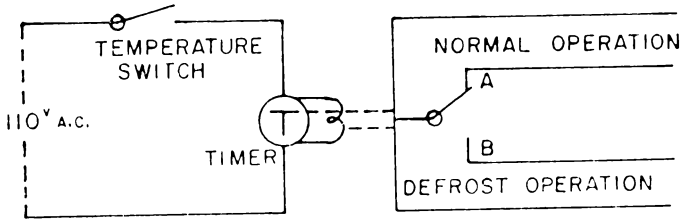

FIGURE 6. Schematic of automatic ice harvest control.

TESTING AND EVALUATION PROGRAM

An experimental program to evaluate pump performance was carried out. The monitoring equipment used, and parameters measured are delineated in Table 1. Sufficient data was collected to evaluate the performance of the ice maker heat pump as a function of ice thickness. A control panel was constructed to facilitate testing. This included all of the switches necessary to operate the system as well as most of the monitoring equipment. To simulate the storage tank environment, a styrofoam enclosure was built around the tank. This caused the air temperature surrounding the evaporator plates to drop to 6°C (43°F). Storage air temperature in the tank is calculated to be 1°C (34°F). The heat pump input electrical power, the tank water temperature, the heat output from the system, and the ice thickness were monitored.

EXPERIMENTAL RESULTS

The original testing of the design concepts concentrated primarily on the operational characteristics of the system during ice formation. The performance change caused by the ice formation is shown by Figure 7 for the design selection. The upper curve is for two parallel plates and the lower for a single evaporator plate at a freon charge of 2.1 kg (4.6 lbs). The required freon charge was analytically determined based on that used in the manufacturer's air evaporators. Future experiments will be run at varying charges to determine the optimum amount of freon for the parallel plate evaporator system.

A comparison of the system performance with the flat plate water evaporators with that of the air evaporator system is shown in Figure 8. This reveals that the heat output, using two parallel water evaporators, exceeds that of the air evaporator for corresponding evaporator temperatures. Tables 2 and 3 present the

TABLE 1. Monitoring equipment used to evaluate evaporator designs.

Equipment	Parameters Measured
Wattmeters	Compressor, condenser fan, and water pump power
Ammeter	Compressor Current
Copper Constantan Thermocouples	Temperature of water, suction and discharge lines, and air entering and exiting the heat pump
Hot Wire Anemometer and Vane Anemometer	Rate of air flow over the condenser
Pressure Gages	Suction and discharge pressures
Vernier Caliper	Thickness of the ice
Stopwatch	Ice harvest time

TABLE 2. Heat pump performance characteristics using sensible heat of storage water. Water flow rate=67 1pm Air flow rate=88 m^3/min.

Water Temperature (°C)	Output Capacity (Watts)	Electrical Input: Compressor and Fan (Watts)	Electrical Input: Water Pump (Watts)	Total (Watts)	COP Output Total Input*	Indoor Temp. Rise (°C)	Operating Pressures: Suction $(kg/cm^2)_g$	Operating Pressures: Discharge $(kg/cm^2)_g$	$\left(\frac{P_d}{P_s}\right)_{abs}$
15	12,300	4,100	300	4,400	2.75	24.3	5.5	10.4	2.99
12	11,500	3,900	300	4,200	2.69	22.7	5.2	17.9	3.05
9	10,600	3,700	300	4,000	2.61	21.9	4.9	17.5	3.14
6	9,800	3,500	300	3,800	2.54	19.4	4.6	17.0	3.21
3	9,000	3,300	300	3,600	2.46	17.	4.3	16.5	3.30
0	8,100	3,100	300	3,400	2.38	26.0	4.0	16.0	3.40

*Includes water pump, condenser fan motor, heat pump controls, and compressor motor.

TABLE 3. Heat pump performance characteristics using latent heat of fusion of storage water. Water flow rate=67 lpm Air flow rate=88 m³/min.

Tine Since Harvest (Min)	Output Capacity (Watts)	Electrical Input Compressor And Fan (Watts)	Water Pump (Watts)	Total (Watts)	COP Output Total Input	Indoor Temp. Rise (°C)	Operating Pressures Suction (Kg/cm²)g	Discharge (Kg/cm²)g	$\left(\frac{P_d}{P_s}\right)_{abs}$
5	7,200	2,700	300	3,000	2.36	14.2	3.7	15.7	3.55
10	7,400	2,900	300	3,200	2.27	14.5	3.6	15.5	3.59
15	7,600	3,020	300	3,320	2.25	1.50	2.4	15.4	3.73
20	7,500	3,000	300	3,300	2.24	14.8	3.3	15.3	3.79
25	7,400	2,980	300	3,280	2.22	14.6	3.25	15.15	3.80
30	7,200	2,900	300	3,200	2.21	14.2	3.2	15.0	3.81
35	7,000	2,850	300	3,150	2.19	13.8	3.2	15.0	3.81
40	6,800	2,780	300	3,080	2.17	13.4	3.15	14.9	3.83
45	6,600	2,700	300	3,000	2.16	13.0	3.15	14.9	3.83

*Includes water pump, condenser fan motor, heat pump controls, and compressor motor.

system performance with the parallel plate evaporators. Table 2 is for operation in a non-ice-making mode using the sensible heat of the water at temperatures above 0°C (32°F). The results during ice formation are given in Table 3.

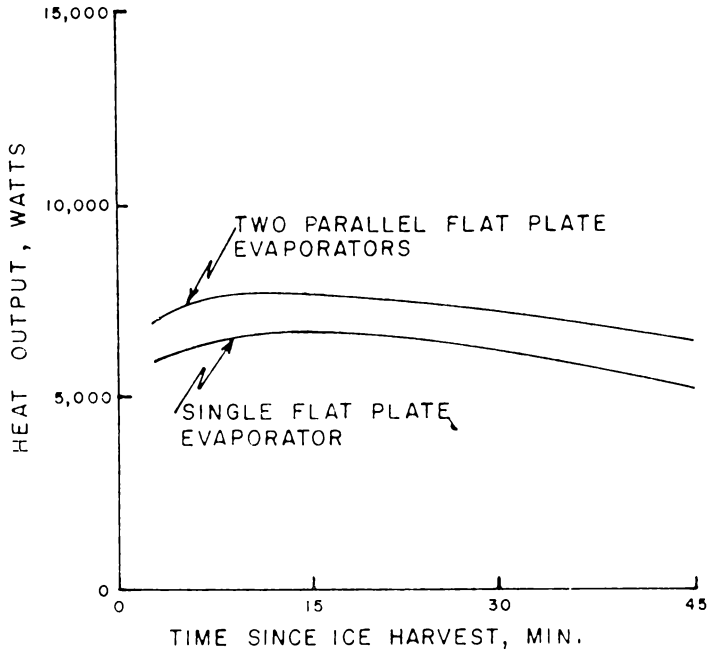

FIGURE 7. Effect of ice formation on output of heat pump.

CONCLUSIONS

The results reveal that heat pumps can efficiently supply the heating requirements of a dwelling while operating in an ice-making mode. The evaporator system components and ice harvest controls described above make use of commercially available equipment, allowing standard heat pumps to be readily adapted to this application. The significant energy savings resulting from using a heat pump in the ACES mode along with the successful laboratory tests justify the installation of this evaporator system in a residential application for continued development and analysis. Continued laboratory studies will involve using the ice-maker evaporators in series with the conventional outside air evaporator in an effort to minimize water storage requirements.

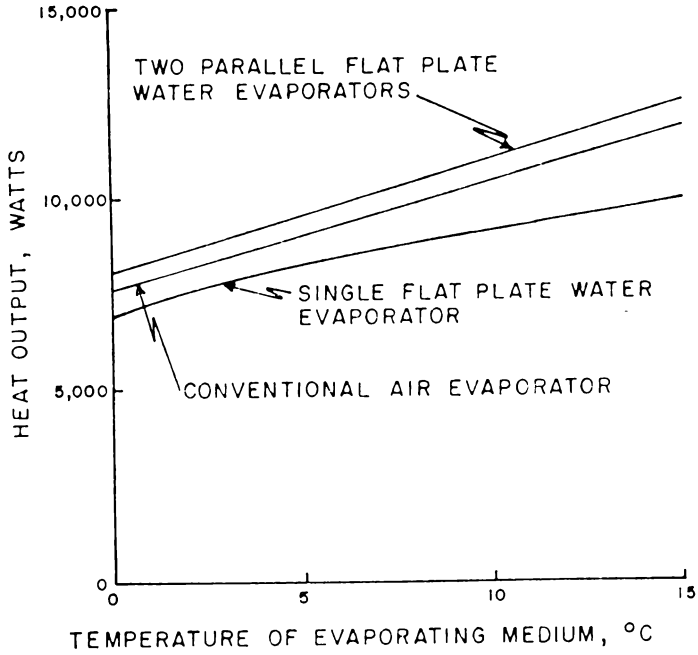

FIGURE 8. Heat pump performance vs. temperature of evaporating medium.

ACKNOWLEDGMENTS

This project was partially supported by the Engineering Experiment Station at the University of North Dakota through a grant made available by Minnkota Power Cooperative. The heat pump used in these tests was donated by Andro Corporation of Columbus, Ohio. Special recognition needs to be extended to Donald Mathsen and Gregory Loken for their advice and assistance in the project. Thanks is also given to Lloyd Nordling for his excellent work in fabricating many of the design concepts tested throughout the project.

LITERATURE CITED

Fischer, H. C. 1976. "Thermal Storage Applications of the Ice-Maker Heat Pump." Oak Ridge National Laboratory. Oak Ridge, Tennessee.

Fischer, H. C. 1976. "The Annual Cycle Energy System." Oak Ridge National Laboratory. Oak Ridge, Tennessee.

THE ECONOMICS OF SOLAR SPACE HEATING AND COOLING

Carl D. Svard
Mason H. Somerville
and
Don V. Mathsen
Engineering Experiment Station
University of North Dakota
Grand Forks, North Dakota 58202

ABSTRACT

An economic analysis of a solar heated and cooled private home is developed. The basis of the analysis is an experimental "solar" home located at Larimore, North Dakota. This 214m² (2,300ft²) home utilizes a solar assisted heat pump heating and cooling system with 97m² (1,050ft²) of forced air solar collector and 15,140-151,400 liters (4,000-40,000 gallons) of water storage capability. This paper includes a comparative study of the costs inherent with this system with those of conventional systems (gas, fuel, and electric) for a similar sized house. Types of costs examined include those for the heating unit, fans, water storage area, evaporators, and pumps. Costs of conventional systems include the heating and cooling units, fans and systems layout. Operational costs of the same systems are simulated with the aid of a computer model of the experimental system.

INTRODUCTION

The use of solar energy as an alternate means of space heating and cooling has become more prominent with the realization of the limits of fossil fuel resources and reserves. Considerable research has been conducted on the engineering and economic feasibility of using a solar-assisted energy package to heat and cool private homes. Such a package consists of heat pumps, solar collectors, and a thermal storage medium. Previous studies have shown the need for large collector areas and large thermal storage capacities in the northern portions of the country (United Nations, 1964). The current high initial cost of solar collectors and storage capacity often makes the solar-assisted alternative economically unattractive when compared to conventional systems (gas, oil, electric resistance).

Fischer (1976) developed an economically feasible heating and cooling system that is not dependent on active solar collectors but is dependent on solar energy. His Annual Cycle Energy System (ACES) utilizes the latent heat of fusion of water to provide the heating and air conditioning requirements of the dwelling. This system needs only a unidirectional heat pump, heat exchangers, water evaporators, and a large storage medium. Thus, it eliminates one of the two costly variables in an alternate energy system—the collectors, replacing them by utilizing naturally occurring solar energy during the summer months.

The economic importance of utilizing solar collectors in a residential heating and cooling system will be examined in this paper. The basis for the study will be an experimental "solar" house containing a solar-assisted heat pump heating and

cooling system. A computer model is used to predict annual operating costs for the solar-assisted system, ACES system, and conventional heating and cooling systems (gas, oil, electric resistance).

MATERIALS AND METHODS

Description of System.—The solar-assisted heat pump system used in this analysis is shown schematically in Figure 1. The system utilizes unidirectional heat pumps, forced air collectors, a water storage capacity, and air-to-water heat

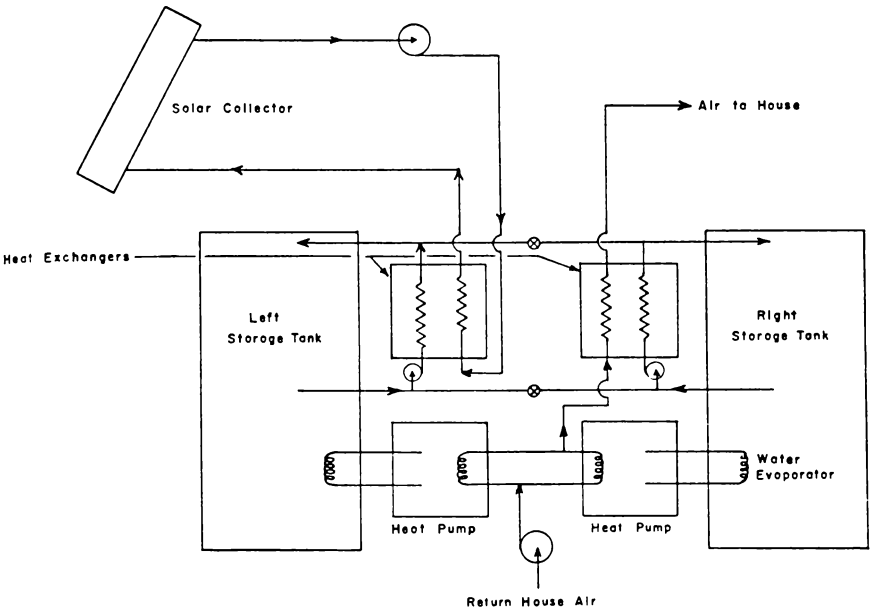

Figure 1. Single Zone solar-assisted heat pump system.

exchangers for effective heat transfer. Somerville (1977) offers a complete system breakdown with operating modes and subsystem functions. Mathsen (1977) describes and discusses the solar collector design and operational performance characteristics.

System Computer Simulation.—Loken (1977) prepared a comprehensive mathematical model of the solar-assist system to predict the operating performance and economy. The computer model consists of a series of differential equations resulting from a first law of thermodynamics analysis of the dwelling,

storage tanks, and collectors. It simulates a yearly run of the solar-assisted system. Also analyzed are the performance and annual operating costs of conventional systems operating under similar conditions as the solar-assisted heat pump system. Design parameters and initial conditions are input at the beginning of the program. Solar isolation on the collector surface is computed using average monthly insolation levels for 48° latitude, interpolated to a daily basis. Energy stored in the storage water and the heating and cooling loads are calculated from system conditions beginning with the initial input. Program output yields the daily, monthly, and yearly heat energy totals, operating performance and cost of the solar assisted system and of the conventional systems.

Analysis Format and Assumptions.—The various systems analyzed were examined in light of local conditions, i.e., local gas, oil, electric rates, equipment, and labor costs. Each system was economically examined as the "installed" heating and cooling system of the test home. Table 1 shows the comparison of

Table 1. Comparison of initial systems cost.

Component	Solar-Assisted Assisted Heat Pump	Oil-Fired Furnace	Gas-Fired Furnace	Electric Resistance	ACES
Water Storage Tanks					
Tank	1,310				2,700
Liners	1,065				
Insulation/Labor	775				
Solar Collectors					
Material	5,065				
Labor	2,500				
Mechanical Equipment					
Heat Pumps	2,000				2,000
Furnace		770	580	810	
Water Evaporators	500				600
Exchanger Coils	1,200				200
Fans	850				425
Water Pumps	540				125
Air-Conditioner		850	850	850	
Fuel Tank		250			
Vent		280			
Controls	200			220	200
Duct Work/Hookup	3,300	1,910	1,910		2,250
Plumbing	600				500
Insulation	440				
Collector Backing					
TOTALS	$20,345	$4,060	$3,340	$1,880	$9,000

initial equipment and labor costs for each system. Annual operational costs for each system were computed on the basis of their respective operating performance characteristics. The total annual cost of each was computed using the initial cost, annual operating cost, and an annual gradient included to simulate inflation and fuel price escalation. Each system was examined for a twenty year life and under two different interest rates. Total annual costs were calculated at 6% interest and 10% interest. The 6% analysis assumes that the owner has the choice of the extra initial investment for the higher priced solar or ACES system. A 6% interest rate is what he could expect had he chosen some other type of investment. The 10% analysis assumes the owner borrowing the initial investment and attaining a mortgage.

The cost of operating the solar-assisted heat pump system to supply building heating and cooling requirements is comprised of three basic components:

1. Heat pump operating costs.
2. Solar collector operating costs.
3. House fan and pump operating costs.

The cost of operating the ACES contains the same components as the solar-assist system without the solar collector operational costs. The cost of operating the heat pumps is a function of the pump Coefficient of Performance (COP). The COP is dependent on evaporator temperature which varies with the water temperature. Heat pump performance data input into the program is used to calculate the COP and operating cost at the various water temperatures. The solar collector operating costs are based on collector fan and pump costs. The cost is calculated from the house heating loads and the local graduated electric rate (NSP, 1977). A base load of 500 kwh/month is assumed in all computations.

Table 2. Cost comparison for solar-assist heat pump system with various collector areas.

Collector Face Area (m^2)	Initial Cost ($)	Salvage Value ($)	Operating Costs* ($)	($) Gradient	Annual Cost ($) 6%	10%
100	20,345	2,035	221	22	2,118	2,721
90	19,195	1,920	232	23	2,033	2,606
80	18,045	1,805	239	24	1,950	2,485
70	16,895	1,690	245	25	1,862	2,362
60	15,745	1,575	251	25	1,776	2,234
50	14,595	1,460	255	26	1,685	2,112
40	13,445	1,345	259	26	1,596	1,985
30	12,295	1,230	262	26	1,503	1,858
20	11,145	1,115	263	26	1,408	1,726
10	9,995	1,000	266	27	1,317	1,598
0	8,250	825	270	27	1,178	1,321

*Includes winter heating and summer cooling.

The solar-assist system's economic performance is examined on the basis of solar collector area. The price of solar collectors is assumed to be $107.64/m^2$ ($10/ft^2$) which includes the price of fans, pumps, and extra ductwork. The system with varying collector area is examined with respect to initial cost, salvage value, annual operating disbursements, a 6% inflation and 4% fuel escalation gradient, and total annual costs. The results are tabulated in Table 2.

The cost of delivering heat to the experimental home by means of an oil-fired furnace with an annual efficiency of 65% is computed on the basis of an assumed fuel cost of .113¢/liter (43¢/gallon). The fuel has an assumed higher heating value of 45,140 J/gr (19,420 Btu/lb) and a volume density of 0.87533 gr/cm^3 (7.305 lb/gallon). The summer cooling load is calculated assuming a central air-conditioning system with a system COP of 2.2.

In this analysis the price of natural gas is determined under the local gas rate structure (NSP, 1977). Unique to regions along the United States-Canadian border is an additional Purchase Gas Adjustment (PGA) for imported natural gas. The PGA assumed in this analysis is $5.91¢/m^3$ ($1.675/1,000ft^3$). This is an additional rate above the basic rate structure set by local distributors. Because of the uncertainty of the PGA in this region, the annual cost calculation assumes an annual gradient of 20% of the first year operating costs instead of the 10% gradient assumed by the other systems examined. The gas system gradient consists of 14% gas escalation and 6% inflation. The heating value for natural gas is assumed to have a value of $27.53 J/cm^3$ (1,000 Btu/ft^3). The gas-fired furnace has a seasonal efficiency of 65% and the summer cooling load costs are calculated assuming a central air-conditioner with a system COP of 2.2.

The all electric-resistance heating system is analyzed with the assumption that all space heating requirements are obtained from electric base board heaters with efficiencies of 97%. Cooling requirements are provided by air-conditioning units with COP's of 2.2.

RESULTS

Table 2 shows the cost comparison for the solar assisted system with varying collector area. As collector area is reduced, the fraction of the heat load provided by the heat pump increases. Therefore, operating costs increase. However, it is interesting to note that the *total* annual cost decreases as collector area decreases for both the 6% and 10% case studies.

Table 3 shows the cost comparison for the various systems examined. Though the conventional systems have a much lower initial cost than the solar-assisted or ACES systems, their annual operating costs are twice those of the ACES system. In total annual costs (on a twenty year basis), ACES system and solar-assisted systems both seem economically competitive to the conventional systems, with ACES being the more attractive. The high annual cost of the natural gas system can be attributed to the PGA of imported gas. At 10% interest, ACES, oil-fired, and electric resistance all appear competitive, while solar-assisted and natural gas have a much higher annual cost.

Table 3. Cost comparison for various heating and cooling systems.

System	Initial Cost ($)	Annual Operating Cost ($)	Total Annual Cost ($) i = 6%	i = 10%
Oil-fired Furnace	4,060	515	1,254	1,323
Gas-fired Furnace	3,340	592	1,779	1,753
Electric Resistance	1,880	643	1,294	1,280
Solar-Assist Heat Pump				
Maximum	20,345	221	2,118	2,721
Minimum	9,995	266	1,317	1,598
ACES	9,000	270	1,241	1,400

CONCLUSIONS

The ACES, oil-fired, and electric resistance systems are economically competitive on a twenty year basis and the assumptions of this study e.g., local energy rates, equipment and construction costs and adequate water storage capacity for the ACES system. The future energy rates, lower future costs of solar collectors and/or changes in construction rates could alter this conclusion. The economics of the solar assist and ACES systems and their overall resource impact (potential doubling of resource life) make them look very attractive for future residential heating application.

ACKNOWLEDGMENTS

This study was supported by the University of North Dakota Engineering Experiment Station and a fellowship provided by Trane Company, LaCrosse, Wisconsin. I wish to thank the people affiliated with these organizations for the help and guidance they provided.

LITERATURE CITED

United Nations, Proceedings of the United Nations Conference on New Sources of Energy, Rome, August 21-31, 1961, Vol. 5, United Nations, 1964.

Fischer, H. C. 1976. Thermal Storage Applications of the Ice-Maker Heat Pump. Energy Division, Oak Ridge National Laboratory, Oak Ridge, Tennessee.

Somerville, M. H., Hatesen, D. V. and Loken, G. R. 1977. Design and Analysis of a North Dakota Annual Cycle Residential Solar Heating System. North Dakota. Proc. North Dakota Academy of Science (I).

Mathsen, D. V., Somrville, M. H., and Loke, G. R. 1977. A Flat-Plate Solar Collector Using Non-Black Absorber Elements. North Dakota. Proc. North Dakota Academy of Science (I).

Loken, G. R., Somerville, M. H., and Mathsen, D. V. 1977. A Computer Model for Performance Analysis of a Solar Heated Residential Home in North Dakota. North Dakota. Proc. North Dakota Academy of Science (I).

Northern States Power Company, Electric Rate Book, North Dakota Divisions, 1-27-76.

Northern States Power Company, Gas Rate Book, North Dakota Divisions, 3-2-77.

THE DESIGN AND ANALYSIS OF A NORTH DAKOTA ANNUAL CYCLE RESIDENTIAL SOLAR HEATING SYSTEM

Mason H. Somerville, Don V. Mathsen, Gregory R. Loken
Carl D. Svard and James C. Wendschlag
The Engineering Experiment Station
University of North Dakota
P.O. Box 8103
Grand Forks, North Dakota 58202

ABSTRACT

The design of an experimental residential solar heating system situated in North Dakota is discussed and described. The system described has been built and provides all of the energy required to heat and, under certain operational modes, air-condition the residence. The system presented is flexible; five different operational modes are examined for the system described. It is unique in the Nation and has value as an experimental tool to evaluate the actual characteristics of different solar systems while eliminating the major variable of the residence.

The results indicate that the annual cycle energy system operational mode is the most economic while reducing procured energy by 61 percent over a conventional system. The maximum energy conservation mode reduced the procured energy base by 72 percent but required over twice the capital investment of the annual cycle system.

INTRODUCTION

The designer of a residential solar based heating and air-conditioning system faces a plethora of decisions which must be addressed. The first is to choose between designing a supplementary solar system (one that supplements a conventional heating and air-conditioning system) or a complete system providing all of the heating and air-conditioning requirements. Only complete systems will be discussed here.

Figure 1 shows that the minimum solar insolation occurs during the winter months while the maximum occurs during the summer months. Maximum heat load occurs during the winter and is shown as the mean degree days curve. Consequently, a system that collected solar energy during the summer would probably require less capital investment per unit energy collected that a system built to operate during the winter months. The time of solar energy collection is the conceptual design difference between an active solar collection system (SCS—winter collection) and a passive solar annual cycle energy system (ACES—summer collection). The system described, located north of Larimore, North Dakota, has the capability of being operated as either an SCS or ACES system. As such, it is an experimental system and is unique in the Nation.

Another design problem is to make the total cost (capital, operational, and maintenance) of the installed system economically competitive. There are also strong incentives, from a business viewpoint, to minimize the capital investment cost in favor of increased operational costs. The latter point is one of the principal

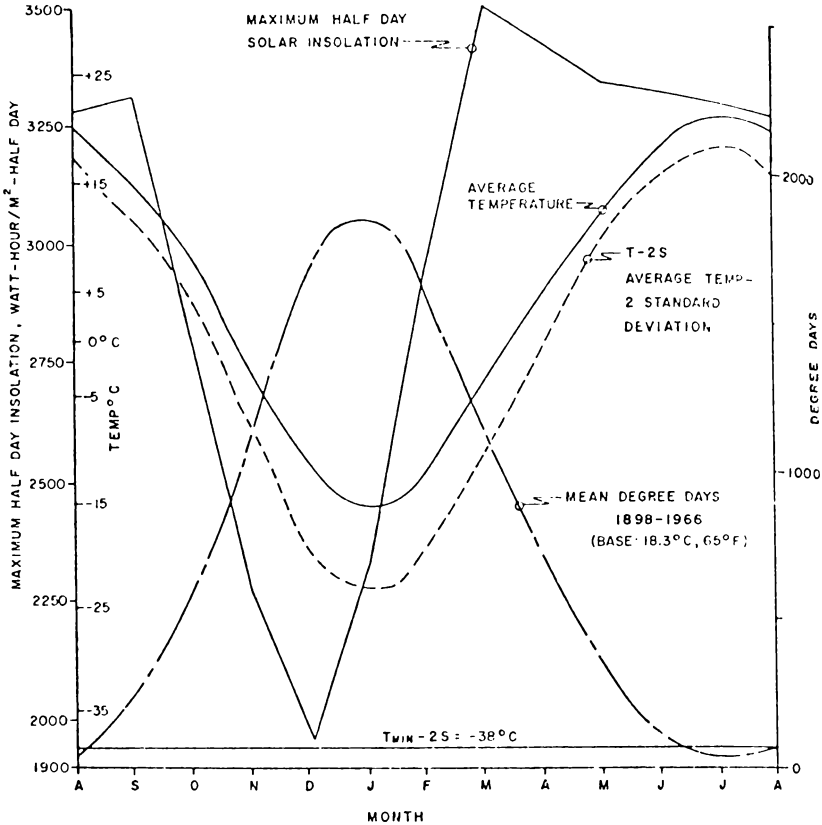

Figure 1. Monthly Solar Insolation, Mean Degree Days, and Average Temperature, Grand Forks, North Dakota, Source: Ashrae 1972.

reasons that solar systems are not widely used today. The system described addresses this capital minimization problem.

Over a thousand solar energy systems exist in the United States today (ERDA 76-144, 1976, 76-1, 1976, 76-127, 1976, 76-128, 1976). Many of these are sponsored by the Energy Research and Development Administration (ERDA). Only nine (ERDA 76-145, 1976) of these are located in a climate approximating that of Grand Forks, North Dakota. None of these are similar to the system described, which the authors believe to be unique to the region and perhaps to the Nation.

The system described has several unique characteristics; which will be discussed here and by Mathsen (1977) and Wendschlag (1977). These characteristics include multiple modes of operation, air-cooled, semi-selective non-black

collector elements, ice-making unitary heat pumps, a flexible but large (15,000 to 150,000 l) water storage volume, and a capability to utilize either or both the sensible and latent heat of fusion storage mechanisms.

The ACES concept was partially developed by Fischer (1976). The ACES system withdraws energy from storage throughout the winter gradually converting the storage liquid (water) to a solid. During the following summer the storage energy is restored by melting solid (ice) formed the preceeding winter. The key to the ACES system is to harvest ice from the evaporator of the system's heat pump at a low or negligible energy cost. Utilization of the sensible and latent heat of fusion effectively increases the thermal storage capacity of a water storage tank by a factor of 2.0 to 2.6 over that of the sensible heat. This has a pronounced beneficial impact on the economics of the system. It also allows the solar collector area to be minimized and, in some cases, allows the solar collector to be completely eliminated.

Institutional constraints represent another area of major concern that the designer faces. Institutional constraints include items such as: solar rights, existing service personnel structure, commercial availability of equipment, unique regional problems, local codes, local utility rate structures, local utility peaking and demand needs, packability of the unit(s), architectural freedom, and retrofit needs. A properly designed solar heating system (SCS or ACES) must address and satisfy most of the instructional constraints listed above.

DESIGN OBJECTIVES

The objectives that are listed below were partially set out at the beginning of the project. Their development continued throughout the project as the design team became more knowledgeable of the problems that had to be addressed.

The design objectives were:

1) The solar heating system was to provide all of the heating and cooling (including dehumidification).
2) The system was to be at least as reliable as a conventional system.
3) The system was to be unique, in an experimental sense, to allow collection of much needed design data.
4) The system was to meet the following institutional constraints:
   a. Conventional house thermostat control was to be used.
   b. The system was to be equivalent to or better than a conventional heating system in regard to utility peaking problems.
   c. The system was to be installed by local contractors.
   d. The system was to be maintained by a local heating and air contractor.
   e. The unit was to have a design life of 20 years.

An economic objective was included in the original objectives. The owner of the system was informed at the beginning of the project that the system would probably not be economically competitive.

DESIGN PROCEDURE

The design procedure consisted of two phases: an approximate design phase and a detailed design phase. Approximately four man-months were devoted to the first phase while forty-eight man-months were expended on the second.

The approximate design phase consisted of four major tasks which were completed for several conceptual designs:

1) Determination of the hourly and seasonal heating and cooling (including dehumidification) loads utilizing standard procedures.
2) Determination of the thermal energy spectrum (energy as a function of collector and environmental temperature) available with different collector designs.
3) Determination of the required storage volumes and evaporator needs for the available heat pumps.
4) Completion of preliminary economic and institutional constraint analyses.

The product of this phase is shown in Figure 2 except that simple coiled copper tubes were to be used as evaporators.

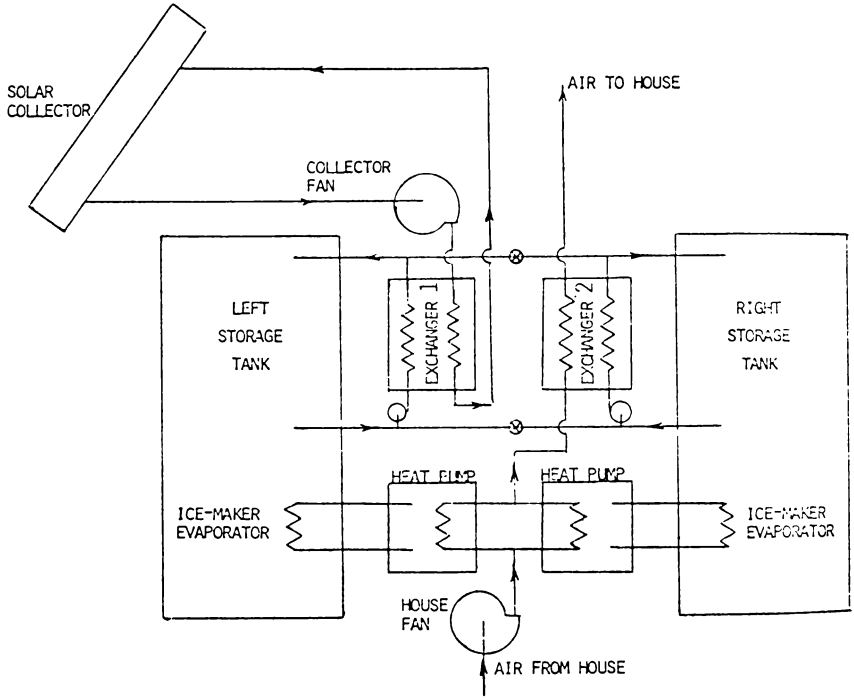

Figure 2. Simplified Schematic of the Solar Energy Heating and Air-Conditioning System.

The detailed design was completed by carrying out several design efforts simultaneously. The following design steps were completed:

1) A detailed research, design, development, and testing program of an air-cooled, semi-selective, non-black collector was completed and is reported by Mathsen (1977).
2) Two mathematical transient models, one of the collector and one of the entire system (collector, storage, heat pumps, ambient conditions, and residence) were written. Algorithms approximating these models were written and the numerical simulations completed. This phase of the work is reported by Loken (1977).
3) A commercially available heating-only heat pump was modified (Wendschlag 1977) to accept ice-maker evaporator plates so that the system could be operated in an ACES mode.
4) A complete economic analysis comparing the SCS and ACES systems with conventional systems was completed by Svard (1977).
5) Commercially available equipment was searched for components that fitted the needs of the system.

The above steps were coordinated and their objectives continually modified so that a practical, economic, flexible heating system would result. The results of this design effort are presented.

DESIGN RESULTS

The major equipment selected and installed in the system (Figure 2) is listed in Table 1 with the manufacturer's specifications. The design specifications of the major items are given in Table 2. These specifications were determined after experimental data for the heat pump and solar collector unit had been gathered and analyzed. The storage volume dimensions are shown in Figure 3; the tanks are 2.6 M (8.5 ft) deep. The choice of two tanks was made on the basis of economic and operational flexibility considerations. The concrete walls shown replaced interior wooden frame structural walls called for by the original design.

The system components key to providing a large degree of flexibility are: two storage tanks, two ice-making heat pumps, the solar collectors, and exchanger number 2. Although not shown in Figure 2, the right storage tank can be mechanically cooled. These items arranged in the manner shown, allow the system to be operated in at least five operation modes.

The objectives of the five operation modes selected for study are listed in Table 3. These modes were selected so that the impact upon energy conservation of different component selection (capital investment) could be determined. The detailed operation of each mode is discussed below. Table 4 summarizes the key operational parameters in the system.

Mode 1.—The first mode of operation was intended to maximize winter energy savings. This is accomplished by operating the solar collector throughout the entire heating season. The collector is turned on September 1, and operates

Table 1. List of mechanical equipment installed in Larimore, North Dakota experimental solar heating system.

Item	Manufacturer	Manufacturer's Specifications	Quantity
Solar Collector Fan	TRANE	220 V, 1 hp, 587 RPM, 3,000 cfm @ 0.82 in. of H_2O, 18FC, type M, #8, ccw, up blast	1
House Fan	TRANE	220 V, 1 hp, 600 RPM, 2,400 cfm @ 67 in. of H_2O, 16FC, type M, #7, ccw, Bottom Horizontal	1
Heat Pumps	JANITROL	#04G03, 35,000 BTUH at 42°F, 38-39 WATT-SAVER	2
Evaporator Pumps	PEABODY BARNES	⅓ hp, SSC27, 25 GPM at 15 ft. head	2
Heat Exchanger Pumps	PEABODY BARNES	SP5, ½ hp, 25 GPM at 70 ft. head	2
Mechanical Cooling	CENTREX	REX 12T, 850 cfm at 2.5 in H_2O, ¼ hp, 1,140 RPM, in line	1
Solar Heat Exchanger	TRANE	type D, 4 row, series 15 with turbulators, 24 x 60	1
House Heat Exchanger	TRANE	type W, 2 row, series 15 with turbulators, 24 x 60	1

until May 1. As a result of this, the temperature of the water storage tank at the beginning of the cooling season will still be very high. This reduces the practicality of air-conditioning with the solar system. The tank will have to be mechanically cooled throughout the entire summer. This mode of operation may increase the energy required to air-condition above that of conventional central air-conditioners. The system, however, maintains the advantage of using off-peak energy for air-conditioning which influences the economics.

Mode 2.—The second mode of operation is a modification of the first with the intent of reducing the amount of mechanical cooling required for air-conditioning. In this mode, the solar collector is turned on September 1. The shut-off point,

Table 2. Design specifications of the major solar heating system components.

	Capacity	
	Metric Units	English Units
Heat Pumps (each)	6.45 KW at 28.3 M^3/min	22 MBTUH at 1,000 CFM
Solar Heat Exchanger	58.6 KW at EAT of 77°C EWT of 32°C	200 MBTUH at EAT of 170°F and EWT of 90°F
House Heat Exchanger	8.8 KW at EAT of 21°C EWT of 35°C	30MBH EAT of 70°F EWT of 95°F
Storage:		
High	151,420 l	40,000 Gal
Startup	94,640 l	25,000 Gal
Low	15,142 l	4,000 Gal
Solar Fan	85 M^3/min @ 2.3 cm of H_2O	3,000 SCFM @ 0.9 in of H_2O
House Fan	56 M_3/min @ 1.5 cm of H_2O	2,000 SCFM @ 0.6 in of H_2O
Evaporator Pumps (each)	94.6 l/min at 4.5 M of H_2O	25 GPM at 15 ft of H_2O
Heat Exchanger Pumps (ea.) (self priming)	94.6 l/min at 12 M of H_2O	25 GPM at 40 ft of H_2O
Solar Collector Area Effective Covered Roof	97.55 M^2 111 M^2	1,050 ft^2 1,200 ft^2

however, is selected early enough so that the remaining heating requirements will drop the storage water temperature to nearly freezing (32°F) by the start of the air-conditioning season (June 1). This will allow much of the total cooling load to be met before mechanical cooling of the tank is required.

Mode 3.—This mode is significantly different from the first and second mode. In this mode, the system is operated as an annual cycle energy system (ACES) and does not require solar collectors. The distinguishing feature of this system is that the storage water becomes a thermal capacitor of sufficient size to cyclically release and absorb a portion of the seasonal heating load and all of the seasonal cooling loads of the dwelling. This is accomplished by utilizing an ice-maker heat pump to remove energy from the water storage tank while heating the house during the winter. This causes the water in the storage tank to freeze. The ice formed during the winter is stored to provide the summer air-conditioning. Melting the ice during the summer returns the energy to the water that was extracted the previous winter. The amount of ice formed exceeds that required for air-

Table 3. Design objectives and equipment arrangement for selected operational modes.

Mode	Objective	Solar Collectors Used	Ice Formed	Single or Dual (Split) Storage Tank Arrangement	
				Winter	Summer
1	Maximize winter energy savings	Yes	No	Single	Dual
2	Maximize winter energy savings consistent with summer conditioning but without ice formation	Yes	No	Single	Single (If properly designed)
3	Operate system as an annual cycle energy system (ACES)	No	Yes	Single	Single
4	Operate system as a series ACES-SCS system	Yes	Yes	Single	Single
5	Operate the system as a parallel ACES-SCS system	Yes	Yes	Dual	Dual

conditioning by a factor of 3 to 4. This excess ice is melted using ambient air (solar energy) as the heat source.

Mode 4.—Operating Mode 4 is a combination of the ACES mode and the direct solar energy operating Mode 2. In this mode, the solar collector is turned on September 1 and shut-off in midwinter. The shutoff point is selected so that the ice formed during the heating cycle will supply the cooling load. This reduces the need to melt excess ice or mechanically cool the storage tanks during summer. Consequently, summer energy requirements are minimized.

Mode 5.—Mode 5, a variation of Mode 4, uses the two tanks as entirely separate systems. One storage tank is used solely in an ACES mode while the other tank is operated in an active solar mode similar to Mode 1. The solar tank is used exclusively for heating when its temperature is above 35°C. The ACES tank is used exclusively for air-conditioning. Mechanical cooling to maintain air-conditioning may or may not be required, depending on the amount of ice generated in the ACES tank. The solar tank is initialized at 43°C in this mode to take into account the solar energy which would be added in August.

SIMULATION RESULTS

Each of the above modes were numerically simulated utilizing Loken's (1977) model. Five yearly simulations initiated at the beginning of heating season, September 1, were completed. Tank temperatures were initialized to 10°C in all

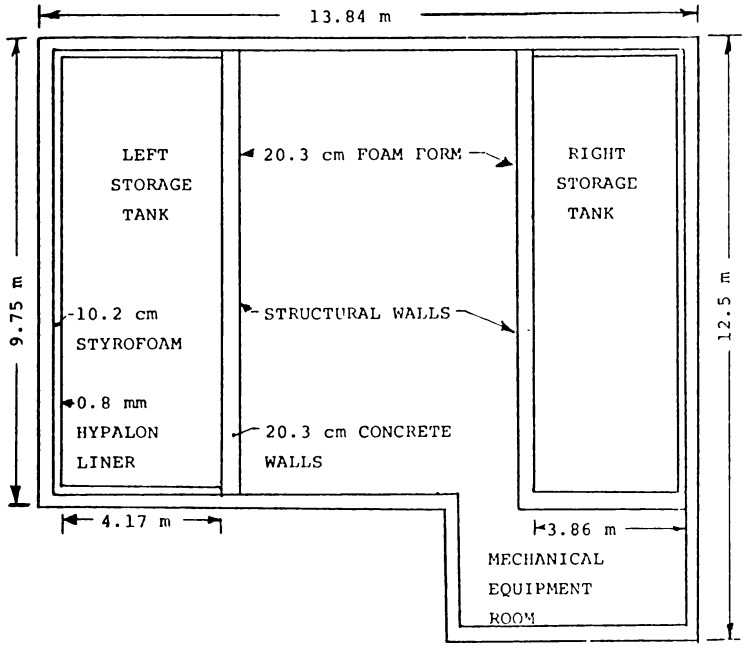

Figure 3. Construction Plans of Basement Storage Tanks.

modes except 5 where it was set to 43°C. The house maintained at 22°C throughout the year. Steady state operation was assumed.

The projected energy usage for each mode is shown in Table 5. The "Energy Furnished" columns represent the total energy supplied to the dwelling on a seasonal or annual basis. The average seasonal heating load for the structure analyzed is 30,540 KW-HR; the average seasonal cooling load is 2,630 KW-HR. The coefficient of performance (COP) is defined as the ratio of the energy furnished to energy procured (electrical input). The seasonal and annual coefficient of performances are also reported in Table 4 with the capital investment required by each mode. Wendschlag (1977) has developed detailed storage tank temperature profiles for each of the simulated operation modes presented.

DISCUSSION

All, except one, of the design objectives have been met or exceeded. The system described provides all of the heating requirements and can provide the required air-conditioning. The reliability of the system is greater than a conventional system's. This is due to the heat pump-storage tank operation. The system is unique in the nation in that it can be operated in several modes which span the entire design range of solar heating systems. The system meets four of

Table 4. Capital investment impact upon selected system operational parameters

Mode	Solar Collector On	Solar Collector Off	Tank Temperature, C Max	Tank Temperature, C Min	Time Weighted Average Temperature, C	Approximate Capital Required	Capital Cost S/Unit COP
1	Sept 1	May 1	38.5	10	23.9	18,000	5,960
2	Sept 1	Mar 16	40.5	1.1	18.3	18,000	5,696
3	NOT USED		12.8	0	1.7	9,000	3,474
4	Sept 1	Feb 4	38.3	0	12.2	18,000	5,678
5	Aug 22	June 1	57.8 Solar 17.2 Aces	13.3 0	26.1	20,500	5,758

Table 5. Simulated system energy usage for selected operational modes.

	Winter			Summer			Annual	
Mode	Energy KW-HRx10³	Electrical KW-HRx10³	Winter COP	Energy KW-HRx10³	Electrical KW-HRx10³	Summer COP	Energy KW-HRx10³	Electrical KW-HRx10³
1	29.77	9.35	3.18	2.64	1.38	1.91	32.41	10.72
2	30.85	9.84	3.13	2.58	0.76	3.38	33.43	10.61
3	30.53	12.51	2.44	2.81	0.37	7.68	33.34	12.89
4	30.74	10.43	2.95	2.72	0.12	22.14	33.46	10.55
5	30.79	8.12	3.79	2.40	1.20	7.00	33.20	9.32

the five institutional constraints set out as design objectives. The projected life of the system is twenty years; however, it is the authors' opinion that the collector's outer convective shield may have a ten to fifteen year life.

The energy data presented (Table 5) indicates that the optimum conservation operation mode is Mode 5 which is a parallel SCS-ACES system. The economic data (Table 4) indicates that the optimum economic operation mode may be Mode 3. This result is substantiated by the work of Svard (1977) which indicates that Mode 3 is economically competitive with conventional systems on a twenty year life basis. The differential percentage energy savings between Modes 3 and 5 are small. Mode 3 saves 61 percent [(1-½.59)*100] of the energy that would have been procurred by a conventional heating and air-conditioning system. Mode 5, the maximum energy conservation mode, saves 72 percent. Although not all of the possible operation modes have been examined, it is unlikely that an energy savings greater than 80 percent can be achieved. To obtain 80 percent, the storage volume (94, 353 l) would be reduced to a somewhat lower volume (approximately 37,400 l) and air-conditioning would be eliminated. However, the system operated in this manner, would become a utility peaking unit. This forces the utility to charge a higher electric rate and would make the system even less economically attractive than it is currently.

The ACES operation mode appears to be a very reasonable compromise between energy savings and capital investment for the North Dakota environment. The ACES system concept is likely to be developed before large SCS systems because of its inherrent advantages of high energy savings at a significantly lower capital cost. The experimental system described that has been built and will provide experimental system data needed in the solar heating and air-conditioning field.

ACKNOWLEDGMENTS

The authors acknowledge the support of the sponsors who donated time, money, and equipment to the project. The authors thank Misses Joan Hanson, Gloria Lembke, and Nancy Carlson for their clerical assistance. The sponsors of this project are listed below.

U.N.D. Engineering Experiment Station, Grand Forks, ND
Mr. Jim Stover, Larimore, ND
Engineering Associates, Grand Forks, ND
Marvin Windows, Warroad, MN
Northern States Power, Grand Forks, ND
Minnkota Power, Grand Forks, ND
Otter Tail Power, Fergus Falls, MN
Nodak Power Cooperative, Grand Forks, ND
Trane Company, LaCrosse, WI
Johnson Controls, Fargo, ND
Andro Corporation, Columbus, OH
B.F. Goodrich General Products Company, Akron, OH

Burke Rubber Company, San Jose, CA
Canton Redwood Yard, Inc., Minneapolis, MN
Foam Form, Inc., Scarborough, Ontario
McIntyre Plumbing Heating & Air-Conditioning, Inc., Grand Forks, ND
Owens-Corning Insulation, Granville, OH
Meland Lumber Company, Larimore, ND
Wholesale Building Supply, Inc., East Grand Forks, MN
Mr. Gary Johnson, Grand Forks, ND
Mr. Arnold Hanson, Devils Lake, ND
Mr. Dick Widseth, Crookston, MN
Mr. Lloyd Nordling, Grand Forks, ND

LITERATURE CITED

Ashrae, Handbook of Fundamentals. 1972. American Society of Heating, Refrigeration, and Air-conditioning Engineers, Inc. New York.

Erda. 1976. Division of Solar Energy. Interim Report: national program plan for research and development in solar heating and cooling. Washington, D.C.

Erda. 1976. A National Plan for Energy Research, Development, and Demonstration: Creating Energy Choices for the Future. Erda 76-1. Washington, D.C.

Erda. 1976. National Program for Solar Heating and Cooling of Buildings: Project Data Summaries. Vol. I: ERDA 76-127, August, 1976; Vol. II: ERDA 76-128, November, 1976; Vol. III: ERDA 76-145, November, 1976. Washington, D.C.

Fischer, H. C., Editor, July, 1976. Annual Cycle Energy System Workshop I. October 29-30, 1975, Oak Ridge National Laboratory, Oak Ridge, Tennessee. ORNL/TM-5243.

Loken, G. R., M. H. Somerville, and D. V. Mathsen, 1977. A Computer Model for Performance Analysis of a Solar Heated Residential Home in North Dakota. *Proc. N. Dak. Acad. Sci.* Grand Forks. Manuscript Submitted for Publication.

Mathsen, D.V., M.H. Somerville, and G.R. Loken, 1977. A Flat Plate Solar Collector using Non-black Absorber Elements. *Proc. N. Dak. Acad. Sci.* Grand Forks. Manuscript Submitted for Publication.

Svard, C.D., M.H. Somerville, and D.V. Mathsen, 1977. The Economics of Solar Space Heating and Cooling. *Proc. N. Dak. Acad. Sci.*, Grand Forks. Manuscript Submitted for Publication.

Wendschlag, J.C., April, 1977. Analysis of a Solar Energy Heating and Air-conditioning System for Operation in North Dakota. Senior Honors Thesis, Department of Mechanical Engineering, University of North Dakota, Grand Forks, North Dakota.

Wendschlag, J.C., and M.H. Somerville, 1977. Development and Testing of an Ice-maker Evaporator for a Heating only Heat Pump. *Proc. N. Dak. Acad,* Grand Forks. Manuscript Submitted for Publication.

A COMPUTER MODEL FOR PERFORMANCE ANALYSIS OF A SOLAR HEATED RESIDENTIAL HOME IN NORTH DAKOTA

Gregory R. Loken
Mason H. Somerville
and
Don V. Mathsen
Engineering Experiment Station
University of North Dakota
P.O. Box 8103
Grand Forks, North Dakota 58202

ABSTRACT

A computer model to simulate the yearly performance of a solar assisted heat pump domestic residence heating system in Larimore, North Dakota, is presented. The house modeled is a two-story structure and has 97m² (1,050 ft²) of solar collector, two water tanks, and two 36.9 MJ/hr (35,000 Btu/h) heat pumps. Differential equations describing the collectors, house, and storage were numerically solved using a Hammings predictor-corrector routine with a Runge-Kutta startup. Other routines were used but were not successful. Local weather records providing hourly temperature and insolation conditions were used to provide the physical boundary conditions. The model provides yearly operating costs for the solar heated residence as a function of equipment and environmental parameters which will assist in selection of the most desirable operating mode and will allow optimization of future designs.

INTRODUCTION

Recent energy shortages have prompted increased interest in developing alternative energy sources to replace or supplement dwindling resources. One of the most abundant and uniformly available sources of energy is sunlight; however, exploitation of solar energy has been frustrated by the diffuse and intermittant nature of solare radiation at the earth's surface. Although these properties constitute serious technical and economic roadblocks to solar development, there are some potentially feasible applications. A case in point is heating ventilating and air-conditioning (HVAC) of structures for human comfort. The potential impact of solar heating systems on United States energy consumption is significant. Reynolds, (1974: 15) indicates that 25 percent of the United States gross energy consumption is used for domestic and commercial space heating. This study is concerned specifically with the space heating application of solar energy to single family domestic residences.

Design of solar HVAC systems which are both functionally and economically competitive with conventional systems represent a challenge to the designer because it is very difficult to reliably predict how well a given system will perform under actual operating conditions. Much research has been devoted to devising analytical techniques and mathematical models to evaluate and simulate the performance of solar HVAC systems. These efforts have been directed to five major

areas: (1) prediction of solar radiation (Liu and Jordan, 1963), (2) solar collector analysis (Klein, et al., 1973), (3) thermal storage analysis (Telks, 1974), (4) structure heating and cooling load analysis ASHRAE, 1972), and (5) overall system analysis (Freemont, et al., 1975). The references cited above comprise only a partial list of the literature available with the number of publications increasing each year.

This study addresses the overall system analysis approach to solar HVAC design by integrating suitable mathematical models of physical processes together. A numerical algorithm written for the digital computer provides solutions to the system model as a function of time throughout the year. The remainder of the paper describes the overall system simulation model and its utility beginning with a description of the dwelling and the solar heating system followed by development of the mathematical model, verification of the model, and results of the analysis of two system design variations.

The house used for the purpose of this study, located in Larimore, North Dakota, is a two-story wood structure with 213m² (2,300 ft²) of floor space and a full basement. Energy conservation features include six inch wall construction with fiberglass insulation, twelve inch attic insulation, and triple pane windows. Design heating and cooling loads are 42.2 and 27.4 MJ/hr (40,000 and 26,000 Btuh) respectively. A conventional forced air distribution system with standard thermostat controls maintains indoor climate conditions. Two storage tanks, each with a capacity of 68m³ (2,400 ft³), are located in the basement and 97.5m² (2,050 ft²) of solar collector is located on the south roof, tilted 63.4° from horizontal.

The heating system can best be described as a "solar assisted heat pump system (Jordan and Threlkeld, 1954)." Solar heating systems are usually comprised of the following basic units: solar collector, thermal storage, backup system, energy transfer equipment, and controls. Figure 1 schematically illustrates the system considered in this study. No backup system is shown because it is not needed. A flat plate solar collector using air as the working fluid transfers heat to the thermal storage medium (water) with an air-water heat exchanger. Two Janitrol heating-only (unitary) heat pumps, each with a condenser capacity of 28.2 MJ/hr at 0°C (32°F) evaporator temperature (Janitrol, 1976), are used to remove heat from storage for house heating when storage temperature is less than 35°C (95°F). If storage temperature drops to freezing, the heat pump evaporators utilize the latent heat of fusion of water by forming ice. At storage temperatures above 35°C, the house is heated directly with hot water via heat exchanger X_H. The house is cooled during the summer by purposely chilling the storage water with the heat pumps (condenser load is dumped to ambient) and circulating the water through exchanger X_H.

An important variation of the solar assisted heat pump system is the annual cycle energy system (ACES) (Fischer, 1976). The discerning feature of this system is that the storage medium becomes a thermal capacitor of sufficient size to cyclically release and adsorb the seasonal heating and cooling load of the dwelling. During the heating season, heat pumps extract heat from thhe storage water

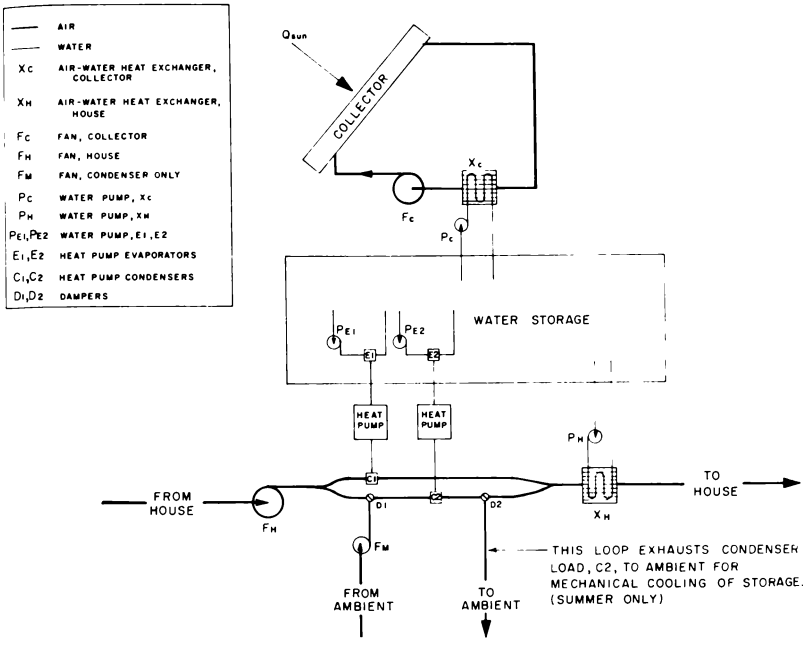

FIGURE 1. Solar Heating and Cooling System for the Larimore House.

making ice in the process which is stored until needed for summer cooling. Amounts of ice in excess of cooling needs will be formed in geographic locations where the heating load exceeds the cooling load. The extra ice may be melted with ambient air or simple solar collectors in the summer. Inexpensive solar collectors may also be used in the heating season to melt ice and thus reduce storage volume requirements.

This study developed a mathematical model of the system described above which simulates yearly performance. The differential equations resulting from a First Law of Thermodynamics analysis of the solar collector, thermal storage medium, and dwelling form the basis for the mathematical model developed. The physical (not mathematical) boundary conditions as a function of time are provided and account for transient solar radiation and environmental temperature phenomena. Numerical solution of the differential equations is accomplished with Hamming's modified predictor-corrector method with a Runge-Kutta startup allgorithm (IBM, 1970: 337-341).

The model provides system performance data in the form of temperatures, heat balances, and operating costs. From this information it is possible to evaluate different combinations of design parameters and operating modes. Operating costs for conventional types of space heating are also calculated for comparison purposes.

MATHEMATICAL MODELS

A brief discussion of the mathematical models devised or adapted for this study will be presented. The models can be catagorized into three general groups: (1) solar collector, (2) thermal storage and dwelling, and (3) physical boundary conditions. Each of these models and the major assumptions are discussed below.

Solar Collector.—This analysis treats the solar collector as a closed system which exchanges energy with the surroundings by means of conduction, convection, and radiation at its boundaries (Brown, 1976). The First Law of Thermodynamics, written for various collector components, reduces to the following system of differential equations:

$$\sum_{k=1}^{n} \frac{dQ_{k,i}}{dt} = m_i(T_i) \cdot C_{vi}(T_i) \cdot \frac{dT_i}{dt} \quad i = 1, p \tag{1}$$

Subject to the initial conditions:

$$T(t_o) = T_o \tag{2}$$

Where mass and specific heat may or may not be functions of temperature. These equations, subject to physical boundary conditions of solar insolation and environmental temperature, govern the transient interchange of energy between the collector coverplates, absorber plates, and working fluid.

In the course of the study it became apparent that solution of equations (1) would be impractical because the thermal time constants are small. As a result, the differential equation solver must choose small timesteps to insure numerical accuracy and stability which leads to excessive computer usage. The problem was overcome by neglecting transient effects. Although thermal capacitance losses are not accounted for, (Klein, et al. 1973) suggests that zero capacitance solar collector models will give performance predictions comparable to transient models.

Transient effects were ignored by making the right hand sides of (1) zero which reduces the set of simultaneous differential equations to a set of simultaneous nonlinear algebraic equations. Collector efficiency as a function of all combinations of solar insolation, environmental temperatures, and thermal storage temperatures was then calculated by a computer program (Brown, 1976) and reduced to simple equation form for the overall system simulation model.

Overall System.—The governing differential equations for the overall system model are derived from a First Law of Thermodynamics analysis of the dwelling and storage units. Both are assumed to be single node lumped capacitance closed systems which exchange heat with the surroundings at system boundaries. This system of equations takes the same form as equations (1) with boundary conditions of solar insolation and environmental temperature. Heat transfer rate ter-

ms follow from the house heating/cooling load analysis (ASHRAE, 1972), heat pump manufacturer data (Janitrol, 1976), and elementary conduction/convention heat transfer analysis.

Boundary Condition-Solar Insolation.—The hourly direct, diffuse, and reflected solar radiation is calculated as a function of time throughout the year by the method of Liu and Jordan (Liu and Jordan, 1963). It is a comprehensive procedure which uses H, the long-term monthly average daily total radiation on a horizontal surface, and K_T, the fraction of extraterrestrial radiation transmitted through the atmosphere, to predict the long-term hourly average total solar radiation on a tilted surface. H was determined from (Hammon, et al., 1954: 145, Figure 5), and K_T was determined from Saint Cloud, Minnesota weather data. Saint Cloud was chosen because it is a nearby weather recording point that measurers K_T.

A computer algorithm was written which generates a one year data set of long-term hourly average total solar insolation for input to the overall simulation model (Brown, 1976). Figure 2 shows the daily total solar insolation on a flat surface tilted 60° from horizontal to the south, plotted as a function of time, as calculated by the simulation program for the Grand Forks area.

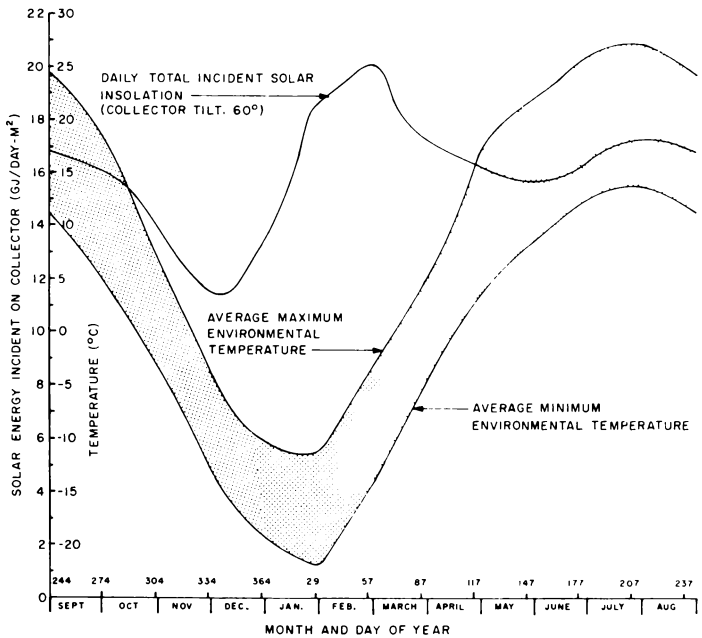

FIGURE 2. Yearly Average Maximum and Minimum Environmental Temperature Distribution and the Total Daily Solar Radiation Incident on a Flat Surface Tilted 60° from Horizontal to the South.

Boundary Condition-Environmental Temperature.—The long-term average hourly variation of environmental temperature is calculated based upon average maximum and minimum daily temperatures and the daily variation of temperature. Local weather records with a 74 year data base were used to provide the daily average maximum and minimum temperatures (Figure 2) (Computer Summary, 1976). The variation of temperature for any day in a specific month is based upon the actual temperature variation for one day in that month. In other words, one representative day was chosen from each of twelve consecutive months (June 1974 - May 1975) and the actual temperature distributions for these days were plotted in a nondimensional manner. As the simulation progresses through each day, the environmental temperature varies between the average maximum and minimum temperatures recorded for that day according to the daily temperature distribution for the appropriate month. This model accounts for both long-term average environmental temperature and the seasonal variations in daily temperature distribution.

COMPUTER PROGRAM

A numerical computer algorithm utilizes each of the mathematical models discussed above to formulate an overall solar heating system computer simulation model. The algorithm consists of a main program, the numerical integration subroutine, and several other subroutines. The algorithm can accommodate both the solar and ACES versions of the system with either single or dual storage tanks. Execution time (CPU) is about thirteen minutes for a one year (8,760 hour) simulation run.

Detailed verification of the model is not possible because of the lack of supporting experimental data; however, it is appropriate to compare the heating and cooling loads calculated by the model with the rule-of-thumb estimates used by local HVAC engineers and the degree-hour method. Figure 3 shows the cumulative heating and cooling loads for the dwelling as calculated by the simulation algorithm, and Table 1 lists the seasonal heating and cooling loads calculated by the model, the degree-hour method, and by rule-of-thumb. The model underpredicts the degree-hour heat load calculation by 4 percent and overpredicts the rule-of-thumb heat load calculation by 38 percent. Cooling load undershoots the degree-hour method by 10 percent and undershoots the rule-of-thumb method by 44 percent. Because many factors which influence the HVAC energy consumption are variable from dwelling to dwelling and even from family to family, the verification and calibration of the model will have to await receipt of actual operating data. Although sophisticated computer software is available for heating/cooling load analysis (Kusudu, 1976), moderate refinement and calibration of the simple model used in this study will probably give performance predictions within acceptable limits of actual operating data with less expenditure of computer storage and run times.

RESULTS

The results of two computer runs, one for a solar operating mode and one for

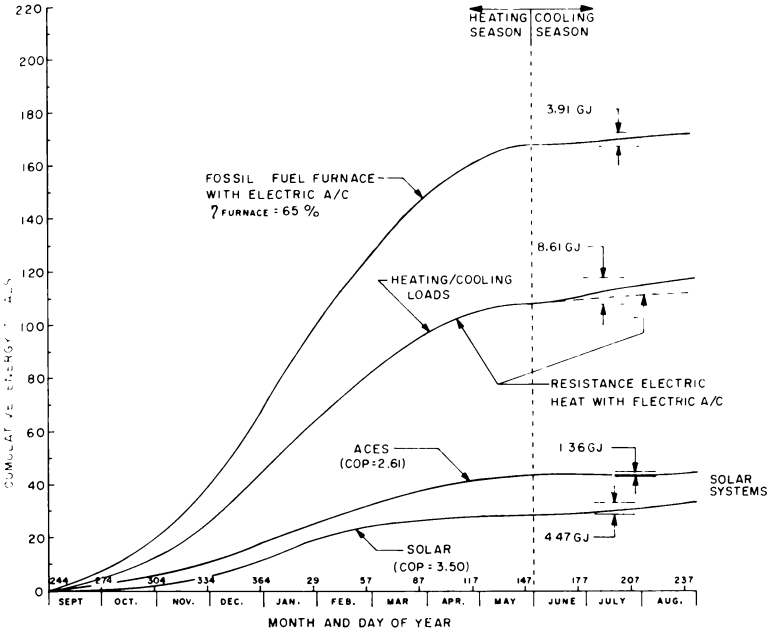

FIGURE 3. Cumulative Heating and Cooling Loads and Cumulative Energy Consumption for Solar, ACES, Fossil, Fuel, and Resistance Electric Heating Systems.

an ACES mode are presented. The following paragraphs briefly outline the operating modes and results. Figure 4, the yearly storage tank temperature distributions presents some of the numerical results of the study and is discussed in detail in the Discussion.

Solar Operating Mode.—In the solar mode, two storage tanks with 49,500 Kg water capacity each are operated independently of each other. Tank 1 is heated by the solar collector throughout most of the year and tank 2 is used for cooling. During the heating season the house may either be heated by hot water if tank 1 temperature is above 35°C (95°F) or by the heat pumps if tank 1 temperature is below 35°C. The storage tanks each have one heat pump; therefore, heat pump operation removes energy from both tanks, but at different rates because heat pump performance depends upon tank temperature. At the beginning of summer (June 1) the collector is turned off allowing tank 1 to cool, and tank 2 is maintained at or below 12.8°C (55°F) by the heat pump for summer cooling. Near the middle of August the solar collector is reactiviated to heat tank 1 in preparation for winter.

ACES Operating Mode.—There are two variations of this mode which assumes one storage tank of 99,000 Kg water capacity and no solar collectors.

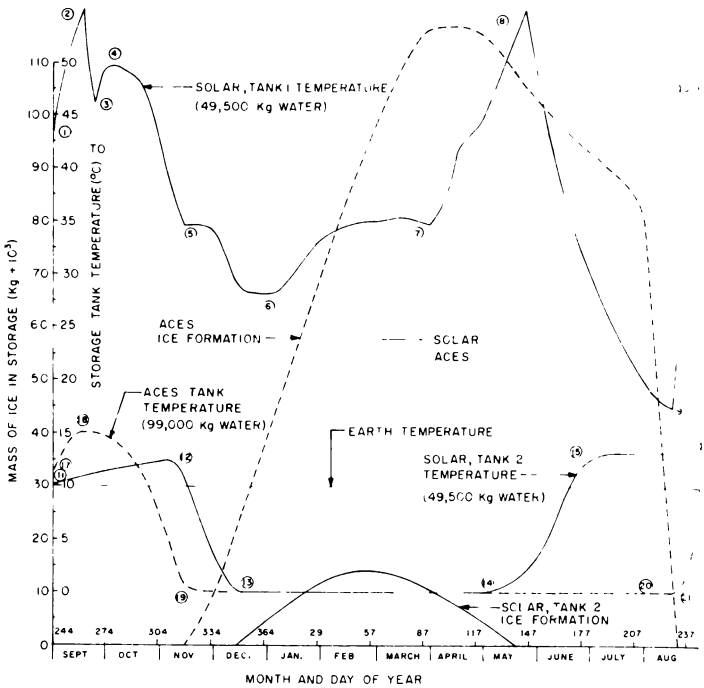

FIGURE 4. Ice Formation and Thermal Storage Temperature Distribution Curves for Solar and ACES Systems.

The first melts ice made during the winter by circulating ambient air through heat exchanger X_H during the summer and fall. A second variation utilizes heat pumps with an ice maker evaporator and an air evaporator. At environmental temperatures above a given set point, say 4.4°C, the heat pumps use ambient air as their low side heat source, and at temperatures below the set point the storage water is used.

Figure 4 indicates that ACES ice formation peaks at 117,000 Kg which would require about 46 percent more storage volume than initially specified if it is assumed that 80 percent of the storage water is frozen. The second scheme described above helps to ease the demand on storage by up to 50 percent depending upon the set point temperature chosen. Other alternatives to building very large storage systems include inexpensive solar collectors and sewage waste heat utilization.

The cumulative energy consumption for each of the systems analyzed is plotted in Figure 3. It is evident that less energy was purchased for solar and ACES operation than was needed to heat and cool the dwelling. This observation is quantified by the coefficient of performance (COP), defined as the ratio of useful

TABLE 1. Heating and Cooling Loads for the Larimore House as Calculated by Computer Simulation, Degree-Hour, and Rule-of-Thumb Methods.

	Heating Load (GJ)	Cooling Load (GJ)
Simulation Model	109	9
Degree-Hour Method	114	10
Rule-of-Thumb Method	68	16

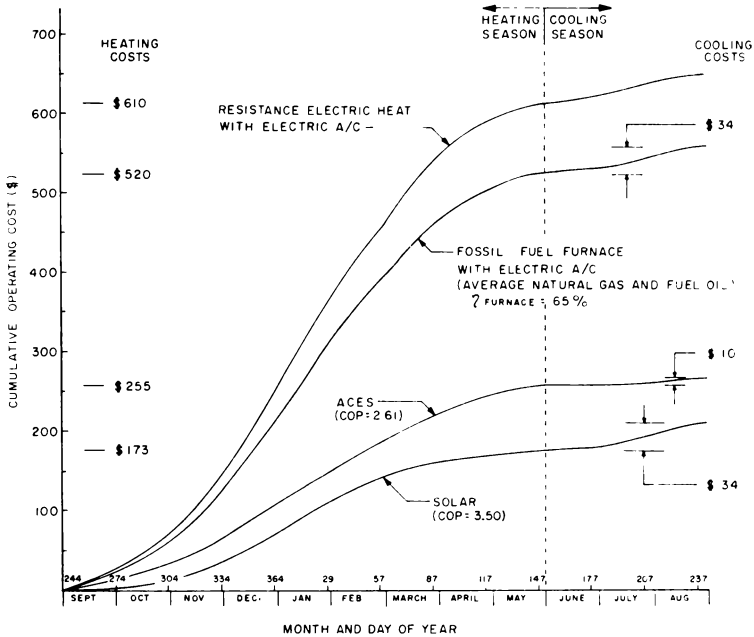

FIGURE 5. Cumulative Operating Costs for Solar, ACES, Fossil Fuel, and Resistance Electric Heating Systems.

energy obtained to energy purchased. For the fossil fuel system, the COP becomes less than unity and is termed efficiency.

Figure 5 shows the cumulative operating costs for resistance electric, fossil fuel (average of local natural gas and fuel oil) ACES, and solar heating systems. Electricity costs reflect the rate structure of a local utility with a 500 Kw-hr base load. The operating cost advantage of solar and ACES heating systems over conventional heating systems is obvious, but operating costs alone do not economically justify one system over another. Capital Costs, equipment life, inflation and other factors must also be considered in an economic analysis. Using

the simulation program and the Larimore house heating system design as data bases, (Svard, 1977) has analyzed the economics of solar and ACES heating in North Dakota.

DISCUSSION

It is sometimes desirable to estimate the primary resource energy consumption of a particular system in order to establish a common reference datum. If electrical energy consumption is divided by the national average electrical generation efficiency of 30.8 percent (Reynolds, 1974: 15), the result is the fossil fuel consumption of the power plant. The resource energy consumption for ACES and solar closely parallels the dwelling load (resource COP is near unity) while electric resistance heat exceeds fossil fuel systems in resource energy consumption.

In order to more effectively interpret the data presented in Figure 4, events denoted by encircled numbers on the figure and the processes occurring between events are described below.

Event 1: initial temperature of tank 1 in the solar operating mode. Process 1-2: temperature increases because solar heat gain exceeds tank heat losses to earth and dwelling.

Event 2: collector has been switched off by tank thermostat on the high temperature setpoint. Process 2-3: temperature decreases because collector is off and heat loss from tank to earth and dwelling remains.

Event 3: collector switched on by tank thermostat on the low temperature setpoint. Process 3-4: temperature increases because solar heat gain exceeds tank heat loss.

Event 4: solar heat gain becomes equal to tank heat loss. Process 4-5: temperature decreases because of decreasing solar radiation and increasing load on the tank from the dwelling heating requirements.

Event 5: switchover from direct hot water to heat pumps at 35°C tank temperature. Process 5-6: curve flattens because heat pump removes less heat from the tank than the heat exchanger. Temperature continues downward as solar radiation and environmental temperature decrease.

Event 6: solar heat gain becomes equal to the tank heat load as solar radiation and environmental temperature bottom out. Process 6-7: temperature increases with increasing solar radiation and environmental temperature.

Event 7: switchover from heat pumps to direct heating with the heat exchanger. Process 7-8: solar heat gain exceeds heat load on tank.

Event 8: collector switched off by tank thermostat on high temperature setpoint and is left off for the summer. Process 8-9: temperature decreases because collector is off and tank transfers heat to the earth and dwelling through its walls.

Event 9: collector is turned on to heat tank in preparation for winter. Process 9-10: temperature increases because solar heat gain exceeds tank heat loss.

Event 10: termination of the simulation run.

Event 11: initial temperature of tank 2 in the solar operating mode. Process

11-12: temperature increases because heat gain from dwelling through the tank walls exceeds heat loss to the earth.

Event 12: switchover from direct hot water heating by tank 1 exclusively to heating from both tanks by the heat pumps. Process 12-13: heat pump evaporator load on tank exceeds heat gain from earth and dwelling.

Event 13: temperature levels out and remains constant because of ice formation. Process 13-14: temperature constant as ice is formed and melted.

Event 14: temperature begins to rise because ice has melted. Process 14-15: temperature increases because heat pump is no longer operating and dwelling begins to require cooling.

Event 15: heat pump begins operating to mechanically cool tank for summer cooling. Process 15-16: temperature maintained at summer cooling setpoint.

Event 16: termination of the simulation run.

Event 17: initial tank temperature for ACES operating mode. Process 17-18: temperature increasing because ambient heat gain via X_H exceeds tank heat loss.

Event 18: ambient heat gain becomes equal to tank heat loss. Process 18-19: temperature decreases as environmental heat load on dwelling causes increased heat load on tank.

Event 19: temperature levels out because of ice formation. Process 19-20: temperature remains constant as ice is formed and melted.

Event 20: Exchanger X_H is allowed to begin melting ice using ambient air. Process 20-21: temperature constant as ice is melted.

Event 21: temperature begins to rise when ice is gone. Process 21-22: temperature increases because tank is being heated by ambient air, the earth, and the dwelling.

Event 22: termination of the simulation run.

CONCLUSIONS AND RECOMMENDATIONS

A mathematical model of a solar assisted heat pump HVAC system has been presented. The model is incorporated into a digital computer algorithm and the ability of the model to predict annual system performance is indicated. Although not precise in an absolute sense, the model allows quantitative comparison of different design alternatives.

Further development of the simulation model should include refinement and calibration of the mathematical models, and extension of program capability to accommodate a variety of system configurations and operating schemes. Finally, the computer program should be made user oriented to permit efficient use by application oriented engineers.

ACKNOWLEDGMENTS

The authors extend their appreciation to the Engineering Experiment Station for support of the above work. In particular, the Otter Tail Power Company sponsored the principle author's graduate study. James Wendschlag and Jeff Brown

assisted with the program and model development, Joan Hanson and Gloria Lembke typed the manuscript, and JoAnn Maloney drafted the figures.

LITERATURE CITED

ASHRAE handbook of fundamentals. 1972. American Society of Heating Refrigerating and Air-Conditioning Engineers, Inc., New York.

Brown, Jeffrey J., 1976. Solar collector analysis computer program. University of North Dakota, Engineering Experiment Station, School of Engineering and Mines, Grand Forks, North Dakota.

Brown, Jeffrey J., 1976. Solar collector analysis notes. University of North Dakota, Engineering Experiment Station, School of Engineering and Mines, Grand Forks, North Dakota.

Brown, Jeffrey J., 1976. Solar insolation computer program: method Liu and Jordan. University of North Dakota, Engineering Experiment Station, School of Engineering and Mines, Grand Forks, North Dakota.

Climatic Data Laboratory, Department of Soils, North Dakota State University, 1976. Computer summary: daily maximum and minimum temperature extremes and means for Grand Forks, North Dakota. Fargo, North Dakota.

Fischer, H. C., 1976. The annual cycle energy system. Oak Ridge National Laboratory, Oak Ridge Tennessee.

Freeman, T. L., W. A. Beckman, J. W. Mitchell, and J. A. Duffie, November, 1975. Computer modeling of heat pumps and the simulation of solar-heat pump systems. ASME paper 75-WA/SOL-3.

Hamon, R. W., L. L. Weiss, and W. T. Wilson, June, 1954. Insolation as an empirical function of daily sunshine duration. U.S. Department of Commerce, U.S. Weather Bureau. Monthly Weather Review 82, No. 6: 141-146.

IBM Subroutine HPCG. August, 1970. System/360 scientific subroutine package. Version III, Programmers Manual, Program IBM 360A-CM-03X: 337-341.

Janitrol Specifications. April, 1976. Series 38 and 39 wattsaver. Janitrol Division of Tapan Corporation, 400 Dublin Avenue, Columbus, Ohio.

Jordan, R. C., and J. L. Threlkeld. February, 1954. Design and economics of solar energy heat pump systems. ASHVE Journal, Section, *Heating Piping and Air-Conditioning:* 122-130.

Klein, S. A., J. A. Duffie, and W. A. Beckman, November, 1973. Transient considerations of flat plate solar collectors. ASME pper 73-WA/SOL-1.

Kusuda, T., 1976. NBSLD, The computer program for heating and cooling loads in buildings. U.S. Department of Commerce, National Bureau of Standards, NBS-BSS-69.

Liu, Benjamin Y. H., and R. C. Jordan, 1963. A rational procedure for predicting the long-term average performance of flat plate solar-energy collectors. Solar Energy 18, No. 2: 53-70.

Reynolds, William C., 1974. Energy from nature to man. McGraw-Hill Inc., New York.

Svard, C. D., M. H. Somerville, and D. V. Mathsen, 1977. The economics of solar space heating and cooling. *NDAS Proceedings.* Grand Forks. Manuscript submitted for publication.

Telks, M. E. R., 1974. Solar energy storage. ASHRAE Journal. September: 38-44.

LIST OF SYMBOLS

C_v constant volume specific heat

$\frac{dT_i}{dt}$ differential rate of temperature change

$\frac{dQ_{k,i}}{dt}$ differential rate of heat transfer

K_T fraction of extraterrestrial radiation transmitted through the atmosphere

H long-term monthly average daily total radiation on a horizontal surface

m_i mass of component i

n number of heat transfer terms

p number of differential equations

T_i temperature of component i

$Q_{k,i}$ heat transfer term k for component i

t time

SELECTED PARAMETERS FROM A BASELINE WATER QUALITY STUDY FOR A PROPOSED COAL GASIFICATION PLANT SITE

Yung-Tse Hung, Guilford O. Fossum, and Earl S. Mason
Department of Civil Engineering
University of North Dakota, Grand Forks, North Dakota 58202

ABSTRACT

A water quality study was conducted from April to October 1975 in Dunn County, North Dakota to provide baseline water quality information for a proposed coal gasification plant site. Sampling stations consisted of ten surface water and six groundwater sampling stations. Water analysis included pH, specific conductance, alkalinity, turbidity, dissolved oxygen (DO), chemical oxygen demand, biochemical oxygen demand, fotal suspended solids, total dissolved solids, total hardness, Ca, Mg, Na, K, SO_4, Cl, SiO_2, NO_3, PO_4, coliforms, and others. Major water quality parameters listed in the North Dakota Water Quality Standard were investigated for their seasonal and spatial variabilities and their interrelationships.

Correlation analysis revealed that streamflow was negatively correlated to TDS and specific conductance, and specific conductance was positively correlated to TDS, Na, and total hardness. High concentration of TSS, low concentration of TDS, and high DO concentration were observed in river waters during the spring runoff period. Lowest DO concentration occurred in July's sampling run. During the study groundwaters sampled from farm wells were found to contain high concentrations of TDS. Water parameters exceeding North Dakota State surface water quality standards included turbidity, TDS and fecal coliforms.

INTRODUCTION

At the present time there are proposals to construct coal gasification plants in the western part of North Dakota to help solve the energy shortage problem in this country. One of the main concerns shared by the residents in western North Dakota is the possible water quality deterioration in the area due to the construction and operation of coal gasification facilities. A water quality study was conducted from April to October 1975 in Dunn County, North Dakota to provide baseline water quality information for the proposed coal gasification plant by the Natural Gas Pipeline Company of America. Future water quality measured in the area could be compared to the baseline data to determine if there is any degradation of either surface or groundwater quality. The complete report of water quality study and surface water hydrology is available in the "Enrivonmental Assessment of a 250 MMSCFD Dry Ash Lurgi Coal Gasification Facility in Dunn County, North Dakota," Volume 3, "Water Quality" (Fossum and Hung, 1976) and Volume 4, "Surface Water Hydrology" (Mason, 1976). This paper is limited to the study of selected water quality parameters, which are of importance in the North Dakota Water Quality Standard (North Dakota State Department of Health, 1973) for the proposed plant site.

MATERIALS AND METHODS

Sampling locations — Four important surface water systems in the develop-

ment area include: (1) the Knife River, (2) the Spring Creek, (3) the Little Missouri River, and (4) the Little Missouri Arm of Lake Sakakawea. The first two systems are recipients of possible pollutants from the coal conversion process. The last two systems are possible sources of water supply for the gasification process water. The proposed project area is largely in the drainage basin of Spring Creek which is a tributary of the Knife River, with a portion within direct drainage of the Knife River itself. The drainage areas are 2,507 and 600 square miles for the Knife River and the Spring Creek, respectively.

The locations of groundwater and surface water sampling stations were carefully selected after consultation with the U.S. Geological Survey and the N.D. Geological Survey engineers. As depicted in Figure 1, a total of ten surface water sampling stations including two stations on the Knife River, three stations on

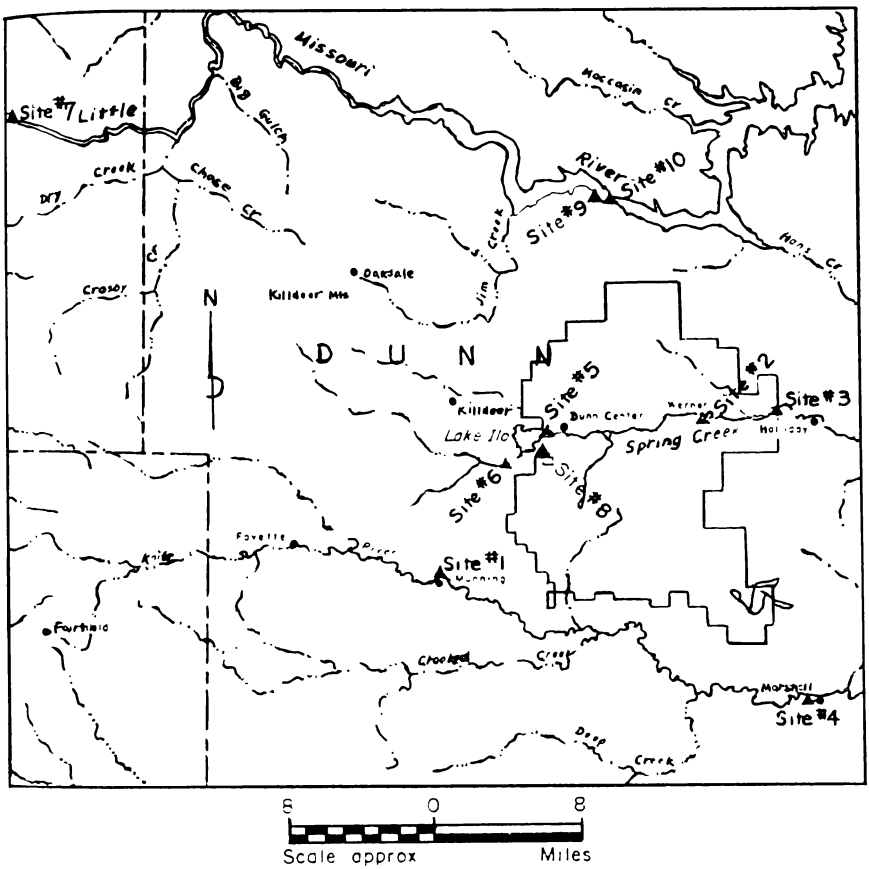

Figure 1. Sampling station locations: surface sites.

Spring Creek and three stations on the Little Missouri River and Lake Sakakawea, were selected as described below:

Station	Description
Site No. 1	USGS station on Knife River near Manning at bridge on North Dakota Highway #22 about ½ mile north of Manning.
2	Spring Creek near Werner. Old bridge on east-west county road ¼ mile west of Werner, on section line between section 24 and 25, T 145 N, R 93 W.
3	Spring Creek near Halliday. Bridge on north-south road about 1¾ miles west and ½ mile north of Halliday by the Neil L. Ferebee farm on section line between sections 22 and 23, T 145 N, R 92 W.
4	USGS station on Knife River at Marshall. At bridge on North Dakota highway #8.
5	Spring Creek near Lake Ilo spillway, at road culvert immediately below the Lake Ilo spillway, S 27, T 145 N, R 94 W.
6	Inflow from Murphy's Slough to Lake Ilo. Temporary station sampled only once due to impassable roads to permanent site #8.
7	USGS station on Little Missouri River near Watford City. At bridge over Little Missouri River on U.S. highway #85, about 17½ miles south of Watford City.
8	Ditch connecting marshland southeast of Lake Ilo to Lake Ilo at culvert with gates on marshland side, S 33, T 145 N, R 94 W.
9	Little Missouri arm of Lake Sakakawea near proposed intake site approximately 100 feet from south shore opposite old American Oil pipeline, NW ¼, SE ¼, S 29, T 147 N, R 93 W.
10	Little Missouri arm of Lake Sakakawea near alternate intake site approximately ½ mile east of site #9.

Six sampling runs were conducted from April to October 1975 to collect water samples from the surface water sampling sites. Groundwater samples were collected at six wells, which were located in, or very near, the proposed mine area and were farm wells currently in use. These wells were the sampling wells of North Dakota Geological Survey for groundwater study in the project area. Well locations are shown in Figure 2 with the following descriptions:

Station	Description
Well No. 1	Edwin Rhode farm well, brown water to house, ahead of basement tank; 210 feet deep; S 23, T 144 N, R 93 W.
2	Bernard Trampe farm well, tap on south side of house; 105 feet deep; S 34, T 144 N, R 94 W.

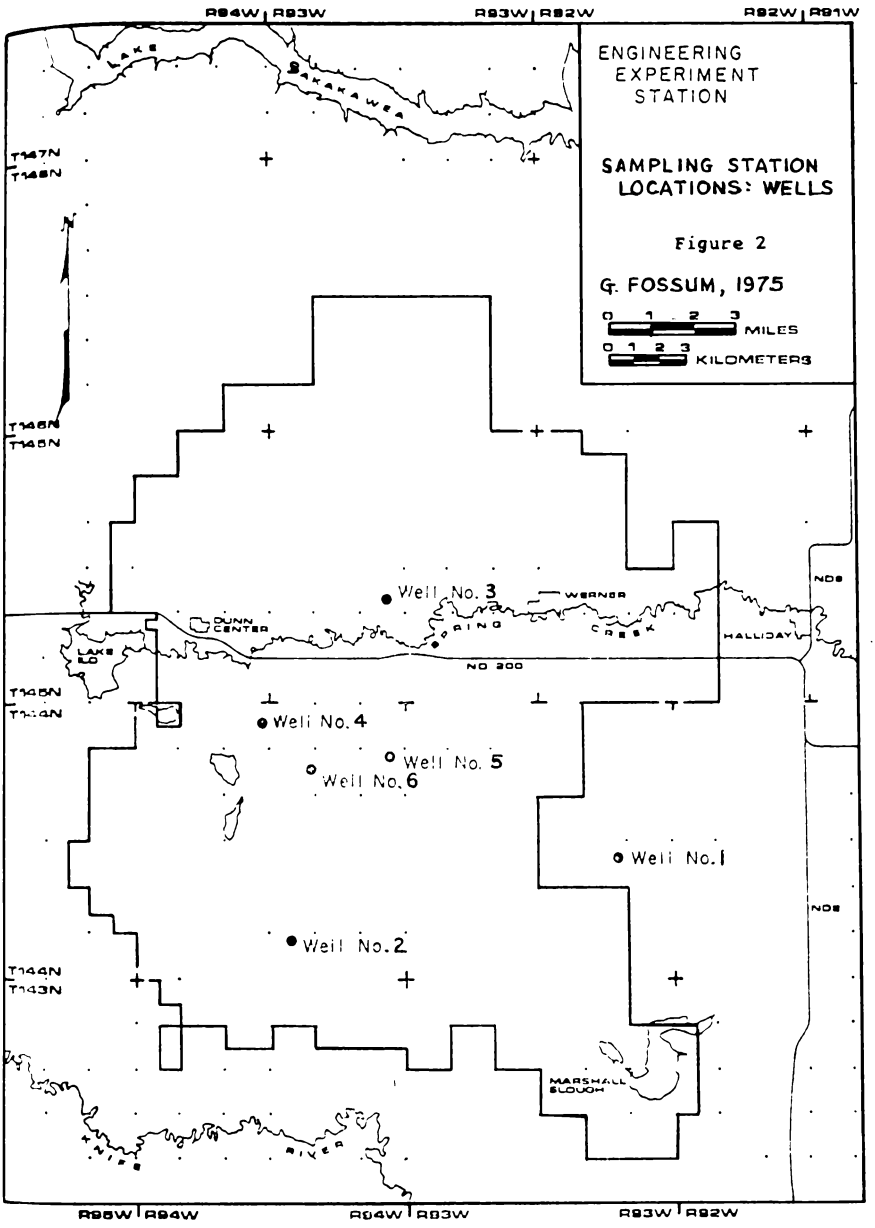

Figure 2. Sampling station locations: wells.

3 G. E. Lynch farm, flowing stock well to stock tank; 100 feet deep; S 21, T 145 N, R 93 W.

4 Iverson Brothers farm well, well with pump jack about 50 feet west of house; 60 feet deep; S 04, T 144 N, R 94 W.

5 Rueben Mjolhus farm well at stock watering tank about 30 feet southeast of barn; about 70 feet deep; S 12, T 144 N, R 94 W.

6 G. E. Schmidt farm, subermersible pump well at northwest corner of stock corral located northwest of buildings; 60 feet deep S 10, T 144 N, R 94 W.

Well No. 3 is an artesian well while the other wells are gravity wells. There were three sampling runs for well water sample collection from June to October 1975.

Procedures — In deep water, such as Lake Sakakawea, samples were collected by means of a home-made integrating sampling device which permitted sample collection from surface to bottom (Fossum and Hung, 1976). In shallow water, such as Spring Creek, samples were collected by a series of dippings without stirring up the stream bottoms. For well water sampling all wells except the artesian well were pumped by mechanical pumps for a duration of time long enough to clear the stagnant water from the well pipings before well samples were collected. Since all wells were used daily for human and stock consumptions, the pumping time required for these wells for draining the stagnant water is shorter than that required for wells not used daily. Immediately after surface and groundwater sample collection, some of the parameters such as pH, temperature and conductance were determined at the site. Portions of samples used for alkalinity and DO (dissolved oxygen) determinations received preliminary treatment to fix the sample as described in the Standard Methods (APHA, 1971); they were then transported back to the field water quality trailer for completion of titrations. Still others were stabilized at once with preservatives as described in the EPA report (USEPA, 1974) for transportation to either the University of North Dakota laboratory or to the commercial laboratories for analysis. The commercial laboratories were LFE Environmental Analysis Laboratories, Richmond, California, and Twin City Testing and Engineering Laboratory, St. Paul, Minnesota. Water analysis included pH, conductance, alkalinity, turbidity, DO, COD, (chemical oxygen demand), BOD (biochemical oxygen demand), TSS (total suspended solids, TDS (total dissolved solids), TH (total hardness), calcium, magnesium, sodium, potassium, sulfate, chloride, silicon dioxide, nitrate, phosphate, coliforms, trace elements and radioactivity. Analytical procedures were in accordance with Standard Methods.

Suspended sediment was also determined for surface water samples taken at Werner and Halliday on Spring Creek, and at Manning and Marshall on the Knife River. At low flows, a depth integrating hand-held sampler US DH-48 was used (USGS 1970). For deeper flows and deep lake sampling, a cable and reel depth integrating sampler, US DH-49 was used (USGS 1970). Since the streams

sampled are relatively narrow, a single vertical sampling system was used (USGS 1970). During the period from April 29 to June 27 when daily values were being taken, single bottle samples were used. During the latter part of the season from June 28 to October 26 when stream flow changes were slight, weekly samples of two bottles were taken. Correlations between daily values or between values of two-bottle samples were good. In addition, a complete cross section of 10 bottles (verticals) were run at the Knife River sites to check the distribution of sediment concentration across the stream. Means from these cross sections were close to values measured near the center of the cross section. Laboratory analysis of suspended sediment was done with a vacuum filter (USGS 1969). Bottom samples from Halliday reservoir were analyzed for size using sieve and hydrometer methods (ASTM 1974).

RESULTS AND DISCUSSION

Surface water quality data are summarized in Tables 1 through 6 for the six sampling runs conducted from April to October 1975. High stream flow occurred in the April sampling run while low stream flow occurred in the August sampling run.

Spring Creek — The quality of Spring Creek water remained relatively constant from Werner, Site No. 2, to Halliday, Site No. 3. Generally the concentrations of minerals at the beginning of Spring Creek below the Lake Ilo spillway, Site No. 5, were considerably less than the corresponding values at Werner. The increase in mineral concentration might be from the runoff over the drainage area. The pickup of minerals by Spring Creek is virtually completed by the time flow reaches Werner and water quality remains relatively constant thereafter. Alkalinity, dissolved solids, sodium and sulfate all were well below the concentrations shown in the Knife River about 15 miles to the south. TDS vs sampling stations are depicted in Figure 3. Spring Creek is less affected by groundwater than the other surface streams in the proposed mine area. Also, Spring Creek did not show an increase in potassium with high flows such as the case with the other surface streams. The surface water of the marshland to the southeast of Lake Ilo, Site No. 8, is very similar to the beginning of Spring Creek, Site No. 5. During late summer considerable algae growth takes place in the marshland and TSS were increased. On the other hand, flow from Lake Ilo into Spring Creek at this time was only by means of siphoning over the spillway or be seepage around the dam and TSS in the Spring Creek were very low. Figure 4 shows TSS vs sampling stations. DO vs sampling stations on Spring Creek is presented in Figure 5. There was an increase in DO concentration from Lake Ilo spillway to Halliday for all sampling runs from April to October 1975 except for July 1975 sampling run where the DO remained constant from Lake Ilo spillway to Werner and decreased to less than 5 mg/l at Halliday. The lowest DO observed during the study was 0.9 mg/l at Lake Ilo spillway in the October 1975 sampling run when there was no flow over the spillway. During the study period, the COD content was from 16 to 103 mg/l where the BOD content varied from 1.7 to 7.5 mg/l in the Spring Creek waters.

TABLE 1 SURFACE WATER QUALITY -SPRING CREEK AT LAKE ILO, SITE NO. 5

Parameter*	Sampling Date 4-26-75	5-27-75	7-8-75	8-5-75	9-16-75	10-7-75
flow (cfs)	480	17	6.5	—	—	—
temp (°C)	4	17	26	24	16	14
pH	7.8	7.6	8.4	8.1	7.3	7.5
conductance (μmhos/cm)	800	450	610	740	827	916
Total alkalinity	280	148	184	231	265	297
turbidity (NTU)	64	130	33	22	27	13
DO	10.3	7.7	7.5	4.1	4.8	0.9
TSS	257	21	9	23	2	17
TDS	440	539	487	549	590	751
TH	128	94	114	144	212	276
Ca	29	29	38	45	66	110
Mg	14	5.3	4.4	7.8	11	7.8
Na	159	99	115	130	150	161
K	10.6	10.6	10.6	10.2	9.5	10.9
sulfate	115	50	163	250	105	230
Cl	2.3	0	0.3	5.5	4.5	0
silicon dioxide	—	12	3	26	9	33
nitrate nitrogen	—	0.27	0.27	0.04	0	0.03
organic nitrogen	—	1.31	1.09	1.52	1.70	1.99
total phosphate	—	0.33	0.12	0.17	0.22	0.30
COD	57	57	31	42	30	103
BOD	—	4.6	1.7	3.4	5.6	>3.0
total coliform (per 100 ml)	—	40	50	—	<10	20
fecal coliform (per 100 ml)	—	30	20	—	<10	20

*Units are in mg/l, if not shown in table.

Knife River — There was considerable increase in the flow of the Knife River between Manning, Site No. 1, and Marshall, Site No. 4, during the period from April to October 1975. The average monthly flow during the period was 2,501 and 5,989 cfs at Manning and Marshall, respectively. Also there was generally an increase in the mineral content of the Knife River between Manning and Marshall during the higher flow period from May to July 1975 when the contribution of minerals from surface runoff is significant. The mineral concentration changed very little during the dry weather flow period from August to October 1975. TDS concentration at sampling stations on the Knife River is shown in Figure 6. TDS increased significantly between Manning and Marshall as the summer progressed until they leveled off in the vicinity of 1400-1500 mg/l. In general, the Knife

River at both Manning and Marshall was moderately hard and quite high in alkalinity, TDS, sodium, and sulfate but low in chlorides. The values obtained at Marshall for conductance and TDS during dry weather flow are quite similar but slightly lower than the same parameters for the farm wells in the proposed mine area. Figure 7 depicts TSS at different sampling stations on the Knife River. The highest TSS concentration of 689 and 734 mg/l for Manning and Marshall, respectively, was observed during the spring runoff period in April 1975. During the dry weather flow period TSS concentration was low along the Knife River as stream flow was maintained by groundwater discharges. The lowest TSS concentration was 2 and 24 mg/l during the September 1975 sampling run at Manning and Marshall respectively. DO content in the Knife River water during the study period was from 5.5 to 9.9 mg/l. Generally, there was an increase in DO content from Manning to Marshall, as shown in Figure 8, due to atmospheric

TABLE 2 SURFACE WATER QUALITY - SPRING CREEK NEAR WERNER, SITE NO. 2

Parameter	Sampling Date					
	4-26-75	5-27-75	7-8-75	8-5-75	9-16-75	10-7-75
flow (cfs)	155	16	5.3	3.0	15	14
temp (°C)	6	17	25	23	17	14
pH	8.2	7.6	8.4	8.5	7.8	8.2
conductance (μmhos/cm)	490	1150	1300	1580	1708	1617
total alkalinity	158	257	347	428	387	434
turbidity (NTU)	93	60	2	23	18	20
DO	9.8	7.7	7.2	6.9	8.9	9.8
TSS	155	88	49	42	1	3
TDS	362	834	937	1231	1251	1283
TH	104	288	314	420	512	420
Ca	26	55	106	139	197	96
Mg	9.7	36	12	17	5	43
Na	87	197	208	265	258	265
K	9.2	10.0	10.6	10.4	11.6	9.8
sulfate	75	310	346	476	530	570
Cl	0.8	1.8	1.5	3.3	3.0	5.0
silicon dioxide	—	16	14	35	21	14
nitrate nitrogen	—	0.31	0.03	0	0.01	0.01
organic nitrogen	—	1.8	1.19	1.08	0.86	0.75
total phosphate	—	0.13	0.05	0.17	0.21	0.10
COD	57	44	33	42	16	28
BOD	—	2.9	3.8	6.7	2.4	2.5
total coliform (per 100 ml)	—	80	140	—	500	80
fecal coliform (per 100 ml)	—	80	30	—	50	60

reaeration. COD values ranged from 21 to 74 mg/l and from 12 to 68 mg/l for Manning and Marshall, respectively. BOD content was generally less than 5 mg/l and ranged from 2.3 to 5.4 mg/l in the Knife River waters.

Correlations between water quality parameters were performed using regressional analysis. The resulting equations with correlation coefficients r are listed below:

Spring Creek: $Na = 18.371 + 0.149$ (sp.cond.), $r = 0.982$
$SO_4 = 103.636 + 0.372$ (sp.cond.), $r = 0.964$
T.H. $= 54.745 + 0.313$ (sp.cond.), $r = 0.973$
TDS $= 24.174 + 0.769$ (sp.cond.), $r = 0.974$

Knife River: $Na = 13.206 + 0.199$ (sp.cond.), $r = 0.992$
$SO_4 = 76.617 + 0.321$ (sp. cond.), $r = 0.969$
T.H. $= 45.627 = 0.163$ (sp.cond.), $r = 0.871$
TDS $= 234.33 + 0.612$ (sp.cond.), $r = 0.972$

TABLE 3 SURFACE WATER QUALITY - SPRING CREEK NEAR HALLIDAY, SITE NO. 3

Parameter	Sampling Date 4-26-75	5-27-75	7-8-75	8-5-75	9-16-75	10-7-75
flow (cfs)	365	24.2	15	1.9	50	48
temp (°C)	6	18	25	24	19.5	14
pH	8.2	8.0	7.7	8.5	8.3	8.4
conductance (μmhos/cm)	375	1300	710	1530	1441	1617
total alkalinity	107	312	199	426	379	430
turbidity (NTU)	91	41	17	28	20	18
DO	9.5	9.0	4.8	7.6	9.7	10.4
TSS	171	69	106	84	11	71
TDS	281	987	452	1159	961	1206
TH	108	360	188	406	416	512
Ca	26	79	62	131	153	143
Mg	11	39	8.3	19	8.2	37
Na	58	211	95	255	211	262
K	8.2	9.6	10.6	9.9	9.7	10.8
sulfate	54	380	224	476	390	510
Cl	1.8	3.0	0	4.3	2.5	5.0
silicon dioxide	—	16	15	35	17	12
nitrate nitrogen	—	0.18	0.19	0	0.01	0.01
organic nitrogen	—	0.72	1.35	1.13	0.84	0.67
total phosphate	—	0.14	0.15	0.17	0.24	0.09
COD	56	46	41	30	7	25
BOD	—	2.9	2.9	7.5	3.3	2.7
total coliform (per 100 ml)	—	150	1100	—	1000	700
fecal coliform (per 100 ml)	—	100	1100	—	550	260

Among the water quality parameters measured in the Spring Creek and Knife River waters, sodium, sulfate, total hardness, total dissolved solids were found to be closely correlated to specific conductance, while there was little correlation between total dissolved solids and stream flow, and between specific conductance and stream flow.

TABLE 4 SURFACE WATER QUALITY - KNIFE RIVER AT MANNING, SITE NO. 1

Parameter	Sampling Date					
	4-26-75	5-27-75	7-8-75	8-5-75	9-16-75	10-7-75
flow (cfs)	420	10	2.8	2.0	3.6	12.4
temp (°C)	7	14	23	19	17.5	12
pH	8.0	8.1	8.1	8.2	8.3	8.3
conductance (μmhos/cm)	315	1625	1150	1785	2134	2075
total alkalinity	103	482	332	558	653	661
turbidity (NTU)	290	27	55	32	7	15
DO	9.3	8.6	5.5	6.3	8.7	7.3
TSS	689	88	95	52	2	37
TDS	649	1161	810	1349	1524	1581
TH	108	326	212	354	448	516
Ca	29	72	70	104	74	149
Mg	8.7	36	8.7	23	64	35
Na	55	307	194	335	400	415
K	12.8	8.8	9.8	9.2	9.0	10.6
sulfate	58	390	242	470	630	690
Cl	2.3	4.0	0	2.5	5.5	5.5
silicon dioxide	—	16	14	32	9	5
nitrate nitrogen	—	0	0.24	0	0	0
organic nitrogen	—	0.34	1.09	1.18	0.90	0.97
total phosphate	0	0.06	0.10	0.14	0.19	0.13
COD	74	49	43	25	21	44
BOD	—	4.0	2.3	5.0	2.7	3.3
total coliform (per 100 ml)	—	<1000	2000	—	600	400
fecal coliform (per 100 ml)	—	2000	700	—	280	190

Little Missouri River and Lake Sakakawea — The average values of water quality data of six sampling runs from April to October 1975 for the Little Missouri River near Watford City, Site No. 7, and proposed intake and alternate intake on Lake Sakakawea, Sites No. 9 and 10, are listed in Table 6. Lake Sakakawea waters were of better quality than that of the Little Missouri River. DO of lake waters was above 9.0 mg/l compared to 8.5 mg/l at Little Missouri River. TSS of lake waters averaged 15 mg/l compared to 1030 mg/l at the Little

TABLE 5 SURFACE WATER QUALITY - KNIFE RIVER AT MARSHALL, SITE NO. 4

Parameter	Sampling Date 4-26-75	5-27-75	7-8-75	8-5-75	9-16-75	10-7-75
flow (cfs)	1000	61	27	13	34	79
temp (°C)	7	18	26	22	17.5	15
pH	7.9	8.3	8.3	8.6	8.3	8.5
conductance (μmhos/cm)	340	2100	1930	1770	2001	1941
total alkalinity	109	522	501	525	603	606
turbidity (NTU)	275	32	24	35	24	25
DO	8.8	9.9	9.6	7.1	8.1	9.7
TSS	734	82	69	61	24	38
TDS	297	1539	1382	1326	1445	1482
TH	116	406	304	292	286	294
Ca	29	94	113	86	99	72
Mg	11	42	5.3	19	9.2	28
Na	56	386	347	365	392	395
K	12.6	10.8	11.9	10.6	9.1	10.8
sulfate	59	680	520	450	510	540
Cl	1.3	4.0	0.8	3.5	3.5	4.8
silicon dioxide	—	16	14	35	10	14
nitrate nitrogen	—	0	0.01	0	0.01	0
organic nitrogen	—	0.9	1.31	1.70	0.79	0.87
total phosphate	—	0.08	0.04	0.11	0.08	0.08
COD	68	54	42	32	12	41
BOD	—	5.4	4.2	3.0	3.0	2.9
total coliform (per 100 ml)	—	30	500	—	20	70
fecal coliform (per 100 ml)	—	<10	650	—	50	30

Missouri. TDS of the Little Missouri was 2175 mg/l which was three times that of the lake waters. The Little Missouri River waters also had higher total hardness than the lake waters. COD values for the Little Missouri and Lake Sakakawea were 59 and 18 mg/l respectively. BOD content for the Little Missouri water was 2.8 mg/l compared to 0.85 mg/l for lake waters. Most water quality parameters in Lake Sakakawea met the recommended standard for public water supplies. Parameters exceeding standards included TDS and sulfate. It should be noted that in spite of relatively good water quality in Lake Sakakawea, each acre-foot of water used in processing would transport approximately one ton of dissolved solids, including one-half ton of sulfates, to the plant site. The fate of these dissolved solids would warrant in-depth study.

TABLE 6 SURFACE WATER QUALITY* - SITES NO. 7-10

Parameter	Little Missouri River	Lake Ilo Area	Lake Sakakawea	
	Site No. 7 (Near Watford City)	Site No. 8**	Site No. 9 (Proposed intake)	Site No. 10 (Alternate intake)
flow (cfs)	--	--	--	--
temp (°C)	18	20	17	16.2
pH	8.3	8.1	8.4	8.2
conductance (μmhos/cm)	1640	653	987	977
total alkalinity	279	293	170	169
turbidity (NTU)	32	46	9	9
DO	8.5	6.9	9.1	9
TSS	1030	54	11	19
TDS	2175	566	706	686
TH	363	140	234	211
Ca	109	47	73	65
Mg	21.7	5.8	12	12
Na	267	149	153	149
K	17.4	12.4	7.0	6.8
sulfate	570	133	322	330
Cl	8.4	0.9	6.6	6.2
silicon dioxide	17	4.8	6	8.3
nitrate nitrogen	0.15	0.92	0.15	0.11
organic nitrogen	0.86	1.64	0.75	0.68
total phosphate	0.11	0.40	1.16	0.18
COD	59	48	13.6	23
BOD	2.8	4.8	0.8	0.9
total coliform (per 100 ml)	527	145	7	5
fecal coliform (per 100 ml)	190	105	6	3

*Average values of 6 sampling runs from April to October 1975

**Site No. 8: Between Lake Ilo and Marshland

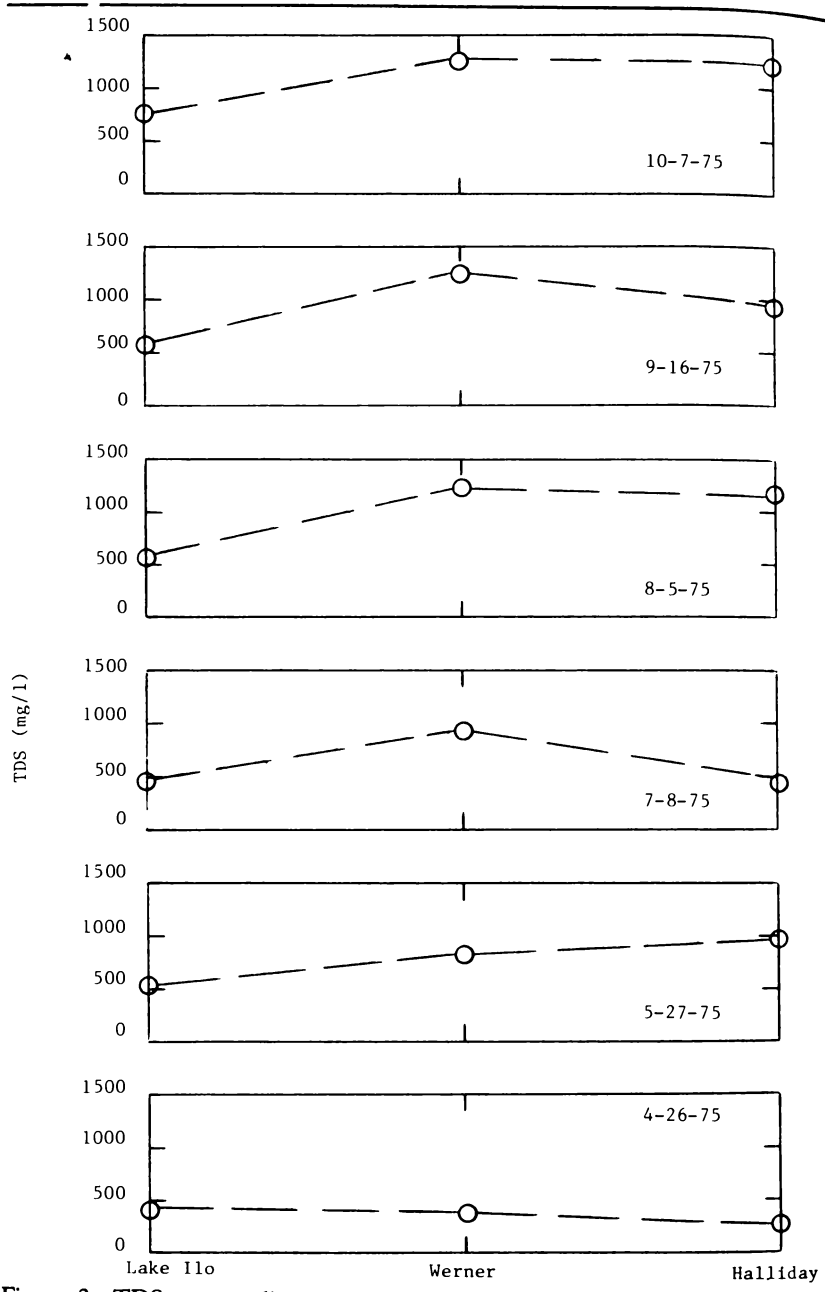

Figure 3. TDS vs. sampling stations - Spring Creek.

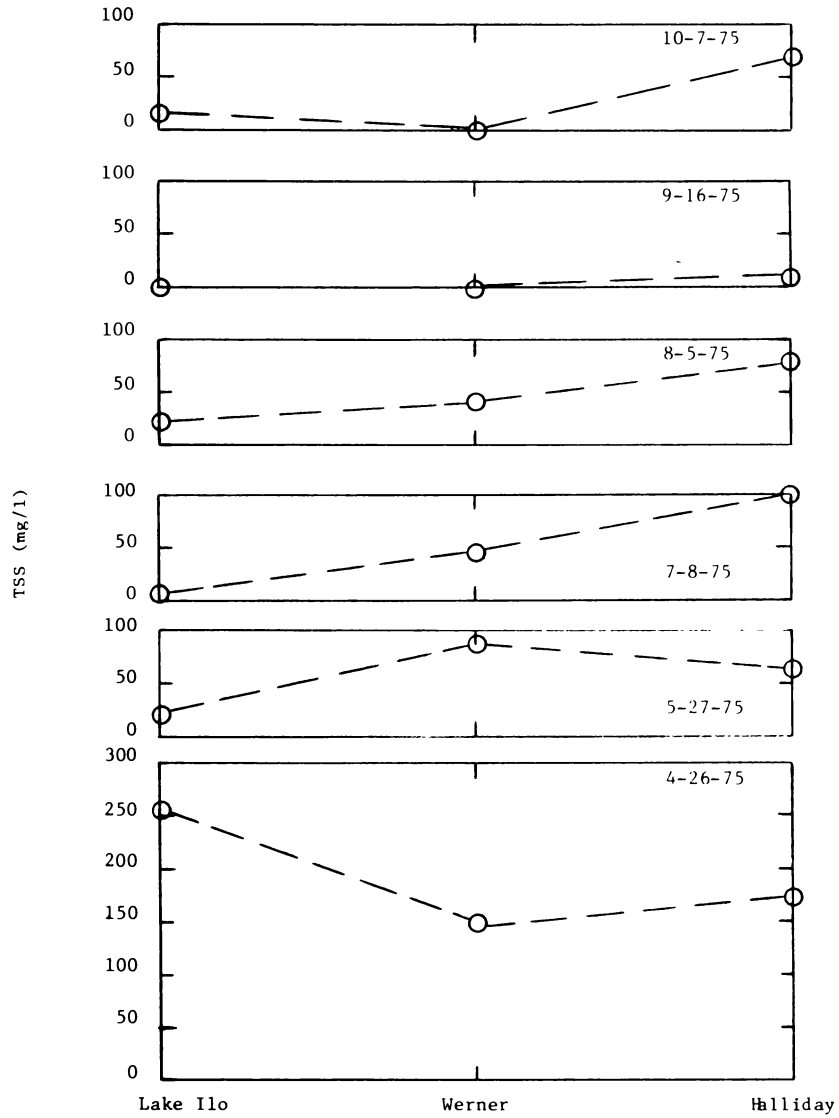

Figure 4. TSS vs. sampling stations - Spring Creek.

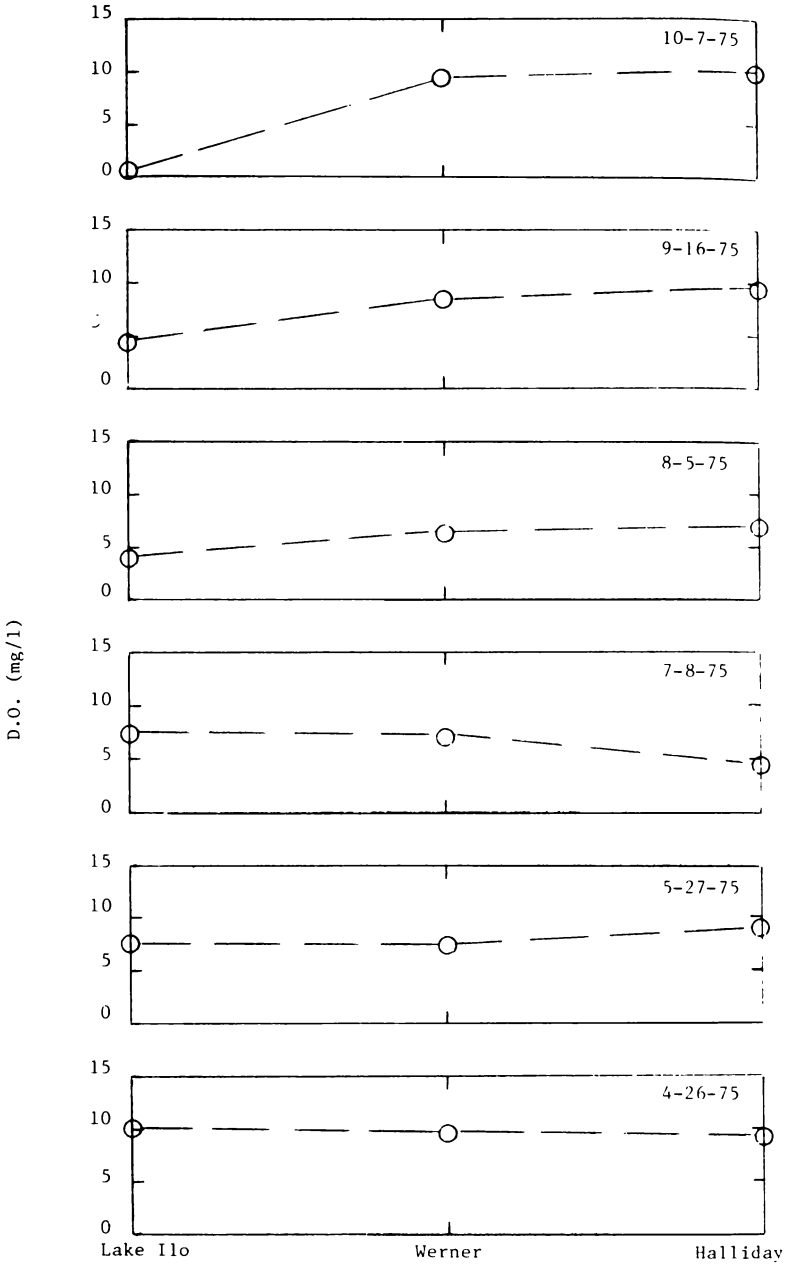

Figure 5. D.O. vs. sampling stations - Spring Creek.

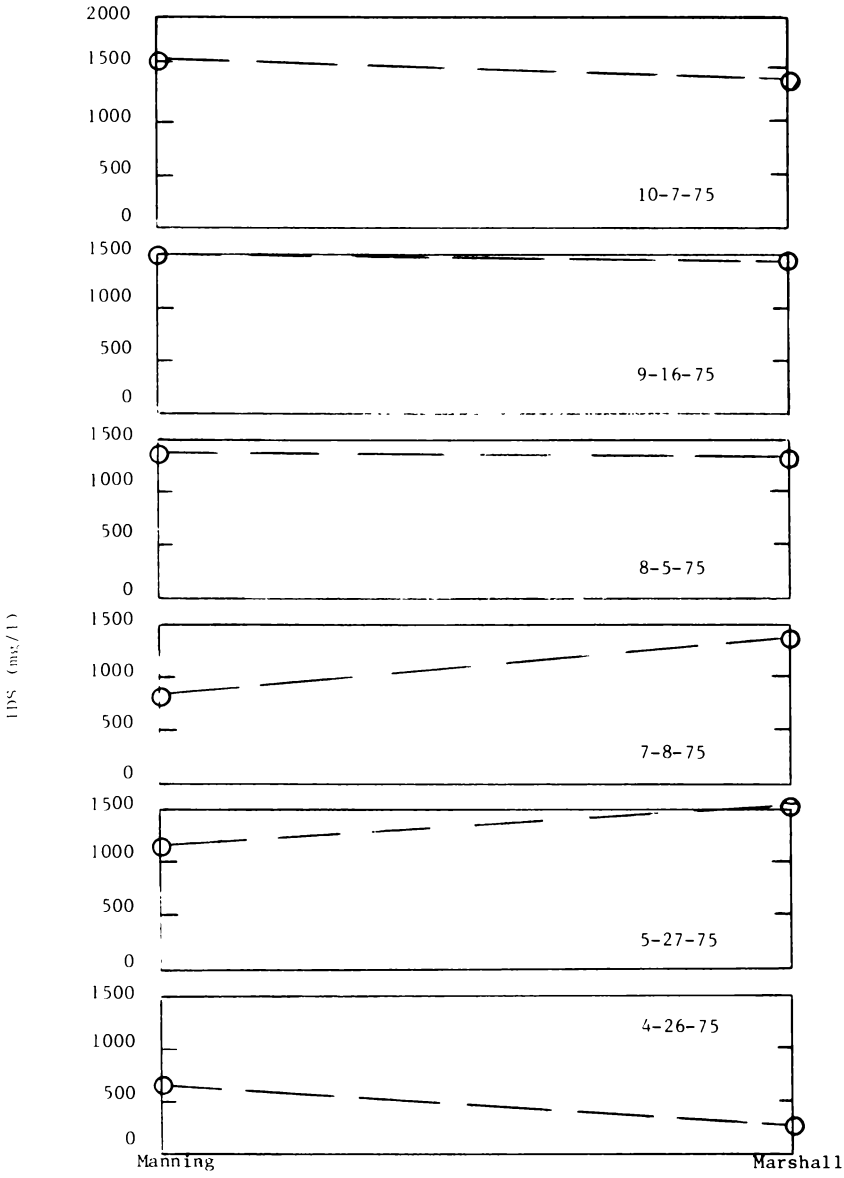

Figure 6. TDS vs. sampling stations - Knife River.

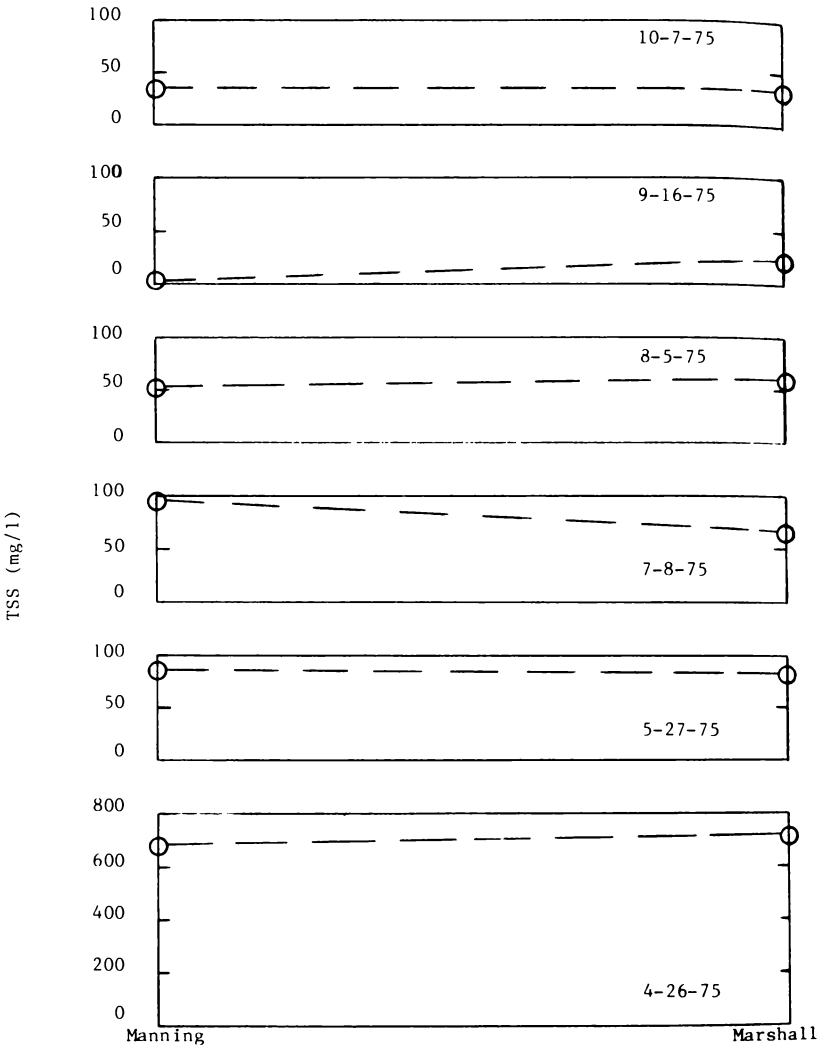

Figure 7. TSS vs. sampling stations - Knife River.

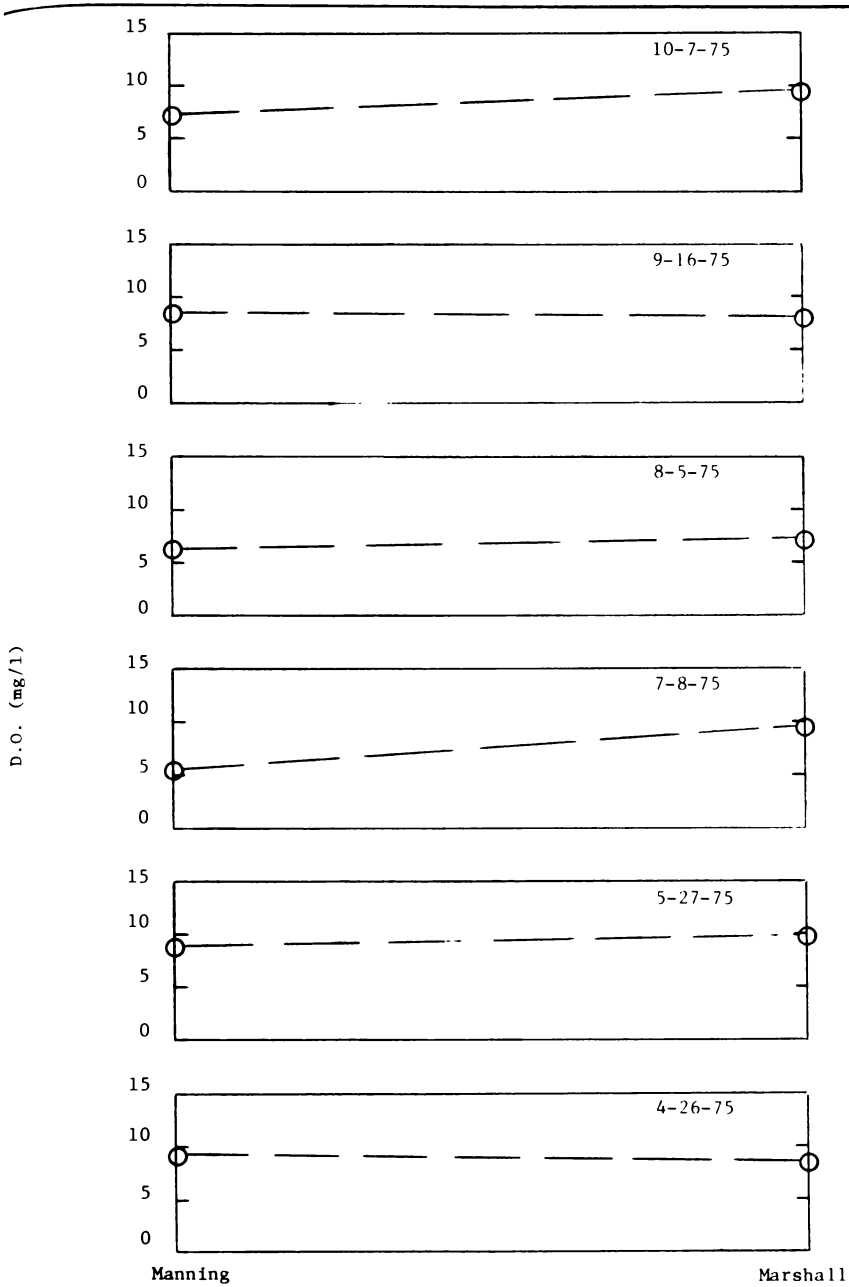

Figure 8. D.O. vs. sampling stations - Knife River.

Comparison to North Dakota Water Quality Standard — In "Standards of Surface Water Quality for State of North Dakota" (North Dakota State Department of Health 1973) streams are classified as Class 1, 1-A, 2, and 3 with Class 1 having the most restrictive standards and Class 3 the least restrictive. In accordance with these classifications, Lake Sakakawea is in Class 1, Spring Creek is in Class 1-A, and the Little Missouri and Knife Rivers are both in Class 2. Based on the average values of water quality data taken during the sampling period from April to October 1975, water quality parameters which exceeded State water quality standards included turbidity, phosphate and fecal coliform for Spring Creek waters; turbidity, TDS and fecal coliform for Knife River waters; turbidity and TDS for Lake Sakakawea waters. Fecal coliforms could originate from either human or animal source.

Selected Wells — Average values of water quality parameters based on three sampling runs from June to October 1975 for six selected wells in the proposed mine area are listed in Table 7. TDS were high for all wells, other major constituents varied widely. The six wells varied in depth from 60 feet for Wells No. 4 and 6, to 210 feet for Well No. 1. All wells were currently being used for either human or animal consumption. The highest nitrate value was found to be 10.5 mg/l for Well No. 5 located near a barn and used for filling the stock watering tank. Total hardness for Wells No. 1 to 3 was less than 100 mg/l while for Wells No. 4 to 6 it varied from 690 to 1112 mg/l. Sulfate was found to range from 138 to 918 mg/l with an average of 573 mg/l which exceeded the 250 mg/l recommended for drinking water standards.

Sediment Transport — Sediment transport study was conducted for four sampling stations on Spring Creek and Knife River from April to October 1975. Table 8 presents sediment transport data with equations relating sediment transport to stream flow at different sampling stations. It was observed that sediment transport was the highest during the high flow period in April 1975 while at the dry weather flow period from June to October 1975 the sediment transport was significantly less. On Spring Creek sediment production was 47 tons/square mile at Werner and 48 tons/square mile at Halliday over the entire study period. The net increase between the two stations amounted to 51 tons/square mile based on drainage area of 195 and 271 square miles at Werner and Halliday, respectively. The low rates were due in part to the large areas in the small watershed that do not flow directly into the stream but end up flowing through Lake Ilo or one of the many swampy areas and thus lose their sediment loads. On the Knife River sediment production rates were higher, 208 tons/square mile at Manning and 137 tons/square mile at Marshall, with a net contribution of 109 tons/square mile for the area between which was based on a drainage area of 205 and 722 square miles at Manning and Marshall, respectively.

CONCLUSIONS

Based on the water quality study conducted during the period from April to October 1975, the following conclusions are presented.

TABLE 7 GROUNDWATER QUALITY* - SELECTED WELLS

Parameter	Well No. 1	Well No. 2	Well No. 3	Well No. 4	Well No. 5	Well No. 6
Temp (°C)	11.0	11.2	9.3	7.8	8.0	9.0
pH	8.2	8.0	8.3	7.0	7.2	6.6
Conductance (μmhos/cm)	2092	2928	1806	1838	2037	1846
total alkalinity	1736	2171	1257	1626	1598	1802
TDS	1221	614	693	347	598	291
TH	54	62	21	890	690	1112
Ca	11.7	15	7.5	230	193	346
Mg	6.0	5.6	0.5	76	51	60
Na	651	780	443	115	227	63
K	6.3	8.0	4	6.1	8.1	5.8
Sulfate	138	918	318	653	540	870
Cl	7.0	2.5	1.4	19.4	45	25
Silicon Dioxide	25.3	19.0	31	32	34	31
Nitrate Nitrogen	0.01	0.002	0.005	4.45	10.5	0.28
Total Phosphate	0.31	0.13	0.15	1.47	0.15	0.09

*Average values of 3 sampling runs from June to October 1975

TABLE 8 SEDIMENT TRANSPORT OF SPRING CREEK & KNIFE RIVER - 1975

	Spring Creek						Knife River					
	Werner			Halliday			Manning			Marshall		
Month	Q (cfs)	Sediment conc. (mg/l)	Sediment Transport (ton/day)	Q (cfs)	Sediment conc. (mg/l)	Sediment Transport (ton/day)	Q (cfs)	Sediment conc. (mg/l)	Sediment Transport (ton/day)	Q (cfs)	Sediment conc. (mg/l)	Sediment Transport (ton/day)
Apr	445	399	478	550	446	661	966	1011	2632	2142	1096	6324
May	51	290	40	62	255	43	42	712	81	233	758	475
June	22	58	3	22	60	3	16	216	10	81	175	38
July	4	56	1	13	244	9	7	382	7	20	81	4
Aug	7	94	2	30	1000	8	3	117	1	13	102	4
Sept	14	47	2	48	70	9	8	84	2	39	67	7
Oct	10	50	1	47	49	6	22	64	4	72	65	13
Equation:	$Q_s^* = 0.074\ Q^{1.36}$			$Q_s = 0.090\ Q^{1.26}$			$Q_s = 0.134\ Q^{1.33}$			$Q_s = 0.046\ Q^{1.47}$		

*Q_s = sediment transport (ton/day)

1. Spring Creek and Knife River waters had a lower TDS content during high stream flow period and higher TDS content during dry weather flow period, whereas TSS and DO content showed the opposite trend. Minimum DO in stream waters occurred during low stream flow period in July and August 1975.

2. Correlation analysis revealed that stream flow was negatively correlated to TDS and specific conductance, and specific conductance was positively correlated to TDS, Na, and total hardness.

3. Based on the average values of water quality data from six sampling runs conducted from April to October 1975 water quality parameters exceeding North Dakota State Water Quality Standards included turbidity, phosphate, and fecal coliform for Spring Creek waters; turbitidity, TDS, and fecal coliform for Knife River waters; turbidity and TDS for Little Missouri River waters; TDS for Lake Sakakawea waters.

4. Six wells selected in the proposed development area were found to contain high concentrations of TDS, which varied from 291 to 1221 mg/l with an average of 627 mg/l and contained high concentrations of sulfate, which ranged from 138 to 918 mg/l with an average of 573 mg/l compared to 250 mg/l recommended for drinking water standards.

5. The stream sediment production in the Knife River was significantly higher than in Spring Creek. Observed values for Spring Creek were 47 and 48 tons/square mile at Werner and Halliday, respectively, while the corresponding figures on the Knife River were 208 and 137 tons/square mile at Manning and Marshall, respectively.

6. The baseline water quality data collected in the vicinity of the coal gasification plant site during the study will serve as useful background information to determine if there is any deterioration in water quality in the future resulting from gasification plant operation. The methodology developed in the study will help coal gasification companies in the preparation of their environmental impact statement reports and in the selection of plant sites.

LITERATURE CITED

American Public Health Association, 1971. Standard methods for the examination of water and wastewater, 13th edition.

ASTM, 1974. Annual book of ASTM standards, part 19, p 70-80.

Fossum, G. O., and Y. T. Hung, 1976. Environmental assessment of a 250 MMSCFD dry ash Lurgi coal gasification facility in Dunn County, North Dakota. Vol. 3, Water quality, University of North Dakota Engineering Experiment Station.

Mason, E. S., 1976. Environmental assessment of a 250 MMSCFD dry ash Lurgi coal gasification facility in Dunn County, North Dakota. Vol. 4, Surface water hydrology. University of North Dakota, Engineering Experiment Station.

North Dakota State Department of Health, 1973. Standards of surface water quality for State of North Dakota.

U.S. Environmental Protection Agency, 1974. Methods for chemical analysis of water and wastes, EPA-625-/6-74-003.

United States Geological Survey, 1969. Laboratory theory and methods for sediment analysis, techniques of water resources, Book 5, Chapter C1, p 12-13.

Ibid, 1970. Field methods for measurement of fluvial sediment, techniques of water resources, Book 3, Chapter C2, p 5-7, and p 27-30.

REAP LAND COVER ANALYSIS OF NORTH DAKOTA USING COMPUTER-PROCESSED LANDSAT IMAGERY

John R. Reid and *A. William Johnson*
North Dakota Regional Environmental Assessment Program
State Capitol
Bismarck, North Dakota 58505

ABSTRACT

One of the projects completed under the sponsorship of the North Dakota Regional Environmental Assessment Program (REAP) is a detailed land cover analysis of the entire State of North Dakota utilizing computerized interpretation of LANDSAT imagery, most of which was collected in 1975. This is the first instance of a complete analysis by this method for an entire state. Nineteen LANDSAT scenes were analyzed utilizing the Bendix Aerospace Systems Division multi-spectral data analysis system (MDAS) together with ground truthing provided through a subcontract with the Institute for Remote Sensing at the University of North Dakota (UNDIRS). The products of this analysis include a geometrically corrected map for each of the 53 counties in the state (1:126,720 - two miles to the inch), a map of the entire state (1:500,000 - approximately eight miles to the inch), a digital tape file for 40-acre cells arranged by township, and area cover tabulations for the state, each of the 53 counties, and the 2,055 townships. The 10 categories of land cover, represented by separate colors on the maps are built-up land, cropland, fallow land, exposed subsoil or saline seep, rangeland, mixed rangeland and pasture, forest, water, wetland, and barren land. The digital data file records land cover data for each pixel (1.12 acres) selected from as many as 36 possible land cover categories. The land cover data will be used in conjunction with other areal data in a computer-based composite geodata analysis system being established by REAP.

INTRODUCTION

The North Dakota Regional Environmental Assessment Program (REAP) was created by the 1975 North Dakota Legislative Assembly as a result of a recognized need for a comprehensive and coordinated source of natural resource-related information. The immediate impetus for such a program was current and prospective large-scale coal development in southwestern North Dakota. House Bill 1004 (Session Law, 1975) directed REAP to carry out studies and research related to natural resources and to develop a comprehensive information and analysis system for the storage, retrieval, and analysis of such information. Furthermore, REAP was especially directed to develop the capability of forecasting the impact of natural resource development alternatives which may be considered by the state.

In order to meet its responsibilities, REAP has undertaken four specific tasks: (1) the collection of existing baseline data, together with a major effort to fill recognized data gaps; (2) the design, development, and installation of a computer-based information system capable of storage, retrieval, representation, and analysis of appropriate data; (3) development of a variety of capabilities, including models, for assessing the impacts of proposed natural resource development; (4) the establishment of a means for the regular monitoring and updating of data so the information system will remain current and the analyses relevant.

With the assistance of 11 technical task forces organized in the fall of 1975, REAP conducted an exhaustive study of the relevant data sources in universities, federal agencies, state agencies, and private industry. One of the final activities of the technical task forces was to identify all information necessary for the conduct of overall environmental assessment, but which was as yet unavailable. Through this effort, it was recognized that there was not comprehensive land cover inventory for the state of North Dakota. Accordingly, REAP identified the completion of such an inventory as a major task requiring early attention (Regional Environmental Assessment Program, 1975).

Several different technologies were considered for inventorying the land cover of the entire state of North Dakota, approximately 180,000 sq. km. (70,665 sq. mi.) in area. The technology chosen was imagery obtained from the LANDSAT satellites launched by the National Aeronautics and Space Administration (NASA) in July 1972 and January 1975. The advantages of LANDSAT imagery include the fact that the entire state of North Dakota is covered every nine days, and therefore repetitive comparative imagery is available. This technology therefore provides a mechanism for conducting a baseline land cover analysis for the state and for monitoring how that land cover changes over time. Since a near-permanent platform for imaging is available at no cost to the state, it is more economical to use such a system than to undertake complete aerial photographic coverage of the state, and to propose frequent repetition of the coverage for monitoring purposes. Another distinct advantage is the large areal coverage for any given image which permits discerning gross land features often not perceivable with aerial photography. LANDSAT imagery is particularly amenable to computer analysis, whereas such techniques have not been well developed for photographic imagery. A disadvantage of utilizing LANDSAT imagery is that a high degree of detail, particularly in urban-type areas, is usually not available. Thus, it is generally not feasible to attempt to obtain a full level II land cover analysis utilizing LANDSAT imagery (Anderson, *et al.*, 1976).

MATERIALS AND METHODS

Satellite characteristics.—Each LANDSAT satellite circles the Earth once every 103 minutes at a height of 918 km. (570 mi.) in a path approximately 13 degrees off true north (DeNoyer, 1976). Because of this path each satellite makes one pass per day over the state for six consecutive days, and passes over a given point in North Dakota at the same local time every 18 days. With two satellites in orbit, a given point in North Dakota was viewed from space every nine days. (As a result of an orbit adjustment completed in January 1977, LANDSAT-I will now follow LANDSAT-II by six days, and LANDSAT-II will follow 12 days later.) Each pass over North Dakota is approximately 100 km. (60 mi.) farther west than the previous pass 24 hours earlier. As the satellite passes over the state, light reflected from the Earth's surface is collected by the satellite's multi-spectral scanner. Reflected light is dispersed into four wave lengths on board the satellite. Two of the bands are of visible light (0.5-0.6 micrometers, green; 0.6-0.7

micrometers, red) and two are in the near infrared (0.7-0.8 micrometers, 0.8-1.1 micrometers). The combination of the four bands provides maximum differentiation of individual land cover types; the green band, for example, is particularly sensitive to water. The smallest element of resolution, the "pixel" (*picture element*) is 1.12 acres, and the spatial resolution is 80 meters. The satellite registers data for a path 190 km. (115 mi.) wide as it passes over the state. Each LANDSAT scene includes the pixels present in an area 190 km. on a side. Nineteen scenes were required to cover all of North Dakota (Figure 1).

LANDSAT scene selection.—The LANDSAT scenes chosen for the REAP land cover analysis were selected by REAP staff, Bendix personnel, and UNDIRS

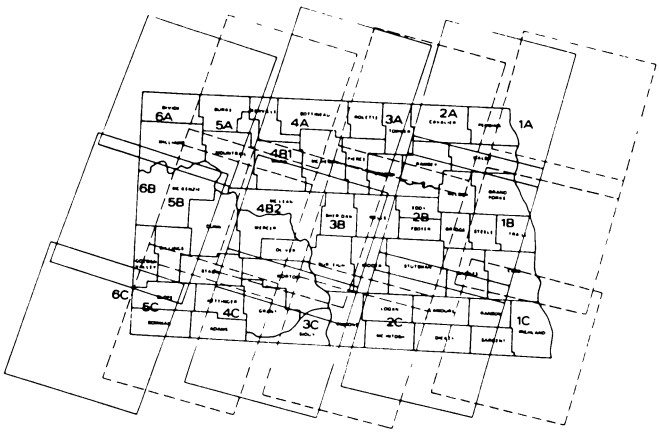

FIGURE 1. Coverage of LANDSAT Scenes Processed for North Dakota Land Cover Analysis. Each scene is individually labelled (e.g. 1A); a single path includes at least three scenes (e.g. 1A, 1B, 1C). See Table 1.

personnel in a joint session at the EROS Data Center, Sioux Falls, South Dakota, after examination of the library of scenes available. The major criteria utilized in the scene selection were as follows:

1. The imagery had to be as recent as possible, preferably from 1975.
2. The imagery should have been collected during the major North Dakota growing season (late June to late July).
3. The image had to be very high in quality.
4. The amount of cloud cover had to be less than 10 percent, and zero percent if at all possible.
5. All four wavelengths had to be recorded.
6. The scene had to be as representative as possible, and therefore imagery of the Red River Valley recorded in July 1975, during and shortly after the Red River flood, had to be excluded if at all possible.

A total of 115 images acquired prior to 1976 was inspected. The final selection included data that had a seasonal range of 47 days (June 20 to August 6), a yearly

range of four years (1973 to 1976), and only two small areas of scattered cloud cover in one scene totaling approximately 200 sq. km. A very small portion of extreme southwestern North Dakota was covered by a part of the 1973 scene, and the 1976 scenes were utilized only after NASA reported the 1972 scenes originally requested were of unsuitable quality and therefore not deliverable. Table 1 details the scenes chosen and Figure 1 illustrates the scene coverage of the State of North Dakota.

The limitations imposed by the scene selection are twofold. First, the 1973 scene is considerably earlier than would have been desired, but it covers a very small portion of the state. Second, because of persistent cloud cover in the Ramsey County region, all imagery through 1975 was found unacceptable. Fortunately, imagery recorded on August 6, 1976, was of extremely high quality and was therefore utilized for the entire path from Cavalier County to Emmons County. However, because 1976 was a relatively dry year, considerable harvesting had already occurred by that time, and satellite discrimination between stubble fields and rangeland may be less than satisfactory.

TABLE 1. LANDSAT Scenes used in REAP Land Cover Analysis.

Scene	Date	Number
1A	06 Aug 1974	1744-16392
1B	06 Aug 1974	1744-16394
1C	10 Aug 1975	2200-16365
2A	15 July 1975	5087-16301
2B	15 July 1975	
2C	15 July 1975	5087-16310
3A	06 Aug 1976	2562-16402
3B	06 Aug 1976	2562-16405
3C	06 Aug 1976	2562-16411
4A	22 July 1974	1729-16570
4B1	22 July 1974	1729-16573
4B2	20 June 1975	2149-16543
4C	26 July 1975	2185-16453
5A	27 July 1975	2186-16592
5B	27 July 1975	2186-16545
5C	27 July 1975	2186-17001
6A	10 July 1975	2169-17053
6B	24 July 1974	2169-17085
6C	23 June 1973	1335-17180

Ground truth.—The land cover analysis depended upon relating information on the actual ground cover in a number of given locations throughout the state of North Dakota to the reflectance properties exhibited by the same piece of land as recorded by the satellite multi-spectral scanner. Such information is called "ground truth information." This information was acquired under contract by the staff of the Institute of Remote Sensing at the University of North Dakota (UNDIRS), Dr. Roland D. Mower, principal investigator. Known key areas on the ground, at least 10 acres in size, were selected from throughout the state as being representative of specific categories of land cover, such as fallow land. These key areas, known as "training sets," were visually inspected by the ground truth team, and 302 such sets were utilized in conjunction with the 19 LANDSAT scenes (Table 2). The UNDIRS team collected information on 500 training sets using on-site observations in the summer of 1976, 470 35mm slides from aerial and ground surveys made in 1975 and 1976, 212 orthophoto and photoquad maps of the western half of the state prepared from aerial photography conducted in August 1974 and 1975, and had available a wide variety of other aerial photography and map information. With the ground truth information thus available, the ground truth team and Bendix personnel jointly participated in categorizing the LANDSAT data, a process of "training" the MDAS computer to recognize areas having the same or similar reflectance properties.

One of the problems associated with the ground truth process is that the on-site information was obtained during visits to the training sets in 1976, whereas the satellite imagery was obtained over the period from 1973 to 1976. Accordingly, it was necessary to relate current land cover information obtained by visual inspection to what the land cover actually was at the time of the satellite overflight.

Preliminary copies of the land cover maps of three western counties, Dunn, Stark, and Hettinger, were subjected to independent ground truth checking in the field by three REAP teams in September 1976. It was concluded that the general categorization results were excellent, but a number of problems were identified and subsequently addressed by the categorization team at Bendix.

Categorization.—Computer processing of the LANDSAT data from computer tapes as received from the EROS Data Center was performed by the Bendix Aerospace Systems Division using a Bendix datagrid digitizer system and the Bendix multi-spectral data analysis system (MDAS) (Rogers, *et al.*, 1975). The process involved identifying an area on a computer display terminal which coincided with the exact shape and location of a given training set. The computer was then coded to identify all areas in that particular scene with a similar reflectance. Finally, a color was assigned to indicate all such areas. In a follow-up process, color-coded areas of a particular category were checked against the available ground truth information to ensure that the computer search for similar cover was complete. This process was repeated for each of the land cover categories. The final result was a "categorized" tape.

The MDAS system is capable of reacting to various spectral ranges of reflec-

TABLE 2. Number and Type of Training Sets.

North Dakota Scene(s)	Number of LANDSAT Training Sets Per Categorization											
	6A	6B	6C*	5A 5B 5C	4A 4B1	4B2	4C	3A 3B 3C	2A 2B 2C	1A 1B	1C	Avg.
Land Cover Type												
Built Up	—	—	—	—	1	1	—	—	—	2	1	.5
Cropland	7	8	5	7	5	5	7	7	6	9	9	6.7
Fallow	6	4	1	6	6	2	4	3	7	8	6	4.8
Exposed Subsoil or Saline Seep	1	—	—	1	1	—	1	—	8	—	—	.4
Rangeland	1	2	2	2	2	3	2	2	1	—	1	1.6
Rangeland, Pasture, and Agricultural (Mixed)	1	1	1	1	2	2	2	—	1	2	2	1.4
Forest	—	1	1	1	1	2	1	1	1	1	1	1.0
Water	10	8	1	8	14	9	8	14	10	3	7	8.4
Wetland	3	—	—	1	2	1	1	2	2	--	1	1.2
Barren	1	1	1	3	2	3	3	2	1	—	—	1.5
TOTAL	30	25	12	30	36	27	29	31	29	25	28	27.5

*Less than five percent of this scene was used in the analysis.

tivity for categorization. With a very narrow range there will be a residue of uncategorized areas in which the reflectance signature does not precisely meet those selected for any of the land cover categories. On the other hand, a wider range results in a diminished amount of uncategorized areas, but leads to the probability of mis-categorized areas. For the REAP land cover analysis program the MDAS system was operated to permit no more than two percent uncategorized cover.

As a result of categorization of the 19 LANDSAT scenes, as few as 12 and as many as 36 different categories were determined. For example, in two different scenes up to 14 different categories of water were identified; as many as nine different categories of cropland were detected but there were only three different wetland categories. All categories identified through this process have been retained on the categorized tapes. However, for purposes of displaying the results of this land cover analysis on colored maps, an extensive merging of categories was undertaken.

Ten different land cover categories were selected for display on maps and a color was assigned for each category (Table 3). The colors assigned for a given land cover were chosen after a consideration of the following criteria: user preferences, the desire to permit a ready association of color to actual land cover color, standard colors for specific features (usually as adopted by national

TABLE 3. REAP Land Cover Categories and Colors.

Category	Color
Built Up Land	Magenta
Agricultural Land	
Cropland	Green
Fallow Land	Brown
Exposed Subsoil	Grey
Rangeland	
Rangeland	Yellow
Pasture, Mixed Agriculture	Orange
Forest	Red
Water	Dark Blue
Wetland	Light Blue
Barren Land	White
Uncategorized	Black

organizations), the desire to more clearly distinguish certain categories, and an attempt to present the most attractive possible combinations.

The 10 categories selected for map display include all seven applicable Level I categories suggested by the U.S. Geological Survey (Anderson, *et al.*, 1976), and five Level II and Level III sub-categories. Modifications were made in the USGS-recommended colors for Level I in order to be able to portray all 10 REAP categories.

Geometric correction.—As satellite imagery is obtained from the EROS Data Center, the only undistorted portion of each scene is the center of the scene. Imagery closer to the edge of the scene is subject to increasingly greater angular distortion. Correction of this distortion is accomplished by selecting a large number of ground control points (GCP's from topographic maps and merging such information with that displayed on MDAS from the LANDSAT scenes. The precise coordinates (latitude and longitude) of each GCP were tied to each feature on the MDAS display terminal, and a computer correction program brought the LANDSAT imagery into conformity with the GCP information.

The most reliable GCP's are those which combine small size with high detectability, and these include such features as sharp bends in rivers, points of land jutting into a water body, unusually shaped inlets, and the intersections of major railroads and/or highways. The data source for such geographic information normally is USGS topographic maps, but the process was complicated by the fact that such coverage of the state of North Dakota is incomplete. Nonetheless, a randomly selected sample of 417 of the 1,250 available 7½-minute (1:24,000) USGS topographic maps was obtained. Of these, 139 yielded a total of 508 usable GCP's, for an average of 1 GCP for every 360 sq. km.

In order to assure that each of the approximately 40,000,000 pixels categorized was properly registered to a given section and township in the state, arrangements were made with the Computer Research Corporation of Arvada, Colorado, to digitize a large-scale map of the state of North Dakota, recording the precise latitude and longitude of every section and township corner within the state. The resulting registration tape was read against the categorized tape in order to identify those pixels which lay within the bounds of each section and township.

RESULTS

North Dakota is the first state for which detailed land cover analysis has been completed utilizing computer processing of digital LANDSAT imagery. Preliminary reports of some of this work have been presented by McKeon *et al.*, and by Mower and Heinrich. The results of this land cover analysis have been incorporated in several different products which will be available for public purchase and technical use. Each of these products will be described in some detail below.

The first product of the land cover analysis is a color-coded map for each of the 53 North Dakota counties at a scale of 1:126,720 (exactly two miles to the inch). On each map, a color is used to designate each of the 10 different land cover categories as indicated in Table 3. Each county map contains information on the

scale, the color legend, the name of the county, a small map of the state with the county darkened, and an outline of the county containing the date(s) of the LANDSAT imagery used for the analysis. To produce these maps Bendix developed a technique to create a high quality color negative merging the land cover and the base map data. The land cover data was produced by the computer processing discussed above, and the map was a "scrubbed" version of the detailed county highway maps. These scrubbed versions, which were purchased from TPI, Inc. of Bismarck, contained only section, township, and county boundaries, and town names and locations. Preparation of the scrubbed versions of the highway maps involved removing all of the irrelevant information normally appearing on such maps, including water bodies, transportation networks, topographic features, etc. The land cover data map was first registered to the detailed county highway map, and then registered to the scrubbed version of the county highway map. A black and white reduced version of a typical county land cover map is shown in Figure 2.

The second product of this analysis is an area tabulation for each township, county, and the state. For each of these geographic units, a table was prepared indicating the acreage covered by each of the 10 land cover analysis categories. The area tabulations were prepared by reading a digital tape file and summing the land cover to the appropriate geographic area. The area tabulation for the entire state is shown in Table 4.

The third product of the land cover analysis is a map of the entire state of North Dakota at a 1:500,000 scale (approximately eight miles to the inch) which contains the land cover illustrated by the appropriate color, the same as used on the county maps, and the county boundaries. The state map is a photomosaic of the 53 county maps. Accompanying each state map which is distributed will be a tabulation of the area of each land cover category for the entire state.

The final product of the land cover analysis is a digital tape file of land cover data prepared in a specified cell format. The objective of this effort was to prepare land cover information aggregated to 40-acre cells. The approach taken was to identify cells, starting at the southeast corner of each section, which are exactly one-fourth of a mile on each edge. Each such cell is typically referred to as a quarter-quarter section. Thus, all pixels with center points lying within the given quarter-quarter section were tabulated and grouped by land cover category. The total number of pixels counted for each cell is typically 34-36.

In the preparation of the digital tape file, it could not be assumed that every section was exactly one mile square nor that each township was precisely six miles square. Of the 2,055 townships in the state, 57 are irregular. Thus, as described earlier in this article, REAP obtained a digital file of the state of North Dakota containing 124,866 latitude and longitude points which describe the precise boundaries of both regular and irregular townships and sections. From this tape, quarter-quarter sections were identified starting at the southeast corner of each section. By this process, any irregularly shaped quarter-quarter section appeared on the westernmost and northernmost border of each section. The digitized registration tape was read against the land cover categorized tape in order to iden-

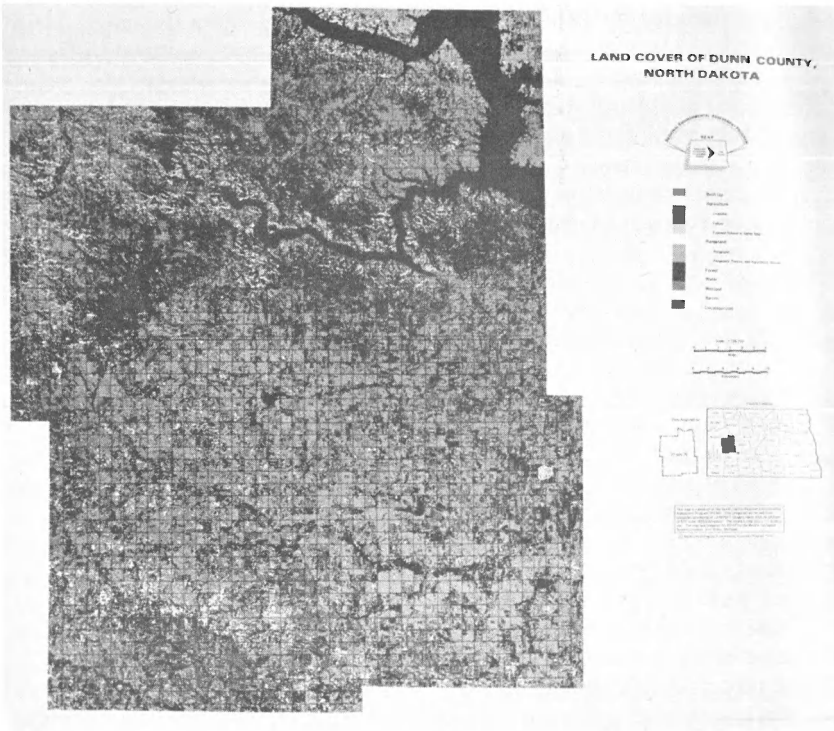

FIGURE 2. Land Cover Map of Dunn County.

TABLE 4. North Dakota Land Cover by Category.

Land Cover Category	Acres	Percent of Total
Built-Up Land	19,777	0.04
Cropland	15,956,690	35.24
Fallow Land	6,189,168	13.67
Exposed Subsoil or Saline Seep	100,952	0.22
Rangeland	11,889,387	26.26
Mixed Range, Agriculture, and Pasture	7,630,329	16.85
Forest	386,823	0.85
Water	1,265,812	2.80
Wetland	780,284	1.72
Barren Land	975,863	2.16
Uncategorized	80,787	0.18
TOTAL	45,275,872	99.99

tify those pixels which fell in each quarter-quarter section. On the digital tape, up to 36 individual land cover categories were recorded for each quarter-quarter section in the state. A header record on the tape provides the township and range number, the LANDSAT scene code, an identification number, and the date of acquisition of the information. This information is grouped into townships and stored on standard-length 800 BPI tape, and will be utilized in the REAP computer system for subsequent analysis and for comparison with other geographically referenced information.

DISCUSSION

This land cover analysis project represents the first time a computerized analysis of LANDSAT imagery has been conducted for an entire state. The fact that this analysis involved 19 different LANDSAT scenes introduced a number of unique problems and difficulties which have not appeared when such analyses have been limited to one scene, or when interpretation of LANDSAT imagery has been conducted manually. Further, it should be recognized that computer analysis of LANDSAT imagery is still a relatively new technique. Thus, while this particular analysis has provided significant information for use in the total REAP system, and has provided an unique analysis of the land cover of the state of North Dakota, it is recognized that there is considerable opportunity for improvement and further analysis of the results of this project. In this section a number of the problems identified in the course of this analysis will be presented and discussed.

There are a number of variables which are uncontrollable and yet have a significant affect on the consistency of the imagery used in the analysis. The fact that scenes covered a range of years from 1973 through 1976 led to inconsistencies. There was considerable difference in the degree of "wetness" of those years, with the early part of 1975 being especially wet, and 1976 being one of the driest years in history in the state of North Dakota. This problem is especially apparent in comparing the analysis of Kidder County with that of Burleigh County adjacent to it. The Burleigh County imagery was recorded in 1975 and the water bodies are relatively full. However, the 1976 imagery shows a considerable amount of barren land that is dried up lake and slough areas. Long Lake, in the southern part of both counties, therefore, appears rather full of deep water in Burleigh County, but appears almost dry in Kidder County. This problem is understandable when the difference follows county lines, but in the case of McKenzie County, the demarcation between the two scenes splits the county on a northeast to southwest line, and is not aesthetically pleasing.

The range in days of scene coverage, from June 20th to August 6th, also created special problems because the vegetative cover significantly changes throughout that period. A particular problem was noted with scenes 3A, 3B, and 3C, recorded on August 6, 1976. That year was an especially dry year, and harvesting of small grains commenced earlier than usual. Accordingly, at the time of the overflight, much of the cropland was already in the form of stubble fields, the reflectance of which is readily confused with rangeland. Therefore, it is apparent that in the acreage tabulations for areas covered by scenes 3A, 3B, and 3C cropland is underrepresented, while rangeland probably is exaggerated. Furthermore, the acreage of wetland probably is considerably understated.

Another limitation is forced by the fact that the minimum period for entire satellite coverage of the state of North Dakota involves one pass per day for six consecutive days, each pass being 100 km. (60 mi.) farther west than the previous pass. It is possible for the moisture conditions of the soil to change from day to day, for example from isolated rains, and therefore provide different reflectance for a similar area from one day to the next. Further, it is almost impossible to find a period of six consecutive days in which the atmospheric conditions are ideal for obtaining top quality imagery.

An important limitation in such an analysis is the amount of information available from other sources on the actual ground cover (i.e. ground truth). The extent of ground truth probably is the key limiting factor for even more detail and accuracy in the categorization. The ground truth information for this project was acquired in 1976, whereas the imagery utilized was from 1973 through 1976. Thus, a number of assumptions were made about what the ground cover actually was for up to three years earlier. In most instances this was not difficult when one understands that North Dakota farming practices usually involve rotating cropland with fallow land.

Another problem is the "averaging" of reflectance. For example, whereas cropland, rangeland, and forest cover each has its own unique reflectance, it ap-

pears that where there is some forest cover on rangeland the reflectance appears the same as cropland. This problem was detected particularly along the borders of Lake Sakakawea and in the Killdeer Mountain areas. Both of these areas show too large an amount of cropland, contrary to that determined from on-site inspection. Wooded draws in rangeland areas of western North Dakota also gave a reflectance characteristic of cropland. A similar problem appears along the border of strip-farmed fields, in western North Dakota particularly. Strip farming typically involves alternating rows of cropland and fallow land. The imagery identified the cropland and the fallow land, but very often perceived rangeland between the two. This is probably due to the pixels recorded along the edge between crop and fallow showing an average reflectivity which happens to be characteristic of rangeland.

It must be kept in mind that the resolution of the satellite is approximately 80 meters. Therefore, many features, such as some highways, railroads, narrow reservoirs, narrow shelterbelts, and narrow wooded draws normally were beyond detection. With the resolution on subsequent LANDSAT satellites to be reduced to approximately 30 meters, the detection of some of these features should be much better. The limited resolution of LANDSAT I and II resulted in poor detection of wooded draws in western North Dakota and shelterbelts in eastern North Dakota. However, in Burleigh and Oliver counties a much larger proportion of forested area was discerned compared to that detected in the remainder of the state. The reason for this is not clear.

There was also considerable difficulty in obtaining a representative and consistent signature for built-up areas (i.e., cities) in the state. Contrary to the perspective we obtain on the ground, indicating that cities are little more than concrete, rooftops, and buildings, from a remote sensor high above, cities appear as a mixture of concrete, asphalt, and rooftops, together with lawns and trees. In some areas where new development was occuring, such as around Dickinson and Bismarck, the area under development appears to be barren land (where the topsoil has been removed) or fallow land (where only the vegetation has been removed). In most cities, however, the typical reflectance is the same as for a mixture of cropland, rangeland, and forest land.

The search for an unique signature for built-up land in western North Dakota led to a serendipitous discovery. The reflected signature for downtown Minot, a rather concentrated built-up area, was found to be the same as for numerous areas appearing in the center of fallow fields, particularly in Stark and Hettinger counties. Subsequent field studies revealed that these were areas where the topsoil had been removed by wind and water erosion, exposing the subsoil. Other areas were sites of saline seepage. It was decided to retain this identification of saline seeps and exposed subsoil because of the potential analytical value of such information. This particular problem revealed one of the unique capabilities of LANDSAT analysis, but also clearly indicates the limitations of such analysis for urban-related studies. It would appear that land cover analyses of urban areas should be reserved to much lower altitude or higher resolution imagery.

SUMMARY

The first complete land cover analysis of the state of North Dakota has been conducted utilizing computerized analysis of LANDSAT imagery. The products of the analysis are color-coded maps of each of the 53 counties in the state and a state map. Tables of area coverage of each land cover category are also available. The digital information for each pixel in the state is recorded on computer tape for subsequent utilization in the REAP computer system.

This analysis has revealed a number of unique capabilities of the LANDSAT imagery process, but has also revealed a number of problems in analyzing such large areas, those utilizing more than a single LANDSAT scene. The products of this analysis are already being used in corridor analysis for transmission lines, resource analysis, water management problems, non-point source pollution studies, and regional environmental analysis. The results provide an essential data base for the REAP system and will serve as the basis for monitoring changes in land cover in the state of North Dakota.

ACKNOWLEDGMENTS

This project involved close cooperation between three groups — the REAP staff, the Bendix team, and the UNDIRS group. We acknowledge the efforts of Bendix personnel under the direction of Dr. John C. McKeon who labored conscientiously to produce a satisfactory final product. The UNDIRS group under the leadership of Dr. Roland D. Mower met their responsibilities effectively. The efforts of Dr. Warren C. Whitman and the group of biologists from North Dakota State University and the University of North Dakota who assisted in the field checking are appreciated. The base map for the state land cover map was prepared by the Cartographic Laboratory of the Geography Department, University of North Dakota.

LITERATURE CITED

Anderson, J. R., Hardy, E. A., Roach, J. T., and Witmer, R. E. 1976. A Land Use and Land Cover Classification System for Use with Remote Sensor Data, U.S. Geological Survey, Professional Paper 964, 28 pp.

DeNoyer, J. M. 1976. ERTS-1, A New Window on our Planet, U.S. Geological Survey, Professional Paper 929, Williams, R. S. and Carter, W.D., Editors, p. 1.

McKeon, J. B., Rogers, R. H., Mower, R. D., Reid, J. R., and Johnson, A.W. 1977. North Dakota Land Cover Analysis from Computer Processed LANDSAT Data, Proceedings of the American Society of Photogrammetry.

Mower, R. D. and Heinrich, M. L. 1977. A Computer Processed (LANDSAT) Land Cover Map of North Dakota, Remote Sensing of Earth Resources, Vol. 5, University of Tennessee Space Institute (in press).

Regional Environmental Assessment Program. 1975. Technical Task Force Reports, 195 pp.

Rogers, R. H., Reed, L. E., Schmidt, N. F., and Schecter, R. 1975. Computer Mapping of LANDSAT Data for Environmental Applications, Proc. of Workshop for Environmental Applications for Multi-Spectral Imagery, Fort Belvoir, Va., p. 118-134.

Session Laws. 1975. State of North Dakota. Chapter 4, Section 4.

PRELIMINARY EVIDENCE OF AN AUTHIGENIC ORIGIN OF KAOLINITE IN THE GOLDEN VALLEY FORMATION (PALEOCENE-EOCENE), NORTH DAKOTA

F. R. Karner, P. F. Bjorlie and O. D. Christensen
Department of Geology
University of North Dakota, Grand Forks, North Dakota 58202

ABSTRACT

Mineralogic, stratigraphic and paleoclimatologic evidence indicates that the kaolinite rich zone of the lower member (Bear Den) of the Golden Valley Formation may have an authigenic origin and is part of a paleosol. X-ray diffraction data show that kaolinite increases in crystallinity toward the top of the kaolinite-rich zone as expected in a soil. Scanning electron microscopy confirms the presence of kaolinite crystals but has not yet provided evidence regarding their origin. The suggested paleosol sequence consists of an upper carbonaceous silty or clayey zone with organic content decreasing downward and underlain by a massive, kaolinite-rich zone containing numerous ferruginous concretions. The lowermost unit of the Bear Den Member consists of unweathered sandstones, siltstones and interbedded clays. The known paleoclimatology at the time of formation would have allowed kaolinite formation in the lowlands of the late Paleocene-early Eocene Great Plains. The kaolinite formation may be correlated with late Cretaceous-early Cenozoic tectonic stability and the development of an extensive erosion surface as presently recognized in the south-central Rocky Mountains.

INTRODUCTION

Recent work by Hickey (1977) summarizes the stratigraphy and paleobotany of the Golden Valley Formation (Paleocene-Eocene) in western North Dakota. About 887 km² of the Golden Valley is exposed in a total outcrop area of about 33,200 km². The lower member (Bear Den) typically ranges from about 6 to 11 m in thickness and consists of kaolinitic, sandy, silty and clayey beds containing limonitic spherules and thin carbonaceous beds. A light colored, kaolinite-rich unit 4-5 m thick is an easily identifiable, laterally consistent unit in the middle of the member. Kaolinite is also present in adjacent silty and sandy units. Freas (1962) and Hickey (1977) have summarized work on the mineralogy and petrography of the Bear Den. In this paper, a preliminary statement in summary form is given of stratigraphic and paleoclimatologic evidence which we believe indicates that the kaolinite may have an authigenic origin and that the Bear Den is a paleosol.

GENERAL GEOLOGIC RELATIONSHIPS

The Bear Den Member conformably overlies olive drab or brown sediments of the upper part (Sentinel Butte) of the Fort Union Formation; the contact is at the base of either the lowest light gray or purplish silt bed or light gray clayey sands (Freas, 1962). The contact with the upper member (Camels Butte) is placed above a carbonaceous zone which is normally capped by the Alamo Bluff lignite or Taylor bed (Hickey, in press). The Bear Den is recognized by its gray to whitish

gray color with characteristic orange staining. Hickey (1977) divided the Bear Den into three zones: a lower gray zone averaging about 2 m in thickness and consisting of kaolinite-bearing siltstone, sandstone and mudstone; a distinctive orange zone about 4-5 m thick consisting of kaolinite-rich silty clay or siltstone with common limonite spherules; and an upper carbonaceous zone about 1 m thick consisting of dark gray kaolinitic shale, mudstone, siltstone and lignite.

Hickey (1977) described a megaflora of 41 species in the Bear Den Member which closely resembles the late Paleocene portion of the Fort Union flora. Lowland forest vegetation is characteristic of the lower zones with swamp and aquatic vegetation more abundant and better distributed upward through the carbonaceous zone. Hickey (1977) concluded that the Bear Den is Late Paleocene in age and that fossil plant, vertebrate, and invertebrate evidence indicates a warm, temperate climate with an estimated mean annual temperature of 15°C changing to a subtropical climate with a mean annual temperature of 18.5°C during deposition of the Camels Butte Member in the Early Eocene. On the basis of sedimentary characteristics, Hickey also concluded that the Bear Den was deposited in a fluvial environment rather than a lacustrine environment as suggested most recently by Freas (1962).

The authors have examined the Golden Valley in the field observing textural, structural and compositional characteristics to verify our use of the data presented by Freas (1962) and Hickey (1977). We have also examined Golden Valley samples in the laboratory utilizing polarized light microscopy, x-ray diffraction and scanning electron microscopy to verify our use of analytical data by Freas (1962) and also to test our hypothesis of the paleosol origin of the Golden Valley.

FORMATION OF KAOLINITE

General conditions facilitiating the formation of kaolinite are summarized by DeSegonzac (1970) and included: (1) hot, humid climate; (2) relatively stable land surface; (3) presence of unweathered silicates and/or clay minerals; (4) low pH; and (5) a leaching environment.

Specific modes of accumulation of kaolinite include: (1) formation in a soil profile (DeSegonzac, 1970); (2) formation beneath acid bogs or peaty soils (Herath, 1963); (3) diagenetic transformation of clayey sediment by acid groundwater (DeSegonzac, 1970); and (4) reworking, transportation and redeposition of previously formed kaolinite (DeSegonzac, 1970).

EVIDENCE THAT THE BEAR DEN IS A PALEOSOL

As a result of study of the literature and an initial field and laboratory study we interpret the Bear Den Member of the Golden Valley Formation to be a kaolinitic soil developed on Late Paleocene, Sentinel Butte sediments in a low, swampy area under subtropical climatic conditions during an Early Eocene period of tectonic quiescence in the Rocky Mountain area of western North America as evidenced by recent studies in the southern Rockies (Epis and Chapin, 1975).

In initial testing of our interpretation we have examined the Bear Den in the field in the area south of Dickinson, North Dakota where we have measured sections and sampled the member. Our laboratory work has included x-ray diffraction examination of samples primarily from a location 3 mi. south of Golden Valley, Mercer Co. N.D., Sec. 2, NW ¼, NE ¼, R. 90 W., T. 43 N. The results agree with those of others (Freas, 1962, Hickey, 1977) regarding general mineralogy of the unit and particularly clay mineral variation as noted below. Scanning electron micrographs confirm the presence of kaolinite. Thin section study shows evidence of partial kaolinitization as noted below.

The following are suggested as major lines of evidence for our interpretation and as subjects for future detailed study. (1) The tripartite division of the Bear Den into an upper carbonaceous, kaolinitic zone, a middle orange kaolinitic zone, and a lower gray, kaolinitic, silty and sandy zone is compatible with a soil profile developed on a Sentinel Butte fluvial sequence. (2) The abundance of kaolinite increases upward in the member as montmorillonite and illite decrease (Freas, 1962). We have confirmed this observation with our own x-ray diffraction work and have also noted that the crystallinity of kaolinite, as evidenced by peak height to width ratios, increases upward. The underlying Sentinel Butte and overlying Camels Butte member are montmorillonitic and illitic. (3) Abundant kaolinite and limonite spherules in the orange zone suggest acid, oxidizing conditions which may account for all or most of the mineralogical differences between the orange zone and lithologically similar Sentinel Butte units. (4) Our thin section study shows that kaolinitization of detrital feldspar, mica and other grains appears to be incomplete and is restricted to the margins of some grains, many of which are angular. Kaolinitization of clay matrix appears to be spatially related to limonite-stained fractures. (5) The Alamo Bluff lignite and the correlative silicified Taylor Bed mark the top of the Bear Den and are the key to reconstructing the geologic and geochemical conditions of formation of the kaolinitic paleosol. (6) Separating the deposition of the Bear Den sediments and the kaolinitization facilitates interpretation of the environment of deposition and the source of the kaolinite, montmorillonite and illite in the Bear Den and associated sediments. (7; Climatic and tectonic conditions in western North America indicate the more or less coincident culmination of a warming trend and a change in tectonics producing an Early Eocene lowland in western North Dakota which received little sediment for a relatively long period of time.

LITERATURE CITED

DeSegonzac, G. D., 1970. The transformation of clay minerals during diagenesis and low grade metamorphism: A review. Sedimentology 15:281-346.

Epis, R. C., and Chapin, C. E., 1975. Geomorphic and tectonic implications of the post-Laramide, late Eocene erosion surface in the Southern Rocky Mountains, in Cenozoic History of Southern Rocky Mountains, Edited by B. F. Curtis. Geol. Soc. America Mem. 144. 45-74.

Freas, D. H., 1962. Occurrence, mineralogy, and origin of the lower Golden Valley kaolinitic clay deposits near Dickinson, North Dakota. Geol. Soc. America Bull. 73:1341-1364.

Herath, J. W., 1963. Kaolin in Ceylon. Econ. Geol. 58:769-773.

Hickey, L. J., 1977. Stratigraphy and paleobotany of the Golden Valley Formation (Early Tertiary) of western North Dakota. Geol. Soc. America Mem. 150. 294p.

PROBABLE CAUSES OF SURFACE INSTABILITY IN CONTOURED STRIP-MINE SPOILS— WESTERN NORTH DAKOTA

G. H. Groenewold
North Dakota Geological Survey
University Station, Grand Forks, North Dakota 58202

and

L. M. Winczewski
Department of Geology
University of North Dakota, Grand Forks, North Dakota 58202

ABSTRACT

Preliminary reconnaissance existing graded strip-mine spoils in western North Dakota indicates that various engineering problems exist within these materials. These include differential subsidence of the surface of the spoil, slope instability, and piping failures. Major variations in texture, composition, and packing, within the spoil, appear to be the primary factors which control spoil stability. These are, in turn, directly related to the original nature of the stripped materials, the methods of stripping, transportation, and emplacement, and the time of year during which these operations occur. Localized movement of groundwater through recontoured spoils is very common in some settings. Permeability of the graded spoils and therefore the rates and directions of groundwater movement are, in part, determined by the method of emplacement and the physical characteristics of the sediments. In addition, the time of year during which emplacement occurs can have a very strong influence on the permeability characteristics of the spoils. Recontouring during the winter months often results in the concentration and burial of large frozen blocks of spoil within the regarded materials. Initially the zones of blocky materials are characterized by a high percentage of void space and corresponding high permeability. Areas of spoil underlain by blocky zones are often highly susceptible to settling. Fractures, resulting from settling, allow surface water to migrate down through the spoils. If sufficient water is available, piping and associated collapse features will result.

INTRODUCTION

The proposed increased development of lignite resources in western North Dakota will lead to large tracts of land, as much as several tens of square miles in a single location, being strip mined and subsequently reclaimed. One of the principal concerns associated with large-scale strip mining in western North Dakota is the return of the mined area to an acceptable level of agricultural productivity. The stated reclamation goal for the state is a return to a level of productivity equal to or greater than that which existed prior to mining. To achieve this goal extensive research has been undertaken to determine the optimum methods of reclamation. The emphasis of most reclamation research, as well as reclamation laws, has been focused almost entirely on that portion of the landscape included within the soil zone. Subsequent agricultural use of a major percentage of the reclaimed areas requires that the replaced material not only maintain a given level of productivity, but also maintain a stable configuration.

Preliminary reconnaissance of existing graded spoils indicates that various

engineering problems exist within these areas. These include differential subsidence of the surface of the spoil, slope instability, and piping failures. For reclamation to be truly meaningful, an entirely new equilibrium landscape must be designed. The landscape includes not only the soils on the surface of the disturbed area, but also the sediments beneath the surface. A complete inventory of this body of materials, including an understanding of the equilibrium of the premining landscape is essential to proper reclamation design. The concept of landscape design reclamation has been discussed in more detail by Moran and others (1975).

MATERIALS AND METHODS

Existing Contoured Site

Preliminary observation of graded spoils began in November, 1974, as part of a project designed to determine the hydraulic characteristics of spoils. The initial area of study involved a 16 hectare site at the Indian Head Mine near Zap, North Dakota. The study site had been contoured in the fall and winter of 1973. Final contouring was completed in the spring of 1974. It was not possible to observe contouring activities at this site. However, it is known that all contouring was done with bulldozers.

Observation of Stripping and Contouring Procedures

It was assumed that surface instability was dependent upon the subsurface characteristics of the materials. In order to gain a better understanding of the factors that determine the internal character of spoils, stripping and contouring procedures at the Indian Head Mine were monitored in detail. Detailed observations of dragline stripping methods and their relationship to spoil characteristics were made. The relationships of thickness of overburden, curvature of cut, and original nature of the overburden to morphology of spoil piles and segregation of materials within the spoils were noted. In this way we have been able to identify a number of potentially significant variables related to stripping procedures.

A second 16 hectare study site, adjacent to the first, was monitored during the contouring phase. Contouring of the rugged spoils was initiated in September, 1975. Contouring continued through the winter and was completed in the summer of 1976.

The first part of the study involved detailed topographic and materials mapping of the area. Distribution of spoil, character of spoil, position of highwalls and cuts, description of undisturbed materials in highwalls, description of interfaces between spoils and undisturbed materials, and locations of ponds and flooded pits were noted in the initial survey.

The second part involved field observation and mapping of contouring procedures. Variations resulting from seasonal effects were noted as were variations in the type of equipment used. After contouring was completed a second topographic survey of the area was made. The site is presently being

monitored periodically. All instability phenomena are being noted and compared to the baseline data for the area. In this way it is possible to correlate these phenomena with variations in the character of the spoil and contouring procedures.

RESULTS AND DISCUSSION

The first indications of differential movement in the spoils at the existing contoured site became evident in the late fall of 1974. Severe subsidence was observed on a 1 hectare test plot designed to monitor surface water runoff. In one instance, 340 cubic metres of material were required to bring the plot back to original slope and gradient. Although the test plot required several surface repairs, similar plots on either side of the one in question showed very little subsidence, indicating the localized nature of the phenomenon.

Figure 1 shows a similar situation at the same site. The photograph shows two of the piezometers which were installed to monitor subsurface water movement. The piezometer in the foreground is 10 cm in diameter, the small piezometer is 2.5 cm in diameter. Both are constructed of plastic pipe. The bottom of the larger pipe is approximately 20 metres below the surface in the basal portion of the spoils. The bottom of the smaller pipe is approximately 35 metres below the surface in unmined bedrock below the spoils.

Both installations were periodically monitored during the winter of 1974-1975. In May, 1975, the cement seal around the larger pipe, originally designed to keep surface water from flowing down the annulus, was observed to be about 0.3 metre above ground surface (figure 1). In addition, the smaller pipe was noticeably rotated from its former vertical position (slightly evident in the photo) and was obstructed at about eight metres below land surface. The toe of a slump block was noted about 20 metres down slope from this site. The piezometers in figure 1 are located on the highest position in the study site area. Subsequently, two other piezometers located elsewhere in the study area (both 2.5 cm in diameter) have broken in the subsurface. These are also located in topographically high positions.

The breakage of the piezometers is apparently the result of shearing related to slumping and associated rotational movements in the spoils. In all three cases, the bottom of the pipe is in unmined bedrock below the spoil. In the case of the larger pipe in figure 1, the slumping did not shear the pipe, but resulted in lowering of the ground surface around the pipe. The increased strength of the larger pipe may have prevented its destruction. Also, the fact that this pipe is totally within the poorly consolidated spoils may have allowed the pipe to move, at least to some extent, with the spoil materials thus reducing some of the shear stresses.

Surface collapse structures are the other type of instability feature commonly found in the study area. These structures ranged in size from small openings a few centimetres in diameter to much larger features several metres in diameter. These features initially occurred as a very small crack or opening at the surface of the spoils. With time and precipitation the opening gradually became larger (figures 2 and 3). In one case a tractor being used to seed the spoils fell into a collapse struc-

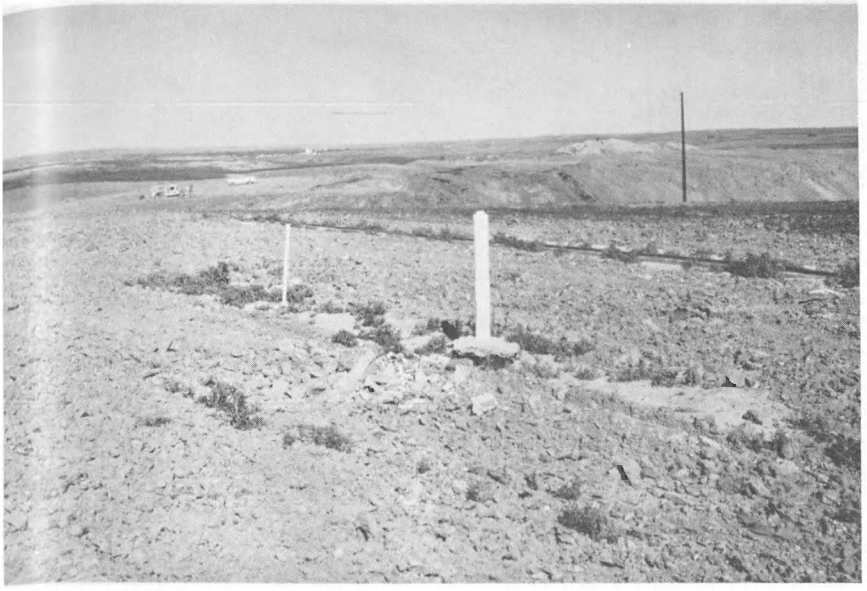

Figure 1. Piezometers in contoured spoils showing settling of spoils around larger pipe (foreground) and rotation of smaller pipe.

ture. As is shown in figure 2, all surface drainage in the immediate area drains toward the depression. All surface runoff in the vicinity of such a feature is observed to flow toward and into the depression, and rapidly disappear into the surface. Of interest is the fact that ponds of surface water may often occur in very close proximity to such collapse features, as shown in figure 3. These observations indicate the highly localized nature of these piping features. These observations also indicate that the various surface instability phenomena are controlled by the varying subsurface characteristics of the spoils.

Probable Causes of Instability

The significant characteristic of all the observed instability phenomena is their localized nature. Area-wide settling of the spoils is also very common but not of major concern. During the mining operations, the rearranged spoil materials assume a volume estimated at 25 percent greater than in the undisturbed state (Van Voast, 1974). With time, the reclaimed area will slowly settle, eventually approaching a density similar to that which existed prior to mining.

It appears that the major cause of localized instability is the concentration of large blocks of overburden or spoils materials in the subsurface. Blocky zones of this type are characterized by a high percentage of void space and a high susceptibility to subsidence and differential movement. Results obtained thus far from

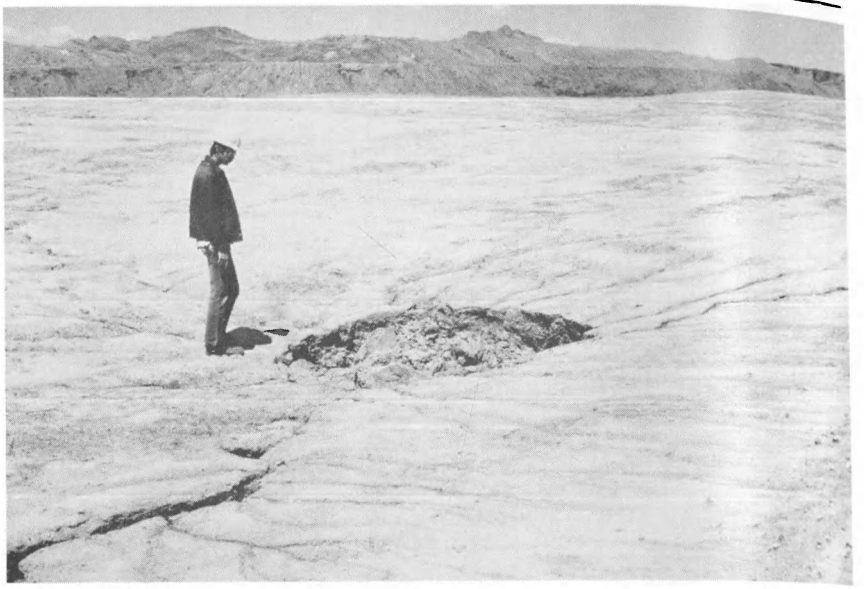

Figure 2. Collapse feature in spoils showing all surface drainage flowing toward the depression.

Figure 3. Collapse feature in spoils showing proximity to standing water body also on spoils.

post-contouring observation of the second study site are preliminary in nature. This site will be monitored periodically for another two years. Monitoring of stripping and contouring operations has enabled us to relate the concentration of blocky materials to a group of mining, material, and reclamation variables. Significant variables include (1) the original nature of the overburden, (2) methods of stripping and resulting spoil morphology, (3) time of year during which stripping and contouring occurs, and (4) method of emplacement of the materials during contouring operations.

Original Nature of the Overburden

The bedrock at the study site is interbedded sand, silt, clay, and lignite of the Sentinel Butte Formation. The Sentinel Butte Formation was deposited in an alluvial floodplain environment (Cherven, 1973; Johnson, 1973). The overburden in the area of the two study sites is predominantly fine-grained silt and clay, typical of natural levee and flood basin settings. Observation of mining techniques at the Indian Head Mine and elsewhere indicate that fine-grained materials of this type have a greater tendency to remain in large blocks than do sandy materials.

Methods of Stripping and Resulting Spoil Morphology

Variations in the methods of stripping by dragline can result in considerable variability in spoil pile morphology. Observation of stripping techniques indicate that blocky materials tend to concentrate in the basal portion of the spoils as well as in the lows between spoil ridges (Winczewski, 1977). These concentrations result from the tendency of large, rounded blocks to roll to the bottom of the spoil bank slope. Concentration of blocky materials between ridges can result in linear areas within the spoils which are potentially susceptible to differential subsidence. The more rugged the topography of the original spoils, the greater the possibility for concentration of blocky materials. The contouring phase of the operation can potentially add to the problem by placing additional blocky materials, if available, between the spoil ridges.

Time of Year During Which Stripping and Contouring Occurs

Observation at the study site indicates that the time of year during which the contouring occurs plays a very significant role in determining subsurface spoil characteristics. If contouring occurs during the winter months frozen blocks of spoil concentrate between ridges. This phenomenon has also been noted by Omodt and others (1975).

Figure 4 shows the area between two spoil ridges. The ridge on the left was contoured in the summer while the ridge on the right was contoured in the winter. Monitoring of the area immediately overlying the frozen materials shown in figure 4 indicates that significant differential subsidence is occurring. The large blocks in the photograph are over 1.5 metres in diameter. The materials con-

toured in the summer are generally less than 0.3 metre in diameter. The original materials comprising both ridges are silty clays. Stripping operations in the winter months can also result in concentrations of frozen blocks of overburden. This is especially true if blasting is required to fracture frozen overburden. Whether stripping or contouring, it seems logical that this problem would be more severe during the winters of years characterized by relatively high levels of precipitation.

Methods of Emplacement of the Materials During Contouring Operations

Two very different methods are used to level spoil ridges. The most common is by leveling the area with a bulldozer. Observation indicates that this technique tends to concentrate blocky materials between spoil ridges. Little or no equipment moves across the area between the ridges. Thus, these areas also tend to be less well compacted than the area underlain by the former ridge and therefore more susceptible to subsidence.

The other method of contouring utilizes large scrapers. The use of these machines is often limited by the morphology of the spoils. The scraper removes a thin layer of spoil from one site and carries the load to a second site. The scraper deposits a thin (generally less than 1.5 metres) layer of spoil. At the same time the weight of the scraper is compacting the materials deposited by previous runs. Preliminary comparisons were made between an area of spoil deposited by a scraper and an area leveled with a bulldozer. Initial results indicate that virtually no movement is occurring in the area contoured with a scraper while various sub-

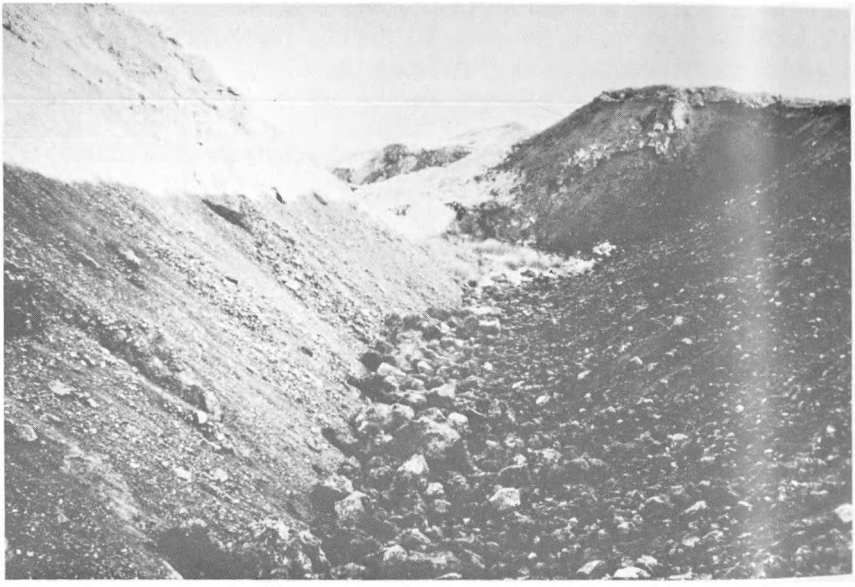

Figure 4. Contrast between summer contouring (left) and winter contouring (right).

sidence features are evident throughout the area contoured with a bulldozer. However, compaction by the scraper will affect essentially only the spoil materials handled by the scraper. If large blocks of material resulting from the stripping operation lie below the compacted zone then the area may still be highly susceptible to subsidence.

Regardless of the initial reason for the blocky materials, it seems likely that with time the voids between the blocks will begin to fill and settling will occur. Fractures, resulting from the settling, allow surface water to migrate down through the spoils. If sufficient water is available, piping and associated collapse or slumping will result. It is hoped that as research continues, we will find ways to avoid these problems and thereby come closer to a truly well designed reclamation landscape.

ACKNOWLEDGMENTS

We would like to acknowledge the cooperation and assistance afforded the researchers of projects associated with this paper by Mr. Robert Murray, President, Western Division of North American Coal Corporation and Mr. Joe Mitzel, Superintendent, Indian Head Mine.

LITERATURE CITED

Cherven, V. B., 1973, High- and low-sinuosity stream deposits of Sentinel Butte Formation (Paleocene) McKenzie County, North Dakota. M.S. Thesis, Univ. N. Dak., 73 p.

Johnson, R. P., 1973, Depositional environments of the upper part of the Sentinel Butte Formation, southeastern McKenzie County, North Dakota. M.S. Thesis, Univ. N. Dak., 63 p.

Moran, S. R., Groenewold, G. H., Hemish, L. A., and Anderson, C. A., 1975, Development of a pre-mining geological framework for landscape design reclamation in North Dakota. Proc. Fort Union Coal Field Symposium, Mont. Acad. Sci., Billings. 3:308-316.

Omodt, H. W., Schroer, F. W., and Patterson, D. D., 1975, The properties of important agricultural soils as criteria for mined land reclamation. N. Dak. Ag. Ex. Sta. Bull. 492, 52 p.

Van Voast, W. A., 1974, Hydrologic effects of strip coal mining in southeastern Montana—emphasis: one year of mining near Decker. Mont. Bur. Mines Geol. Bull. 93, 24 p.

Winczewski, L. M., 1977. Western North Dakota lignite strip mining processes and resulting subsurface characteristics. M.S. Thesis, Univ. N. Dak., 433 p.

A COMPARATIVE STUDY OF THE NUCLEI AND MEMBRANE SYSTEMS OF THE BLASTODERM EMBRYOS OF INSECTS WITH SCANNING ELECTRON MICROSCOPY

S. G. Sears
Metabolism and Radiation Research Laboratory
Agricultural Research Service
U.S. Department of Agriculture
Fargo, North Dakota 58102

ABSTRACT

A scanning electron microscopy study was done to examine the cytological features of early blastoderm membrane systems in two species of insects, *Oncopeltus fasciatus* (Dallas) and *Pectinophora gossypiella* (Saunders). Fertilized eggs were fixed in glutaraldehyde saturated heptane and/or 4% glutaraldehyde and then postfixed in 1% osmium tetroxide. Two tissue fracture methods were used: (1) a modified ethanol cryofracture (CF), and (2) a room temperature ethanol fracture (RF). The CF method produced fractures through nuclei, whole cells, and certain other embryonic structures; the RF method produced cleavage around cells and yolk granules, giving a three-dimensional view of the cell surfaces. Fractured nuclei containing chromosomes were seen, as were whole cells with small finger-like cytoplasmic projections that connected the cells to each other and to the yolk-rich interior of the embryo. Both species of insect embryos studied were similar in general appearance; however, differences were noted in the size and type of surface structures of cytoplasmic projections, etc. Smaller cellular structures such as ribosomes, centrioles, etc., were not identified in these preparations.

INTRODUCTION

To date, the majority of investigations in the field of insect embryology have dealt with the events occurring after blastoderm formation. In these studies, researchers have utilized light and transmission electron microscopes (TEM) to elucidate the structure and functions of the embryo and to identify the cells, nuclei, chromosomes, yolk granules, and membrane systems existing in the embryo at certain stages of development (Counce and Waddington, 1972, pp. 166-242). However, recent studies of early embryology in *Oncopeltus fasciatus* (Dallas) (Gassner and Sears, 1976, pp. 39-51) and *Pectinophora gossypiella* (Saunders) (Berg, 1976, pp. 85-87) have demonstrated that some of the more conventional ideas about nuclear division are not valid until some time during or after the blastoderm. In fact, transmission electron micrographs indicate that in the preblastoderm embryo, the directional flow of the nucleoplasm and the nuclear envelope appear to play a role in chromosome separation and that nuclear divisions occur in the absence of spindle-fiber apparatus.

The present scanning electron microscopy (SEM) study was undertaken to observe membrane systems in the early insect blastoderm embryo, particularly the cellular and nuclear membranes, and to help visualize the three-dimensional structure of objects previously observed only by TEM.

MATERIALS AND METHODS

Fertilized eggs from the large milkweek bug, *Oncopeltus fasciatus*, and the pink bollworm, *Pectinophora gossypiella*, were collected within ½ hr after oviposition and allowed to mature to the early blastoderm stage of development (6-8 hr for the bollworm and 18 hr for the milkweed bug). The eggs were then dechorionated in diluted chlorine bleach solution (Gassner and Sears, 1976, p. 40) and washed with a .1 M phosphate buffer, pH 7.3. The eggs were then treated in either of two ways: (1) emersion in a glutaraldehyde saturated heptane solution (Limbourg and Zalokar, 1973, p. 383) for 1 min. followed by fixation overnight in 0.05 M phosphate buffered 4% glutaraldehyde; or (2) fixation overnight in 0.05 M phosphate buffered 4% glutaraldehyde containing 2% acrolein. The eggs were postfixed overnight in 0.05 M phosphate buffered 1% osmium tetroxide, washed well with distilled water, and dehydrated in a graded series of ethanols. The tissue was then either cryofractured in solid ethanol with a razor blade (Humphreys, Spurlock, and Johnson, 1975, p. 120) or fractured in ethanol at room temperature (Turner and Mahowald, 1976, p. 96) with a fine needle. All fractured eggs were then dehydrated in 100% ethanol and were critical-point dried by using carbon dioxide as transition fluid (Flechon *et al.*, 1975, p. 326). Finally, the dried embryos were mounted on stubs with silver adhesive paint and gold coated before they were viewed in a JEOL JSM-35 scanning electron microscope operated at 10-40 kV.

RESULTS

The blastoderm embryos of pink bollworms and milkweed bugs viewed with the SEM were similar in general appearance (Figures 1 and 2). Both had an outer membranous covering, the chorion, and an inner vitelline membrane between the chorion and the embryo itself. In both species the vitelline membrane was strongly attached to the layer of dividing embryonic cells that surrounded the yolk-rich interior.

The two techniques used to fracture the embryos, cryofracture and room temperature fracture, together yielded a more complete picture of the embryo than either method yielded alone. The cryofracture method (Figure 2) showed planar fractures through the cytoplasm with a number of protruding yolk granules, which gave a "peanut brittle" appearance to the fracture surface. The vitelline membrane appeared to have a flakey texture. The internal structure of cells, nuclei, and numerousyolk granules was revealed by cleaving. The cleaved nuclei (Figures 3 and 4) showed a nuclear membrane and masses of chromatin located centrally or peripherally in the nucleus. The cleaved yolk granules revealed several different internal morphologies. Undigested granules were of a homogeneous nature and were probably bounded by a membrane (Figure 5). The filamentous remnants of yolk (Figure 6) that were sometimes attached to the surrounding tissue.

The room temperature fractured embryos yielded a three-dimensional picture that showed fractures around cells and yolk granules instead of through them

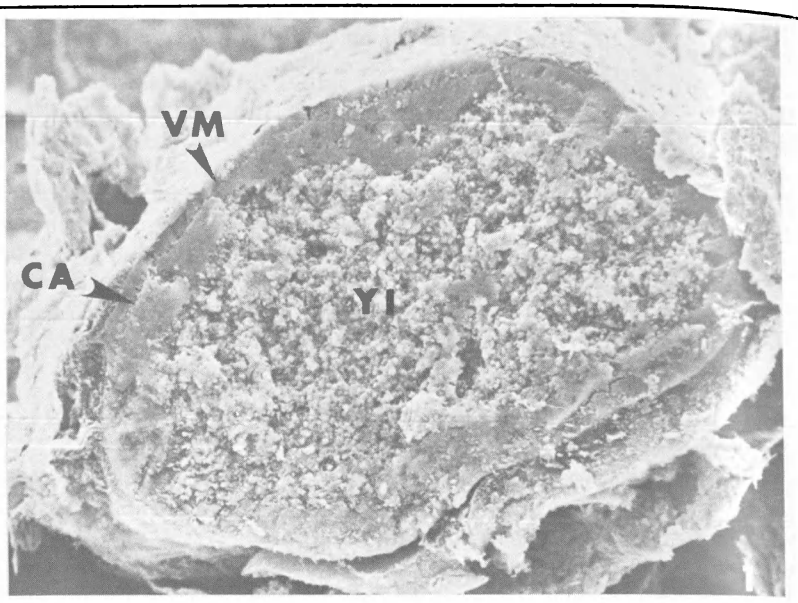

Figure 1. A cryofractured pink bollworm embryo showing the vitelline membrane (VM), the cytoplasmic area (CA) containing the nuclei, and the yolk-filled interior (YI). (Glutaraldehyde/acrolein fix) X 370.

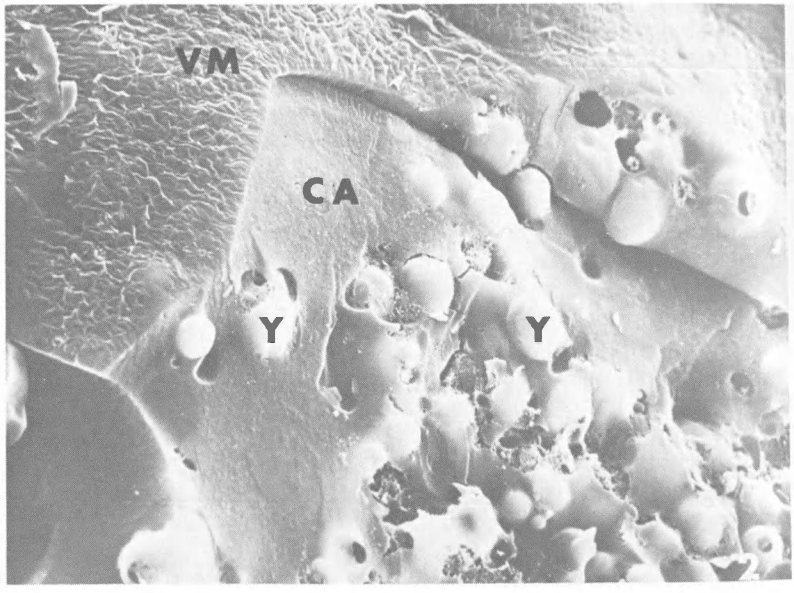

Figure 2. A cryofractured milkweed bug embryo showing the vitelline membrane (VM), the cytoplasmic area (CA), and the individual yolk granules (Y). (Glutaraldehyde/acrolein fix) X 720.

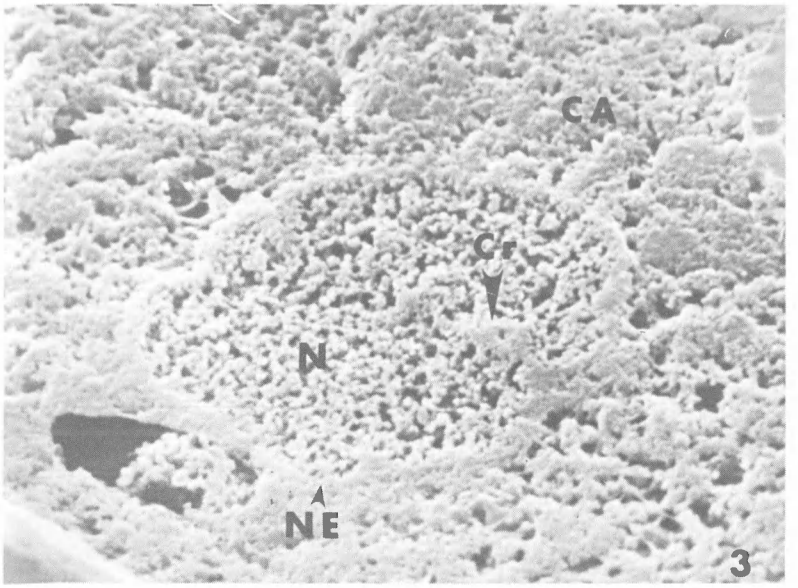

Figure 3. High magnification of a milkweed bug nucleus showing the cytoplasmic area (CA), nucleus (N), nuclear envelope (NE), and condensed chromatin (Cr). (Glutaraldehyde/acrolein fix) X 7,300.

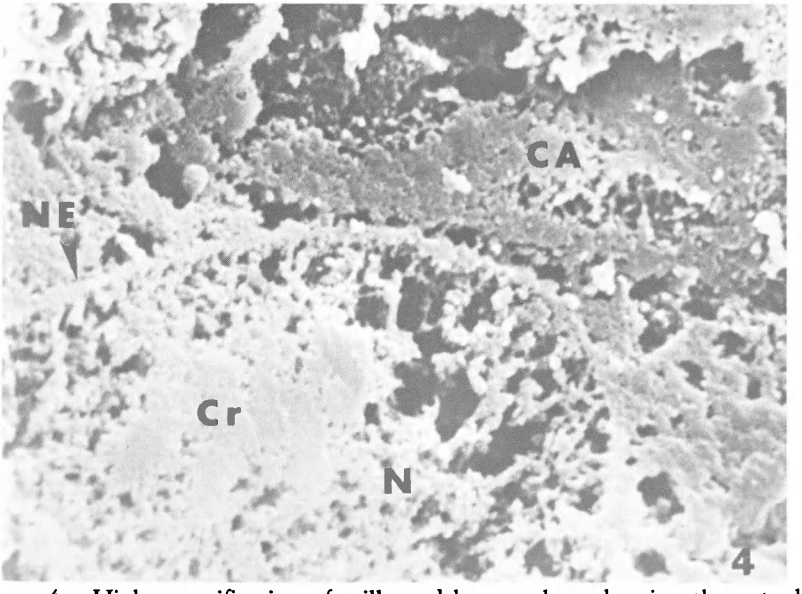

Figure 4. High magnification of milkweed bug nucleus showing the cytoplasmic area (CA), nucleus (N), nuclear envelope (NE), and condensed chromatin (Cr). (Heptane/gluraldehyde fix) X 8,300.

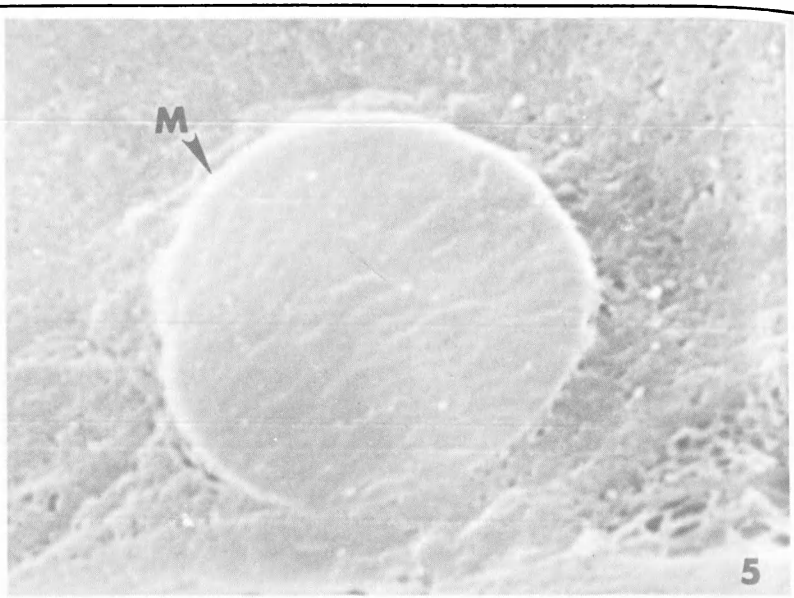

Figure 5. A cryofractured, undigested yolk granule showing smooth, homogeneous interior. Note possible membrane (M) around yolk. (Glutaraldehyde/acrolein fix) X 16,400.

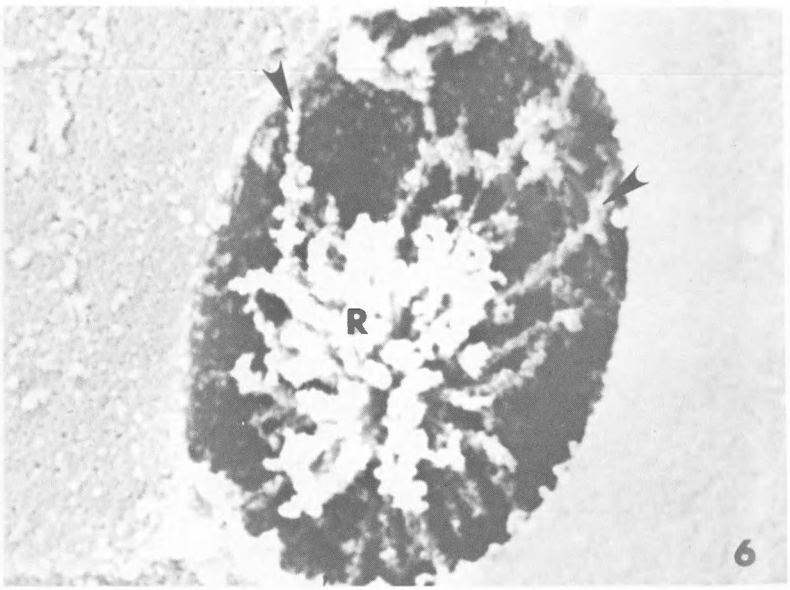

Figure 6. A crofractured digested yolk granule showing the remains of yolk (R). Note the filamentous attachments (arrows) of remnants to the surrounding tissue. (Heptane/glutaraldehyde fix) X 12,000.

(Figure 7). Thus, when a whole embryo was viewed (Figure 8), the individual cells of the blastoderm layer were seen in their spatial relationship to each other and to the yolk-filled interior. This particular bollworm embryo was one cell layer thick, with the cell layer and the yolk area separated by a membrane. Finger-like projections (microvilli) (Figure 9) were seen connecting the cells to the membranous covering of the yolk interior. Other microvilli connected the cells (Figure 10) to each other and possibly connected the cells to the vitelline membrane, which had been removed from this embryo. In the milkweed bug embryo (Figure 11), the blastoderm cells appeared similar in shape to those of the bollworm. However, the milkweek bug embryo was not as developed as the bollworm embryo, and the cells were still rounded. Also, fewer microvilli were present over the cell surfaces (Figure 12), and the individual cells had a more wrinkled appearance. There was also a venous network that ran along the side of the cells and appeared to connect the cells, and this differed from the finger-like connections between bollworm cells. Small protruberances were also observed in the cell membranes of the milkweed bug embryos, and numerous small spheres, possibly mitochondria, were seen attached to the cells. A large, oblong yolk granule capped by a multi-branched membranous structure appeared near the cell layer (Figure 13) in another milkweek bug preparation. The nature of this membrane "cap" is open to conjecture.

A comparison was also made between the average cell size and the largest yolk granule size for the pink bollworm and milkweed bug (this study) and for *Drosophila* (Turner and Mahowald, 1976, p. 99). Sizes were as follows: *Drosophila* yolk size, 5.3 μm; bollworm yolk size, 6μm; milkweed bug yolk size, 6.4μm; *Drosophila* cell size, 12.6 μm; bollworm cell size, 14.5 μm; milkweed bug cell size, 13.5 μm.

DISCUSSION

In any SEM study there is a question of how well the fixed tissue actually represents living tissue. In the present study, several methods of tissue fixation and fracture were used with varying results. The fixation procedure, including dechorionation, emersion in heptane to permeabilize the vitelline membrane, and fixation in glutaralde or glutaraldehyde/acrolein, sometimes damaged the eggs. The bleach also stripped away cytoplasm as well as chorion, and the heptane rendered the eggs extremely sensitive to changes in osmotic pressures. There appeared to be little difference in fixation quality with or without heptane in the eggs observed; however, the heptane emersion has been used with good success in the fixation of *Drosophila* embryos (Limbourg and Zalokar, 1973, p. 383).

The cryofracture method yielded mainly two-dimensional views of embryonic cells, some appearing quite like TEM pictures. The room temperature fractures gave three-dimensional data on whole cells, microvilli, and cellular protruberances.

The presence of microvilli has been noted in vertebrate preimplantation embryos (Flechon *et al.*, 1976, p. 249; Calarco, 1975, p. 312) as well as in invertebrate blastoderm embryos (Turner and Mahowald, 1976, p. 99). However,

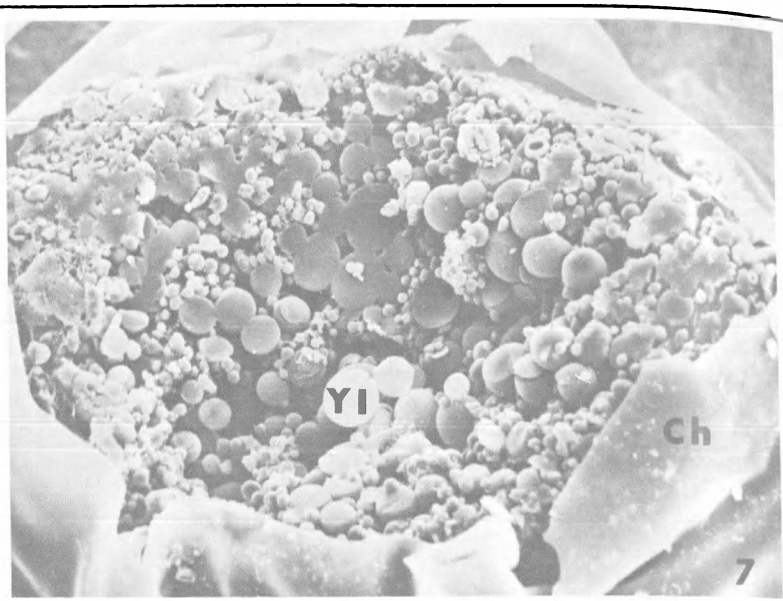

Figure 7. A room temperature fracturd milkweed bug embryo showing the chorion (Ch) and the yolk-filled interior (YI). Note the spherical nature of the yolk granules. (Heptane/glutaraldehyde fix) X 230.

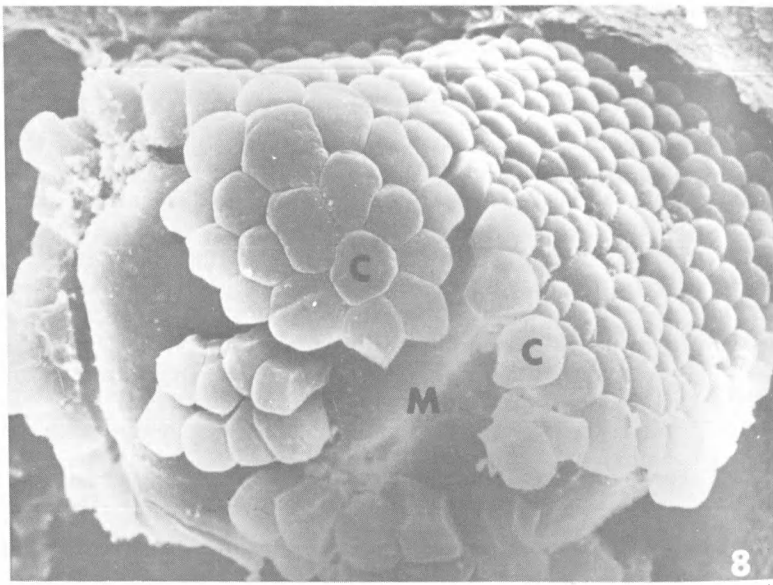

Figure 8. A pink bollworm blastoderm embryo showing a well developed cell layer in which individual cuboidal cells (C) are clearly visible. Note the membrane (M) between the cell layer and the yolk interior. (Heptane/glutaraldehyde fix) X 440.

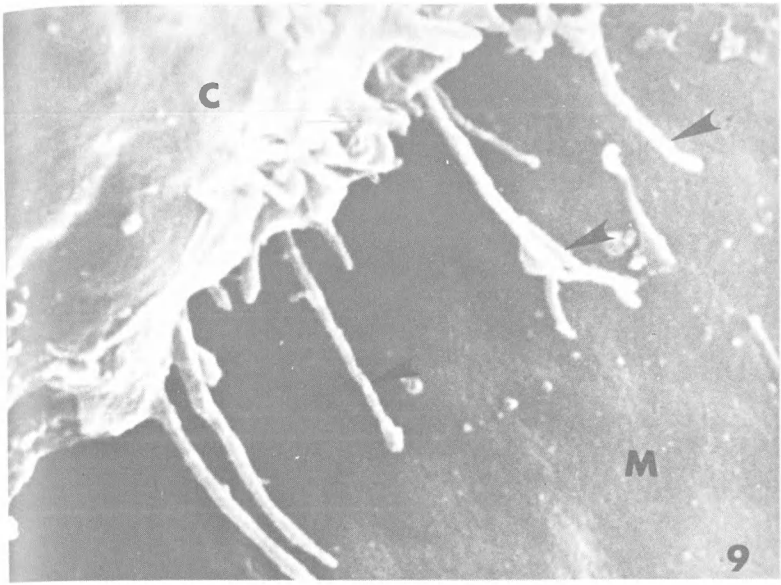

Figure 9. High magnification of Figure 8 showing microvilli (arrows) that connect the cells (C) to the membrane covering the yolk (M). (Heptane/glutaraldehyde fix) X 11,400.

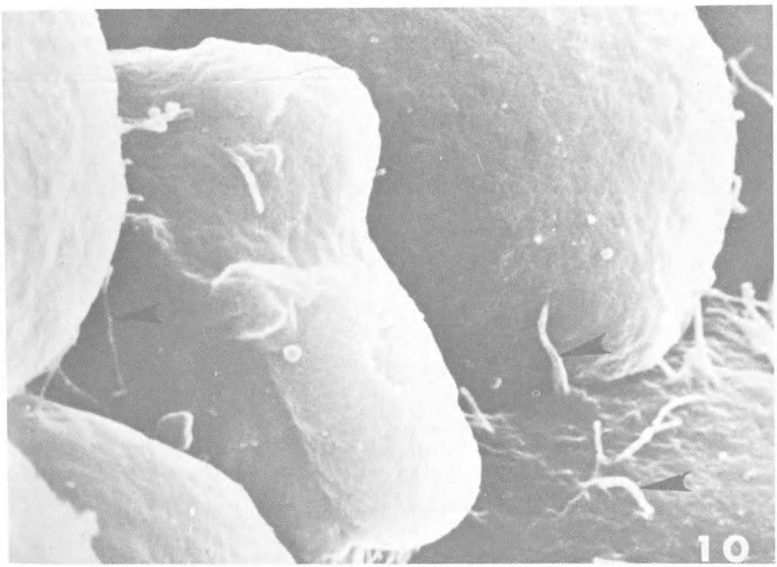

Figure 10. High magnification of cells in Figure 8 showing microvilli (arrows) that connect the cells to each other and to the vitelline membrane. Note the fairly smooth, unwrinkled surface of the cells. (Heptane/glutaraldehyde fix) X 6,300.

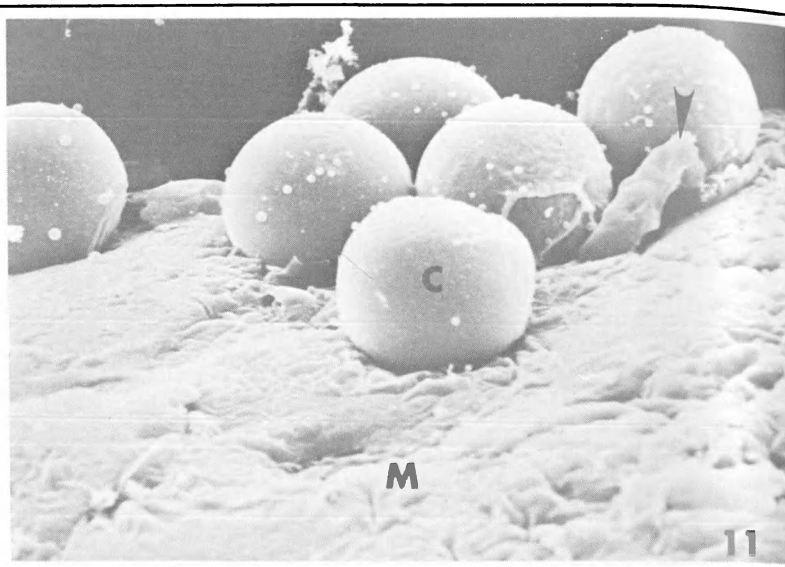

Figure 11. Spherical blastoderm cells (C) of the milkweed bug showing a slightly earlier stage of blastoderm development than is shown in Figure 8. Note slightly rumpled membrane (M) separating the yolk area from the cells and the crumpled cell membrane (arrows) from a ruptured cell. (Heptane/glutaraldehyde fix) X 2,000.

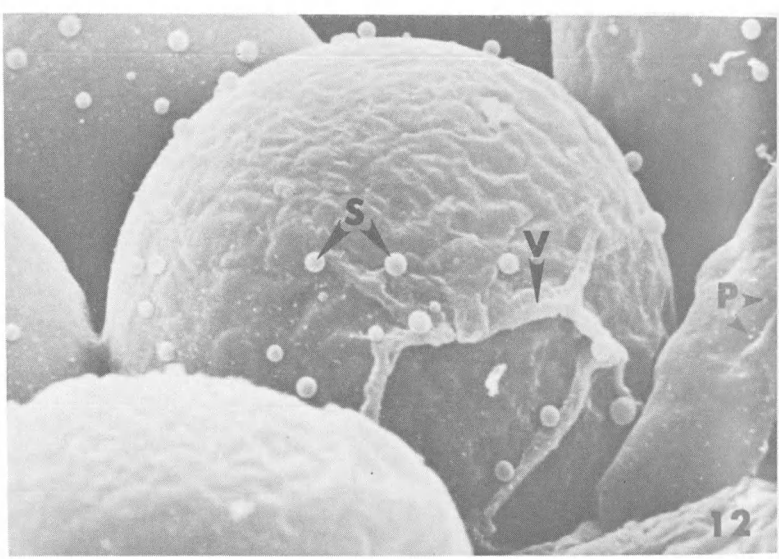

Figure 12. High magnification of cells seen in Figure 11 showing the wrinkled cell surface containing numerous protruberances (P) and the venous structure (V) that appears to connect the cells to each other. Note the small spherical bodies (S) that may be mitochondria. (Heptane/glutaraldehyde fix) X 6,000.

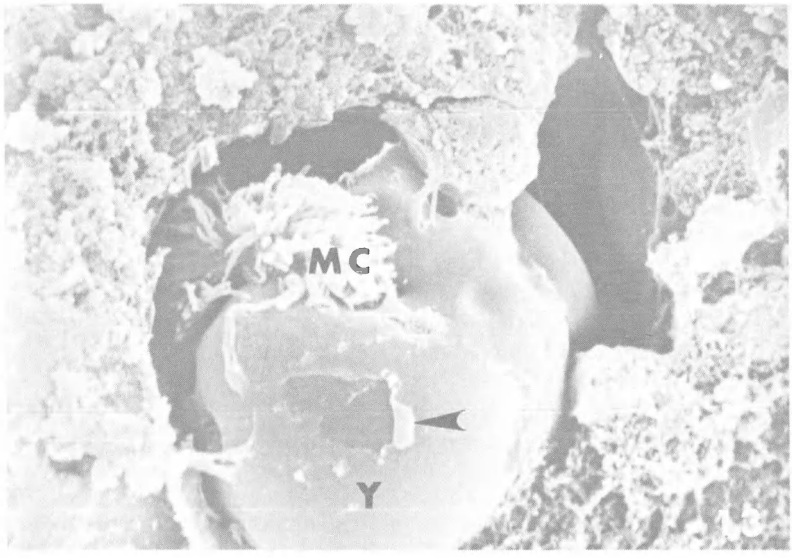

Figure 13. A fracture showing a yolk granule (Y) that is covered with a membrane (arrow). Note the membranous "cap" (MC) that sits atop the yolk granule. (Heptane/glutaraldehyde fix) X 6,400.

the number, size, and shape of these microvilli appeared to vary from species to species. For example, the *Drosophila* embryos studied by Turner and Mahowald (1976, p. 99) showed numerous microvilli on the cell surface. It was not noted whether these projections were also present between individual cells or between the cell-yolk area interface.

From the data it appeared both the yolk granules and cells of the milkweed bug, pink bollworm, and *Drosophila* were similar in size. This was interesting, since the blastoderm embryos of these insects vary considerably in size (Counce and Waddington, 1972, pp. 100, 167).

The preliminary steps taken in this study showed that the techniques used did not produce the type of fracture required for studying chromosome-membrane associations. However, several features of blastoderm embryos that could not be made readily available by either light microscopy or TEM were observed by using SEM, for example, the three-dimensional views of the whole embryo with its many varied, interrelating parts. The visualization afforded by the SEM of early embryogenesis by using the techniques of this study would be adequate for future work on surface interactions of ooplasmic organelles.

ACKNOWLEDGMENTS

Thanks are extended to Thomas Freeman, North Dakota State University,

for taking the SEM pictures and to George Gassner, Metabolism and Radiation Research Laboratory, for advice and support. Supported in part by U.S. Energy Research and Development Administration Contract P7603214.

LITERATURE CITED

Berg, G. J., 1976. RNA synthesis and blastoderm ultrastructure in the pink bollworm embryo. Publ. Ph.D. Dissertation, North Dakota State University, Fargo, N. Dak.

Counce, S. J., and C. H. Waddington (eds.), 1972. *Developmental Systems*, Vol. I. Academic Press, London-New York.

Calarco, P. G., 1975. Cleavage (mouse). *In: Scanning Electron Microscopic Atlas of Mammalian Reproduction*. pp. 306-317. Hafez, E. S. E. (ed.), Springer-Verlag, New York.

Flechon, J. E., S. Bergstrom, S. Jaszczak, and E. S. E. Hafez, 1975. Techniques for critical point drying of gametes and embryos. Scan. Elect. Microsc. (I): 325-332.

Flechon, J. E., M. Panigel, D. C. Kraemer, S. S. Kalter, and E. S. E. Hafez, 1976. Surface ultrastructure of preimplantation baboon embryos. Anat. Embryol., 149: 289-295.

Gassner, G., and S. G. Sears, 1976. Preblastoderm nuclear division in the embryo of the large milkweed bug, *Oncopeltus fasciatus* (Dallas). Differentiation 7: 39-51.

Humphreys, W. J., B. O. Spurlock, and J. S. Johnson, 1975. Transmission electron microscopy of tissue prepared for scanning electron microscopy by ethanol-cryofracture. Stain Technol. 50: 119-125.

Limbourg, B., and M. Zalokar, 1973. Permeabilization of *Drosophila* eggs. Develop. Biol. 35: 382-387.

Turner, R., and A. P. Mahowald, 1976. Scanning electron microscopy of *Drosophila* embryogenesis. 1. The structure of the egg envelopes and the formation of the cellular blastoderm. Develop. Biol. 50: 95-108.

BLOOD ALCOHOL CONCENTRATIONS IN DRIVERS APPREHENDED FOR DRIVING WHILE UNDER THE INFLUENCE OF INTOXICATING LIQUOR IN NORTH DAKOTA, 1972-1976

N. G. S. Rao and *Alphonse Poklis*
Office of the State Toxicologist
State University Station
Fargo, North Dakota 58102

ABSTRACT

The distribution of blood alcohol concentrations (BAC) from drivers apprehended in North Dakota during the past five years for the violation of "Driving While Under the Influence of Intoxicating Liquor" is presented. BAC's were determined by gas chromatographic analysis of blood samples and by analysis of alveolar air samples by the "Breathalyzer®". From 1972 through 1976, 21,090 blood alcohol determinations were concluded in North Dakota. The statutory restriction for operating a motor vehicle in North Dakota is a BAC of 0.10% or greater. The average BAC of the apprehended drivers was substantially higher than the legal limit, being 0.18% for breath test and 0.22% for blood test. Fewer than one per cent of the samples analyzed had a BAC below 0.05%, while more than thirty-five percent were in excess of 0.20%.

INTRODUCTION

Ninety-five million Americans engage in social drinking and 9-10 million Americans are chronic alcoholics. Both social drinkers and alcoholics have adverse effects on society. Chief among these is the loss of life, limb and property due to the operation of a motor vehicle while under the influence of alcohol (ethanol, ethyl alcohol).

In 1959, the North Dakota legislature, to ensure the public safety, enacted chemical test and implied consent laws. The law states ". . . No person shall drive or be in actual physical control of any vehicle upon a highway in this state if he is under the influence of intoxicating liquor . . ." (NDCC-39-08-01, 1959). According to state law " 'Intoxicating liquor' shall mean and include any beverage containing alcohol . . ." (NDCC-39-01-01, 1959). The law further states, ". . . any person who operates a motor vehicle upon the public highways of this state will be deemed to have given consent—to chemical test, or tests, of his blood, breath, saliva or urine for the purpose of determining the alcohol content of his blood. . .", (NDCC-39-20-01, 1959). Numerous studies (American Medical Association, 1968), have established the relationship between the concentration of alcohol in a person's blood and his physiological status, Table 1. Using such

TABLE 1. States of Alcohol Intoxication[A]

BLOOD ALCOHOL CONCENTRATION Per Cent (wt./vol.)	STATE OF ALCOHOLIC INFLUENCE	CLINICAL SIGNS/SYMPTOMS
0.01 - 0.05	Sobriety	No apparent influence Behavior nearly normal by ordinary observations Slight changes detectable by special tests
0.03 - 0.12	Euphoria	Mild euphoria, sociability, talkativeness Increased self-confidence; decreased inhibitions Dimunition of attention, judgment and control
0.09 - 0.251	Excitement	Emotional instability; decreased inhibitions Loss of critical judgment Decreased sensitory response; increased reaction time
0.18 - 0.30	Confusion	Disorientation, mental confusion Decreased pain sense Impaired balance; muscular incoordination; stggering gait, slurred speech
0.27 - 0.40	Stupor	Apathy Marked muscular incoordination; inability to stand or walk Vomiting; sleep or stupor
0.35 - 0.50	Coma	Coma; depressed or abolished reflexes Embarrassment of circulation and respiration Possible death
0.45 +	Death	Death from respiratory paralysis

[A]Prepared by Kurt M. Dubowski, Ph.D., FAIC, Director, Department of Clinical Chemistry and Toxicology, University of Oklahoma, School of Medicine, Oklahoma City, Oklahoma.

studies as a basis, the law states that a person having a blood alcohol concentration (BAC) of less than 0.05% (w/v) is presumed not to be under the influence of intoxicating liquor. A person having a BAC of more than 0.05% and less than 0.10% could be intoxicated, but the BAC value shall not be given as prima facie evidence of intoxication. A person having a BAC of 0.10%, or greater, shall be presumed to be under the influence of intoxicating liquor, (ND-CC-39-20-07, 1959). To obtain a BAC of 0.10%, a 150 lb man would have to drink approximately five to seven ounces of 80 proof whiskey.

The type of specimen collected for analysis is determined by the arresting officer. Almost all specimens analyzed in North Dakota are either blood or breath. Blood samples from apprehended drivers are drawn at local hospitals or clinics and then submitted to the Office of the State Toxicologist for analysis. Breath samples are analyzed at various law enforcement centers throughout the state by "chemical test operators" who are trained and certified by the State Toxicologist. A commercially available instrument, the Breathalyzer® (Smith & Wesson Electronics, Springfield, Mass.), is used to determine the BAC by the analysis of breath.

This communication presents the blood alcohol concentrations of persons charged in North Dakota with driving while under the influence of intoxicating liquor (DWI) over the five-year period of 1972 to 1976.

MATERIALS AND METHODS

Analysis of Blood Samples: The blood alcohol concentrations were determined by gas chromatography. The procedure for each sample involved the analysis of the blood sample, a distilled water blank and a standard solution of 0.150% (w/v) ethanol. Two 1.0-ml of aliquots of the sample were diluted with 3.0 ml of an internal standard of 0.120% (w/v) *n*-propanol in distilled water. The blank and standard solution were diluted in the same manner. Three 1-μl injections of the prepared solutions were chromatographed on a Hewlett-Packard Model 5711 a gas chromatograph containing a 1/8" id x 6' stainless steel column filled with 50-80 mesh Porapak Q and equipped with a flae ionization detector. The temperatures of the column, injection port and detector were 180°C, 250°C and 250°C, respectively. The flow rates of the air, hydrogen and nitrogen gas were set at 220, 40 and 30 ml/min., respectively. The concentration of the alcohol was determined by comparing peak height ratios of ethanol to that of *n*-propanol. A response factor of the standard was calculated as the ratio of the ethanol to *n*-propanol peak heights divided by the concentration of the ethanol. The response factor was linear throughout the range of 0.01 to 0.70% (w/v) ethanol.

Analysis of Breath Samples: Analysis of breath alcohol in order to determine the BAC depends upon the fundamental principles that the distribution of alcohol between circulating pulmonary blood and alveolar air occurs by simple diffusion and, like that of other volatile substances, obeys Henry's Law. Henry's Law states "The mass of a gas dissolved by a given volume of solvent, at constant temperature, is proportional to the pressure of gas with which it is equilibrium." This

means the concentration of alcohol in alveolar air at body temperature is directly proportional to the concentration of alcohol in pulmonary blood. The mean value of the Ostwald partition ratio of the BAC to the alveolar air concentration at the average temperature of exhaled air, 34°C, is 2,100 to 1.

Breath analysis in North Dakota is performed on the Breathalyzer®. The instrument in the "Take" position traps a known volume of the gaseous sample submitted for analysis. In the "Analyze" position the trapped gas passes through a 3-ml solution of 0.025% potassium dichromate and 0.025% silver nitrate in 50% sulfuric acid. The oxidation of alcohol by the reagent causes a color change in the solution. The resulting color change is photometrically determined and the BAC is read directly from the instrument. The approved procedure includes in sequence, the testing of, a room air sample, the subject's breath and a vapor of a standard solution which simulates an equivalent of 0.11% BAC. A complete analysis requires approximately 20 min.

RESULTS AND DISCUSSION

The number of blood and breath tests conducted on drivers in North Dakota charged for "driving while under the influence of intoxicating liquor" (DWI), for each year from 1972 to 1976, are presented in Table 2. A total of 21,090 cases occurred over the five-year period of the study. Approximately 75% of the tests performed each year were on breath samples. A slight increase in the number of blood analyses occurred in a six-month period from late 1974 to early 1975, due to rulings of the North Dakota Supreme Court in State *vs* Ghylin (1974), State *vs* Fuchs (1974) and State *vs* Salhus (1974). Breath analysis is generally preferred by law enforcement officials, as the results are readily available and the procedure precludes problems of sample handling, preservation and transportation.

The distribution of the blood alcohol concentrations (BAC) in blood and breath tests for each of the years from 1972 to 1976 are presented in Table 3 and 4, respectively. More than 92% of the blood tests and 94% of the breath tests gave a BAC in excess of the 0.10% presumptive level for DWI. Approximately 58% of the blood tests gave a BAC in excess of 0.20%. The largest group in the

TABLE 2. Blood and breath tests conducted for violation of driving while under the influence of intoxicating liquor (DWI)

Type of Test	Year				
	1972	1973	1974	1975	1976
Breath Tests	2336	2637	3262	3136	4096
Blood Tests	732	796	1219	1611	1265
Total	3068	3433	4481	4747	5361

TABLE 3. Distribution of the blood alcohol concentration (BAC) in blood tests

BAC Range	Number of DWI[A] Cases				
Per cent (wt./vol.)	1972	1973	1974	1975	1976
0.00 - 0.04	30	31	48	67	50
0.05 - 0.09	22	33	68	61	64
0.10 - 0.14	80	82	122	205	149
0.15 - 0.19	158	159	256	387	316
0.20 - 0.24	216	256	352	431	355
0.25 - 0.29	142	147	225	288	208
0.30 - 0.34	64	61	102	125	87
0.35 - 0.39	19	23	31	32	25
0.40 +	1	4	25	15	11
Blood Tests	732	796	1219	1611	1265

[A]DWI, Driving While Under The Influence of Intoxicating Liquor.

TABLE 4. Distribution of the blood alcohol concentration (BAC) in breath tests

BAC Range	Number of DWI[A] Cases				
Per cent (wt./vol.)	1972	1973	1974	1975	1976
0.00 - 0.04	27	24	39	33	63
0.05 - 0.09	116	116	181	146	185
0.10 - 0.14	489	550	745	769	973
0.15 - 0.19	833	911	1125	1127	1437
0.20 - 0.24	619	721	811	721	1027
0.25 - 0.29	196	231	297	246	317
0.30 - 0.34	50	67	56	64	77
0.35 - 0.39	3	13	6	7	15
0.40 +	3	4	2	3	2
Total Breath Tests	2336	2637	3262	3116	4096

[A]DWI, Driving While Under The Influence of Intoxicating Liquor.

blood tests, 29% were in the BAC range of 0.20-0.24%. Persons with a BAC in this range may exhibit muscular incoordination, mental confusion and disorientation. They are undoubtedly a hazzard operating a motor vehicle. The largest group in the breath test, 35% were in the BAC range of 0.15-0.19%. While 10% of the blood tests gave a BAC of 0.30% or greater, only 2.4% of the breath test gave BAC's in this range. This is due to several factors; the Breathalyzer procedure gives a result approximately 10% lower than the actual BAC, and breath samples are difficult to collect from persons who are periodically vomiting or losing consciousness. The latter are common symptoms of alcoholic intoxication at BAC's above 0.30%.

Eight per cent of the blood tests and 6% of the breath tests gave a BAC of less than 0.10%. Many of the drivers charged with DWI at these lower BAC's were under the influence of drugs, alone or in a combination with alcohol. Finkle et al. (1968) surveyed 3,409 DWI cases in Santa Clara County, California, and found 21% of the drivers had taken other drugs.

Carlson et al. (1971) in a road-side survey, found that 4% of all automobile drivers have a BAC in excess of 0.10%. However, Beitel et al. (1975) have estimated the probability of arrest for DWI at a BAC of 0.10% is only 1 in 200. Borkenstein et al. (1969) have established that the relative probability of causing an accident increases to seven times that of non-drinking drivers at a BAC of 0.10%. The probability increases to twenty-five times at a BAC of 0.15%. In the North Dakota survey presented here, 55% of all DWI cases involved a BAC in excess of 0.15%.

Contrary to the popular complaint, persons apprehended for DWI have not inbibed only "a drink or two". The mean BAC of persons charged with DWI in this survey was 0.22%. A man weighing 150 lbs would have to consume a minimum of eight to nine drinks of 100 proof whiskey to obtain a BAC of 0.22%. Over the five years of this survey, there has been a 75% increase in number of DWI cases, but the distribution of the BAC in those arrested has remained constant. The increased efforts of law enforcement agencies to apprehend "drunk drivers" has not resulted in the harassment of the driving public. These efforts are a necessary attempt to make the highways of North Dakota a safe place to drive.

ACKNOWLEDGMENT

This work was funded by the National Highway Traffic Safety Administration through the Traffic Safety Programs Division of the North Dakota Highway Department.

The authors wish to thank the members of the State Toxicology Laboratory who have been active participants in the Alcohol and Highway Safety Program; Wallace Kunerth, Kathleen Lee, Margaret Pearson, David Shelton and John Warner.

LITERATURE CITED

American Medical Association, ed. 1968. Alcohol and the Impaired Driver. American Medical Association, Chicago. 35-39 pp.

Beitel, G. A., C. S. Michael and W. D. Glauz. 1975. Probability of arrest while driving under the influence of alcohol. J. Stud. Alcohol 36:109-116.

Borkenstein, R. F., R. F. Crowther, R. P. Shumate, W. B. Ziel and R. Zylman. 1969. The Role of the Drinking Driver in Traffic Accidents, 4th ed. Indiana University. 141-170 pp.

Carlson, W. L., M. M. Chapman, C. D. Clark, L. D. Filkins and A. C. Wolfe. 1971. Washentaw County BAC Roadside Survey. University of Michigan. 16-24 pp.

Finkle, B. S., A. A. Biasotti, M. Crim and L. W. Bradford. 1968. The occurrence of some drugs and toxic agents encountered in drinking driver investigations. J. Forensic Sci. 13:236-245.

State *v* Fuchs. 1974. 219 N.W. 2d 842. North Dakota.

State *v* Ghylin. 1974. 222 N.W. 2d 864. North Dakota.

State *v* Salhus. 1974. 220 N.W. 2d 852. North Dakota.

PLASMALEMMAL MICROAPPENDAGES: FINE STRUCTURAL ALTERATIONS IN RESPONSE TO CYTOCHALASIN B AND BCG

David J. Friedenbach, Randall E. Merchant and Paul A. Stagno
Department of Anatomy
University of North Dakota, Grand Forks, North Dakota 58202

ABSTRACT

Surface contours of mesodermal cells of early chick embryos and leukocytes of canine leptomeningeal sheaths were examined by scanning and transmission electron micrscopy. Normally, these cells possess plasmalemmal microappendages (microvilli, blebs, and ruffles) in variable degrees. Microvilli are cell surface extensions of variable lengths and uniform diameter (0.1 μm). In contrast, blebs display bulbous configurations of inconsistent diameter and size. Ridge-like ruffles are primarily found near the cell margins. When endodermal cells are exposed to variations in extracellular pH or cytochalasin B, the appearance and distribution of the microappendages are altered. Similar results are obtained when subarachnoid leukocytes are challenged by the foreign protein, bacillus Calmette Guerin (BCG). Microappendages thus appear to reflect changes within the extracellular environment and degrees of leukocyte activation in response to antigen.

INTRODUCTION

Lewis and Gey (1923) were the first to describe elaborate folding of the plasmalemma. They termed these folds ruffles. Ruffles are most commonly observed on cells active in phagocytosis and locomotion. They are often referred to as pseudopodia or lamellipodia because of their appearance at the leading edge of moving cells (Abercrombie, *et al.*, 1970). Ruffles are one of the three major forms of cell surface extensions and along with microvilli and blebs are collectively termed microappendages.

Microvilli and blebs are often difficult to observe by common light microscopic techniques because of their small size. However, with the use of good phase optics, Gey (1954) was able to demonstrate surface extensions beautifully. He refers to them as "microfibrils" on both normal and cancer cells. Previous to this work, Costero and Pomerat (1951) also observed bleb formation and retraction on cultured nerve cells. They called this phenomena zeiosis. Gey (1954) notes the tendency of microvilli to grow in a crystalline fashion from the cell surface, then stiffen and either pivot about their point of attachment or deliquesce into the surface. This process is relatively rapid and it demonstrates the dynamic nature of these structures.

The development of the scanning electron microscope (by McMullan, 1953 and further improved by Oatley, 1966) opened a new dimension of cell surface study. The scanning electron microscope (SEM) has the capability to produce a three dimensional effect because of its great depth of field and high resolution. It has both low and high power capabilities (20X - 100,000X). Use of the SEM has greatly enhanced the study of microappendages.

Microvilli.—Microvilli are accepted to be small surface extensions of about 0.1 μm diameter and can be of variable lengths. Microvilli are well known on various absorptive surfaces such as the small intestine and proximal convoluted tubules of the nephron. Although less commonly associated with other areas, they are often present in surprising numbers on free surfaces.

Microspikes (Taylor's terminology for microvilli) according to Taylor (1966) possess as internal structures, small microtubules (150 Å diameter) aligned parallel to the longitudinal axis of the microvilli. This discovery has not been confirmed. However, other laboratories (Follett and Goldman, 1970; Taylor, 1966) have noted that microvilli contain axial bundles of 40-60 Å filaments.

Blebs—Blebs are bulbous extensions of the cell surface. They are of variable sizes and are most commonly observed on cells during the G_1 period of the cell cycle (Porter, *et al.*, 1973). Their shape is spherical when viewed from above and their attachment site has a smaller diameter. There seems to be no special arrangement of blebs over the surface, except that they are perhaps more numerous over the nuclear area.

Internally, blebs are relatively free of "major" cell organelles. However, transmission electron microscopy on human epithelial cells demonstrates numerous polyribosomes (Price, 1967). Similar findings have resulted from studies of CHO cells by Porter, *et al.* (1973).

Ruffles—Ruffles are recognized as broad folds at the cell surface. They are commonly observed originating at the leading edge of advancing cells (Abercrombie et al., 1970; Ingram, 1969). Although ruffles are often seen at leading edges, they are usually absent at edges in confluence with other cells. Vertically, ruffles may project 6-8 μm. Along the cell margin they often extend 8-10 μm.

Transmission electron microscopy of these structures reveals relatively little about their internal structure. They contain no identifiable organelles; however, a few small vesicles are often seen at their base. Abercrombie *et al.* (1971) report what they term "granular" and "vague filaments" in the ground substance of the ruffles.

Although microappendages are similar in the respect that they all arise from the cell surface as extensions of the plasmalemma, there are no common internal structures which can be found. In addition, it should be noted that although they are described separately in terms of their external morphology, they cannot be catagorized definitively.

Pleomorphicity has been compounded by one structure arising from an other (i.e. microvilli from a ruffle). Commonly microvilli terminate in a bleb-like structure.

Microappendages, to some extent, have been observed on almost every free cell surface which has been examined by electron microscopy. They are rapidly becoming recognized as important structures related to vital cell functions, locomotion, phagocytosis, diffusion, active transport, receptor sites of agglutinins and many others. Since there are differences in microappendages on transformed cells, especially neoplastic cells, their normal pattern needs to be established. Furthermore, the responses of microappendages to physiologic conditions and

stresses are very important. With the establishment of a normal pattern of development and response, similar structures on abnormal cells can be more fully understood.

Chick embryos offer the advantage of possessing a histologically organized cell layer; the endoderm which composes the ventral surface. Endodermal cells express pleomorphism of surface microappendages typical of rapidly growing areas (Harri and Low, 1974). Microappendages are concentrated at, and outline, cell margins where cells are in contact.

Environmental factors appear to be important in regulating cell function. The pH of most vertebrate cells is held constant at pH 7.2 ± 0.1. Proper growth and development of cells require that pH be closely regulated (Ceccarini and Eagle, 1971).

Cytochalasin B (CB) possesses unusual cytoactive properties first described by Carter (1967). Cytochalasins are a group of mold metabolites to which a multitude of cellular responses have been attributed. Among those are: inhibition of cell movements (membrane ruffling), multinucleation (inhibition of cytokinesis), nuclear extrusion and disruption of the cytoskeleton (microfilaments, Wessells, *et al.*, 1971). Another cell type readily accessible to the study of microappendages is found in the central nervous sytem. The brain and spinal cord of vertebrates are covered by three distinct connective tissue layers, collectively termed the meninges. Two of these layers, the arachnoid mater and pia mater, are often referred to together as the leptomeninges. An interval between the leptomeningeal sheaths, the subarachnoid space, is occupied by a fine trabecular network of arachnoid tissue, blood vessels, nerve rootlets and cerebrospinal fluid.

Many investigations of the subarachnoid space have demonstrated free cells resting on the leptomeningeal linings of normal animals (Pease and Schultz, 1958; Shabo and Maxwell, 1968; Morse and Low, 1972a, b; Oehmichen and Gruninger, 1974). Generally these cells possess a highly vacuolated cytoplasm, an indented nucleus, some mitochondria, rough endoplasmic reticulum, lipid inclusions and free ribosomes (Morse and Low, 1972b; Malloy and Low, 1976). More recent studies utilizing SEM have made reference to the extreme pleomorphism of the subarachnoid free cell and its wealth of microappendages; microvilli, blebs and ruffles (Cloyd and Low, 1974; Malloy and Low, 1974, 1976; Allen and Low, 1975). Malloy and Low (1976) performed a coordinated SEM and TEM investigation of these cells and concluded that the leptomeningeal free cell possesses the morphological characteristics of a macrophage.

We recently reported an approximate ten-fold increase in the number of free cells adherent to the leptomeningeal sheaths twelve days after an intrathecal injection of bacillus Calmette-Guerin (BCG) (Merchant and Low, 1977b). Nearly eighty percent of these cells were macrophages, as indicated by low power TEM. The remainder of the population was composed of neutrophils and lymphoblasts (Merchant and Low, 1976). Each of these cell types of the leukocyte series displayed a characteristic topography and compliment of microappendages,

making identification possible solely from the evidence of SEM alone (Merchant and Low, 1977a). Moreover, it became apparent that under conditions of BCG challenge, macrophages frequently entered into close apposition with cells of a similar or different type. Adjacent cells often appeared to contact one another through their plasmalemmal extensions.

Therefore it is the aim of this communication to describe changes in microappendage distribution and morphology under several systems and several insults. The extracellular effect of pH and cytochalsin B will be examined on the ventral surface of the chick embryo. The effect of BCG on subarachnoid leukocytes will also be investigated. Special attention will be given to the possible functional significance of cell surface topography at the ultrastructural level.

MATERIALS AND METHODS

Preparation of chick embryos.—Fresh pullet eggs (White Leghorn variety) were incubated 24-48 hours (Hamilton, 1952). Blastoderms from eggs designated experimentals were removed by the paper ring method (Low, 1967) and immersed for five minutes in buffered chick ringers solution at a pH of either 6.0 or 9.4. Samples were fixed in isotonic Tyrode's fluid (249-254 mOsm) containing 0.8% glutaraldehyde for one to two hours and post-fixed in buffered 2% OsO_4 for 45 minutes. Samples were processed routinely for SEM and mounted for viewing with the ventral surface exposed.

Blastoderms were exposed to CB (10 or 40 μg/ml) by either immersion in buffered chick ringers solution; a dimethylsulfoxide (DMSO) solution; or by subblastodermic injection for 5-15 minutes. DMSO is utilized due to its high CB solubility. Fixation was carried out as previously described. Preparation for SEM and TEM was routine.

Controls for both groups were fixed either *in ovo* or by the paper ring immersion technique and subsequently prepared for electron microscopic (SEM and TEM) examination by standard methods.

Preparation of macrophages.—Macrophages were activated, then processed by a combination of techniques previously described in detail (Malloy and Low, 1976; Merchant and Low, 1977a, b). Dogs anesthetized intraperitoneally with sodium phenobarbital, were administered 4-9 million BCG microorganisms intrathecally. Subarachnoid space entrance was made into the cisterna magna with care being made not to substantially modify cerebral spinal fluid pressures. Following twelve days incubation, the dogs were reanesthetized and perfused through the left cardiac ventricle. Initial fixation was accomplished with a washout solution of cacodylate-buffered paraformaldehyde - glutaraldehyde mixture. Peripheral vasoconstriction was avoided by the addition of procaine hydrochloride (0.1%) to the washout solution (Forssman *et al.* 1967). Final fixation was continued with Karnovsky fixative (Karnovsky, 1965) adjusted to pH 7.4 at 560 mOsm. Representative leptomeningeal samples were removed (Cloyd and Low, 1974) following laminectomy. Samples were post-fixed for one hour in 2% OsO_4 and routinely prepared for SEM. Control dogs were carried through the same protocol, omitting BCG intrathecal administration.

Selected SEM specimens were embedded and sectioned for TEM.

Electron Microscopy.—Preparations for SEM were dehydrated through graded series of acetone, critical point dried utilizing carbon dioxide and coated with carbon and gold-palladium (60:40). Preparations for TEM were dehydrated through graded alcohols and embedded in Epon 812. Thin sections were obtained on the Porter-Blum MT-2 ultramicrotome. Selected sections were picked up on grids and double stained with uranyl acetate and lead citrate. Observations were made on a Cambridge Stereoscan S4 Scanning Electron Microscope or a Phillips 200 Transmission Electron Microscope.

RESULTS

Chick Embryo; Control.—Endodermal cells of the ventral surface have a characteristic surface morphology within the incubation times examined (24-48 hours). Figure 1 displays the normal surface contours found on the ventral surface of early chick embryos. Cells fixed *in ovo* are flat except for numerous bulges due to previous phagocytosis of yolk (Litke and Low, 1975). Cilia, usually centrally located, are found one per cell (fig. la). Microappendages (microvilli, blebs and ruffles) may arise anywhere on the free surface but tend to be concentrated near the cell borders (fig. la). Figure 1b demonstrates a typical transmission electron micrograph of the ventral surface. Endodermal cells possess a distinct basal lamina overlying the processes of mesodermal cells.

Dimethylsulfoxide controls differ from *in ovo* controls in distribution of microappendages. Endodermal cells are flat overall, and yolk bulges are less prominent (fig. lc). Cilia are still present. Small blebs, however, are more numerous. Figure 1c demonstrates a typical increase in large ruffled plasmalemmal extensions on the majority of cells.

Chick Embryo; Cytochalasin B.—Extracellular introduction of cytochalasin B elicits dynamic alterations in plasmalemmal morphology. Regardless of whether embryos were immersed or injected sub-blastodermally, similar results were obtained.

Figure 2 illustrates the rapid effects of CB on cell surface appearance of endodermal cells. Cells exposed to 10 μg/ml CB (5 or 15 minutes) reveal a surface heavily populated with microvilli, small blebs and ruffles (fig. 2a). Bulging cells, indistinct cell margins, and branching of microappendages are commonly observed. Isolated areas demonstrate a second major effect; that of cell dissociation (fig. 2b). Figure 2b displays cells separating from each other, rounding up and leaving filopodia (long attenuated cell processes) behind. Dissociated cells are devoid of microappendages except for the persistent cilium.

Figure 3 and 4 illustrate the effects of a high concentration of CB (40 μg/ml) at 5 minutes exposure. Large blebs (2-10 μm diameter) are the predominent surface feature of these cells (figs. 3a, 3b, 4a), although microvilli and small blebs (2μm) are still numerous. Figure 3b reveals microvilli and small blebs populating the surface of a large bleb. Arrangements of microappendages often take on this pleomorphic appearance. Correlated with TEM, large blebs reveal that they are devoid of cell organelles except for numerous membranous vesicles (fig. 3c).

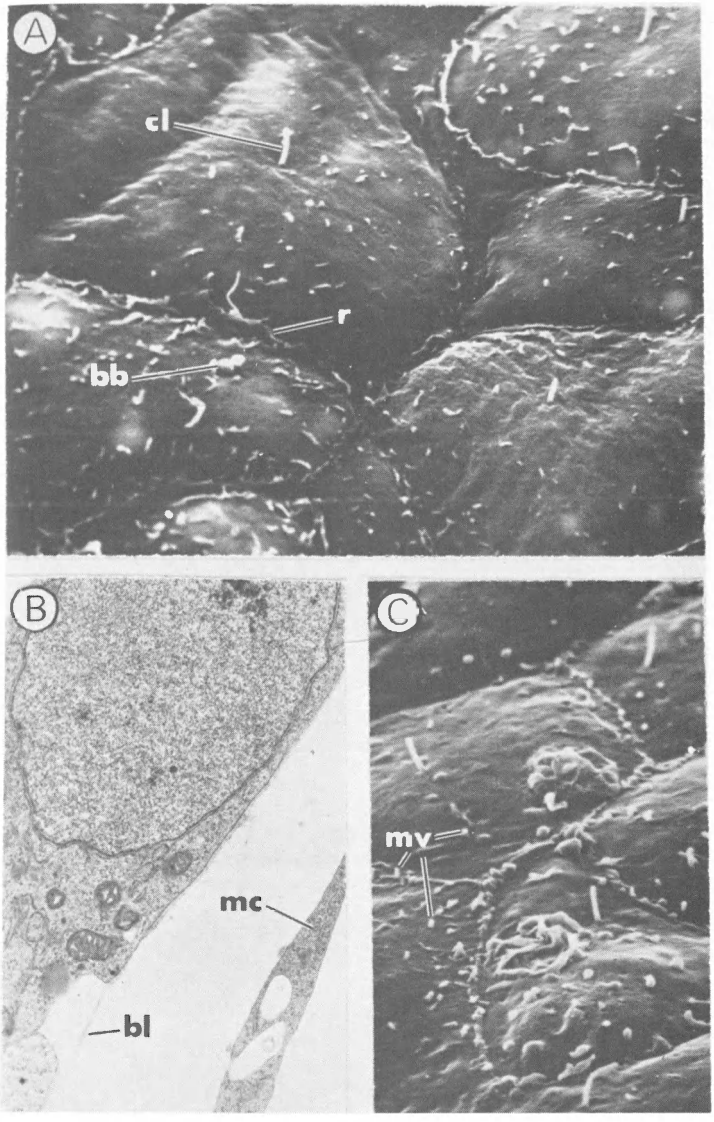

Figure 1. *Chick Embryo; Control.*—A—Central cilia (cl), ruffles (r), and blebs (bb) populate the surface of endodermal cells predominantly at cell margins. (X 3,000) B—Transmission electron microscopy reveals typical ventral surface structures. Basal lamina (bl) underlies endodermal cells with subjacent mesoblast cell (mc) processes. (X 13,000) C—Dimethylsulfoxide controls possess numerous microvilli (mv), blebs and large ruffled areas. (X 3,000)

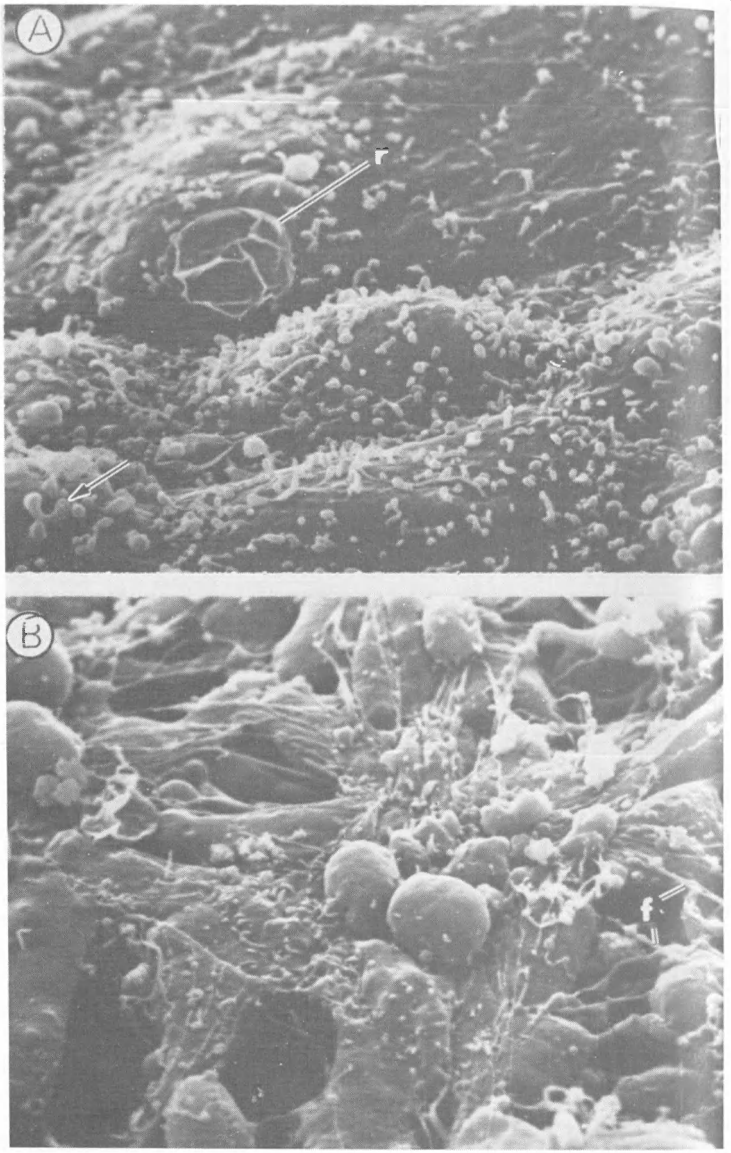

Figure 2. *Chick Embryo; Cytochalasin B (10μg/ml, 5 mins).*—A—Cell surfaces are heavily populated with microappendages often exhibiting branching (arrow) and large ruffled areas (r). Cell rounding is apparent with indistinct cell margins. (X 2,800) B—Cytochalasin B induces cell dissociation, associated with cell rounding and retraction of cell processes except for filopodia (f). (X 2,500)

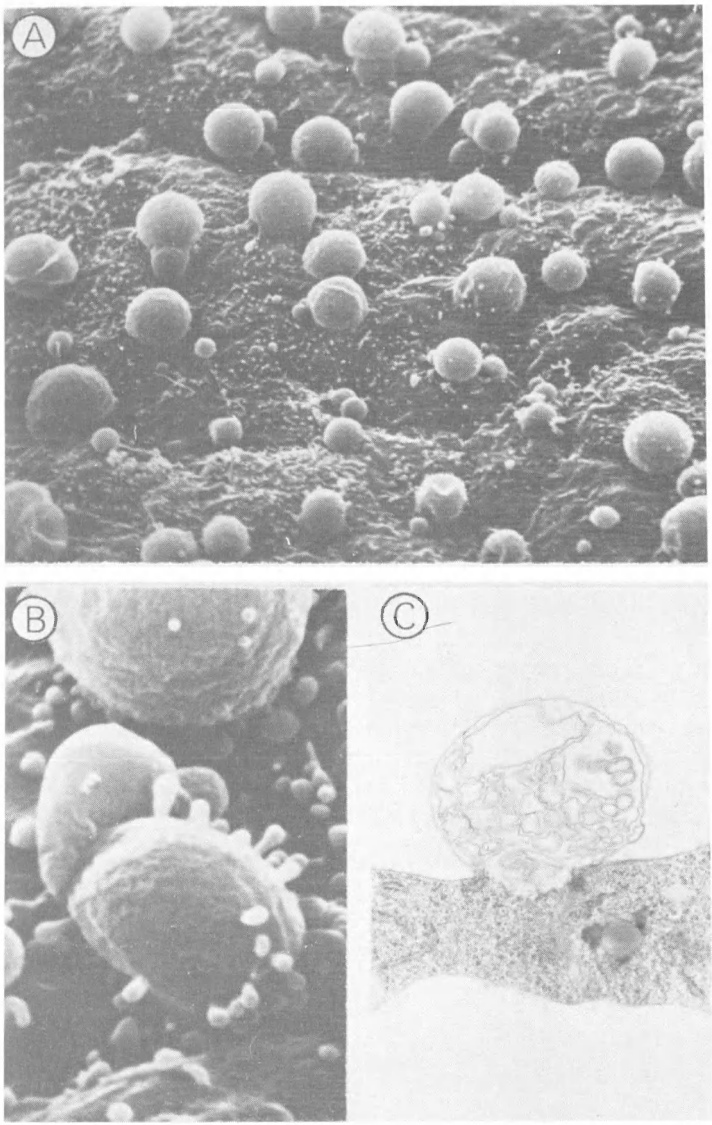

Figure 3. *Chick Embryo; Cytochalasin B (40μg/ml, 5 mins).*—A—Large blebs (2-10μm) are the predominant surface feature of these cells. Microappendages still cover the remaining cell surface. (X 1,500) B—Blebs often give rise to microvilli and smaller blebs (0.5μm) over there surface. (X 7,000). C—Transmission electron microscopy reveals that large blebs contain numerous membranous vesicles. (X 19,000)

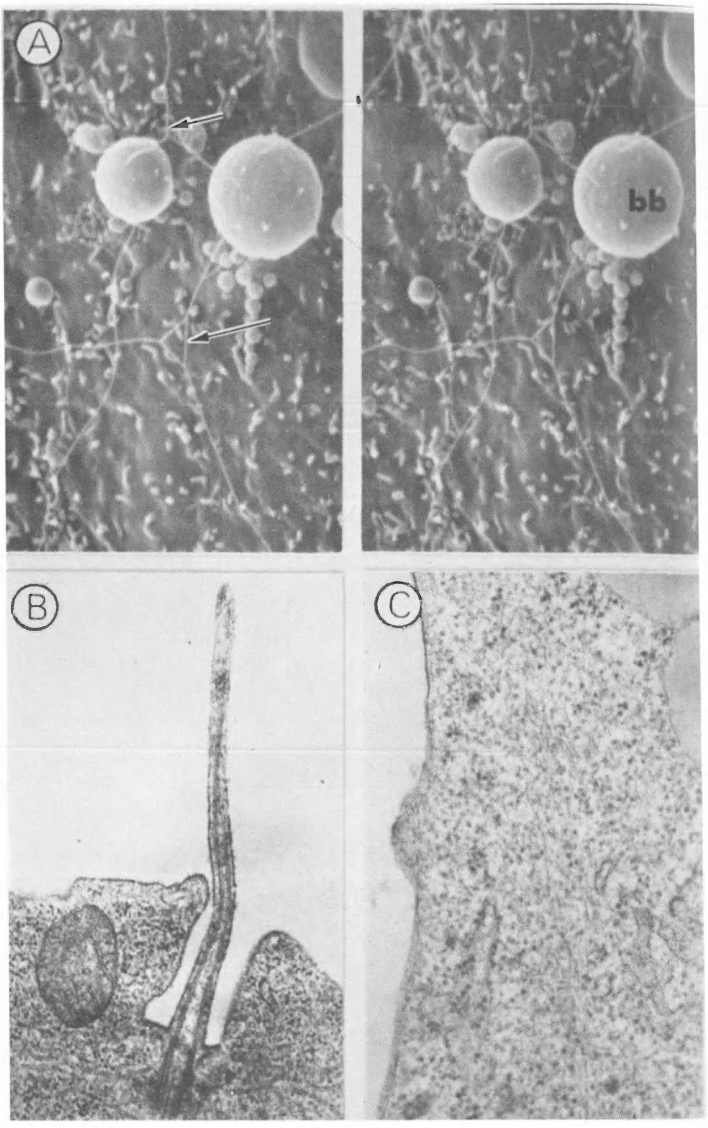

Figure 4. *Chick Embryo; Cytochalasin B (40μg/ml, 5 mins).*—A—Stereopairs demonstrate the true three dimensional relationships of some microappendages. Filamentous processes (arrows) are shown interconnecting blebs (bb) and microvilli. (X 5,000) B—Cilia retain internal morphology, often arising from the base of an invagination. (X 31,000) C—Microfilaments are seen traveling parallel to the cell surface in discrete bonds. (X 43,000)

Stereoscopy of microappendages displays their true three-dimensional relationship Figure 4a represents a stereopair of endodermal cells demonstrating long filamentous processes often interconnecting microappendages. Microvilli are easily distinguished from small blebs with this technique.

Transmission electron microscopy of endodermal cells reveals that cellular components are normal in distribution and morphology (figs. 4b, 4c). Figure 4b illustrates a typical cilia with its complement of microtubules and basal body. The plasmalemma at the base of a cilia is usually invaginated, giving the appearance of a pit in SEM (fig. 4a, upper right). Microfilaments are found in discrete bands near the cell surface, showing no disruptive affect due to exposure to CB (fig. 4c). Observations indicate that no cellular organoids appear to be associated with bleb formation, retention, or retraction.

Chick Embryo; pH alteration.—Alteration in the environmental pH results in changes in microappendage patterns. Figure 5 illustrates surface morphology as revealed by scanning electron microscopy.

Exposure of endoderm to alkaline pH results in an increase in number and length of microvilli (fig. 5a). Figure 5a also demonstrates that microvilli now possess bulbous terminations as well as greater length. The plasmalemma appears smooth in contrast to cells exposed to acid pH which present a somewhat pitted surface (fig. 5b). Figure 5b reveals that acidic pH (6.0) causes disappearance of microappendages except for cilia. Changes in pH do no elicit formation of large blebs.

Subarachnoid Leukocytes; Control.—Scanning and transmission electron microscopy of the leptomeningeal sheaths of normal animals reveal a randomly scattered population of macrophages with morphological characteristics consistent with those reported previously (Cloyd and Low, 1974; Allen and Low, 1975; Malloy and Low, 1976). These free cells are associated with all structures lining and traversing the subarachnoid space. Figure 6 dramatically illustrates the extreme pleomorphism exhibited by two members of this population. Their surfaces vary from smooth (fig. 6a) to highly ruffled and blebbed (fig. 6b). Macrophage microvilli display wide variations in length and often times contact adjacent cells or their underlying, leptomeningeal substrate (fig. 6a). Pial microvilli as well may touch a nearby free cell (fig. 6b).

Subarachnoid Leukocytes; BCG Challenged.—Animals injected with BCG are asymptomatic for adverse systemic reaction to the antigen. They appear instead to be outwardly healthy and indistinguishable from controls. Scanning and transmission electron microscopy demonstrate not only macrophages but also lymphoblasts and neutrophils on the leptomeningeal sheaths of infected animals.

Figure 7 illustrates the wide array of plasmalemmal contours displayed by BCG-challenged macrophages. Blebs, ruffles, and microvilli erupt from each cell's surface. Some processes appear to associate with similar structures of neighboring cells (fig. 7a,c). Although expressing the normal variety of microappendages, the macrophage's surface is dominated by blebs (fig. 7a,b). The majority of blebs are between 0.5 and 2.5 μm in diameter. Apical blebs can be

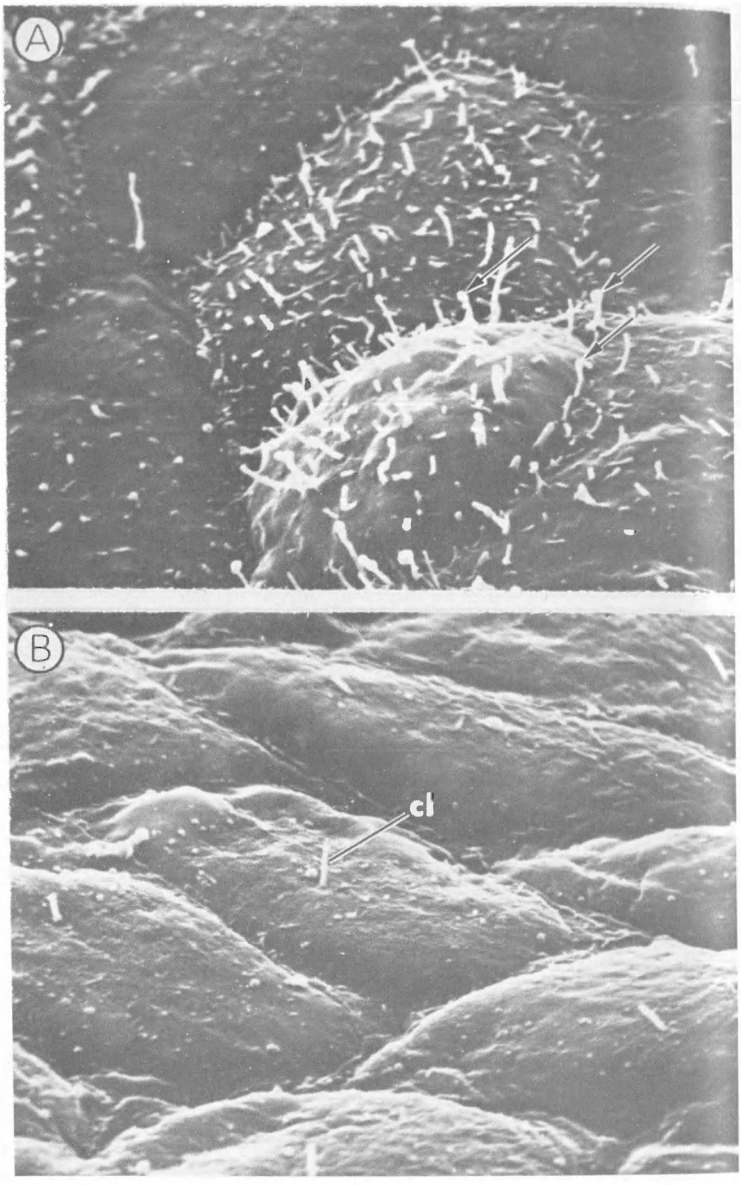

Figure 5. *Chick Embryo; pH Alteration.*—A—Alkaline pH (9.4) causes increase in length and number of microvilli which possess bulbous terminations (arrows): (X 3,000) B—Acid pH (6.0) induces loss of microappendage without cell swelling. Cilia (cl) persist throughout treatment. (X 3,000)

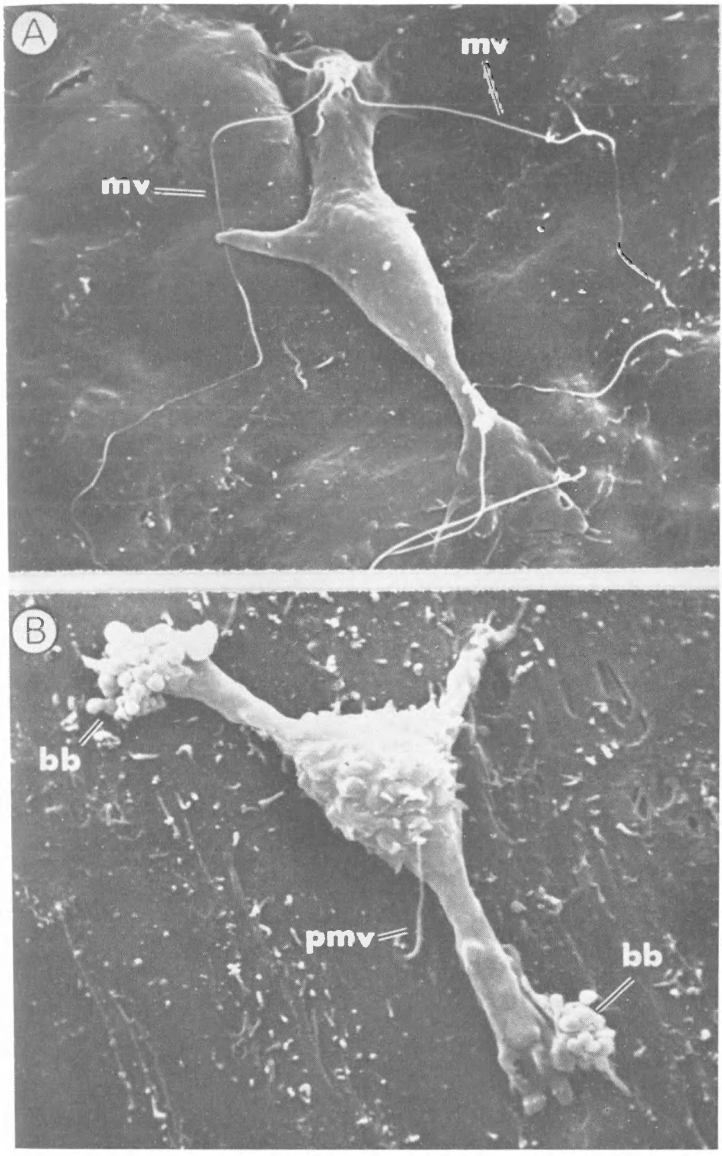

Figure 6. *Leptomeningeal Macrophages; Control.*—A—This smooth-surfaced macrophage possesses tenuous microvilli (mv). (X 4,000) B—This cell exhibits a highly ruffled central lobe with two pseudopod-like extensions. Blebs (bb) on the distal surfaces of the pseudopodia are frequently seen. A pial microvillus (pmv) contacts this cell. (X 2,900)

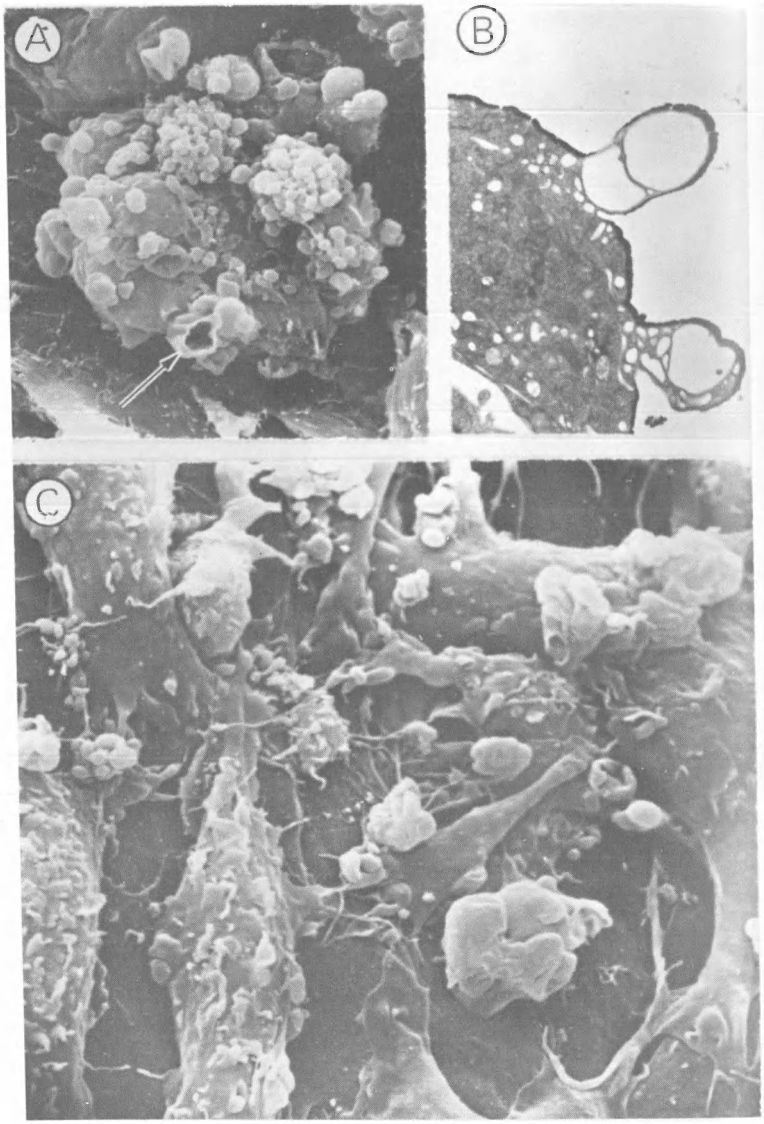

Figure 7. *Leptomeningeal Macrophages; BCG Challenged.*—A—Blebs dominate the surfaces of stimulated macrophages. One bleb appears to have burst (arrow) revealing a vacuolar interior. (X 1,500) B—Macrophage blebs are composed of large vacuoles surrounded by a highly attenuated portion of cytoplasm. (X 8,500) C—Macrophage microappendages contact adjacent free cells and the pial surface. (X 2,300)

identified by TEM of comparable cells (fig. 7b). These structures are composed of vacuoles surrounded by a highly attenuated cytoplasm. Scanning elctron microscopy of burst blebs reveals their vacuolar interior (fig. 7a).

Lymphoblasts from the same experimental model are presented in figures 8 and 9. These cells display a characteristic surface morphology; a smooth, rounded cell body with many basal microvilli projecting to the underlying pia (fig. 8a). Although certain microvilli appear by SEM to perforate the pial surface, TEM demonstrates that these processes do not perforate but, rather, indent the pial cell plasmalemma (fig. 8b). Frequently lymphoblasts exhibit blunt microvilli at the margins of lamellipodia (fig. 8c).

Two modes of macrophage-lymphoblast interaction are reported in figure 9. One consists of an intimate plasmalemmal association encompassing much of each cell's surface (fig. 9a), while the other involves the extended, basal microvillus of a lymphoblast contacting an adjacent macrophage (fig. 9b).

Neutrophils are demonstrated in figure 10. These cells are nearly spherical and have extremely irregular surfaces composed largely of thick, tapering microvilli (fig. 10a, b). Scanning and transmission electron microscopy suggest that neutrophils approach adjacent macrophages with their microvillar processes (fig. 10b) and that this might lead to more closely proximated plasmalemmal associations (fig. 10c, d). Transmission electron microscopy demonstrates a conspicuous morphological feature of the macrophage-neutrophil junction: indentations of each cell's plasma membrane by surface processes of the other (fig. 10d).

DISCUSSION

This contribution shows that cytochalasin B and change in extracellular pH cause alteration in microappendage prominence and morphology. Large blebs are the prominent morphological feature of endodermal cells of the chick embryo exposed to CB. Transmission electron microscopy correlates reveal that blebs contain membranous vesicles. The observed phenomena support the idea that initial effects are induced in the plasmalemma. In addition, plasmalemmal manifestations due to changes in pH have been demonstrated. This ramification has not previously been investigated.

Bleb formation following exposure to CB is reported frequently in the literature (Carter, 1972; Krishan, 1971; Bhisey and Freed, 1975; Mayhew and Maslow, 1974). Blebs usually contain ectoplasm and polyribosomes but otherwise are devoid of major organelles (Krishan, 1971; Bhisey and Freed, 1975). In contrast, the present study shows that large blebs contain only membranous vesicles. Blebs are free of cell structures which confer shape or rigidity upon them. Apparently either passive expansion or plasmalemmal ultrastructure is responsible for maintenance of these microappendages. Cytochalasin B elicits rapid (< 5 minutes) induction of microappendages without affecting internal cell structures.

Microfilaments, which are primarily contractile structures, are implicated by some investigators as the primary site of CB's action (Wessells, *et al.*, 1971; Axline and Reaven, 1974). Since these authors observe disruption of

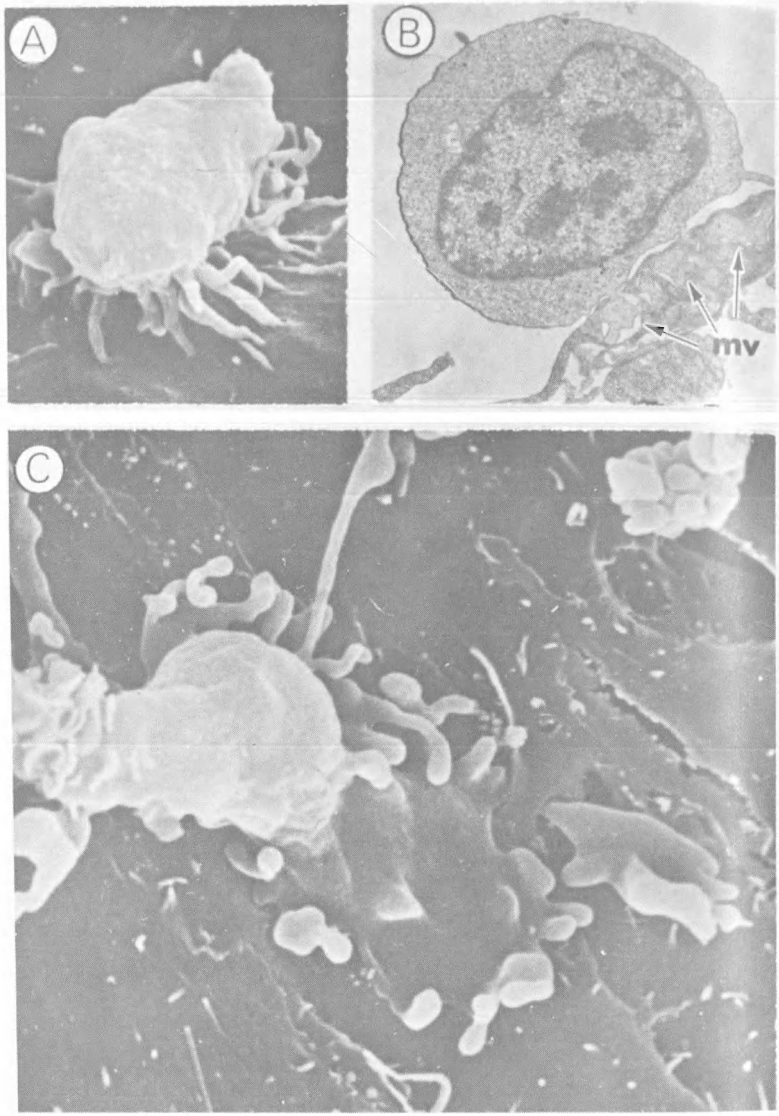

Figure 8. *Leptomeningeal Lymphoblasts; BCG Challenged.*—A—Smooth-surfaced lymphoblasts possess many basal microvilli extending to the pial substrate. Some microvilli appear to perforate the pial cell's plasmalemma. (X 5,000) B—The basal microvilli (arrows) do not perforate a pial cell's plasmalemma but rather indent its membranes. (X 9,800) C—Lymphoblasts often exhibit lamellapodia with blunt microvilli at the margin. (X 3,600)

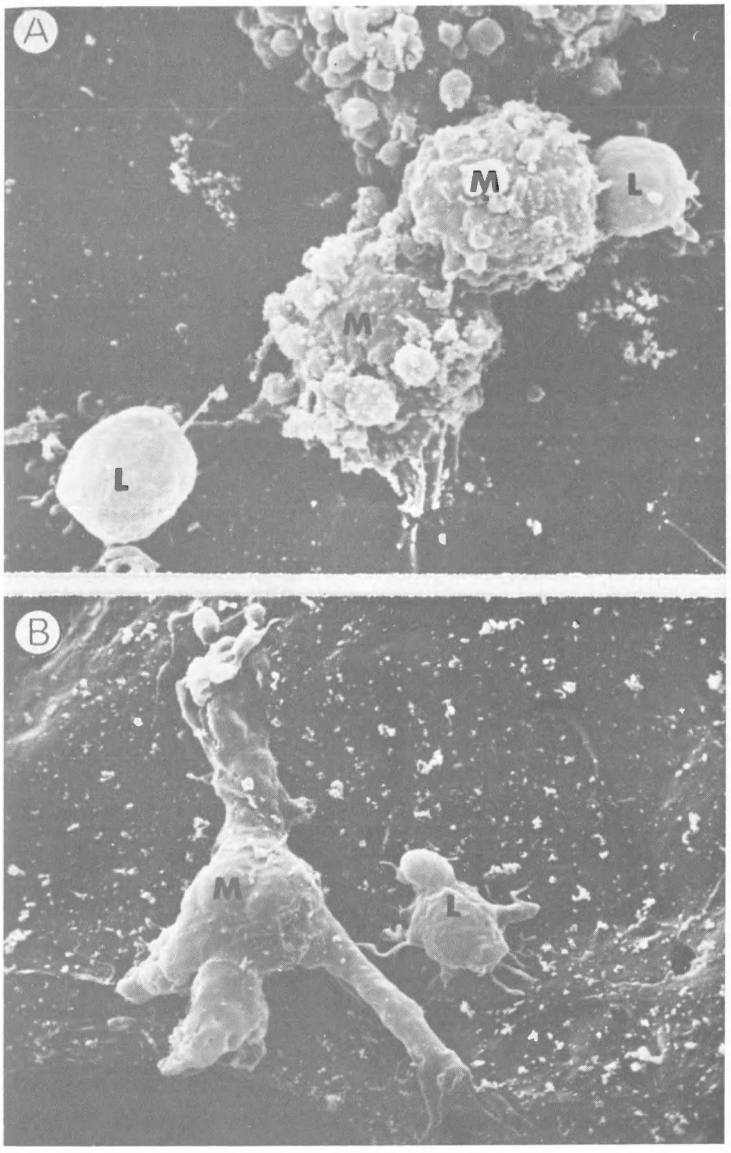

Figure 9. *Leptomeningeal Lymphoblasts and Macrophages; BCG Challenged.*—A—Some macrophage (M) - lymphoblast (L) interactions consist of a close association encompassing much of each cell's plasmalemma. (X 3,000) B—Lymphoblasts contact neighboring macrophages by way of their basal microvilli. (X 2,000)

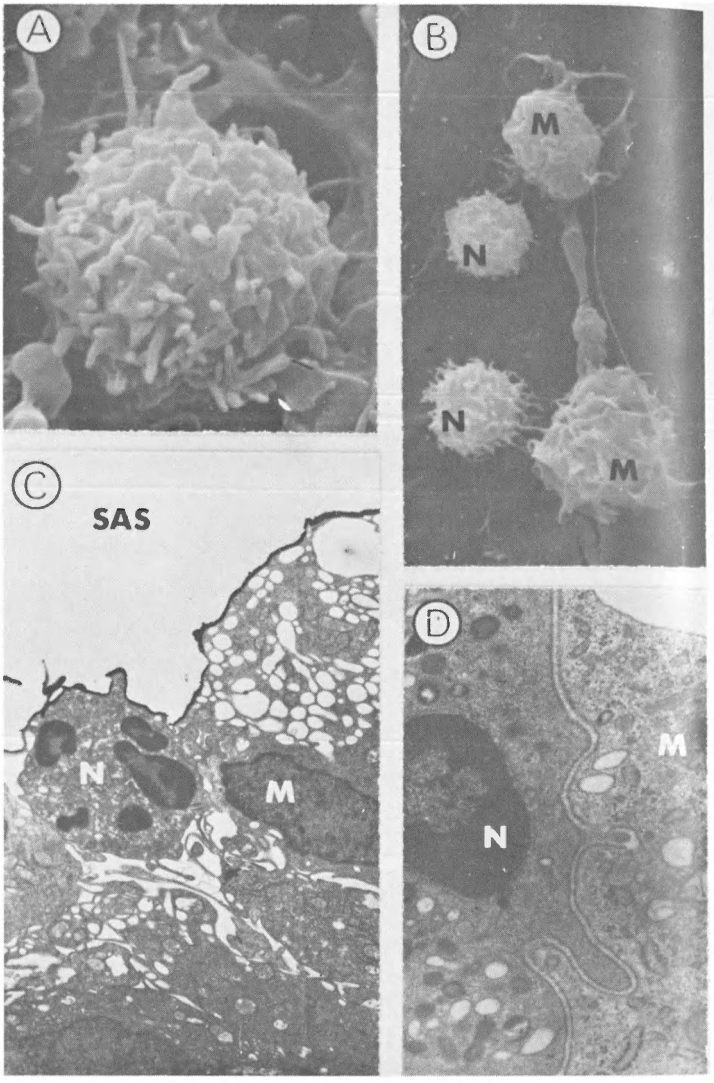

Figure 10. *Leptomeningeal Neutrophils and Macrophages; BCG Challenged.*—A—Neutrophils are nearly spherical and display numerous microvilli over their surfaces. (X 5,300) B—Neutrophils (N) contact macrophages (M) through microvillar processes. (X 2,000) C—Interactions may involve a large portion of each cell's surface. (X 6,300) D—Macrophages and neutrophils indent or interdigitate with each other through surface processes. (X 18,000)

microfilaments in the presence of CB they suggest that most, if not all, of CB's effects are due to microfilament inhibition. However, there is no direct evidence that the affected microfilaments are involved with the cell processes which are inhibited by CB (Carter, 1972; Estensen, *et al.*, 1971). Therefore, it remains to be determined whether there is a causal relationship between microfilaments and the effects of cytochalasin B. This present study shows no disruption of microfilaments, within the short term exposure to CB, and no relationship between these structures and blebs. The speed of action and its nature (microappendage formation; cell dissociation) both implicate the plasmalemma as the most likely site of primary action.

Mammalian cells, especially as shown in culture, are extremely sensitive to extracellular environmental factors such as pH (Ceccarini and Eagle, 1971; New, 1966). Proper maintenance of growth and metabolic functions are dependant upon optimal pH. Scanning and transmission electron microscopy reveal that microappendages undergo modification when stressed by non-physiological pH. Microvilli develop bulbous teminations as well as elongation at alkaline pH while disappearing at acid pH. Although the functional implications are not known, microappendage morphology is dependent on environmental conditions. Related to these findings is the work of Litke and Low (1977) which demonstrates that variations in fixative tonicity affects endodermal cells similar to acid pH. Cell bulging and loss of microappendages are consistent with hypotonic fixation. Alteration in pH conceivably might alter cell permeability resulting in uptake of excess fluid associated with retraction of microappendages. A similar mechanism could explain the effects of CB on cell dissociation as reported herein.

Scanning and transmission electron microscopy indicate that the free cells resting on the leptomeningeal linings of normal animals possess the morphology of macrophages (Morse and Low, 1972b; Malloy and Low, 1976). The unstimulated macrophages of controls present a topography suggestive of a high level of plasmalemmal activities; including blebs, microvilli and ruffles.

Electron microscopy of the subarachnoid space of BCG-challenged animals shows that approximately 80% of the free cell population expresses a macrophage morphology. Activated macrophages differ from controls in two respects. First, SEM demonstrates that plasmalemmal blebbing is greatly enhanced and dominates the macrophage surface. Some cells are totally covered by these rounded eruptions of the plasma membrane. Transmission electron microscopy not only illustrates that challenged macrophages, possess a greater wealth of vacuoles but also that these vacuoles compose much of the interior of apical blebs. The vacuoles may represent heightened ingestion of cerebrospinal fluid and analysis of its composition by the stimulated macrophage.

Second, microvilli increase in number on the surfaces of challenged macrophages. This trait may relate to enhanced phagocytic capacity since these microvilli appear to probe the meningeal sheaths in a searching fashion. The present study demonstrates cellular interactions between adjacent macrophages via microvilli. Such associations may be reasonably interpreted as a mechanism by which cells are recruited for specific immunologic or phagocytic activities and that

the intimate proximity of some plasmalemmal extensions may serve as an intercellular pathway for this communication.

Electron microscopy of experimental animals uncovers at least two other members of the leukocyte series, neutrophils and lymphoblasts. Their appearance in infected animals only suggests that in the presence of an antigen their ability to adhere to a substrate is enhanced. Both cell types display microvillar processes which appear to anchor the cells to the substrate.

The present study reveals extensive inderdigitating processes between neutrophils and macrophages. Since degenerating neutrophils are occasionally observed with macrophage phagosomes, these plasmalemmal invaginations may represent early events of phagocytosis (Leibovich and Ross, 1975). Regardless of the fate of the neutrophil, the elaborate junction formed by this cell and the macrophage, would suggest this as a site of information exchange between the two cell types.

Numerous studies have demonstrated lymphocytes physically interacting with macrophages during the immune response (Farr and DeBruyn, 1975; Nielson, *et al.*, 1974; Schoenberg, *et al.*, 1964; Werdelin, *et al.*, 1974). These studies indicated that for most antigens, macrophage-lymphoblast interactions were required for immune reactions to be fully potentiated. In the present study, the close apposition of their respective plasmalemmas and microappendages may facilitate the presentation of macrophage, surface-bound antigen to the lymphocyte (Cline and Swett, 1968). A functional cooperation could also be mediated through soluble factors or "altered" antigens released by macrophages and therefore the close proximity of cell processes might serve in the conservation and concentration of such liberated factors (Fishman and Adler, 1963).

Electrophysiological studies have demonstrated electronic coupling between closely apposed cells (Revel, *et al.*, 1971; Sheridan, 1966). Levy *et al.* (1976) have reported similar communication occurring between cultured macrophages. Therefore, the intimate cell surface associations mediated through the cell surface processes of leptomeningeal leukocytes may not only allow for chemical factors to be transferred from cell to cell more easily but an electrical field as well. It therefore appears that portions of the microappendage plasmalemma may represent specialized areas where the transport function is more essential than the barrier function.

In summary then, plasmalemmal microappendages are differentiated, highly active functional components of the cell. They exhibit purposeful activity and responsiveness to extrinsic change. The former has been demonstrated within the chick embryo model in response to changes in pH and the insult cytochalasin B. The extent, prominence and distribution of microappendages are modified indicating variable states of cellular activity or response. Further analysis defines this response as being membrane-associated. With the subarachnoid space-leukocyte model we observe a further refinement in the activity of plasmalemmal morphology. Evidence has been presented to indicate an active communicative as well as passive function. That macrophages and other leukocytes are intimately involved in the immune response, demands that they possess highly capable

methods of interpreting foreign from endogenous antigenic substances. Also the requirement of certain leukocyte interactions to express some immunological effects predisposes a method of intercellular communication. Evidence for both of these ideas has been presented.

As cytochalasin B has been shown to inhibit a variety of microfilament dependent activities, however, and that microfilaments per se are not found to be direct controllers of microappendage alteration as seen with CB administration, evidence is enhanced for a passive or concomitant mechanism for bleb formation.

The mechanisms of microappendage formation and function, nevertheless, remain largely unknown. However, as per this communication it is plausible to investigate intramembranous activity with respect to motility, receptive and communicative modalities. This laboratory is currently investigating related intramembranous morphology with the freeze-fracture technique.

ACKNOWLEDGMENTS

The authors wish to thank Doctor Frank N. Low for his guidance and support throughout the course of this study. Special thanks are extended to Joy Brew and Debra Beck for their valuable technical assistance. This work was supported by United States Public Health Science Grants NS 09363 and NS 12106 from the Institute of Neurological and Communicative Disorders and Stroke.

LITERATURE CITED

Abercrombie, M., J. E. M. Heaysman and S. M. Cegrum. 1970. The locomotion of fibroblasts in culture. II. Ruffling. Exp. Cell Res., *60*:437-450.

_____. 1971. The locomotion of fibroblasts in culture. III. Electron microscopy of the leading lamella. Exp. Cell Res., 67:359-382.

Allen, D. J. and F. N. Low. 1975. Scanning electron microscopy of the subarachnoid space in the dog. III. Cranial levels. J. Comp. Neur., *161*:515-540.

Axline, S. G. and E. P. Reaven. 1974. Inhibition of phagocytosis and plasma membrane mobility of the cultivated macrophage by cytochalasin B. J. Cell Biol., *62*:647-659.

Bhisey, A. N. and J. J. Freed. 1975. Remnant motility of macrophages treated with cytochalasin B in the presence of colchicine. Exp. Cell Res., *95*:376-384.

Carter, S. B. 1967. Effects of cytochalasins on mammalian cells. Nature, *213*: 261-264.

_____. 1972. The cytochalasins as research tools. Endeavor, *31*:77-82.

Ceccarini, C. and H. Eagle. 1971. Induction and reversal of contact inhibition of growth by pH modification. Nature New Biol., *233*:271-273.

Cline, M. J. and V. C. Swett. 1968. Interaction of human monocytes and lymphocytes. J. Exp. Med., *128*:1309-1320.

Cloyd, M. W. and F. N. Low. 1974. Scanning electron microscopy of the subarachnoid space in the dog. I. Spinal cord levels. J. Comp. Neur., *153*: 325-368.

Costera, I. and C. M. Pomerat. 1951. Cultivation of neurons from the adult human cerebral and cerebellar cortex. Am. J. Anat., *89*:405-432.

Estensen, R. D., M. Rosenburg and J. O. Sheridan. 1971. Cytochalasin B: Microfilaments and "contractile processes". Science, *173*:356-357.

Farr, A. G. and P. P. H. DeBruyn. 1975. Macrophage-lymphocyte clusters in lymph nodes: A possible substrate for cellular interactions in the immune response. Am. J. Anat., *144*:209-232.

Fishman, M. and F. L. Adler. 1963. Antibody formation initiated in vitro. II. Antibody synthesis in x-irradiated recepients of diffusion chambers containing nucleic acid derived from macrophages incubated with antigen. J. Exp. Med., *117*:595-609.

Follett, E. A. C. and R. D. Goldman. 1970. The occurrence of microvilli during spreading and growth of BHK 21/C13 fibroblasts. Exp. Cell Res., *59*: 124-136.

Forssman, W. G., G. Siegrist, L. Orci, L. Girardier, R. Pictet and C. Rouiller. 1967. Fixation par perfusion pou la microscopie electronique. Essai de generalisation, J. Microscopie, *6*:279-304.

Gey, G. O. 1954-55. Some aspects of the constitution and behavior of normal and malignant cells maintained in continuous culture. Harvey Lect. Ser. L., pp. 154-229, Academic Press, New York, 1956.

Hamilton, H. H. 1952. Lillie's Development of the Chick. Third Edition. Holt, Rinehart and Winston, New York.

Harri, J. E. and F. N. Low. 1974. Microappendages on the ventral surface of the primitive streak chick embryo. Am. J. Anat., *141*:569-574.

Ingram, V. M. 1969. A side view of moving fibroblasts. Nature (London) *222*: 641-652.

Krishan, A. 1971. Fine structure of cytochalasin - induced multi-nucleate cells. J. Ultrastruct. Res., *36*:191-204.

Leibovich, S. J. and R. Ross. 1975. The role of the macrophage in wound repair. A study with hydrocortisone and antimacrophage serum. Am. J. Path., *78*:71-98.

Levy, J. A., R. M. Weiss, E. R. Dirksen and M. R. Rosen. 1976. Possible communication between murine macrophages oriented in linear chains in tissue culture. Exp. Cell Res., *103*:375-385.

Lewis, W. H. and G. O. Gey. 1923. Clasmatocytes and tumor cells in cultures of mouse sarcoma. Bull. J. Hopk. Hosp., *34*:369-378.

Litke, L. L. and F. N. Low. 1975. Scanning electron microscopy of yolk absorption in early chick embryos. Am. J. Anat., *142*:527-530.

_____. 1977. Fixative tonicity for scanning electron microscopy of delicate chick embryos. Am. J. Anat., *148*:121-127.

Low, F. N. 1967. Developing boundary membranes in the chick embryo. Anat. Rec., *159*:231-238.

Malloy, J. J. and F. N. Low. 1974. Scanning electron microscopy of the subarachnoid space in the dog. II. Spinal nerve exits. J. Comp. Neur., *157*: 87-108.

_____. 1976. Scanning electron microscopy of the subarachnoid space in the dog. IV. Subarachnoid macrophages. J. Comp. Neur., *167*:257-284.

Mayhew, E. and D. E. Maslow. 1974. Cytochalasin B and the sialic acids of Ehrlich ascites cells. Exp. Cell Res., *83*:255-260.

New, D. A. T. 1966. The Culture of Vertebrate Embryos. Loops Press Ltd., London.

McMullan, D. 1953. An improved scanning electron microscope for opaque specimens. Inst. Elect. Eng. Proc., *100*:245-256.

Merchant, R. E. 1976. Scanning and transmission electron microscopy of subarachnoid free cells; interactions stimulated by bacillus Calmette-Guerin. J. Cell Biol., *70*:171A.

Merchant, R. E. and F. N. Low. 1977a. Identification of challenged subarachnoid free cells. Am. J. Anat., *148*:143-148.

_____. 1977b. Scanning electron microscopy of the subarachnoid space in the dog. V. Macrophages challenged by bacillus Calmette-Guerin. J. Comp. Neur., *172*:381-408.

Morse, D. E. and F. N. Low. 1972a. The fine structure of the pia mater in the rat. Am. J. Anat., *133*:349-368.

_____. 1972b. The fine structure of subarachnoid macrophages in the rat. Anat. Rec., *174*:469-476.

Nielsen, M. H., H. Jensen, O. Braendstrup and O. Werdelin. 1974. Macrophage-lymphocyte clusters in the immune response to soluble protein antigen in vitro. II. Ultrastructure of clusters formed during the early response. J. Exp. Med., *140*:1260-1282.

Oatley, C. N. 1966. The scanning electron microscope. Sci. Prog., *54*:483-495.

Oehmichen, M. and H. Gruninger. 1974. Cytokinetic studies on the origin of cells of the cerebrospinal fluid with a contribution to the cytogenesis of the leptomeningeal mesenchyme. J. Neurol. Sci., *22*:165-176.

Pease, D. C. and R. L. Schultz. 1958. Electron microscopy of rat cranial meninges. Am. J. Anat., *102*:301-321.

Porter, K., D. Prescott and J. Frye. 1973. Changes in the surface morphology of Chinese hamster ovary cells during the cell cycle. J. Cell Biol., *57*: 815-836.

Price, L. H. 1967. The micromorphology of zeiotic blebs in cultured human epithelial (HEp) cells. Exp. Cell Res., *48*:82-103.

Revel, J. P., A. G. Yee and A. J. Hudspeth. 1971. Gap junctions between electronically coupled cells in tissue culture in brown fat. Proc. Nat. Acad. Sci. U.S.A., *68*:2924-2927.

Schoenberg, M. D., V. R. Mumaw, R. D. Moore and A. S. Weisberger. 1964. Cytoplasmic interaction between macrophages and lymphotic cells in antibody synthesis. Science, *143*:964-965.

Shabo, A. L. and D. S. Maxwell. 1968. Electron microscopic observations on the fate of particulate matter in the cerebrospinal fluid. J. Neurosurg., *29*: 464-474.

Sheridan, J. D. 1966. Electrophysiological study of special connections between cells in the early chick embryo. J. Cell Biol., *31*:C1-C5.

Taylor, A. C. 1966. Microtubules in the microspikes and cortical cytoplasm of isolated cells. J. Cell Biol., *28*:155-171.

Werdelin, O., O. Braendstrup and E. Pederson. 1974. Macrophage-lymphocyte clusters in the immune response to soluble protein antigen in vitro. I. Roles of lymphocytes and macrophages in cluster formation. J. Exptl. Med., *140*:1245-1259.

Wessells, N. K., B. S. Spooner, J. F. As, M. O. Bradley, M. A. Luduena, E. L. Taylor, J. T. Wrenn and K. M. Yamada. 1971. Microfilaments in cellular and developmental processes. Science, *171*:135-143.

A SCANNING ELECTRON MICROSCOPIC STUDY OF THE CHOROID PLEXUS IN THE RABBIT

Bruce Persky and Frank N. Low
Department of Anatomy, School of Medicine
University of North Dakota, Grand Forks, North Dakota 58202

ABSTRACT

This study depicts the surface morphology of the choroid plexus of the lateral ventricle in the rabbit. Numerous pleomorphic epiplexus (Kolmer cell) macrophages were noted, often occupying the sulcus found between adjacent choroid plexus ependymal cells. The ventricular surface of each ependymal cell resembled a low, rounded mound covered with numerous microvilli. The microvilli varied in length and were more heavily distributed on the top of the cell than at the periphery. The sulcus positioning apparently allowed the epiplexus macrophage to attain a closer physical proximity to the underlying epithelial cells.

The cytoplasmic processes of some epiplexus macrophages were long, thin, and delicate while others were thick and proboscis-like. Occasionally pits and crater-like depressions were observed on both the cell body and cytoplasmic processes. Generally, the cytoplasmic processes flattened out and blended with the ependymal cells.

INTRODUCTION

Scientific observations of the choroid plexus and ventricles began in 1836 with a light microscopic study of the ventricular epithelium of sheep. Since then numerous studies, many using transmission electron microscopy (TEM), have focused on the ultrastructure of the ventricular ependymal lining cells, the choroid plexus epithelium, and associated macrophages. The basic structure of the mature choroid plexus is now known to consist of a single layer of flattened cuboidal epithelial cells resting on a basement membrane. An interposing layer of connective tissue separates all basement membranes, as especially seen when the choroid plexus bulges into the ventricular space. Superficially the epithelial cells are covered with microvilli and cilia.

Some eighty-five years later, Kolmer (1921) observed phagocytic cells resting on the choroid plexus of lower vertebrates. Subsequent light microscopic studies during the 1930's, '40's, and early '50's confirmed the presence of phagocytic cells (Kolmer cells) in other vertebrates (Biondi, 1934). Ariëns Kappers (1953) reported the Kolmer cell morphology and phagocytic behavior in the salamander and the guinea pig, and he also coined the name "epiplexus cell" to designate the Kolmer cell's epi-epithelial position on the choroid plexus.

Detailed studies of the cat's epiplexus cells uncovered such ultrastructural features as free ribosomes, multiple Golgi, indented nucleus, coated surface invaginations and microvesicles and dense lysosomal bodies (Carpenter, 1970). The cat's epiplexus cells appeared to be of hematogenous origin, but evidence was lacking. This came in 1975 from research done on humans (Schwarze, 1975). Schwarze noted that the polymorphous mononuclear epiplexus cells could not be distinguished from cells which are found as macrophages in the blood vessels and the stroma of the plexus. He formulated this conclusion due to the fact that

neither a light and electron microscope comparison nor a phagocytosis experiment could show a difference. The epiplexus cells were highly similar to or identical with macrophages of other locations. It is currently believed that the epiplexus cells are hematogenous in origin and are therefore monocytogenetic macrophages.

Schwarze also positively determined that a second type of phagocytic epiplexus cell, which had been found by other investigators as early as 1953, was indeed a lymphocyte. He based his identification on morphologic and cytochemical criteria. These lymphocytes, which are not often seen on the surface of the plexus epithelium, wander through the stroma and epithelium of the choroid plexus as hematogenous cells and then enter the cerebrospinal fluid.

One of the earliest scanning electron microscopic (SEM) studies of the epiplexus cells was reported by Hosoya and Fujita (1973) on the rat choroid plexus. They divided the epiplexus cells into two types by differences noted in their topography. Type 1 cells possessed only fibrous processes projecting from a centrally located cell body. Type 2 cells possessed pseudopod-like processes of considerable length and thickness. They suggested that Type 1 cells represented a resting stage while Type 2 cells represented a motile stage.

A later study (Chamberlain, 1974) performed in the fetal cat brain found large epiplexus cells (8-10 μm) typified by folds, flange-like surface projections, and long, thin pseudopodia interdigitating with subjacent choroid plexus microvilli. Discrete, periodic enlargements were observed at intervals along the pseudopodial processes. The periodic swellings may represent surface protrusions of migrating subplasmalemmal organelles, such as lysosomes and microtubules.

A still later study (Allen, 1975) examined the epiplexus cells of the dog. Allen's work demonstrated that the numerous epiplexus cells exhibit extreme polymorphism and also that TEM used in conjunction with SEM positively identified epiplexus cells as being macrophages. Because of the epiplexus cell's special characteristics of polymorphism, Allen concluded that external morphological classification would have to rely on generalizations. Flattened supraependymal macrophages had processes that tend to flatten out and blend with the ependymal cells. Star shaped supraependymal macrophages had a smooth oval body with a number of radiating cellular processes. Rounded up supraependymal macrophages had many fine, filamentous processes. Some of the filamentous processes possessed bulbous-like projections. Most of the processes of the macrophages were intimately associated with the ependymal surface, but these were not macrophage-ependymal tight junctions. This absence supported the belief that the polymorphism was due to the Kolmer cells moving about on the ependymal lining.

SEM studies of the choroid plexus have indicated substantial differences in the surface morphology between various vertebrate species. The present work is a descriptive study of the choroid plexus in the rabbit so that further vertebrate comparisons may be made.

MATERIALS AND METHODS

Four female rabbits of varying ages were anesthetized by intraperitoneal and intrathoracic injection of 6.5% sodium pentobarbital and perfused under near normal physiological pressure by a cannula inserted into the exposed left ventricle. The perfusates were buffered aldehyde solutions (Karnovsky, 1965) modified by techniques from Palay et al., (1962), Sabatini et al., (1963) and Rosen et al., (1967). The initial fixation and washing out of blood was accomplished by a washout solution of a cacodylate-buffered paraformaldehyde-glutaraldehyde mixture which contained 0.1% procaine hydrochloride to prevent peripheral vasoconstriction (Forssman et al., 1967). After flushing 1,000 - 1,500 ml of washout solution through the circulatory system, the perfusion was completed with 1,000 - 1,500 ml of Karnovsky fixative.

The animals were decapitated, and the bony vault of the skull was stripped free of soft tissue. A complete coronal section just anterior to the orbits allowed access to the cranial cavity. The calvarium was split midsagitally (anterior to posterior) and reflected laterally. The brain was lifted from the cranial vault as the cranial nerves and blood vessels were severed. The entire brain was then immediately immersed in Karnovsky fixative for further dissection. The brain was sectioned midsagitally, and the lateral ventricles opened via entry through the Foramen of Monroe. The choroid plexus was excised from the lateral ventricles and placed in fresh Karnovsky fixative. The tissues were subjected to a cleansing stream of fixative for several minutes to prevent surface contamination.

The choroid plexuses were prepared for scanning electron microscopy by postfixing for 60-90 minutes in either 1% or 2% OsO_4 buffered with 0.144 N sodium cacodylate. An electric stirrer provided a constant slow swirl during all phases of postfixation. After rinsing in 0.144 N sodium cacodylate buffer, the tissue samples were dehydrated through an ascending series of acetone. Samples were dried in a Sorvall Critical Point Drying System using carbon dioxide as the drying agent. The dried tissues were quickly mounted on metal specimen stubs with either silver paste or double-stick tape, and coated with palladium-gold in a Technics Hummer I vacuum evaporator. Specimens were viewed in a Cambridge Stereoscan S4 scanning electron microscope.

RESULTS AND DISCUSSION

Scanning electron microscopy of the rabbit choroid plexus at low magnification reveals a tortuous, convoluted epithelium projecting into the ventricular cavity (Figures 1-6). Regional differences in the overall topography of the plexus tissue were noted but appear to be limited only to the degree of tortuosity.

The cuboidal epithelial cells which comprise the choroid plexus are rounded up on the ventricular side (Figures 1, 5, 6). Numerous microvilli and cilia cover the plexus surface (Figures 1-6). The cilia appear to encircle pore-like structures on the cell surface. Thus the cilia outline an apparent passageway through the plexus plasmalemma (Figure 2). Microvilli blanket the plexus ventricular surface, especially the ventricular apex. Cell junctions between adjacent ependymal cells in

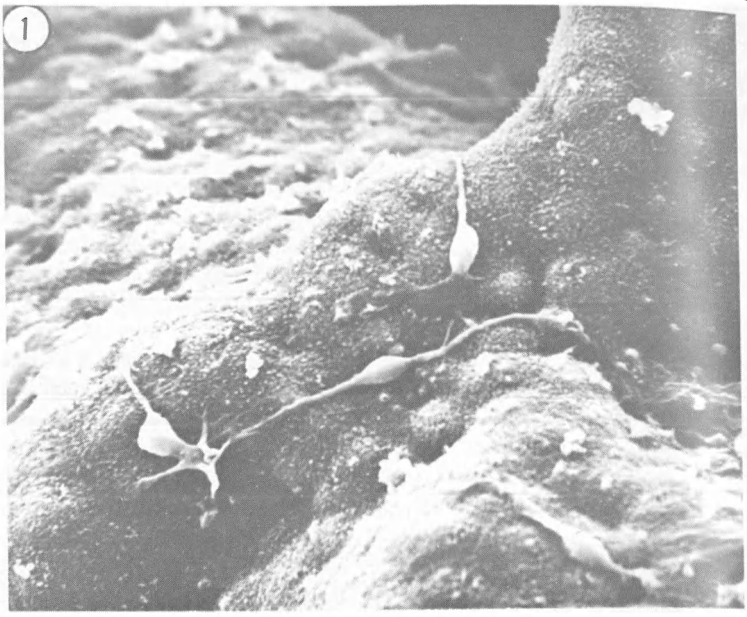

Figure 1. Low power scanning electron micrograph showing the convolutions of the choroid plexus. The entire ventricular surface is covered with microvilli. Note that the ventricular surface of each ependymal cell is rounded up towards the ventricular lumen. Four pleomorphic Kolmer cells are seen on the epithelial sbustrate. x 650.

this study were obscured by the microvilli lining the intercellular sulci. Transmission electron microscopy, however, shows such cellular junctions near the ventricular surface to be tight junctions (Millen, 1956; Carpenter, 1966; Tennyson, 1968; Carpenter, 1970; Edvisson, 1975; and Milhorat, 1976).

Smooth surfaced cells (Kolmer cells, epiplexus cells, macrophages) are frequently noted resting on top of the choroid plexus' ridges (Figure 2). These smooth-surfaced Kolmer cells are indiscriminantly spread over the entire choroid plexus epithelium. Generally the individual Kolmer cell favors a location in the sulcus between the ependymal cells (Figures 4, 6). Yet, the Kolmer cells are often seen straddling an ependymal cell (Figure 5).

The nuclear region of the Kolmer cell always appears enlarged. Most often in SEM, the nuclear region appears ovoid (Figure 2) or round (Figure 5), or some intermittent pleomorphic state. One or more processes radiate out from the centrally located nuclear region. Sometimes the processes are very long, thin and

delicate (Figures 3, 5, 6). Such long structures may stretch across several epithelial cells, and may or may not be in physical contact with the substrate. The long, thin processes may show periodic enlargements along their length (Figure 3). These periodic swellings may represent surface protrusions of migrating subplasmalemmal organelles (Chamberlain, 1974). The terminal ends of the long processes either taper to a narrow point (Figure 3) or into a thin, veil-like process (Figure 3). In other instances, the radiating processes are thick and proboscis-like. Still another variation of the cytoplasmic extension is a pseudopoid-like process emerging directly from the central nucleus area (Figure 2). Such processes appear similar to those seen at the terminal end of a long, thin process except for the obvious size difference, the latter being smaller. The veil-like process is known to

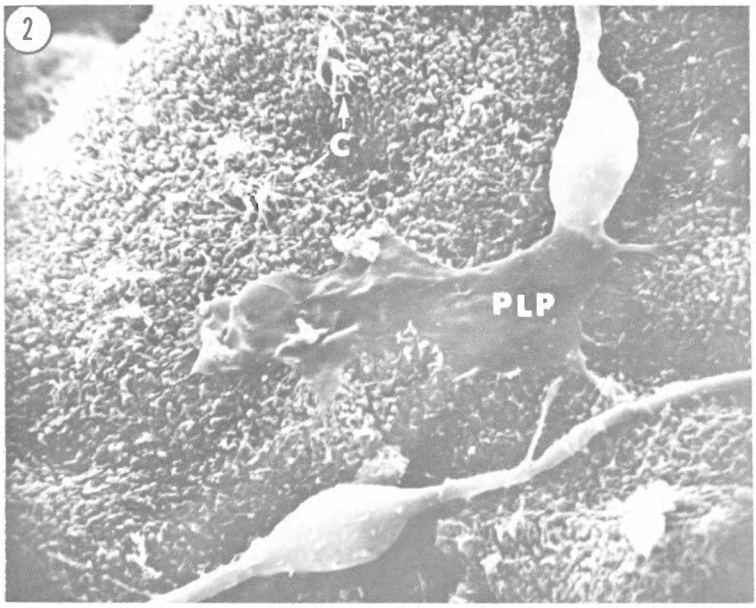

Figure 2. This enlargement of Figure 1 depicts the pseudopod-like process (PLP) seen in some Kolmer cells. The pseudopod-like process appears to make contact with the underlying microvilli. In fact the contour of the underlying microvilli may help give rise to the topography of the overlying pseudopod-like process. Two clumps of cilia (C) surround apparent apertures into the cell plasmalemma. The shorter microvilli are seen to blanket the cell's ventricular surface. x 2000.

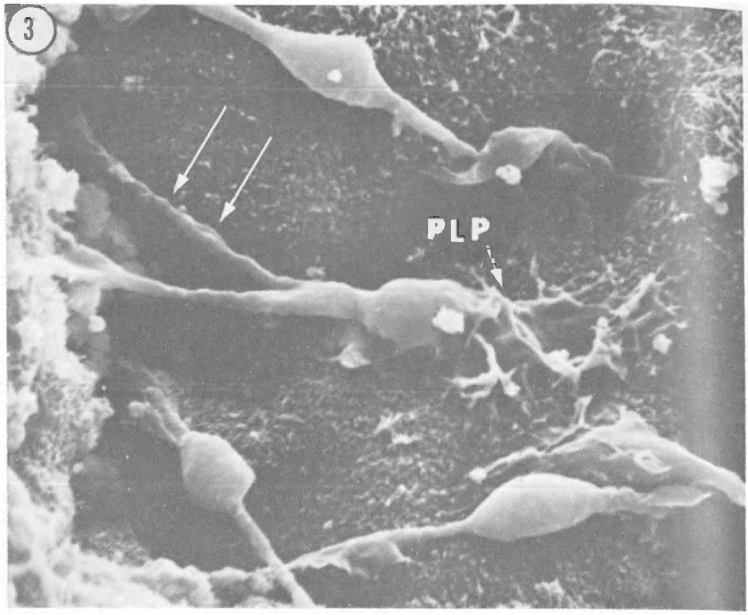

Figure 3. Pronounced periodic enlargements in the thin processes (arrows) are exhibited by this scanning electron micrograph. The enlargements are believed to be caused by the passage of small subplasmalemmal material through the thin process. The ovoid nuclear region of the same Kolmer cell gives rise to a pseudopoid-like process (PLP). This latter process looks both discontinuous and continuous with the microvilli substrate. x 1750.

adhere closely to the substrate as microvilli impressions may be seen on the ventricular surface of the veil (Figure 2). The purpose of this interdigitating with microvilli of subadjacent choroid plexus epithelial cells is not yet clearly understood. It may be responsible for an amoeboid type of movement by the Kolmer cell to traverse the epithelial substrate.

In general the choroid plexus of the rabbit closely resembles that of the cat, rat, guinea pig and dog as previously reported. The Kolmer cells are found in the same general position but have a tendency toward more processes that are slender and flatten out on the surfaces of the epithelial cells.

ACKNOWLEDGMENTS

This study was supported by USPHS grant NS 09363 from the Institute of Neurological and Communicative Disorders and Stroke. Thanks are extended to Joy Brew for typing the manuscript.

LITERATURE CITED

Allen, Delmas J. 1975. Scanning electron microscopy of epiplexus macrophages (Kolmer Cells) in the dog. J. Comp. Neur., 161:197-214.

Ariens-Kappers, J. 1953. Beitrag zur experimentellen Untersuchung von Funktion and Herkunft der Kolmerschen Zellen des Plexus choroideus beim Axolotl und Meerschweinchen. Z. Anat. Entwickl. Gesch., 117:1-19.

Biondi, G. 1934. Zur Histopathologie des menschlichen Plexus choroideus und des Ependyms. Arch. Psychiat. Nervenkr., 101:666-728.

Carpenter, R. S. 1966. An electron microscopic study of the choroid plexus of Necturus maculosus. J. Comp. Neur., 127:413-434.

Carpenter, S. J., L. E. McCarthy and H. L. Borison. 1970. Electron microscopic study of the epiplexus (Kolmer) cells of the cat choroid plexus. Z. Zellforsch., 110:471-486.

Chamberlain, J. 1974. Scanning electron microscopy of epiplexus cells (macrophages) in the fetal rat brain. Am. J. Anat., 139:443-447.

Edvinsson, L., R. Hakanson, M. Lindvall, Ch. Owman and K. G. Svensson. 1975. Ultrastructural and biochemical evidence for a sympathetic neural influence on the choroid plexus. Exp. Neurology, 48:241-251.

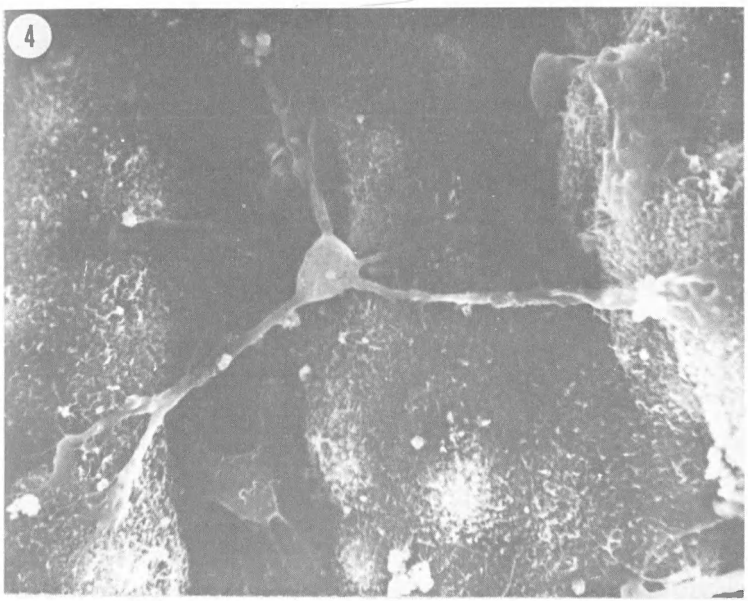

Figure 4. Found stretched between a few ependymal cells, this Kolmer cell has very long, yet thin processes. x 1150.

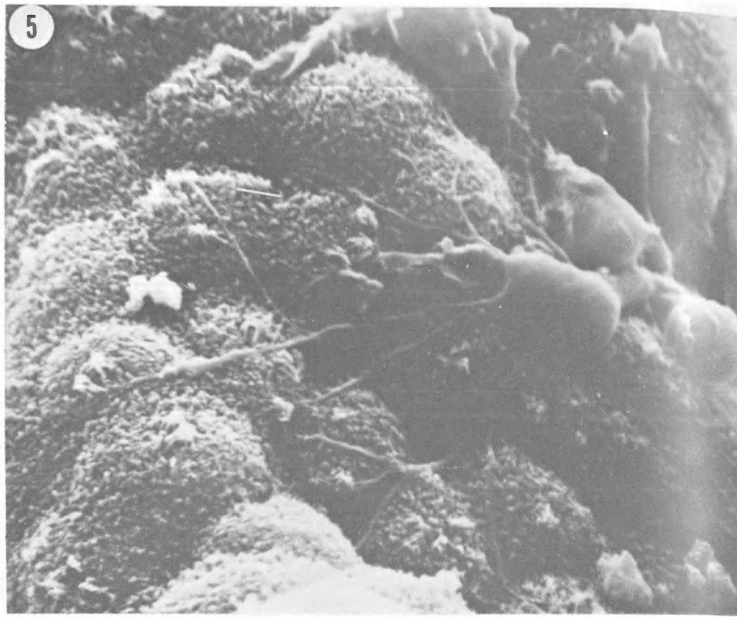

Figure 5. This scanning electron micrograph illustrates multiple radiating processes from the central nuclear region. In addition, the processes are highly branched and often traverse several ependymal cells. x 1300.

Forssman, W. G., G. Siegrist, L. Orci, L. Girardier, R. Pictet and C. Rouiller. 1967. Fixation par perfusion in pour la microscopie electronique. Essai de generalisation. J. Microscopie, 6:279-304.

Hosoya, Y. and T. Funita. 1973. Scanning electron microscope observations of intraventricular macrophages (Kolmer Cells) in the rat brain. Arch. Hist. Jap., 35:133-140.

Karnovsky, M. J. 1965. A formaldehyde-glutaraldehyde fixative of high osmolality for use in electron microscopy. J. Cell Biol., 27:137A-138A.

Kolmer, W. 1921. Uber eine eigenatige Beziehung von Wanderzellen zu den Chorioidealplexus des Gehirns der Wirbeltiere. Anat. Anz., 54:15-19.

Milhorat, Thomas H. 1976. Structure and function of the choroid plexus and other sites of cerebrospinal fluid formation. International Review of Cytology, 47:225-288.

Millen, J. W. and G. E. Rogers. 1956. An electron microscopic study of the choroid plexus the rabbit. J. Biophys. Biochem. Cytol., 2:407-416.

Palay, S. L., S. M. McGee-Russell, S. Gordon, Jr. and M. A. Grillo. 1962. Fixations and neural tissue for electron microscopy by perfusion with solutions of osmium tetraoxide. J. Cell Biol., 12:385-410.

Rosen, W. C., C. R. Basom and L. L. Gunderson. 1967. A technique for the light microscopy of tissues fixed for fine structure. Anat. Rec., 158:223-237.

Sabatini, D. D., K. G. Bensch and R. J. Barrnett. 1963. Cytochemistry and electron microscopy: The preservation of cellular ultrastructure and enzymatic activity by aldehyde fixation. J. Cell Biol., 17:19-58.

Schwarze, Ernst-Wilhelm. 1975. The origin of (Kolmer's) epiplexus cells—A combined histomorphological and histochemical study. Histochemistry, 44:103-104.

Tennyson, V. M. and G. D. Pappas. 1968. The fine structure of the choroid plexus: Adult and development stages. Prog. Brain Research, 29:63-85.

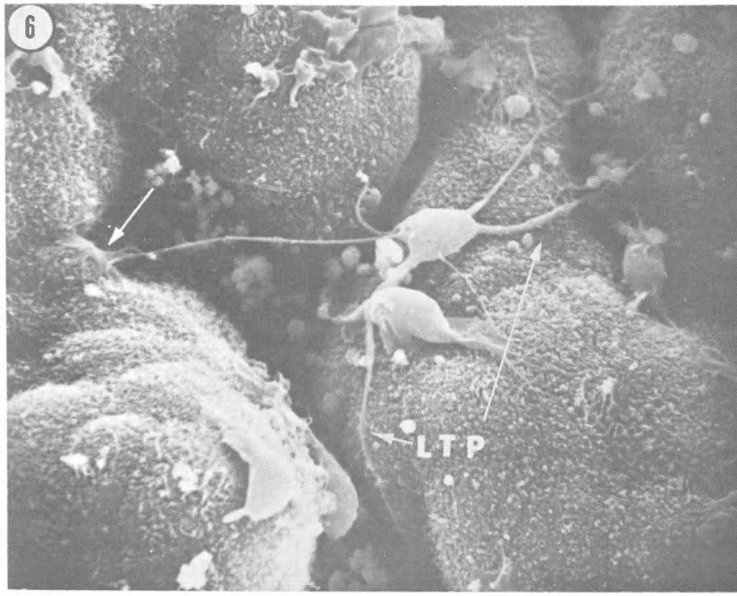

Figure 6. Several long thin processes (LTP) radiate out from these two Kolmer cells. The top cell illustrates pleomorphism well, having a long thin process terminate in a veil-like structure (arrow). x 1000.

PROBABILITY AMPLITUDES FOR TWO-PHOTON ABSORPTION: RARE EARTH AND ACTINIDE ION SYSTEMS

J. B. Gruber, E. D. Larson, D. N. Olsen and T. R. Stoner
Department of Physics
College of Science and Mathematics
North Dakota State University, Fargo, North Dakota 58102

ABSTRACT

Probability amplitudes have been derived for two-photon spectroscopy using time-dependent perturbation theory. Two cases are considered in detail: (1) absorption of a laser photon and an incoherent light-source photon, and (2) absorption of two laser photons. Expressions for two-photon absorption coefficients are compared with results obtained by Kleinman in 1962. Contrary to Kleinman's approach, our expressions give first-order probability amplitudes that do not contain or require intermediate states. We find these amplitudes depend upon the polarization and intensity of the incoming laser beams. The second-order probability amplitudes are calculated by assuming that the charge transfer band acts as intermediate states, an assumption also made by Kleinman. As an example, we quantify our expressions by performing a ratio calculation between two-photon and single-photon absorption by rare earth or actinide ion (nf^N) systems.

INTRODUCTION

With the advent of laser technology in the early sixties, it became possible to generate powerful, coherent, and tunable laser sources which allow one to examine many low-probability non-linear optical phenomena. One such phenomenon includes multiphoton spectroscopy which is the interaction between the quantized electromagnetic field and matter, accompanied by absorption or emission (or both) of not *less* than two photons from the radiation field per elementary act. Prediction of such a phenomenon, however, actually predates the laser, and was made as early as 1931 by Marie Goeppert-Mayer who made use of time-dependent perturbation theory associated with the then emerging theory of quantum mechanics. Quantum mechanical time-dependent perturbation theory organizes interaction of the radiation field with matter rather logically into a sequence of events of decreasing probability in which the occupation numbers of the quantized electromagnetic field change by integer amounts of increasing magnitude. These events are usually referred to as one, two, or higher multiphoton processes. The high intensity, monochromaticity and coherence of the laser source can overcome in many cases the experimental difficulties in dealing with low-probability multiphoton events.

Lasers are particularly useful in studying the optical properties of rare earth and actinide ions where single-photon electric-dipole transitions within the nf^N subshell, usually appearing in the visible and ultraviolet spectra, are precluded or are of low-probability due to selection rules arising from obvious parity considerations. Two-photon spectroscopy is particularly suited to studying $nf^N \rightarrow nf^N$ electronic transitions since two-photon absorption matrix elements in the electric-

dipole approximation achieve their maximum probability between states of the same parity.

The approach presented in this paper uses the time-dependent perturbation theory also used by Kleinman (1962) whose results were taken by Kaiser and Garrett (1961) to show qualitatively that two-photon absorption can take place in CaF_2 crystals doped with Eu^{2+} if a pulsed ruby laser of modest energy output (<1.0 joule at 6943 A) is used. Our results agree to within a constant factor with those reported by Kleinman (1962), the difference being that we have included contributions ignored by Kleinman. Our results give rise to expressions that do not contain or require intermediate states that serve no physical role in the actual process. Moreover, we find that calculated probability amplitudes for two-photon processes depend upon polarization of the photon beams. A critique is given near the end of the paper to show why this approach is more suitable and more physically sound. Also a ratio calculation is presented which indicates two-photon absorption is roughly a thousand times less likely than single-photon absorption for a typical rare earth ion.

In the following sections an expression is developed for a single-photon absorption coefficient in order to illustrate the procedure. Then expressions are derived for absorption coefficients for two-photon processes using second-order time-dependent perturbation theory (Merzbacher, 1970). Two types of absorption spectroscopy are considered.

1. A laser beam, frequency ω_b, is incident upon an absorbing medium having a sharp absorption line, frequency ω_{kg}. On the basis of the following calculation, a second, much weaker beam is then expected to experience absorption at frequencies $\omega_{kg} \pm \omega_b$.

2. A laser beam, frequency ω_b, is incident upon a medium having an absorption band at frequency $\omega_{kg} \sim 2\omega_b$. In both of these situations it is assumed, of course, that no states exist below the state of interest such that two single-photon absorptions occur.

BASIC ASSUMPTIONS AND DEVELOPMENT OF PERTURBATION COEFFICIENTS

The first assumption to be made in this semi-classical treatment is that transitions of importance may be characterized by a single-electron transition, and the perturbation Hamiltonian is chosen to have the form

$$H(t) = \frac{e\hbar}{mc\iota}\vec{A}(t)\cdot\vec{\nabla} + \frac{e^2}{2mc^2}(\vec{A}(t)\cdot\vec{A}(t)) \tag{1}$$

where all symbols have their usual meaning. Equation (1) comes from the total Hamiltonian

$$\mathcal{H} = \frac{1}{2m}\left[\vec{p} - \frac{e}{c}\vec{A}(t)\right]^2 + V, \tag{2}$$

where V is the unperturbed potential. There is no contribution to the scalar potential by the radiation field since the Coulomb gauge is chosen

$$\vec{\nabla}\cdot\vec{A} = 0, \qquad \phi = 0$$

$$\nabla^2\vec{A} - \left[\frac{n}{c}\right]^2 \frac{\partial^2\vec{A}}{\partial t^2} = 0. \tag{3}$$

In this treatment the time-dependent lattice perturbations are neglected so that V, in Eq. (2), is assumed static. This assumption is appropriate, for example, for rare earth and actinide ions in solids, liquids or gaseous media where the f electrons are usually well shielded from the environment and are not involved as bonding electrons. There are a number of other systems that can be studied as well for cases of localized electrons undergoing transitions. A vector potential of the form

$$\vec{A}(\vec{r},t) = \vec{A}_b \exp[i\omega_b(t-\tilde{n}_b\cdot\vec{r}/c)] + \vec{A} \exp[i\omega(t-\tilde{n}\cdot\vec{r}/c)] + c.c. \tag{4}$$

is taken, where $\omega_b\tilde{n}_b/c$ and $\omega\tilde{n}/c$ are wave vectors in the medium for the laser and weaker source, respectively. The expression c.c. means the complex conjugate of the first terms in Eq. (4). Taking only monochromatic forms here instead of Fourier transforms is based upon the practical fact that such forms are much simpler to use.

Combining Eq. (4) and Eq. (1) yields the perturbation Hamiltonian

$$\begin{aligned} H(t) = {} & \frac{e\hbar}{mci}\left\{\vec{A}_b \exp[i\omega_b(t-\tilde{n}_b\cdot\vec{r}/c)] + \vec{A} \exp[i\omega(t-\tilde{n}\cdot\vec{r}/c)] + c.c.\right\}\cdot\vec{\nabla} \\ & + \frac{e^2}{2mc^2}\left\{\vec{A}_b\cdot\vec{A}_b \exp[i2\omega_b(t-\tilde{n}_b\cdot\vec{r}/c)] + c.c. + \vec{A}_b\cdot\vec{A}_b^* + c.c.\right. \\ & + 2\left[\vec{A}_b\cdot\vec{A} \exp[i(\omega_b+\omega)t] \exp[-i(\omega_b\tilde{n}_b+\omega\tilde{n})\cdot\vec{r}/c] + c.c.\right] \\ & + 2\left[\vec{A}_b\cdot\vec{A}^* \exp[i(\omega_b-\omega)t] \exp[-i(\omega_b\tilde{n}_b-\omega\tilde{n})\cdot\vec{r}/c] + c.c.\right] \\ & \left. + \text{neglected terms in } \vec{A}\cdot\vec{A}\right\}. \end{aligned} \tag{5}$$

The perturbation theory is based upon the assumption that ψ may be expanded as

$$\Psi = \sum_k \{\delta_{kg} + a_k^{(1)} + a_k^{(2)}\} \phi_k \exp(-iE_k t/\hbar), \tag{6}$$

the initial, ground state being denoted by the subscript g (notice $\psi(0) = \phi_g$) and ϕ_k is an eigenfunction of the unperturbed Hamiltonian (which is the difference between Eq. (2) and (1)), and E_k is the corresponding eigenvalue. The

perturbation corrections in 2nd order time-dependent perturbation theory are given by

$$a_k^{(1)}(t) = \frac{1}{i\hbar}\int_0^t H_{kg}(t')\exp(i\omega_{kg}t')\,dt' \tag{7}$$

and

$$a_k^{(2)}(t) = \frac{1}{i\hbar}\int_0^t \sum_m a_m^{(1)}(t')\,H_{km}(t')\exp(i\omega_{km}t')\,dt' \,. \tag{8}$$

The matrix element of Eq. (7) is written

$$\begin{aligned}\langle k|H(t)|g\rangle = {} & \frac{e\hbar}{mci}\left\{\vec{A}_b\cdot\vec{B}_{kg}(\omega_b\tilde{n}_b)e^{i\omega_b t} + \vec{A}\cdot\vec{B}_{kg}(\omega\tilde{n})e^{i\omega t} + \text{c.c.}\right\} \\ & + \frac{e^2}{2mc^2}\left\{\vec{A}_b\cdot\vec{A}_b\, C_{kg}(2\omega_b\tilde{n}_b)e^{i2\omega_b t} + \text{c.c.}\right. \\ & + 2\left[\vec{A}_b\cdot\vec{A}\, C_{kg}(\omega_b\tilde{n}_b-\omega\tilde{n})e^{i(\omega_b+\omega)t} + \text{c.c.}\right] \\ & \left. + 2\left[\vec{A}_b\cdot\vec{A}^*\, C_{kg}(\omega_b\tilde{n}_b-\omega\tilde{n})e^{i(\omega_b-\omega)t} + \text{c.c.}\right]\right\}\end{aligned} \tag{9}$$

where $\vec{B}_{kg}(\omega\tilde{n}) = \langle k|\exp(-2\pi i\nu\tilde{n}\cdot\vec{r}/c)\vec{\nabla}|g\rangle$ and $C_{kg}(\omega\tilde{n}) = \langle k|\exp(-2\pi i\nu\tilde{n}\cdot\vec{r}/c)|g\rangle$ and the constant term has vanished for $k \neq g$.

Combining Eq. (7) and Eq. (9) now gives

$$\begin{aligned}a_k^{(1)}(t) = -\frac{e}{mc}\Bigg\{ & \vec{A}_b\cdot\vec{B}_{kg}(\omega_b\tilde{n}_b)\,\frac{\exp[i(\omega_b+\omega_{kg})t]-1}{i(\omega_b+\omega_{kg})} \\ & + \vec{A}_b^*\cdot\vec{B}_{kg}^*(\omega_b\tilde{n}_b)\,\frac{\exp[-i(\omega_b-\omega_{kg})t]-1}{-i(\omega_b-\omega_{kg})} \\ & + \vec{A}\cdot\vec{B}_{kg}(\omega\tilde{n})\,\frac{\exp[i(\omega+\omega_{kg})t]-1}{i(\omega+\omega_{kg})} \\ & + \vec{A}^*\cdot\vec{B}_{kg}^*(\omega\tilde{n})\,\frac{\exp[-i(\omega-\omega_{kg})t]-1}{-i(\omega-\omega_{kg})}\Bigg\}\end{aligned}$$

$$+\frac{e^2}{2i\hbar mc^2}\left\{\vec{A}_b\cdot\vec{A}_b C_{kg}(2\omega_b\tilde{n}_b)\,\frac{\exp[i(2\omega_b+\omega_{kg})t]-1}{i(2\omega_b+\omega_{kg})}\right.$$

$$+\vec{A}_b^*\cdot\vec{A}_b^* C_{kg}^*(2\omega_b\tilde{n}_b)\,\frac{\exp[-i(2\omega_b-\omega_{kg})t]-1}{-i(2\omega_b-\omega_{kg})}$$

$$+2\vec{A}_b\cdot\vec{A}\,C_{kg}(\omega_b\tilde{n}_b+\omega\tilde{n})\,\frac{\exp[i(\omega_b+\omega+\omega_{kg})t]-1}{i(\omega_b+\omega+\omega_{kg})}$$

$$+2\vec{A}_b^*\cdot\vec{A}^* C_{kg}^*(\omega_b\tilde{n}_b+\omega\tilde{n})\,\frac{\exp[-i(\omega_b+\omega-\omega_{kg})t]-1}{-i(\omega_b+\omega-\omega_{kg})}$$

$$+2\vec{A}_b\cdot\vec{A}^* C_{kg}(\omega_b\tilde{n}_b-\omega\tilde{n})\,\frac{\exp[i(\omega_b-\omega+\omega_{kg})t]-1}{i(\omega_b-\omega+\omega_{kg})}$$

$$\left.+2\vec{A}_b^*\cdot\vec{A}C_{kg}^*(\omega_b\tilde{n}_b-\omega\tilde{n})\,\frac{\exp[-i(\omega_b-\omega-\omega_{kg})t]-1}{-i(\omega_b-\omega-\omega_{kg})}\right\} \tag{10}$$

Now we obtain the second-order coefficients by combining (9) and parts of (10) in Eq. (8). This leads to the following expression: (See Appendix B).

$$a_k^{(2)}(t)=\int_0^t\frac{1}{i\hbar}\sum_\ell\frac{-e}{mc}\left\{\vec{A}_b\cdot\vec{B}_{\ell g}(\omega_b\tilde{n}_b)\,\frac{\exp[i(\omega_b+\omega_{\ell g})t']-1}{i(\omega_b+\omega_{\ell g})}\right.$$

$$+\vec{A}_b^*\cdot\vec{B}_{\ell g}^*(\omega_b\tilde{n}_b)\,\frac{\exp[-i(\omega_b-\omega_{\ell g})t']-1}{-i(\omega_b-\omega_{\ell g})}$$

$$+\vec{A}\cdot\vec{B}_{\ell g}(\omega\tilde{n})\,\frac{\exp[i(\omega+\omega_{\ell g})t']-1}{i(\omega+\omega_{\ell g})}$$

$$\left.+\vec{A}^*\cdot\vec{B}_{\ell g}^*(\omega\tilde{n})\,\frac{\exp[-i(\omega-\omega_{\ell g})t']-1}{-i(\omega-\omega_{\ell g})}\right\}$$

$$\times\frac{e\hbar}{mci}\left[\vec{A}_b\cdot\vec{B}_{k\ell}(\omega_b\tilde{n}_b)e^{i\omega_b t'}+\vec{A}\cdot\vec{B}_{k\ell}(\omega\tilde{n})\,e^{i\omega t'}+\text{c.c.}\right]\,e^{i\omega_{k\ell}t'}\,dt', \tag{11}$$

which we write as (neglecting $\vec{A}\cdot\vec{A}$ term)

$$a_k^{(2)}(t) = \left[\frac{e}{mc}\right]^2 \sum_{\ell} \frac{\vec{A}_b\cdot\vec{B}_{\ell g}(\omega_b\tilde{n}_b)}{i(\omega_b+\omega_{\ell g})}$$

$$\times\left\{\vec{A}_b\cdot\vec{B}_{k\ell}(\omega_b\tilde{n}_b)\left[\frac{\exp[i(2\omega_b+\omega_{kg})t]-1}{i(2\omega_b+\omega_{kg})} - \frac{\exp[+i(\omega_b+\omega_{k_\ell})t]-1}{+i(\omega_b+\omega_{k\ell})}\right]\right.$$

$$+\vec{A}_b^*\cdot\vec{B}^*_{k\ell}(\omega_b\tilde{n}_b)\left[\frac{\exp[i\omega_{kg}t]-1}{i\omega_{kg}} - \frac{\exp[-i(\omega_b-\omega_{k\ell})t]-1}{-i(\omega_b-\omega_{k\ell})}\right]$$

$$+\vec{A}\cdot\vec{B}_{k\ell}(\omega\tilde{n})\left[\frac{\exp[i(\omega_b+\omega+\omega_{kg})t]-1}{i(\omega_b+\omega+\omega_{kg})} - \frac{\exp[i(\omega+\omega_{k\ell})t]-1}{i(\omega+\omega_{k\ell})}\right]$$

$$+\vec{A}^*\cdot\vec{B}^*_{k\ell}(\omega\tilde{n})\left[\frac{\exp[i(\omega_b-\omega+\omega_{kg})t]-1}{i(\omega_b-\omega+\omega_{kg})} - \frac{\exp[-i(\omega-\omega_{k\ell})t]-1}{-i(\omega-\omega_{k\ell})}\right]$$

$$+\left[\frac{e}{mc}\right]^2 \sum_{\ell} \frac{\vec{A}^*_b\cdot\vec{B}^*_{\ell g}(\omega_b\tilde{n}_b)}{-i(\omega_b-\omega_{\ell g})}$$

$$\times\left\{\vec{A}_b\cdot\vec{B}_{k\ell}(\omega_b\tilde{n}_b)\left[\frac{\exp[i\omega_{kg}t]-1}{i\omega_{kg}} - \frac{\exp[i(\omega_b+\omega_{k\ell})t]-1}{i(\omega_b+\omega_{k\ell})}\right]\right.$$

$$+\vec{A}^*\cdot\vec{B}^*_{k\ell}(\omega_b\tilde{n}_b)\left[\frac{\exp[-i(2\omega_b-\omega_{kg})t]-1}{-i(2\omega_b-\omega_{kg})} - \frac{\exp[-i(\omega_b-\omega_{k\ell})t]-1}{-i(\omega_b-\omega_{k\ell})}\right]$$

$$+\vec{A}\cdot\vec{B}_{k\ell}(\omega\tilde{n})\left[\frac{\exp[i(\omega-\omega_b+\omega_{kg})t]-1}{i(\omega-\omega_b+\omega_{kg})} - \frac{\exp[i(\omega+\omega_{k\ell})t]-1}{i(\omega+\omega_{k\ell})}\right]$$

$$+\vec{A}^*\cdot\vec{B}^*_{k\ell}(\omega\tilde{n})\left[\frac{\exp[-i(\omega+\omega_b-\omega_{kg})t]-1}{-i(\omega+\omega_b-\omega_{kg})} - \frac{\exp[-i(\omega-\omega_{k\ell})t]-1}{-i(\omega-\omega_{k\ell})}\right]\Bigg\}$$

$$+\left[\frac{e}{2mc}\right]^2 \sum_{\ell} \frac{\vec{A}\cdot\vec{B}_{\ell g}(\omega\tilde{n})}{i(\omega+\omega_{\ell g})}$$

$$\times\left\{\vec{A}_b\cdot\vec{B}_{k\ell}(\omega_b\tilde{n}_b)\left[\frac{\exp[i(\omega_b+\omega+\omega_{kg})t]-1}{i(\omega_b+\omega+\omega_{kg})} - \frac{\exp[i(\omega_b+\omega_{k\ell})t]-1}{i(\omega_b+\omega_{k\ell})}\right]\right.$$

$$+ \vec{A}^*_b \cdot \vec{B}^*_{k\ell}(\omega_b \tilde{n}_b) \left[\frac{\exp[i(-\omega_b+\omega+\omega_{kg})t]-1}{i(-\omega_b+\omega+\omega_{kg})} - \frac{\exp[i(-\omega_b+\omega_{k\ell})t]-1}{i(-\omega_b+\omega_{k\ell})} \right]$$

$$+ \left[\frac{e}{2mc}\right]^2 \sum_{\ell} \frac{\vec{A}^* \cdot \vec{B}^*_{\ell g}(\omega\tilde{n})}{-i(\omega-\omega_{\ell g})}$$

$$\times \left\{ \vec{A}_b \cdot \vec{B}_{k\ell}(\omega_b \tilde{n}_b) \left[\frac{\exp[i(\omega_b-\omega+\omega_{kg})t]-1}{i(\omega_b-\omega+\omega_{kg})} - \frac{\exp[i(\omega_b+\omega_{k\ell})t]-1}{i(\omega_b+\omega_{k\ell})} \right] \right.$$

$$\left. + \vec{A}^*_b \cdot \vec{B}^*_{k\ell}(\omega_b \tilde{n}_b) \left[\frac{\exp[i(-\omega_b-\omega+\omega_{kg})t]-1}{i(-\omega_b-\omega+\omega_{kg})} - \frac{\exp[i(-\omega_b+\omega_{k\ell})t]-1}{i(-\omega_b+\omega_{k\ell})} \right] \right\} \tag{12}$$

SINGLE-PHOTON ABSORPTION

We begin by obtaining an expression for ordinary single-photon absorption. Assume for the moment that $\vec{A}_b = 0$. If g labels the ground state $\omega_{kg} > 0$, $k \neq g$ and the interesting part of Eq. (10) is surely

$$^s a_k^{(1)}(t) = \frac{e}{imc} \vec{A}^* \cdot \vec{B}^*_{kg}(\omega\tilde{n}) \frac{\exp[-i(\omega-\omega_{kg})t]-1}{(\omega-\omega_{kg})} \tag{13}$$

The transition probability is the squared modulus of $a_k(t)$.

$$^s W(t,\omega_{kg}) = |^s a_k^{(1)}(t)|^2 = 4\left[\frac{e}{mc}\right]^2 |\vec{A}^* \cdot \vec{B}^*_{kg}(\omega\tilde{n})|^2 \frac{\sin^2[\frac{1}{2}(\omega-\omega_{kg})t]}{(\omega-\omega_{kg})^2} \tag{14}$$

This is the probability of finding the system in state $|k\rangle$ at time t. In a real situation a collection of atoms will have a distribution of states $|k\rangle$ since each atom experiences a different environment. Thus, a distribution exists for the characteristic frequency $\zeta(\omega_{kg})$. The probability of transition should be averaged over $\zeta(\omega_{kg})$ to give

$$^s W(t) = \int_{-\infty}^{\infty} W(t,\omega_{kg})\zeta(\omega_{kg})d\omega_{kg}$$

$$= 4\left[\frac{e}{mc}\right]^2 |\vec{A}^* \cdot \vec{B}^*_{kg}(\omega\tilde{n})|^2 \int_{-\infty}^{\infty} \zeta(\omega_{kg}) \frac{\sin^2[(\omega-\omega_{kg})t/2]}{(\omega-\omega_{kg})^2} d\omega_{kg} \tag{15}$$

If t is taken large enough, $W(t,\omega_{kg})$ will be so sharply peaked that $\zeta(\omega_{kg})$ may be taken out of the integral; and since

$$\int_{-\infty}^{\infty} \frac{\sin^2 xt/2}{x^2}\, dx = \frac{\pi t}{2},$$

$$s_{W(t\to\infty)} = 2\pi \left[\frac{e}{mc}\right]^2 |A^*\cdot B^*_{kg}(\omega\tilde{n})|^2 \zeta t. \tag{16}$$

Thus, the probability of transition is proportional to time, and the transition rate for single-photon absorption is

$$s_R = \frac{d}{dt}\, s_{W(t\to\infty)} = 2\pi\left[\frac{e}{mc}\right]^2 |\vec{A}^*\cdot\vec{B}^*_{kg}(\omega\tilde{n})|^2 \zeta(\omega). \tag{17}$$

It must be remembered that $\zeta(\omega)$ is a distribution function for characteristic frequency ω_{kg} and hence also for the separation of state $|k\rangle$ from the ground state. In this treatment it is assumed that this function depends only on the medium and its inherent fluctuations and that the incoming radiation will not affect its shape. It may be, however, that a high power laser pulse will perturb the system to such an extent that this function will require more attention.

The intensity is related to the amplitude of the vector potential by

$$I = \frac{n\omega^2}{2\pi c} A^2; \tag{18}$$

then if $\vec{A} = A\tilde{e}$ ($\tilde{e}$ = unit vector) Eq. (17) can be written

$$s_R = 4\pi^2 \left[\frac{e}{mc}\right]^2 \frac{cI}{n\omega^2} |\tilde{e}\cdot\vec{B}^*_{kg}(\omega\tilde{n})|^2 \zeta(\omega).$$

The rate of absorption of energy is

$$N\hbar\omega s_R = -\frac{dI}{dz}, \tag{19}$$

and the absorption coefficient is defined as

$$\alpha = -\frac{1}{I}\frac{dI}{dz} = \frac{N\hbar\omega}{I} s_R; \tag{20}$$

so

$$\alpha = 4\pi^2 \left[\frac{e}{mc}\right]^2 \frac{\omega\hbar}{n\omega} |\tilde{e}\cdot B^*_{kg}(\omega\tilde{n})|^2 \zeta(\omega)\, N, \tag{21}$$

where N is the concentration of absorbers. From Appendix A Eq. (A2)

$$\vec{B}^{*}_{kg}(\omega n) = \frac{m\omega_{kg}}{\hbar}\vec{r}_{kg} \quad , \tag{22}$$

in the dipole approximation, and

$$\vec{r}_{kg} = \langle k|\vec{r}|g\rangle \quad . \tag{23}$$

So. Eq. (20) can be written

$$s_{\alpha} = 4N\pi^2\left[\frac{e^2}{\hbar c}\right]\frac{\omega_{kg}}{n}|\tilde{e}\cdot\vec{r}_{kg}|^2\,\zeta(\omega) \quad ; \tag{24}$$

where $e^2/\hbar c = 1/137$, the fine structure constant. The derivation of Eq. (24) establishes the procedure; that which follows is done in a similar way.

DOUBLE-PHOTON COEFFICIENTS FROM $a_k^{(1)}$

Both $a_k^{(1)}$, Eq. (10), and $a_k^{(2)}$, Eq. (12), contain terms which may be interpreted as pertaining to two-photon effects. We look first at terms deriving from $a_k^{(1)}$ which might describe absorption at $\nu_c \pm \nu_b$ where ν_c is a sharp line in the spectrum of a medium. We take $\omega_{kg}=\omega_c=2\pi\nu_c > 0$ and note the terms with the proper resonant behavior are

$$\begin{aligned} {}^{1}a_k^{(1)}(t) = \frac{e^2}{i\hbar mc^2}\Bigg[& \vec{A}^{*}_{b}\cdot\vec{A}^{*}C^{*}_{kg}(\omega_b\tilde{n}_b+\omega\tilde{n})\ \frac{\exp[-i(\omega_b+\omega-\omega_{kg})t]-1}{-i(\omega_b+\omega-\omega_{kg})} \\ & + \vec{A}_{b}\cdot\vec{A}^{*}C_{kg}(\omega_b\tilde{n}_b-\omega\tilde{n})\ \frac{\exp[i(\omega_b-\omega+\omega_{kg})t]-1}{i(\omega_b-\omega+\omega_{kg})}\Bigg] \end{aligned} \tag{25}$$

where the pre-superscript denotes the first of the experiments outlined in the Introduction.

Equation (25) has some interesting characteristics. Contrary to Kleinman's approach in 1962, Eq. (25) will give an amplitude for a two-photon absorption which does not contain intermediate states. Our result does not seem unreasonable since the intermediate states seem to serve a purely formal, nonphysical role, and they appear as a consequence of assuming that the unperturbed eigenvectors form a basis sufficient to describe the behavior of the system. Thus, one should not infer that in undergoing a transition a system actually traverses all or any of these intermediate states. Equation (25) also exhibits a *dependence*

upon polarization of the beams through the dot products. We can write the matrix element as

$$C_{kg}(\omega_b \tilde{n}_b - \omega \tilde{n}) = \frac{-i(\omega_b \tilde{n}_b - \omega \tilde{n})}{c} \cdot \vec{r}_{kg} \tag{26}$$

by expanding the exponential and retaining the first nonvanishing term in the dipole approximation (first nonvanishing term); hence, if the dipole matrix element between the ground state and excited state is appreciable, contributions from $a_k^{(1)}$ will contribute in describing this two-photon process. This leads to an absorption coefficient for the source equal to

$$1_\alpha(1)(\omega) = N(2\pi)^3 \left[\frac{e^2}{\hbar c}\right]^2 \frac{\hbar}{(mc)^2} \frac{I_b}{n n_b \omega \omega_b} |\tilde{e}_b \cdot \tilde{e}|^2 \, |(\omega_b \tilde{n}_b \pm \omega \tilde{n}) \cdot \vec{r}_{kg}|^2 \zeta(\omega \pm \omega_b). \tag{27}$$

Again, we note that $\zeta(x)$ is the line shape of the ω_{kg} transition. The subscript b denotes the laser frequency and $\tilde{e}$, $\tilde{e}_b$ are unit vectors describing the polarization of the radiation. Notice *this coefficient depends upon the intensity of the laser beam*, and as mentioned before, *is sensitive to the relative polarization of the two beams.* It will also be noticed that the factor involving the dipole moment may be expected to *depend upon directions of propagation in crystals of low symmetry.*

Equation (10) also has a term which may be interpreted as describing transitions due to simultaneous absorption of two laser photons. It is

$${}^2a_k^{(1)}(t) = \frac{e^2}{2i\hbar mc^2} \vec{A}_b^* \cdot \vec{A}_b^* C_{kg}(2\omega_b \tilde{n}_b) \frac{\exp[-i(2\omega_b - \omega_{kg})] - 1}{-i(2\omega_b - \omega_{kg})} . \tag{28}$$

The pre-superscript 2 denotes the second of the experiments outlined in the Introduction. Hence,

$${}^2R(1) = 2\pi \left[\frac{e^2}{2\hbar mc^2}\right]^2 |\vec{A}_b^*|^2 \, |C_{kg}(2\omega_b \tilde{n}_b)|^2 , \tag{29}$$

but here, rather than Eq. (20),

$${}^2\alpha = \frac{2\hbar\omega}{I} \, NR , \tag{30}$$

so

$$2_\alpha(1)(2\omega_b) = 4N\pi^3 \left[\frac{e^2}{\hbar c}\right]^2 \frac{\hbar}{(mc)^2} \frac{I_b}{n_b^2 \omega_b} |\tilde{n}_b \cdot \vec{r}_{kg}|^2 \zeta(2\omega_b) \tag{31}$$

Here again, the absorption coefficient depends upon the intensity and crystal symmetry. Equation (31) can be written in terms of oscillator strengths. Oscillator strength is defined by

$$f_{kg} = \frac{2m\omega_{ks}}{\hbar} |x_{gk}|^2 \quad , \tag{32}$$

and obeys

$$\sum_k f_{kg} = 1 \ . \tag{33}$$

In an isotropic medium

$$\overline{|\tilde{n}_b \cdot \vec{r}_{kg}|^2} = \frac{n_b^2}{3} |\vec{r}_{kg}|^2 = n_b^2 |x_{kg}|^2 = \frac{\hbar n_b^2}{2m\omega_{kg}} f_{kg} \ . \tag{34}$$

Using $\omega_{kg} = 2\omega_b$ and Eq. (34) changes Eq. (32) to

$$2_\alpha(1)(2\omega_b) = \frac{N\pi^3}{4} \left[\frac{e^2}{mc^2}\right]^2 \frac{I_b f_{kg}}{m\omega_b^2 n_b^2} \zeta(2\omega_b) \ . \tag{35}$$

DOUBLE-PHOTON COEFFICIENTS FROM $a_k^{(2)}$

Let us continue by considering cases wherein the transition is forbidden in the dipole approximation. It may be that the following $a_k^{(2)}$ coefficients will dominate in describing the two-photon absorption.

$$
{}^{1}a_k^{(2)}(t) = \left[\frac{e}{mc}\right]^2 \sum_{\ell} \left\{ \frac{\vec{A}_b \cdot \vec{B}_{\ell g}(\omega_b \tilde{n}_b)\vec{A}^* \cdot \vec{B}^*_{k\ell}(\omega\tilde{n})}{i(\omega_b + \omega_{\ell g})} \left(\frac{\exp[i(\omega_b - \omega + \omega_{kg})t] - 1}{i(\omega_b - \omega + \omega_{kg})} \right) \right.
$$

$$
+ \frac{\vec{A}^*_b \cdot \vec{B}^*_{\ell g}(\omega_b \tilde{n}_b)\vec{A}^* \cdot \vec{B}^*_{k\ell}(\omega\tilde{n})}{-i(\omega_b - \omega_{\ell g})} \left(\frac{\exp[-i(\omega + \omega_b - \omega_{kg})t] - 1}{-i(\omega + \omega_b - \omega_{kg})} \right)
$$

$$
+ \frac{\vec{A}^* \cdot \vec{B}^*_{\ell g}(\omega\tilde{n})\vec{A}_b \cdot \vec{B}_{k\ell}(\omega_b \tilde{n}_b)}{-i(\omega - \omega_{\ell g})} \left(\frac{\exp[i(\omega_b - \omega + \omega_{kg})t] - 1}{i(\omega_b - \omega + \omega_{kg})} \right)
$$

$$
\left. + \frac{\vec{A}^* \cdot \vec{B}^*_{\ell g}(\omega\tilde{n})\vec{A}^*_b \cdot \vec{B}^*_{k\ell}(\omega_b \tilde{n}_b)}{-i(\omega - \omega_{\ell g})} \left(\frac{\exp[i(-\omega_b - \omega + \omega_{kg})t] - 1}{i(-\omega_b - \omega + \omega_{kg})} \right) \right\} \tag{36}
$$

Calculating $|a_k^{(2)}(t)|^2$ directly is obviously too involved and not pertinent; many terms would be generated which would be uninteresting for these processes, so let us proceed by approximation. Kleinman (1962) assumed the existence of a very strong band lying well above the frequencies ω, ω_b, and ω_{kg}. These so dominate the scene that the sum in Eq. (37) can be dispensed with as follows. Take $\omega_{lg} >> \omega$, ω_b, ω_{kg} and assume the matrix elements connecting the intermediate states with the final state and with the ground state are essentially the same. Then, combining Eqs. (32), (34), and (36) results in the following form for ${}^{1}a_k^{(2)}(t)$.

$$
{}^{1}a_k^{(2)}(t) \simeq \left[\frac{e}{mc}\right]^2 \sum_{\ell} \left\{ A_b A^* \frac{m^2}{i\hbar^2 \omega_{\ell g}} |X_{\ell g}|^2 \frac{\exp[i(\omega_b - \omega + \omega_{kg})t] - 1}{i(\omega_b - \omega + \omega_{kg})} \right.
$$

$$
+ A^*_b A^* \frac{m^2}{i\hbar^2 \omega_{\ell g}} |X_{\ell g}|^2 \frac{\exp[-i(\omega + \omega_b - \omega_{kg})t] - 1}{-i(\omega + \omega_b - \omega_{kg})}
$$

$$
+ A_b A^* \frac{m^2}{i\hbar^2 \omega_{\ell g}} |X_{\ell g}|^2 \frac{\exp[i(\omega_b - \omega + \omega_{kg})t] - 1}{i(\omega_b - \omega + \omega_{kg})}
$$

$$
\left. + A^* A^*_b \frac{m^2}{i\hbar^2 \omega_{\ell g}} |X_{\ell g}|^2 \frac{\exp[i(-\omega_b - \omega + \omega_{kg})t] - 1}{i(-\omega_b - \omega + \omega_{kg})} \right\} \tag{37}
$$

The time dependent parentheses and the A amplitudes in the equation above can be removed from the sum, leaving a sum of the form

$$\sum_{\ell} m^2 \frac{\omega_{\ell g}}{i\hbar^2} |X_{\ell g}|^2 . \tag{38}$$

Using Eqs. (32) and (33), Eq. (38) becomes

$$\frac{m}{2i\hbar} \sum_{\ell} f_{\ell g} = \frac{m}{2i\hbar} . \tag{39}$$

Thus, the assumption of a strong absorption band with characteristic frequency much greater than ω, ω_b, and ω_{kg} results in the following expression for $1a_k^{(2)}(t)$.

$$1a_k^{(2)}(t) \simeq \left[\frac{e}{mc}\right]^2 \frac{m}{i\hbar} \left\{ A_b A^* \frac{\exp\{-i[\omega-(\omega_{kg}+\omega_b)]t\}-1}{-i[\omega-(\omega_{kg}+\omega_b)]} + A_b^* A^* \frac{\exp\{-i[\omega-(\omega_{kg}-\omega_b)]t\}-1}{-i[\omega-(\omega_{kg}-\omega_b)]} \right\} \tag{40}$$

In squaring this term to get the transition probability, we note that cross terms give incomplete as well as uninteresting results; therefore, we omit them and obtain for the transition probability

$$\left| 1a_k^{(2)}(t) \right|^2 = 2 \left[\left(\frac{e}{mc}\right)^2 \frac{m}{\hbar} \right]^2 \frac{|A_b A|^2 \, 4\sin^2\{[\omega-(\omega_{kg}\pm\omega_b)]t/2\}}{[\omega-(\omega_{kg}\pm\omega_b)]^2} . \tag{41}$$

Thus,

$$1R(2) = 4\pi \left[\left(\frac{e}{mc}\right)^2 \frac{m}{\hbar} \right]^2 |A_b A|^2 \, \zeta(\omega\pm\omega_b) . \tag{42}$$

Using Eqs. (17) and (19) with (42) gives the absorption coefficient for frequencies near $\omega = \omega_{kg}\pm\omega_b$

$$1\alpha^{(2)}(\omega) = 4N\pi^3 \left[\left(\frac{e}{mc}\right)^2 \frac{m}{\hbar} \right]^2 \frac{2cI}{n\omega^2} \frac{2cI_b}{n_b\omega_b^2} \zeta(\omega\pm\omega_b) \frac{\hbar\omega}{I}$$

$$= 16N\pi^3 \left(\frac{e^2}{hc}\right)^2 \frac{\hbar I_b}{nn_b m^2 \omega\omega_b^2} \zeta(\omega\pm\omega_b) . \tag{43}$$

Finally, the double-photon, $2\omega_b$, absorption coefficient is desired. The interesting term in Eq. (12) is

$$2a_k^{(2)}(t) = \left[\frac{e}{mc}\right]^2 \sum_{\ell} \frac{\vec{A}_b^* \cdot \vec{B}_{\ell g}^* (\omega_b \tilde{n}_b) \vec{A}_b^* \cdot \vec{B}_{k\ell}^* (\omega_b \tilde{n}_b)}{-i(\omega_b - \omega_{\ell g})} \quad \frac{\exp[-i(2\omega_b - \omega_{kg})] - 1}{-i(2\omega_b - \omega_{kg})} \tag{44}$$

Using the same assumptions that lead to Eq. (40) results in

$$2a_k^{(2)}(t) = \left(\frac{e}{mc}\right)^2 \frac{m}{2i\hbar} (\vec{A}_b^*)^2 \frac{\exp[-i(2\omega_b - \omega_{kg})t] - 1}{-i(2\omega_b - \omega_{kg})} \tag{45}$$

which results in the transition rate

$$2R^{(2)} = 2\pi \left[\left(\frac{e}{mc}\right)^2 \frac{m}{2\hbar}\right]^2 |A_b^*|^4 \zeta(2\omega_b) . \tag{46}$$

Replacing in Eq. (30) gives

$$2\alpha^{(2)}(2\omega_b) = 16N\pi^3 \left(\frac{e^2}{\hbar c}\right)^2 \frac{I_b \hbar}{m^2 n_b^2 \omega_b^3} \zeta(2\omega_b). \tag{47}$$

Notice that Eq. (43) becomes Eq. (47) in the limit $\omega = \omega_b$, as it should.

DISCUSSION OF RESULTS

Equations (43) and (47) are identical, except for a constant factor, with Kleinman's expressions for a two-photon absorption process. Equation (47) was used by Kaiser and Garrett (1961) to discuss their double-photon absorption experiment in CaF_2:Eu^{++}. This appears to be proper even though there is probably an appreciable dipole matrix element connecting the ground state with the $2\gamma_b$ state (~3472 A, half the ruby laser wavelength). If the dipole matrix element is appreciable, Eq. (31) (or Eq. (35)) will apply. On the other hand, the assumptions leading to Eq. (47) are probably fairly good and since Eq. (47) is much greater (ratio is $mc^2/f_{kg}\hbar\omega_b$ it will dominate in describing the process.

To estimate the probability of two-photon absorption, we compare its absorption coefficient to that for a single-photon absorption. That is, we take the ratio of Eqs. (43) and (24)

$$\frac{1\alpha^{(2)}(\omega)}{s\alpha} = 4\pi \left(\frac{e^2}{\hbar c}\right) \frac{\hbar I_b}{n_b m^2 \omega \omega_b^2 \omega_{kg} |\tilde{e} \cdot \vec{r}|^2} . \tag{48}$$

Suppose $\vec{e} = (1,0,0)$, then $\omega_{kg}|\vec{e}\cdot\vec{r}|^2 = \omega_{kg}|X_{kg}|^2 = \hbar f_{kg}/2m$ where Eq. (32) is used.

Hence, Eq. (48) becomes

$$\frac{I_\alpha(2)(\omega)}{S_\alpha} = 8\pi \left(\frac{e^2}{\hbar c}\right) \frac{I_b}{n_b m\omega\omega_b^2 f_{kg}} \quad . \tag{49}$$

One can estimate expression (49) by using the following nominal values for a rare earth ion in a crystal lattice where $f^N \rightarrow f^N$ transitions can be considered.

Then we have

$$\frac{e^2}{\hbar c} = \frac{1}{137},\ I_b \sim 50MW,\ n_b \sim 1.5,\ \omega \sim \frac{2\pi c}{(1 \text{ micron})} = 2 \times 10^{15}\ \text{sec}^{-1}$$

$$\omega_b \sim \frac{2\pi L}{(.7 \text{ micron})} = 3 \times 10^{15}\ \text{sec}^{-1},\ \text{and}\ f_{kg} \sim 10^{-6}$$

The ratio then takes the value of 10^{-3}. By focusing the laser it is possible to increase I_b to the extent that the ratio (Eq. (49)) becomes of the order of unity. Thus, one would expect an absorption of the weaker source at frequency $\omega_{kg} - \omega_b$ just as strong as that which occurs at frequency ω_{kg} in an ordinary absorption experiment. The practical difficulty here is that focusing the laser decreases the effective size of the sample to $\sim 10^{-5}$ cm^3 (if the sample is 1 mm thick).

At least two problems must be avoided if the effect for which the previously noted cross-section $[\alpha_{(2)}]$ applies is not to be obscured. First, care must be taken to choose a system which has no states of energy $E = h\nu$ above the ground state where ν is the source or pump frequency. Secondly, in order to exclude the complications of second harmonic generation followed by single-photon absorption at the second harmonic frequency it is best to choose a system with inversion symmetry. The second harmonic susceptibility coefficient is zero if one uses a system having inversion symmetry. Since $P_{2\omega} = X(2\omega)E^2$, where $P_{2\omega}$ = polarization, x = susceptibility, E = electric field. In the case of inversion symmetry reversing the field leaves $P_{2\omega}$ invariant. Hence, $-P_{2\omega} = X(2\omega)(-E)^2 = X(2\omega)E^2 = P_{2\omega}$, which implies $X(2\omega) = 0$.

HISTORICAL NOTE

J. B. Gruber began this study nearly ten years ago at Washington State University, Pullman, with assistance from graduate students T. R. Stoner and D. N. Olsen at WSU. Part of the present manuscript was submitted on behalf of T. R. Stoner to WSU in partial fulfillment of the Ph.D. degree in physics awarded posthumously in 1970. Details of the calculation have not been published elsewhere. Subsequent research in this area is being continued by J. B. Gruber at North Dakota State University with assistance from graduate students E. D. Larson and J. Daly.

LITERATURE CITED

Bonch-Bruevich, A. M. and V. A. Khodovoĭ. 1965. Multiphoton Processes. Sov. Phys. 85:1-38.

Condon, E. U. and G. H. Shortley. 1957. The Theory of Atomic Spectra. Cambridge Univ. Press, England.

DiBartolo, B. 1968. Optical Interactions in Solids. John Wiley and Sons, New York.

Fiutak, J. 1963. The Multipole Expansion in Quantum Theory. Can. J. of Phys. 41:12-20.

Goeppert-Mayer, M. 1931. Time Dependent Perturbation Theory. Ann. Physik 9:273-278.

Gruber, J. B. 1968. Optical Transitions in Rare Earth Crystals. Prog. Sci. and Tech. of the Rare Earths 3:38-60.

Jackson, J. D. 1962. Classical Electrodynamics. John Wiley and Sons, New York.

Kaiser, W. and C. G. B. Garrett. 1961. Two-Photon Excitation in $CaF_2:Eu^{2+}$. Phys. Rev. Lett. 7:229-231.

Kleinman, D. A. 1962. Laser and Two-Photon Processes. Phys. Rev. 125:87-88.

Messiah, A. 1965. Quantum Mechanics. North Holland Publ. Co., Amsterdam.

Merzbacher, E. 1970. Quantum Mechanics. John Wiley and Sons, New York.

Peticolas, W. L. 1967. Multiphoton Spectroscopy. Ann. Rev. of Phys. Chem. 18:233-260.

Appendix A. Matrix Element $B^*_{mn}(\nu\tilde{n})$

Taking the first nonvanishing term in $B_{mn}(\nu\tilde{n})$ gives

$$\vec{B}^{d*}_{mn}(\nu\tilde{n}) = \langle m|\vec{\nabla}|n\rangle \quad .$$

The unperturbed Hamiltonian is

$$H_0 = \frac{p^2}{2m} + V = -\frac{\hbar^2}{2m}\nabla^2 + V$$

$$H_0\vec{r} = V\vec{r}$$

$$\vec{r}H_0 = -\frac{\hbar^2}{2m}\vec{r}\nabla^2 + \vec{r}V \quad .$$

Assuming $[\vec{r},V] = 0$,

$$\left[\vec{r},H_0\right]\Psi = -\frac{\hbar^2}{2m}\left[\vec{r}\nabla^2 - \nabla^2\vec{r}\right]\Psi \quad . \qquad \text{(A1)}$$

A typical term in the last term in (A1) is

$$\partial_{x_\alpha}\partial_{x_\alpha}\chi_\beta\psi = \partial_{x_\alpha}\delta_{\alpha\beta}\psi + \partial_{x_\alpha}\chi_\beta\partial_{x_\alpha}\psi$$

$$= \delta_{\alpha\beta}\partial_{x_\alpha}\psi + \delta_{\alpha\beta}\partial_{x_\alpha}\psi + \chi_\beta\partial_{x_\alpha}\partial_{x_\alpha}\psi$$

$$= 2\,\delta_{\alpha\beta}\partial_{x_\alpha}\psi + \chi_\beta\partial_{x_\alpha}\partial_{x_\alpha}\psi$$

Hence,

$$\dot{\nabla}^2\vec{r} = \vec{r}\nabla^2 + 2\vec{\nabla}$$

so (A1) becomes

$$\vec{\nabla} = -\frac{m}{\hbar^2}\left[\vec{r},H_0\right]$$

so that

$$\vec{B}^{d*}_{mn}(\nu n) = -\frac{m}{\hbar^2}\,\langle m|\left[\vec{r},H_0\right]|n\rangle = -\frac{m}{\hbar^2}(E_n-E_m)\vec{r}_{mn} = \frac{m\omega_{mn}}{\hbar}\vec{r}_{mn}\,. \qquad \text{(A2)}$$

Appendix B.

In determining Equation 11, a total of sixty terms were dropped. The justification for this is readily seen by comparing the largest neglected term to the smallest retained term.

Retained was:

$$\frac{ie^2}{m^2c^2}\sum_{\ell}\frac{\vec{A}\cdot\vec{B}_{\ell g}(\omega_b\tilde{n}_b)\;\vec{A}\cdot\vec{B}_{k\ell}(\omega_b\tilde{n}_b)}{(\omega_b+\omega_{\ell g})}\left\{\exp[i(2\omega_b+\omega_{\ell g}+\omega_{k\ell})t] - \exp[i(\omega_b+\omega_{k\ell})t]\right\}$$

Neglected was:

$$\frac{e^4}{4\hbar m^2c^4}\sum_{\ell}\frac{(A^*_b\cdot A^*_b)^2 C_{\ell g}(2\omega_b\tilde{n}_b)C_{k\ell}(2\omega_b\tilde{n}_b)}{(2\omega_b-\omega_{\ell g})}\left\{\exp[-i(3\omega_b-\omega_{\ell g})t] - \exp(-i\omega_b t)\right\}$$

Considering one term in each expansion and the amplitude only, we must show that

$$\frac{-i\vec{A}\cdot\vec{B}_{\ell g}(\omega_b\tilde{n}_b)\;\vec{A}\cdot\vec{B}_{k\ell}(\omega_b\tilde{n}_b)}{\omega_b+\omega_{\ell g}} \gg \frac{e^2}{4hc^2}\;\frac{(\vec{A}^*_b\cdot\vec{A}^*_b)^2 C_{\ell g}(2\omega_b\tilde{n}_b)C_{k\ell}(2\omega_b\tilde{n}_b)}{2\omega_b-\omega_{\ell g}}$$

or that

$$\frac{-i\vec{A}\cdot\vec{B}_{\ell g}(\omega_b \tilde{n}_b)}{\omega_b + \omega_{\ell g}} \gg \frac{e^2}{4hc^2} \frac{(\vec{A}_b^* \cdot \vec{A}_b^*) C_{\ell g}(2\omega_b \tilde{n}_b)}{2\omega_b - \omega_{\ell g}}$$

This can be done quite simply by using hydrogenic wave functions to determine the matrix elements. One finds that the inequality does hold.